Université du Québec
Institut National de la Recherche Scientifique
Centre Énergie Matériaux Télécommunications

Low-Cost Localization Algorithms for Wireless Sensor Networks

Par
Ahmad El Assaf

Thèse présentée pour l'obtention
du grade de philosophiae doctor (Ph.D.)

Président du jury	Serioja Ovidiu Tatu INRS-EMT
Examinateur	Wessam Ajib UQAM
Examinateur	Mohamed Ibnkahla Carleton University
Directeur de recherche	Nahi Kandil UQAT
Co-directeur de recherche	Sofiène Affes INRS-EMT

Remerciements

Je tiens, tout d'abord, à remercier mon directeur de recherche Prof. Nahi Kandil d'avoir supervisé cette thèse. Je lui suis également reconnaissant de m'avoir assuré un encadrement rigoureux tout au long de ces années, tout en me donnant toutefois la possibilité de trouver par moi-même mon cheminement personnel. Prof. Kandil a su diriger mes travaux avec beaucoup de disponibilité, de tact et d'intérêt.

Je remercie aussi très chaleureusement mon co-directeur de recherche, Prof. Sofiène Affes qui, malgré ses nombreuses occupations, a accepté de prendre la direction de cette thèse en cours de route, transformant ainsi les difficultés rencontrées en une expérience enrichissante. Je lui dois ma profonde reconnaissance pour son soutien continu et ses précieux conseils qui m'ont permis de réaliser une recherche de qualité.

Je suis grandement reconnaissante au Prof. Serioja Ovidiu Tatu qui m'a fait l'honneur de présider le jury. Les examinatrices qui ont accepté de siéger sur le jury de cette thèse doivent aussi trouver ici l'expression de ma reconnaissance, soit Dr. Wessam Ajib et Dr. Mohamed Ibnkahla.

Je suis aussi redevable à la contribution de mon adorable ami et collègue Dr. Slim Zaidi, qui a consacré, beaucoup de temps et d'énergie pour l'avancement du projet. Qu'il trouve ici l'expression de ma profonde gratitude.

Je souhaite aussi remercier mes chers frères et sœurs qui m'ont toujours soutenue à dépasser les moments les plus difficiles durant mes études doctorales.

Enfin, Mes remerciements vont particulièrement au mes deux grands héros, ma mère et mon père, les êtres les plus généreux et attentionnés qu'ils ont tout donné pour avoir fait de moi ce que je suis aujourd'hui. Le mot merci est à mon avis insuffisant pour exprimer ma gratitude envers vous. Mille mercis.

Table des matières

Liste des figures

Liste des tableaux

Résumé

Cette thèse propose de nouveaux algorithmes de localisation à faible coût pour les réseaux de capteurs sans fils (“wireless sensor networks (WSNs)”). Jusqu'ici, la nature hétérogène des WSNs a été ignorée lors de la conception de tels algorithmes. Ceci nous a motivé a développé un nouvel algorithme adapte aux WSNs hétérogènes (HWSN)s. On a prouvé que l'algorithme proposé est capable de localiser les capteurs avec une grande précision. En plus, on a développé dans le cadre de cette thèse, un nouvel algorithme de localisation qui exploite en plus du nombre minimal de sauts d'autres informations localement disponible au niveau de chaque capteur. Malgré leur précision, les performances de ces algorithmes se détériorent rapidement dans les environnements anisotropes plus réaliste où plusieurs obstacles (murs, personnes, immeubles, machines, etc.) peuvent exister entre deux nœuds. Afin de résoudre ce problème, on a développé une stratégie de sélection d'anchors fiable à faible coût. Afin d'augmenter encore plus la robustesse de nos algorithmes, on a développé un mécanisme de correction qui tient en compte le phénomène d”atténuation anisotrope du signal. En exploitant les réseaux de neurones artificiels (ANNs), ce mécanisme est capable de corriger les erreurs d'estimation de distance due à ce phénomène. Étant donné que la précision de localisation est étroitement liée aux positions des anchors, cette thèse propose aussi une stratégie novatrice de placement optimal des anchors. En recourant à l'optimisation par essaim de particules bien connu (“Particle swarm optimization PSO”), il a été démontré que cette nouvelle stratégie offre des gains de précision significatifs.

Introduction

Les progrès récents dans les communications sans fil et l'émergence de nouvelles technologies à faible coût ont conduit à la prolifération des réseaux de capteurs sans fil (WSN). Un WSN est un ensemble de capteurs sans fil complétement indépendants, autonomes, de taille réduite, et à faible coût qui sont souvent équipés avec une ressource énergétique limitée et irremplaçable. Ces unités sont déployées généralement en grande densité d'une façon aléatoire dans des environnements hostiles. Ils ont pour rôle la détection et la mesure de certains phénomènes physiques sus tels que la température, la lumière, la pression, etc.. Afin de préserver leurs énergies, ces capteurs collaborent souvent dans la transmission des données vers un point d'accès (AP). Ces données sont malheureusement inutiles si la position de l'endroit où elles ont été mesurées est inconnue, ce qui rend la localisation des nœuds une tâche essentielle dans les WSNs. De nombreuses solutions intéressantes existent dans la littérature qui peuvent être classifiées en deux grandes catégories : *range-based* et *range-free*.

Pour localiser correctement un capteur, les algorithmes *range-based* exploitent des données pertinentes obtenus à partir des signaux radio reçus, tels que le temps d'arrivée (TOA), l'angle d'arrivée (AOA), ou la puissance reçu (RSS). Ces signaux sont, en fait, transmis par des nœuds ayant une connaissance préalable de leurs positions, appelées "anchors" (ou points de repère). Bien que les algorithmes *range-based* sont très précis, nous ne pouvons négliger l'impact énergétique de ces algorithmes sur la survie de l'ensemble du réseau, et par suite ils ne conviennent pas aux WSNs. Ils nécessitent en effet une forte puissance pour assurer la communication entre les capteurs, alimentés par de petites batteries. De plus, du matériel supplémentaire est généralement requise au niveau des capteurs, augmentant ainsi le coût global du réseau. En outre, les performances de ces algorithmes peuvent être gravement affectées par le bruit, les interférences, l'évanouissement (fading), effet de masque (shadowing).

Contrairement à ces derniers, les algorithmes *range-free* sont originalement proposés comme

des algorithmes plus économes en énergie et qui ne nécessitent pas de matériel supplémentaire au niveau des nœuds et, par conséquent, sont plus appropriés pour WSNs. Les algorithmes relevant de ce type de stratégie exploitent les informations de connectivité de réseau pour estimer les positions des nœuds régulières. Afin de bénéficier de ces nombreux avantages, les algorithmes de localisation *range-free* ont attiré l'attention de la communauté des chercheurs dans le domaine de localisation. La plupart de ces algorithmes sont incontestablement basés sur des variations de DV-HOP dont la mise en œuvre dans WSNs multi-sauts nécessite la dérivation d'un facteur de correction h_{av} (i.e., distance moyenne entre deux nœuds intermédiaires consécutifs) pour estimer la distance entre un nœud régulier et un nœud d'ancre comme $n_h h_{\text{av}}$, où n_h représente le nombre minimale de sauts (i.e., nombre de liens radios empruntés par un message du nœud d'ancre au nœud régulier à travers des nœuds intermédiaires ("hop-count")) entre ces deux nœuds. En effet, h_{av} est calculé d'une manière non-localisée au niveau des nœuds ancres et diffusé dans le réseau par chaque ancre. Ceci induit inévitablement de l'*overhead* (qui augmente linéairement avec le nombre des ancres) et de consommation d'énergie indésirables, augmentant ainsi le coût global du processus de localisation. Lorsque le réseau est dense, cet *overhead* peut devenir excessif ce qui entraîne un épuisement sévère des batteries des terminaux. Ce défis majeur a motivé beaucoup de rechercher visant à développer les meilleures algorithmes capables de réduire l'*overhead* des algorithmes heuristiques.

Visant à atteindre cet objectif, de nombreuses alternatives populaires appropriées pour WSNs multi-sauts ont été développées. Ces algorithmes évaluent analytiquement la valeur de h_{av} en utilisant les caractéristiques statistiques du déploiement du réseau. La valeur obtenu de h_{av} est en fait localement calculable à chaque nœud régulier, évitant ainsi l'*overhead* et la consommation d'énergie inutile encourus par les algorithmes heuristiques si, de même, il a dû être diffusé dans le réseau. Malgré leur précieuse contribution, les algorithmes de localisation développées jusqu'à présent ne fournit pas malheureusement de précision suffisante, en raison de grandes erreurs se sont produites lors de la cartographie le nombre de sauts n_h en unités de distance. Ceci est principalement causé soit par le fait que les algorithmes existant se basent sur une hypothèse irréaliste (i.e., tous les nœuds ont les mêmes capacités de transmission), ou bien soit par le manque des informations fournies lors de la dérivation de h_{av}. Il a été prouvé que les performances d'algorithmes existants sont malheureusement, très médiocres surtout dans les réseaux hétérogènes de capteurs sans fil(HWSNs) où les portées de transmission de capteurs

sont très souvent différentes.

L'objective de cette thèse est donc :

- Fournir de nouvelles algorithmes analytiques de localisation novatrices en prenant plusieurs phénomènes en considération lors de la conception de ces algorithmes tels que, la nature hétérogène de réseaux de capteurs, l'existence des obstacles dans le réseau, le phénomène d'atténuation anisotrope de la portée de transmission de capteurs etc., tout en évitant les inconvénients respectifs (l'énorme *overhead*).
- Prouver l'efficacité des algorithmes développés dans des conditions d'implémentation réelles.
- Proposer une stratégie de placement optimal de nœuds d'ancre capables de garantir une haute précision de localisation peu importe la technique de localisation utilisée.

Structure de la Thèse et Contributions

Le reste de cette thèse est organisé comme suit. Chapitre 1 introduit les réseaux de capteurs sans fils et le concept de la localisation. Les défis à surmontés pour garantir un algorithme de localisation robuste et précis dans des conditions réelles sont aussi détailles et discutés dans ce chapitre.

Chapitre 2 propose un algorithme de localisation distribué plus approprié pour les réseaux de capteurs heterogene (HWSNs). La distance entre le capteur régulier et les anchors est localement calcule en exploitent uniquement les informations disponibles au niveau de chaque capteur, réduisant ainsi l'*overhead* nécessaire a la localisation. En plus, nous développons un mécanisme de correction capable d'améliorer encore plus la précision de notre algorithme sans pour autant nécessiter des couts supplémentaire. Il a été prouvé que notre algorithme offre plus de précision que la plupart des algorithmes dans la littérature : DV-hop, LAEP et EPHP dont la conception ne prend pas en compte l'hétérogénéité des WSNs.

Étant donné que des obstacles peuvent également existes dans les environnements pratiques, il est très probable que le chemin le plus court entre un anchor et un capteur soit courbé ce qui entraîne une surestimation de la distance entre ces deux nœuds. Ceci rend évidemment la localisation moins précise. En estimant seulement les distances entre un nœud régulier et un sous-ensemble d'anchors fiables, on a réussi à résoudre ce problème dans le chapitre 3. En plus, un mécanisme d'économie d'énergie visant à améliorer la durée de vie WSN est proposée. Il a

été démontré que notre algorithme pourrait facilement surpasser la plupart des algorithmes de la littérature.

Chapitre 4 améliore encore plus la précision de la localisation en utilisant non seulement l'information du nombre minimal de sauts entre les nœuds mais, aussi, d'autre informations localement disponibles au niveau de ces derniers. Dans ce chapitre, L'expression analytique de la moyenne de l'erreur de l'estimation de positon a été calculée pour la première fois en *closed-form*. Il a été démontré que, en utilisant notre algorithme, les erreurs d'estimation de la position et de leurs écart-type tendent vers zéro dans les réseaux très denses.

Chapitre 5 propose un nouvel algorithme de localisation robuste contre l'atténuation anisotrope du signal. Une nouvelle approche capable de calculer efficacement les distances estimées en *closed-form* a été développée dans ce chapitre. En exploitant les réseaux de neurones artificiels (ANNs), on a réussi à développer un mécanisme de correction des distances estimées à faible coût. La précession et la robustesse de notre algorithme a été prouve.

Étant donné que la précision de localisation est étroitement liée aux positions des anchors, chapitre 6 a élaboré une stratégie novatrice de placement optimal de ces derniers. En recourant à l'optimisation par essaim de particules bien connu ("Particle swarm optimization PSO"), il a été prouvé que la nouvelle stratégie de placement des anchors offre des gains de précision considérables.

Chapitre 1

La localisation dans les réseaux de capteurs sans fil : revue de la littérature et illustration

1.1 Concept des réseaux de capteurs sans fils

Durant les dernières années, les réseaux de capteurs sans fil ont été introduits dans de nombreuses applications, ces réseaux sont constitués des nœuds de capteurs sans fil dispersés aléatoirement dans le terrain d'intérêt. Un capteur sans fil est un petit dispositif électronique capable de surveiller, mesurer et de collecter périodiquement des données relatives aux conditions physiques ou environnementales telles que la température, la présence de substances toxiques, de pression, mouvement, son, et d'autres phénomènes [1]-[3].

Un réseau de capteurs (WSN) est donc défini comme un réseau de dispositifs de capteurs sans fil qui se communiquent entre eux et avec une station de base (BS) en utilisant des liens radio sans fil, et qui coopèrent les uns avec les autres afin de partager l'information par un traitement coopératif. Par conséquent, un capteur sans fil n'est pas seulement responsable de la détection et de la collecte des données, mais aussi une unité de traitement, de communication, de stockage, de corrélation et la fusion de ses propres données et des données provenant d'autres nœuds de capteurs [3].

1.2 Applications des WSNs

De nos jours, la réduction de plus en plus importante de la taille des capteurs, leur faible coût, ainsi que leur fonctions configurables de traitement du signal (filtre, gains, etc.), permettent aux réseaux de capteurs d'envahir de très nombreux applications dans plusieurs domaines telles que le militaire, la santé, l'environnemental, le réseau électrique intelligent, l'automatisation de la maison, etc..

Plusieurs projets ont été lancés pour aider les unités militaires dans le champ de bataille et protéger les villes contre des attaques, tels que le projet DSN (Distributed Sensor Network) au DARPA (Defense Advanced Research Projects Agency) qui était l'un des premiers projets dans les années quatre-vingt ayant utilisé les réseaux de capteurs pour rassembler des données distribuées. Un réseau de capteurs peut être déployé dans un endroit stratégique ou hostile afin de surveiller les mouvements des forces ennemies, ou analyser le terrain avant d'y envoyer des troupes (détection des armes chimiques, biologiques ou radiations).

De nombreuses applications ont été proposées dans le domaine de la santé pour les réseaux de capteurs sans fil, y compris le suivi des patients atteints de la maladie de Parkinson, l'épilepsie, les patients cardiaques, les patients de la réhabilitation des AVC ou une crise cardiaque, et les personnes âgées. Contrairement aux autres types d'applications abordés jusqu'à présent, les applications dans le domaine de la santé ne fonctionnent pas comme des systèmes autonomes. Dans ce domaine, les réseaux de capteurs peuvent être utilisés pour assurer une surveillance permanente des organes vitaux de l'être humain.

Un autre domaine d'application pour les réseaux de capteurs sans fil c'est au niveau de l'environnement, où les réseaux de capteurs sont beaucoup utilisés dans les forêts (peut aider à détecter un éventuel début de feu), dans les milieux urbains (détecter la pollution et analyser la qualité de l'air), dans les sites industriels (empêche les risques industriels comme la fuite des gaz toxiques). De plus, les réseaux de capteurs sont utilisés pour surveiller les volcans actifs et même pour la surveillance des pipelines (monitoring of gas, water,and oil pipelines). Les réseaux de capteurs sans fil sans également appliqués dans le domaine de l'agriculture, par exemple pour suivre la progression d'une tige d'une plante.

1.3 La localisation dans les WSNs

Dans de nombreuses applications mentionnées ci-dessus, les informations de position de chaque nœud de capteur dans le réseau est essentiel pour le service. En effet, normalement les utilisateurs ont besoin de savoir non seulement ce qui se passe, mais aussi où les événements intéressants se produisent. Par exemple, durant la surveillance du champ de bataille, la connaissance de l'endroit exacte d'où l'ennemi vient est beaucoup plus important que seulement savoir l'apparence de l'ennemi dans la zone de surveillance. Plus simplement, il faut répondre à la question fondamentale : "mais où suis-je ?". D'autre part, les informations de position des nœuds de capteurs sont supposées être disponibles dans de nombreuses opérations de gestion du réseau, telles que les algorithmes de routage, le contrôle de topologie du réseau qui utilise

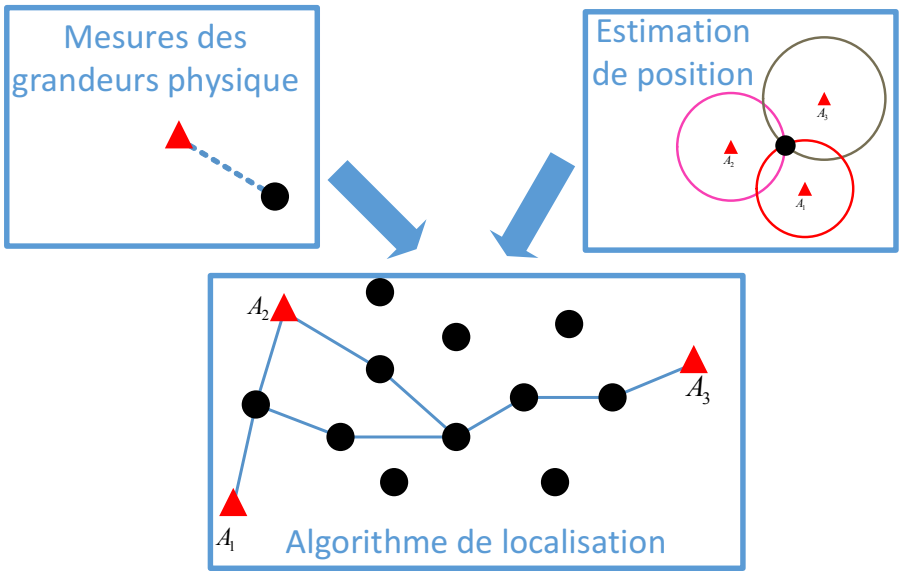

FIGURE 1.1 – Les deux principaux composants d'un système de localisation.

les informations de positionnent des nœuds comme une connaissance a priori pour ajuster la connectivité du réseau pour les économies d'énergie,etc..

L'origine de nombreuses techniques de localisation c'est la connaissance du monde physique. Fondamentalement, comme illustré par la Fig. 1.1, tout système de localisation peut être divisé en deux composantes distinctes [6]-[30] :

- Mesures des grandeurs physique
- Derivation de position

1.3.1 Mesures des grandeurs physique

Dans cette phase les nœuds communiquent entre eux et collectent diverses caractéristiques à propos du signal radio entre les deux nœuds, à partir desquelles les distances et/ou les angles entre les nœuds peuvent être estimées, ainsi qu'une connaissance globale sur la connectivité du réseau peut être fournis.

Selon la caractéristique du signal à récupérer, nous présentons dans ce qui suit les techniques de mesures des grandeurs physique les plus populaires dans la littérature [6]-[30].

1.3.1.1 Temps d'arrivée (TOA)

Cette méthode s'enregistre le temps d'arrivée (TOA), ce concept est indiqué dans la Fig. 1.2. Le temps de propagation peut être directement traduit en distance, sur la base de la vitesse de propagation de signal connue [6]. Cette méthode peut être appliquée à de nombreux signaux

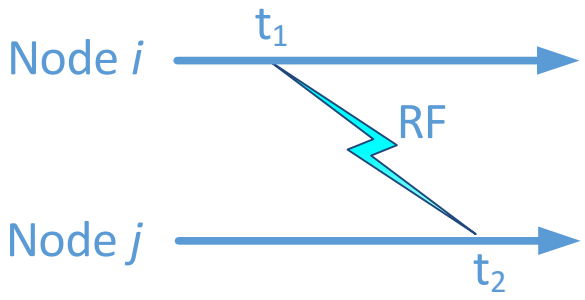

FIGURE 1.2 – TOA

différents, tels que RF, acoustique, infrarouge. La distance entre deux nœuds i et j peut être déterminée comme suit :

$$d_{i-j} = (t_2 - t_1)\, V \tag{1.1}$$

où t_1 et t_2 sont les instants de l'envoi et de réception du signal (mesurée à l'émetteur et au récepteur, respectivement) et V est la vitesse du signal.

1.3.1.2 Différence de temps d'arrivée (TDOA)

Les méthodes TDOA sont remarquablement précises sous les conditions de visibilité directe LOS. Mais cette condition (LOS) est difficile à respecter dans certains environnements comme

le cas de l'environnement minier. En outre, la vitesse du signal dans l'air varie avec la température de l'air et l'humidité, ceci est causé par une inexactitude dans l'estimation de la distance. L'approche TDOA utilise deux signaux qui voyagent à des vitesses différentes (Fig. 1.3). Le ré-

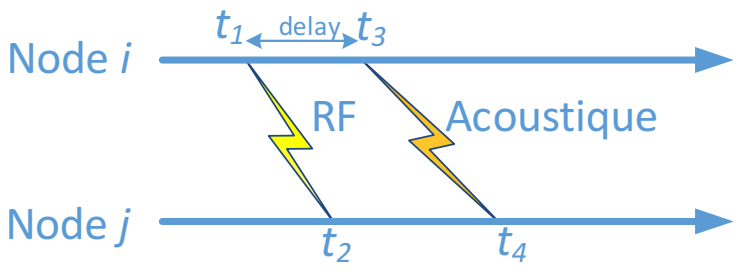

FIGURE 1.3 – TDOA

cepteur est alors en mesure de déterminer sa position similaire à l'approche TOA. Par exemple, le premier signal pourrait être un signal radio (émis à l'instant t_1 et reçu à t_2), suivi par un signal acoustique (immédiatement ou après un intervalle de temps fixe $t_{\text{delay}} = t_3 - t_1$). Par conséquent, le récepteur peut déterminer la distance par :

$$d_{i-j} = (v_1 - v_2)\,(t_4 - t_2 - t_{\text{delay}}) \tag{1.2}$$

L'approche TDOA n'exige pas les horloges de l'émetteur et du récepteur pour être synchronisée et peut obtenir des mesures très précises. L'inconvénient de l'approche TDOA est le besoin de matériel supplémentaire, par exemple, un microphone et haut-parleur pour l'exemple ci-dessus.

1.3.1.3 Indicateur de puissance de signal reçu (RSSI)

L'indicateur de puissance de signal reçu (RSSI) mesure la puissance du signal au niveau du récepteur basé sur une puissance d'émission connue. La perte de propagation efficace peut être calculée. En utilisant des modèles théoriques et empiriques, nous pouvons traduire cette perte en une estimation de la distance [5]. Cette méthode a été utilisée principalement pour les signaux RF. RSSI est une solution relativement pas chère sans aucun périphérique supplémentaire, parce que tous les nœuds de capteurs sont susceptibles d'avoir des signaux radios. Cependant, la performance n'est pas aussi bonne que d'autres techniques de position parce que la propagation se fait par trajets multiples. Il y a trois paramètres principaux qui jouent un rôle dans la détermination de la puissance du signal reçu : les pertes dues à la distance parcourue (path loss), les

effets de masque (shadowing) provoqués par des obstacles, et les évanouissements (fadings) dus aux effets induits du multi-trajet. Le modèle de signal le plus largement utilisé est le modèle log-Normal avec effet de masque (log-normal shadowing) [5] :

$$P(d) = P_T - P(d_0) - 10n(\frac{d}{d_0}) + X_\sigma \tag{1.3}$$

où :

- $P(d)$: puissance reçue à la distance d ;
- P_T : puissance de transmission ;
- $P(d_0)$: est la perte de trajet sur une distance de référence d_0 ;
- n : coefficient d'atténuation (entre 3 et 5) ;
- d : distance qui sépare l'émetteur du récepteur ;
- d_0 : distance de référence ;
- X_σ : une variable aléatoire qui suit une loi normale de moyenne nulle et d'écart-type σ (déviation standard en dB).

En pratique, l'atténuation réelle dépend des effets de propagation par trajets multiples, des réflexions, du bruit, etc.

1.3.1.4 Angle d'arrivée (AOA)

Une autre technique utilisée dans la localisation est de déterminer la direction de propagation du signal, typiquement en utilisant un réseau d'antennes. L'angle d'arrivée (AOA) est alors l'angle entre la direction de propagation et la direction d'une référence connue sous le nom d'orientation [8]. AOA estime l'angle sous lequel les signaux sont reçus et utilise les relations géométriques simples pour calculer les positions des nœuds. En règle générale, les techniques de l'AOA fournissent des résultats de localisation plus précis que les techniques à base de RSSI, cependant, par rapport à ceux à base de TDOA , aucune amélioration significative n'est pas obtenue. Compte tenu du fait que le coût du matériel d'AOA est très élevé, seulement quelques algorithmes de localisation nécessite absolument l'information d'AoA dans la pratique.

1.3.1.5 Nombre de sauts (hop-count)

Le nombre des sauts ("hop-count") est l'un des paramètres les plus exploités par les algorithmes de localisation *range-free* [4]-[13]. Il s'agit du nombre de liens radios empruntés par

un message de la source à la destination à travers des nœuds intermédiaires. Comme première étape, le k- ème ancre diffuse à travers le réseau un paquet de donnée spécial qui se compose d'un en-tête suivi d'une charge utile de données (data). L'en-tête contient la position d'ancre(x_k, y_k), tandis que la charge utile de données contient le nombre de sauts n initialisée à un.

Chaque nœud reçoit ce paquet, il stocke la position du k-ème ancre ainsi que le nombre de sauts reçu $n_k = n$ dans sa base de données, incrémente ce dernier (i.e, $n = n + 1$), et il diffuse ensuite le paquet résultant. Une fois que ce paquet est reçu par un autre nœud, ses informations de base de données sont vérifiées. Si les informations du k-ème ancre est déjà disponible et la valeur de nombre de sauts reçu n est plus petite que celle précédemment stockée n_k, le nœud met à jour ce dernier, incrémente n par 1, puis rediffuse le paquet résultant.Si n_k est plus petit que n, le noeud rejette tout simplement le paquet reçu. Toutefois, lorsque le nœud est inconscient à la position du k-ème ancre, il ajoute cette information à sa base de données et transmet le paquet reçu après l'incrémentation de n par 1.

Ce mécanisme continuera jusqu'à ce que tous les nœuds prennent conscience de les positions des tous les ancres et leurs nombres minimales de sauts correspondantes. Cette information est ensuite combinée à la taille moyenne d'un saut pour estimer la distance séparant les nœuds réguliers des ancres.

1.3.2 Les techniques de derivation de position

Le but de cette phase est de trouver les positions des nœuds en exploitant une ou plusieurs mesures de grandeurs phtisiques décrites ci-dessus. Selon l'information utilisée, plusieurs méthodes peuvent être utilisées pour calculer la position d'un nœud. Ces méthodes comprennent triangulation, trilatération, multilatération, approches probabilistes, etc. Le choix de la méthode à utiliser a également un impact sur la précision de localisation. Un tel choix dépend des limitations du processeur et l'information disponible au niveau du noeud. Lorsqu'un nœud a suffisamment d'informations sur les distances et/ou des angles lui-même et les nœuds des ancres, il peut dériver sa propre position en utilisant l'une des méthodes étudiées dans cette section.

1.3.2.1 Triangulation

La triangulation utilise les propriétés géométriques de triangles pour estimer la position de capteur. Cette méthode est utilisée lorsque la direction du nœud est estimée au lieu de la distance,

comme dans l'AOA. Les positions de nœuds sont calculées dans ce cas en utilisant les lois de la trigonométrie sinus et cosinus. Fig. 1.4 illustre le concept de la triangulation en utilisant trois nœuds d'ancre avec des emplacements connus (x_i,y_i), et des angles mesurés α_i (exprimée par rapport à une ligne de référence fixe, par exemple, la ligne verticale dans la fig. 1.4). Supposons

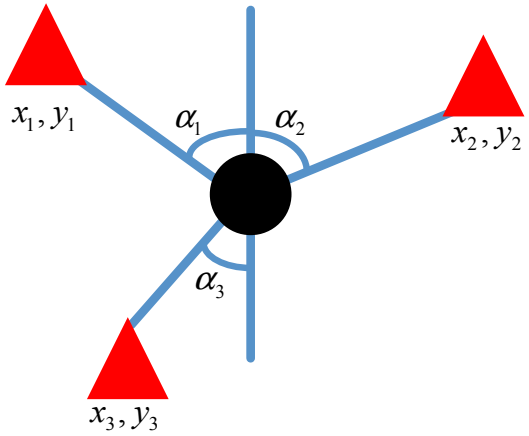

FIGURE 1.4 – Triangulation

que la position du récepteur inconnu est $x_r = [x_r, y_r]^T$, les mesures de l'angle d'arrivés à partir de N noeuds d'ancre sont exprimés en $\beta = [\beta_1, \ldots, \beta_N]^T$, et les positionnements des ancrages sont connus par $x_i = [x_i, y_i]^T$. Mais à cause du bruit, les angles d'arrivés mesurées ne reflètent pas parfaitement les angles réels qui sont exprimés par $\theta(x) = [\theta_1(x), \ldots, \theta_N(x)]^T$. La relation entre les valeurs mesurées et réelles est donnée par :

$$\beta = \theta(x_r) + \delta\theta \tag{1.4}$$

où $\delta\theta = [\delta\theta_1, \ldots, \delta\theta_N]^T$, est le bruit gaussien avec une moyenne nulle. Diverses méthodes statistiques ont été appliquées à l'estimation de la position d'un capteur. L'estimation par le maximum de vraisemblance ML (Maximum Likelihood) estime la position d'un nœud en minimisant les différences entre les distances mesurées et les distances estimées. Selon l'estimateur ML, la position du récepteur est donnée par :

$$\begin{aligned} \hat{x}_r &= \text{argmin} \frac{1}{2} \left[\theta(\hat{x}_r) - \beta\right]^T S^{-1} \left[\theta(\hat{x}_r) - \beta\right] \\ &= \text{argmin} \frac{1}{2} \sum_{i=1}^{N} \frac{(\theta_i(\hat{x}_r) - \beta_i)^2}{\sigma_i^2} \end{aligned} \tag{1.5}$$

où $S = \text{diag}\,(\sigma_1^2, \ldots, \sigma_N^2)$.

1.3.2.2 Trilatération hyperbolique

La méthode la plus simple et intuitive est appelée trilatération hyperbolique. Elle consiste à localiser un nœud en calculant l'intersection de trois cercles. La trilatération désigne le procédé de calcul de la position d'un nœud sur la base de distances mesurées entre lui-même et un certain nombre de points d'ancres. Étant donné l'emplacement d'une ancre et la distance d'un capteur à l'ancrage, il est connu que le capteur doit être positionné quelque part le long de la circonférence d'un cercle centré sur la position de l'ancre, avec un rayon égal à la distance entre le capteur et l'ancre. Dans un espace bidimensionnel, les mesures de distance d'au moins de trois points d'ancrage non colinéaires sont nécessaires pour obtenir un positionnement unique (c'est-à-dire l'intersection de trois cercles).

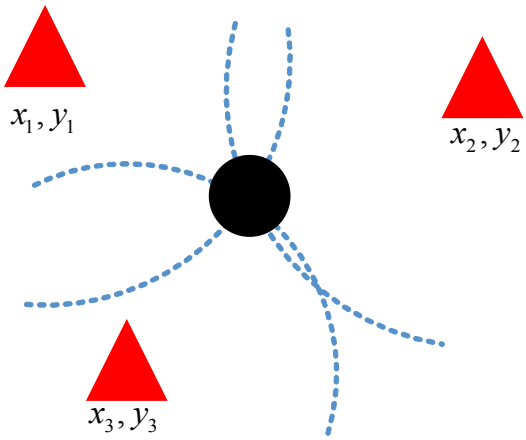

FIGURE 1.5 – Trilatération

Fig. 1.5 illustre un exemple dans le cas bidimensionnel. Pour obtenir les mesures de distance dans le cas de trois dimensions, quatre ancres non coplanaires au moins sont nécessaires. Supposons que les emplacements des N_a nœuds d'ancre sont donnés par (x_i, y_i), $i = 1, \ldots, N_a$ et que les distances entre un noeud régulier (x, y) et ces nœuds d'ancre sont également connus par $d_i, i = 1, \ldots, N_a$. En utilisant cette information on obtient le système d'équations non linéaires suivant :

$$\begin{cases} (x_1 - \hat{x})^2 + (y_1 - \hat{y})^2 = & \hat{d}_1^2 \\ (x_2 - \hat{x})^2 + (y_2 - \hat{y})^2 = & \hat{d}_2^2 \\ \vdots & \vdots \\ (x_{N_a} - \hat{x})^2 + (y_{N_a} - \hat{y})^2 = & \hat{d}_{N_a}^2 \end{cases}, \tag{1.6}$$

où $(\hat{x}, \hat{y})$ sont les coordonnées estimées du noeud régulier. Après quelques réarrangements qui

linéarisent le système ci-dessus, nous obtenons :

$$\boldsymbol{\Upsilon}\hat{\boldsymbol{\alpha}} = -\frac{1}{2}\boldsymbol{\kappa}, \tag{1.7}$$

où $\hat{\boldsymbol{\alpha}} = [\hat{x}, \hat{y}]^T$,

$$\boldsymbol{\Upsilon} = \begin{bmatrix} x_1 - x_{N_a} & y_1 - y_{N_a} \\ x_2 - x_{N_a} & y_2 - y_{N_a} \\ \vdots & \vdots \\ x_{(N_a-1)} - x_{N_a} & y_{(N_a-1)} - y_{N_a} \end{bmatrix}, \tag{1.8}$$

and

$$\boldsymbol{\kappa_i} = \begin{bmatrix} \hat{d}_1^2 - \hat{d}_{N_a}^2 + x_{N_a}^2 - x_1^2 + y_{N_a}^2 - y_1^2 \\ \hat{d}_2^2 - \hat{d}_{N_a}^2 + x_{N_a}^2 - x_2^2 + y_{N_a}^2 - y_2^2 \\ \vdots \\ \hat{d}_{(N_a-1)}^2 - \hat{d}_{N_a}^2 + x_{N_a}^2 - x_{(N_a-1)}^2 + y_{N_a}^2 - y_{(N_a-1)}^2 \end{bmatrix}. \tag{1.9}$$

Puisque $\boldsymbol{\Upsilon}$ est une matrice non inversible, $\hat{\boldsymbol{\alpha}}$ peut être estimée par le pseudo-inverse de $\boldsymbol{\Upsilon}$ comme suit

$$\hat{\boldsymbol{\alpha}} = -\frac{1}{2}\left(\boldsymbol{\Upsilon}\boldsymbol{\Upsilon}^T\right)^{-1}\boldsymbol{\Upsilon}^T\boldsymbol{\kappa}. \tag{1.10}$$

1.4 Les algorithmes de localization range-free

Les différentes techniques utilisées dans les approches "*range-based*" sont basées sur les estimations de distance et/ou de l'angle. En revanche, les algorithmes "*range-free*" sont plus économique en matériel car ils se contentent de l'information de connectivité liée à la portée radio au lieu des mesures de distance ou d'angle. Les sections suivantes décrivent ces différentes algorithmes de localisation.

1.4.1 L'algorithme MDS

L'algorithme MDS (Multidimensional Scaling) utilise la technique de localisation centralisée, où un dispositif central puissant (par exemple, la station de base) recueille de l'information à partir du réseau, détermine les positions des nœuds, et propage cette information dans le réseau [13]. Bien qu'il existe de nombreuses variantes de MDS, la version la plus simple (dite classique MDS) a une solution analytique permettant des implémentations efficaces. Définissons

la matrice des carrés des distances entre les nœuds est écrite comme suit :

$$D^2 = c1^{'} + 1c^{'} - SS^{'} \tag{1.11}$$

Où 1 est un vecteur de longueur $n \times 1$ où touts les éléments sont égaux à 1, S est la matrice de similarité pour les n points, où chaque ligne représente les coordonnées du point i le long des coordonnées m ($m < n$ qui sont des nœuds ancres et qui connaissent leurs emplacements), $SS^{'}$ est appelée matrice du produit scalaire, et c est un vecteur contenant les éléments diagonaux de la matrice du produit scalaire. En multipliant les deux côtés de l'équation (1.11) par la matrice de centrage $T = I - \frac{[11]^{'}}{n}$, où I est la matrice identité on obtient :

$$TD^2T = T(c1^{'} + 1c^{'} - SS^{'})T = Tc1^{'}T + T1c^{'}T - T(2B)T \tag{1.12}$$

Où $B = SS^{'}$, l'utilisation d'une matrice de centrage des uns rend à un vecteur de zéros, et par conséquent :

$$TD^2T = -T(2B)T \tag{1.13}$$

En outre, multipliant les deux côtés avec $-\frac{1}{2}$ nous donne :

$$B = -1/2TD^2T \tag{1.14}$$

B est une matrice symétrique et donc elle peut être décomposée en :

$$B = Q\Lambda Q^{'} = (Q^{'}\Lambda^{\frac{1}{2}})(Q^{'}\Lambda^{\frac{1}{2}})^{'} = SS^{'} \tag{1.15}$$

Une fois que B a été obtenu, les coordonnées S peuvent être calculées par décomposition d'une matrice en éléments propres (“Eigendecomposition”) :

$$S = Q\Lambda^{\frac{1}{2}} \tag{1.16}$$

Sur la base de ce concept, une méthode de localisation pour les réseaux de capteurs appelée MDS-MAP [13] peut être appliquée.

1.4.2 Système de positionnement Ad-hoc (APS)

APS est un exemple d'un algorithme de localisation basé sur la connectivité distribuée qui estime la position des nœuds avec le soutien d'au moins trois nœuds d'ancre, où les erreurs de localisation peuvent être réduites en augmentant le nombre de nœuds d'ancre. Chaque nœud d'ancre propage son emplacement à tous les autres nœuds du réseau en utilisant le concept de l'échange de vecteur de distance (DV), où les nœuds dans un réseau échangent périodiquement leurs tables de routage avec leurs voisins à un seul saut. L'algorithme le plus fondamental de l'APS, qui est appelé DV-hop [4], chaque nœud maintient une table X_i, Y_i, n_i, où X_i, Y_i est l'emplacement du nœud i, n_i est le nombre de saut minimal entre ce nœud et le nœud i. lorsqu'un nœud d'ancre obtient les distances vers des d'autres ancres, il détermine alors une taille moyenne d'un saut C_i(appelé le facteur de correction) qui peut être calculée comme suit :

$$c_i = \frac{\sum \sqrt{(X_i - X_j)^2 + (Y_i - Y_j)^2}}{\sum n_i} \tag{1.17}$$

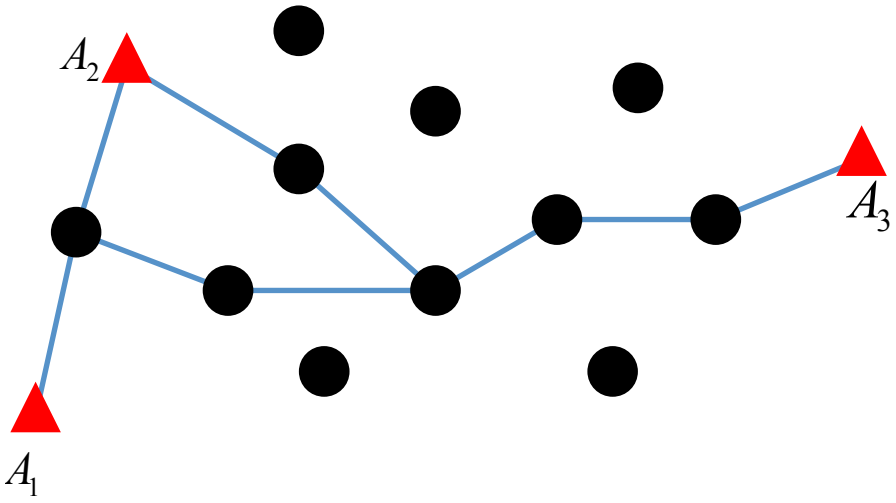

FIGURE 1.6 – Algorithme DV-hop

Pour mieux comprendre cette technique, nous prenons cet exemple qui est illustré dans la Fig. 1.6. Dans cet exemple, nous avons trois nœuds d'ancre A_1, A_2, A_3. Pour l'ancre A_1, les distances euclidiennes entre l'ancre A_1 des ancres A_2 et A_3 sont $d_{A_1-A_2} = 50$m et $d_{A_1-A_3} = 110$m, respectivement. En plus, les nombres des sauts séparant l'ancre A_1 des ancres A_2 et A_3 sont deux et six sauts successivement. Le facteur de correction pour A_1 est calculé alors par $\frac{50+110}{2+6} = 20$m, qui représente la distance estimée moyenne d'un saut. De la même façon, nous calculons le facteur

de correction pour A_2 comme $\frac{50+80}{2+5} = 18.57$m. Une fois que toutes les ancres dérivent leur propre taille moyenne d'un saut ils les diffusent à travers le réseau aux autres nœuds réguliers. À la réception de ces messages au niveau de nœuds réguliers ils sauvegardent seulement la valeur de la taille moyenne d'un saut reçu de l'ancre le plus proche.

1.4.3 L'algorithme APIT

La méthode d'APIT (Approximate Point In Triangulation) est une approche similaire à l'APS. Elle repose sur la présence de plusieurs nœuds d'ancrage qui connaissent leurs propres positions. Toute combinaison de trois points d'ancrage constitue une région triangulaire et la présence d'un nœud à l'intérieur ou à l'extérieur d'une telle région permet à un nœud d'affiner sa positon possible [10]. La puissance du signal entre les nœuds et l'ancre peut être utilisée pour estimer quel nœud est le plus proche de l'ancre, puis si aucun voisin du nœud M n'est ni proche ni loin des trois ancres A_1, A_2, A_3 simultanément, M suppose qu'il est à l'intérieur du triangle $A_1A_2A_3$. Sinon M suppose qu'il est à l'extérieur du triangle. Ce concept est illustré dans la Fig. 1.7. Dans la partie gauche de la Fig. 1.7, le nœud M a quatre voisins, aucun de ces nœuds ne

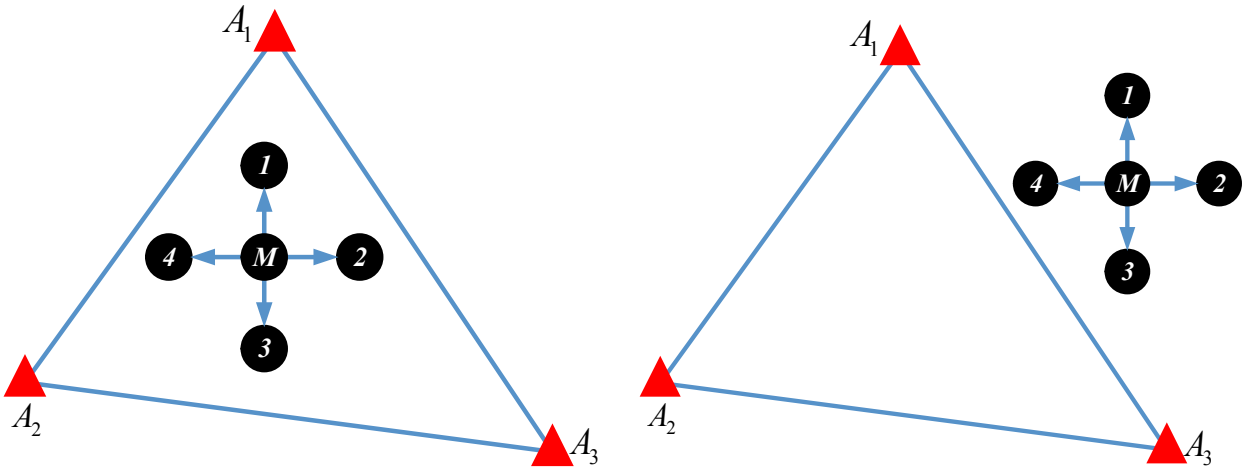

(a) Cas à l'intérieur. (b) Cas à l'extérieur

FIGURE 1.7 – Algorithme APIT

sont proches ou loin des trois ancres. Donc M conclut correctement qu'il est à l'intérieur du triangle $A_1A_2A_3$. La situation est différente dans la partie droite de la figure, par exemple le voisin 4 est proche de tous les trois nœuds d'ancre que le nœud M, tandis que le nœud 2 est

loin des nœuds d'ancre que le nœud M, par suite le nœud M conclut qu'il est à l'extérieure du triangle $A_1A_2A_3$.

Dans ce schéma, un nœud peut prendre de mauvaises décisions, par exemple dans la partie gauche de la figure, si les mesures du distance du nœud 4 indiquent qu'il est plus loin du nœud A_2 que le nœud M (à cause d'un obstacle entre l'ancre A_2 et le nœud 4), le nœud M conclurait qu'il doit être en dehors du triangle $A_1A_2A_3$. L'avantage d'APIT réside dans sa simplicité et sa facilité de mise en œuvre. Mais l'APIT exige un ratio élevé de nœuds d'ancre. Pour un faible nombre d'ancres, cet algorithme ne saura pas donner des résultats précis.

1.5 Défis de localisation dans le WSN

A la lumière des informations présentes dans les sections précédentes, les algorithmes de localisation doivent inévitablement faire face aux défis suivants

1.5.1 Hétérogénéité des noeuds

Les nœuds de capteurs sont conçus en utilisant différentes technologies pour réaliser différentes tâches, leur détection ainsi que leurs capacités de transmission sont très souvent différentes. En outre, si une technologie de récolte d'énergie ("Energy Harvesting (EH)") est localement intégrée à chaque nœud, ce qui est le cas dans les WSNs développés récemment [30]-[33], la puissance récoltée disponible au niveau des nœuds serait alors aléatoire. Ce phénomène résulte en fait dans la randomisation de capacités de transmission des nœuds (Fig. 1.8), puisque les lettres sont étroitement liées aux ressources énergétiques disponibles des nœuds. Au cours du processus de localisation, il est donc très probable que les capacités de transmission des nœuds soient différentes. Puisque les approches traditionnelles de localisation [4]-[30] assument la même capacité de transmission à travers le réseau, leur précision de localisation se détériore gravement dans les WSNs hétérogènes (HWSNs). Au meilleur de notre connaissance, il n'y a pas d'algorithme de localisation qui tient compte à ce jour pour la nature hétérogène de WSN.

Pour combler cet écart, nous proposons dans les prochains chapitres un nouvel algorithme de localisation spécifiquement conçu pour le HWSNs.

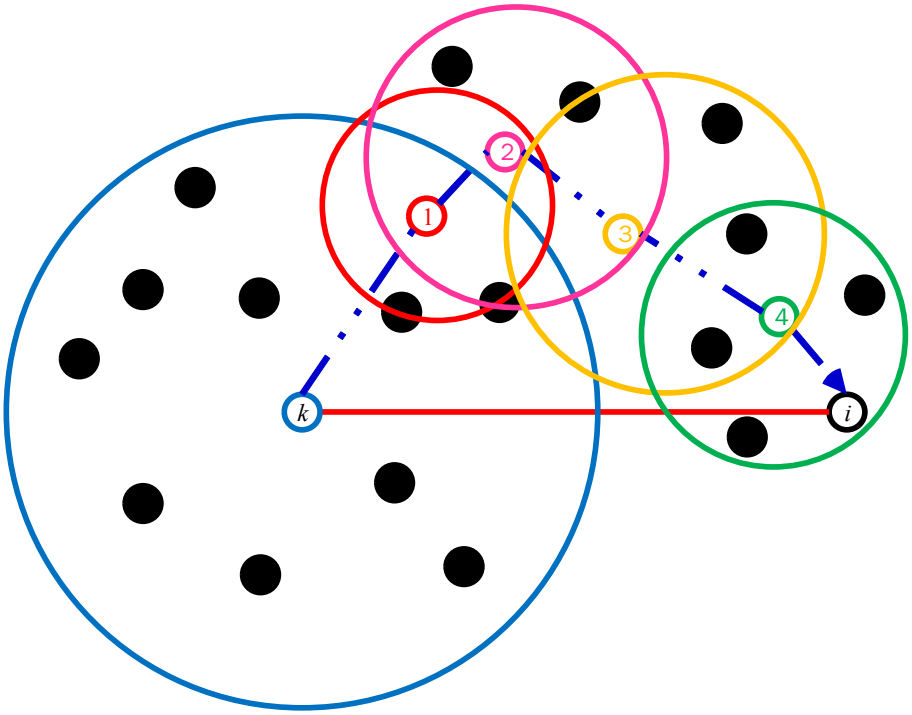

FIGURE 1.8 – Réseau hétérogène de capteurs sans fil.

1.5.2 Communication à visibilité indirecte (NLOS)

Comme il a été discuté dans la section 1.3, afin de localiser les capteurs dans les algorithmes *range-free*, chaque nœud doit être en mesure de compter le nombre minimal de sauts entre lui-même et au moins trois ancres. Malheureusement, dans les milieux anisotropes, plusieurs obstacles et/ou des trous peuvent exister, ce qui rend la majorité des algorithmes *range-free* incapable de fournir une précision de localisation suffisante en raison de grandes erreurs qui se produisent lors de la cartographie du nombre de sauts en unités de distance. En effet, dans de tels environnements, il est très probable que le chemin le plus court entre une ancre et un nœud régulier est recourbé, ce qui conduit à une surestimation de la distance entre ces deux nœuds et par suite à une localisation imprécise.

1.5.3 Anisotrope de la portée de transmission

Jusqu'au présent, lors de la conception des algorithmes de localisation, on a ignoré le phénomène de l'atténuation anisotrope du signal (i.e., la portée de transmission est différente d'une direction à l'autre) présent, en pratique, dans tous les milieux de propagation. Par conséquent,

si ce dernier n'est pas correctement prises en compte, les erreurs de l'estimation de la distance augmentent considérablement et entravent gravement la précision de la localisation.

1.5.4 Répartition des ancres

Finalement, il existe encore plusieurs informations pouvant être intégrées au processus de Localisation qui ne sont pas directement utilisées dans le calcul de la position mais servent à assurer l'implémentation de l'algorithme. L'une des plus élémentaires est la répartition optimale des ancres dans le réseau. Il a été prouvé que la stratégie de placement des ancres sur le périmètre est optimale dans des environnements isotropes (sans d'obstacles) mais pas dans les milieux anisotropes.

Bibliographie

[1] D.P. Agrawal and Q.-A. Zeng, *Introduction to Wireless and Mobile Systems,* 3^{rd} edition Cengage Learning, USA, 2010.

[2] S. Zaidi and S. Affes "Distributed collaborative beamforming in the presence of angular scattering," *IEEE Trans. Commun.,* vol. 62, pp. 1668-1680, May 2014.

[3] F. Akyildiz, W. Su, Y. Sankarasubramaniam, and E. Cayirci, "A survey on sensor networks," *IEEE Commun. Mag.,* vol. 40, no. 8, pp. 102-114, August 2002.

[4] J.N. Al-Karaki and A.E. Kamal, "Routing techniques in wireless sensor networks : a survey," *IEEE Wireless Commun.* vol. 11, no. 6, pp. 6-8, December 2004.

[5] F. Gustafsson and F. Gunnarsson, "Mobile Positioning Using Wireless Networks : Possibilities and Fundamental Limitations Based on Available Wireless Network Measurements," *IEEE Signal Process. Mag.,* vol. 22, no. 4, pp. 41-53, July 2005.

[6] H. Shen, Z. Ding, S. Dasgupta, and C. Zhao, "Multiple Source Localization in Wireless Sensor Networks Based on Time of Arrival Measurement," *IEEE Trans. Signal Process.,* vol. 62, no. 8, pp. 1938-1949, February 2014.

[7] J. Rezazadeh, M. Moradi, A.S. Ismail and E. Dutkiewicz, "Superior Path Planning Mechanism for Mobile Beacon-Assisted Localization in Wireless Sensor Networks," *IEEE Sensors J.,* vol. 14, no. 9, pp. 3052-3064, May 2014.

[8] D. Niculescu and B. Nath, "Ad Hoc Positioning System (APS) Using AOA," *IEEE INFOCOM'2003,* San Francisco, California, USA, 30 March-3 April, 2003.

[9] V. Lakafosis and M.M. Tentzeris, "From single-to multihop : The status of wireless localization," *IEEE Microw. Mag.,* vol. 10 , no. 7, pp. 34-41, December 2009.

[10] D. Niculescu and B. Nath, "Ad hoc positioning system (APS)," *Proc. IEEE GLOBECOM'2001,* San Antonio, TX, USA, November 25-29, 2001.

[11] Z. Ziguo and T. He,"RSD : A Metric for Achieving Range-Free Localization beyond Connectivity," *IEEE Trans. parallel and distributed Sys.,* vol. 24, no. 11, pp. 1943-1951 , November 2011.

[12] A. Boukerche, H.A.B.F. Oliveira, E.F. Nakamura, A.A.F. Loureiro, "DV-Loc : a scalable localization protocol using Voronoi diagrams for wireless sensor networks," *IEEE Wireless. Commun. Mag.,* vol. 16, no. 2, pp. 50-55, April 2009.

[13] Y. Shang, W. Rumi, Y. Zhang, M. Fromherz, "Localization from connectivity in sensor networks," *IEEE Trans. Parallel Distrib. Syst.,* vol. 15, no. 11, pp. 961-974, November 2004

[14] D. Ma, MJ. Er, B. Wang , "Analysis of Hop-Count-Based Source-to-Destination Distance Estimation in Wireless Sensor Networks With Applications in Localization," *IEEE Trans. Veh. Technol.,* vol. 59, no. 6, pp. 2998-3011, July 2010.

[15] D. Ma, MJ. Er, B. Wang , "A novel approach toward source-to-sink distance estimation in wireless sensor networks," *IEEE Commun. Lett.,* vol. 14, no. 5, pp. 384-386, May 2010.

[16] X. Ta, G. Mao, and B. D. Anderson, "On the probability of k-hop connection in wireless sensor networks," *IEEE Commun. Lett.,* vol. 11, no. 9, pp. 662-664, August 2007.

[17] Y. Wang, X. Wang, D. Wang, and D. P. Agrawal, "Range-Free Localization Using Expected Hop Progress in Wireless Sensor Networks," *IEEE Trans. Parallel Distrib. Syst.,* vol. 25, no. 10, pp. 1540-1552, October 2009.

[18] T. He, C. Huang, B. M. Blum, J. A. Stankovic, and T. Abdelzaher, "Range-free localization schemes for large scale sensor networks," *Proc. ACM MobiCom'03,* San Diego, California, USA, September 14-19, 2003.

[19] S. Vural and E. Ekici, "On Multihop Distances in Wireless Sensor Networks with Random Node Locations," *IEEE Trans. Mobile Comput.,* vol. 9, no. 4, pp. 540-552, April 2010.

[20] M. Haenggi, "On distances in uniformly random networks," *IEEE Trans. Inf. Theory,* vol. 51 , no. 10 , pp. 3584-3586, October 2005.

[21] JC. Kuo, W. Liao, "Hop Count Distribution of Multihop Paths in Wireless Networks With Arbitrary Node Density : Modeling and Its Applications," *IEEE Trans. Veh. Technol.,* vol. 56, no. 4, pp. 2321-2331, July 2007.

[22] M. Li and Y. Liu,, "Rendered path : Range-free localization in anisotropic sensor networks with holes," *IEEE/ACM Trans. Netw.,* vol. 18, no. 1, pp. 320-332, February 2010.

[23] Z. Shigeng, C. Jiannong, L.-J. Chen , C. Daoxu Chen, "Accurate and Energy-Efficient Range-Free Localization for Mobile Sensor Networks," *IEEE Trans. Mobile Comput.,* vol. 9, no. 6, pp. 897-910, June 2010.

[24] B. Xiao, L. Chen, Q. Xiao, M. Li , "Reliable Anchor-Based Sensor Localization in Irregular Areas," *IEEE Trans. Mobile Comput.,* vol. 9, no. 1, pp. 60-72, January 2010.

[25] Q. Xiao, B. Xiao, J. Cao, J. Wang, "Multihop Range-Free Localization in Anisotropic Wireless Sensor Networks : A Pattern-Driven Scheme," *IEEE Trans. Mobile Comput.,* vol. 9, no. 11, pp. 1592-1607, November 2010.

[26] A. Kansal, J. Hsu, S. Zahedi, and M. B. Srivastava, "Power Management in Energy Harvesting Sensor Networks," *ACM Trans. Embedded Computing Systems,* vol. 6, no. 4, pp. 1-38, September 2007.

[27] A. P. Sample, D. J. Yeager, P. S. Powledge, A. V. Mamishev, and J. R. Smith, "Design of an RFID-Based Battery-Free Programmable Sensing Platform," *IEEE Trans. Instrum. Meas.,* vol. 57, no. 11, pp. 2608-2615, November 2008.

[28] Y. Luo, J. Zhang, and K. B. Letaief, "Optimal Scheduling and Power Allocation for Two-Hop Energy Harvesting Communication Systems," *IEEE Trans. Wireless Commun.,* vol. 12, no. 9, pp. 4729-4741, September 2013.

[29] S. Sudevalayam and P. Kulkarni, "Energy Harvesting Sensor Nodes : Survey and Implications," *IEEE Commun. Survey and tutorials,* vol. 13, no. 3, pp. 443-461, Third Quarter 2011.

Chapitre 2

Low-Cost Localization for Multi-Hop Heterogeneous Wireless Sensor Networks

Ahmad El Assaf, Slim Zaidi, Sofiène Affes and Nahi Kandil

IEEE Transactions on Wireless Communications, vol. 15, no. 1, pp. 472-484, January 2016.

Résumé : Ce chapitre propose de développer et d'évaluer un nouvel algorithme novateur de localisation à faible coût visant une utilisation dans le contexte de réseaux hétérogènes de capteurs sans fil (HWSNs) où les portées de transmission de nœuds sont différentes. Le fait d'ignorer cette dernière caractéristique lors de la conception de l'algorithme de localisation, peut nuire fortement à la précision de l'algorithme. En supposant que les portées de transmission sont différentes, nous développons dans ce chapitre, deux approches différentes pour dériver analytiquement la taille moyenne d'un saut ("Expected Hop Progress (EHP)"). En exploitant celle-ci, on a réussi à concevoir un nouvel algorithme de localisation à faible coût qui tient compte de l'hétérogénéité du réseau de capteurs, et qui est aussi capable de localiser avec précision les nœuds de capteurs. En outre, nous développons un mécanisme de correction qui est conforme à la nature hétérogène de WSNs pour améliorer encore la précision de localisation sans encourir de frais supplémentaires. Il est aussi prouvé que l'algorithme proposé, qu'il soit appliqué avec ou sans le mécanisme de correction, surpasse en termes de précision les algorithmes de localisation les plus représentatives dans la littérature.

Abstract

In this paper, we propose a novel low-cost localization algorithm tailored for multi-hop heterogeneous wireless sensor networks (HWSNs) where nodes' transmission capabilities are different. This characteristic, if not taken into account when designing the localization algorithm, may severely hinder its accuracy. Assuming different nodes' transmission capabilities, we develop two different approaches to derive the expected hop progress (EHP). Exploiting the latter, we propose a localization algorithm that is able to accurately locate the sensor nodes owing to a new low-cost implementation. Furthermore, we develop a correction mechanism which complies with the heterogeneous nature of WSNs to further improve localization accuracy without incurring any additional costs. Simulations results show that the proposed algorithm, whether applied with or without correction, outperforms in accuracy the most representative WSN localization algorithms.

2.1 Introduction

Recent advances in wireless communications and low-power circuits technologies have led to proliferation of wireless sensor networks (WSNs). A WSN is a set of small and low-cost sensor nodes often equipped with small batteries. The latter are often deployed in a random fashion to sense or collect from the surrounding environments some physical phenomena such as temperature, light, pressure, etc. [1]-[3]. Since power is a scarce resource in such networks, sensor nodes usually recur to multi-hop transmission in order to send their gathered data to an access point (AP). However, the received data at the latter are often fully or partially meaningless if the location from where they have been measured is unknown [3]- [2], making the nodes' localization an essential task in multi-hop WSNs. Owing to the low-cost requirements of WSNs, unconventional paradigms in localization must yet be investigated. Many interesting solutions exist in the literature [6]-[30]. To properly localize each regular or position-unaware node, most of these algorithms require the distance between the latter and at least three position-aware nodes called hereafter anchors. Since it is very likely in multi-hop WSNs that some regular nodes be unable to directly communicate with all anchors, the distance between each anchor-regular nodes pair is usually estimated using their shortest path. The latter is obtained by summing the

distances between any consecutive intermediate nodes located on the shortest path between the two nodes. Depending on the process used to estimate these distances, localization algorithms may fall into three categories : measurement-based, heuristic, and analytical [6]-[30].

Measurement-based algorithms exploit the measurements of the received signals' characteristics such as the received signal strength (RSS) [6]-[5] or the time of arrival (TOA) [6], etc. Using the RSS measurement, the distance between any sensors' pair could be obtained by converting the power loss due to propagation from a sensor to another based on some propagation laws. Unfortunately, due to the probable presence of noise and interference, the distance's estimate would be far from being accurate, thereby leading to unreliable localization accuracy. Using the TOA measurement, nodes require high-resolution clocks and extremely accurate synchronization between them. While the first requirement may dramatically increase the cost and the size of sensor nodes, the second results in severe depletion of their power due to the additional overhead required by such a process. Furthermore, in the presence of noise and/or multipath, the TOA measurement is severely affected thereby hindering nodes' localization accuracy. As far as heuristic algorithms [4]-[12] are concerned, they also have a major drawback. Indeed, most of these algorithms are based on variations of DV-HOP [4] whose implementation in multi-hop WSNs requires a correction factor derived in a non-localized manner and broadcasted in the network by each anchor. This causes an undesired prohibitive overhead and power consumption, thereby increasing the overall cost of the network.

Popular alternatives, more suitable for multi-hop WSNs, are the analytical algorithms [13]-[30] which evaluate theoretically the distance between any two consecutive intermediate nodes. The latter is in fact locally computable at each node, thereby avoiding unnecessary costs incurred if it is fully or partially computed at other nodes and then broadcasted in the network, such as in heuristic algorithms. In spite of their valuable contributions, the approaches developed so far in [13]-[30] to derive that distance are based on the unrealistic assumption that all nodes have the same transmission capabilities (i.e., the WSN is homogenous). However, due to the fact that these sensor nodes are designed using various technologies to achieve different tasks, their sensing as well as transmission capabilities are very-often different. Furthermore, if an energy harvesting (EH) technology is locally integrated at each node, which is the case in the most recently developed WSNs referred to hereafter as EH-WSNs [30]-[33], the available harvested power at nodes would then be random. This phenomenon actually results in the randomization

of the nodes' transmission capabilities, since the latters are closely related to the nodes' available powers. During the localization process, it is then very likely that nodes' transmission capabilities be different. As the approaches in [13]-[30] assume the same transmission capability throughout the network, their localization accuracy substantially deteriorates in the so-called heterogeneous WSNs (HWSNs) making them unsuitable for such networks. To the best of our knowledge, there is no analytical algorithm that accounts so far for the heterogeneous nature of WSNs.

To bridge this gap, we propose in this paper a novel analytical algorithm tailored for multi-hop HWSNs where nodes have different transmission capabilities. Taking into account this characteristic, two approaches are developed to accurately derive the distances between any consecutive nodes. Using the so-obtained distances, the proposed algorithm is able to accurately locate the nodes owing to a new low-cost implementation. Furthermore, we develop a correction mechanism which complies with the heterogeneous nature of WSNs to further improve localization accuracy without incurring any additional costs. Simulations results show that the proposed algorithm, whether applied with or without correction, outperforms in accuracy the most representative multi-hop WSNs localization algorithms.

The rest of this paper is organized as follows : Section 4.2 describes the system model and discusses the motivation of this work. Section 2.3 derives the distance between consecutive sensors using two approaches. A novel localization algorithm for HWSNs is proposed in section 5.4. Its implementation cost is discussed in Section 2.6. Simulation results are discussed in Section 3.8 and concluding remarks are made in section 5.6.

Notation : Uppercase and lowercase bold letters denote matrices and vectors, respectively. $[\cdot]_{il}$ and $[\cdot]_i$ are the (i,l)-th entry of a matrix and i-th entry of a vector, respectively. $\mathbf{I}$ is the identity matrix. $(\cdot)^T$ denotes the transpose. $D(i,x)$ denotes the disc having the i-th sensor as a center and x as a radius.

2.2 Network model and overview

Fig. 6.1 illustrates the system model of N sensor nodes uniformly deployed in a 2-D square area S. The transmission coverage of each node is assumed to be circular, i.e., the i-th node could directly communicate with any node located in $D(i, Tc_i)$, the disc having this node as a center and its transmission capability Tc_i as a radius. In a multi-hop transmission, note that

the i-th node could also communicate with any node located outside its coverage area $D\left(i, Tc_i\right)$. Due to the heterogonous nature of WSNs, nodes are assumed here to have different transmission capabilities. It is also assumed that only a few nodes commonly known as anchors are aware of

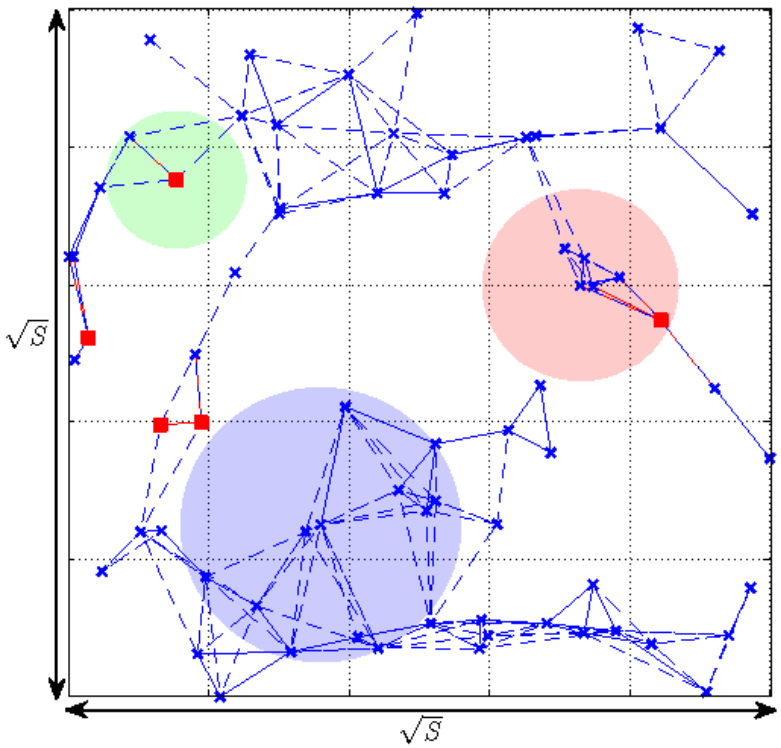

FIGURE 2.1 – Network model.

their positions. The other nodes, called hereafter position-unaware or regular nodes for the sake of simplicity, are oblivious to this information. As shown in Fig. 6.1, the anchors are marked with red squares and the regular nodes are marked with blue crosses. If a node is located within the coverage area of an another node, the two nodes are linked with a dashed line that represents one hop.Three discs were drawn as few illustrative examples of the coverage areas of the corresponding nodes. Let N_a and $N_u = N - N_a$ denote the number of anchors and regular nodes, respectively. Without loss of generality, let $\left(x_i, y_i\right)$, $i = 1, \ldots, N_a$ be the coordinates of the anchors and $\left(x_i, y_i\right)$, $i = N_a + 1, \ldots, N$ those of the regular nodes.

As a first step of any localization algorithm for multi-hop WSNs aiming to estimate the regular nodes' positions, the k-th anchor broadcasts through the network a message containing its position. As it can be seen in fig. 2.2, if the $(i - N_a)$-th regular node (or the i-th node) is located outside the anchor coverage area, it receives this message through multi-hop transmission.

For simplicity, let us assume that only one intermediate node j located over the shortest path

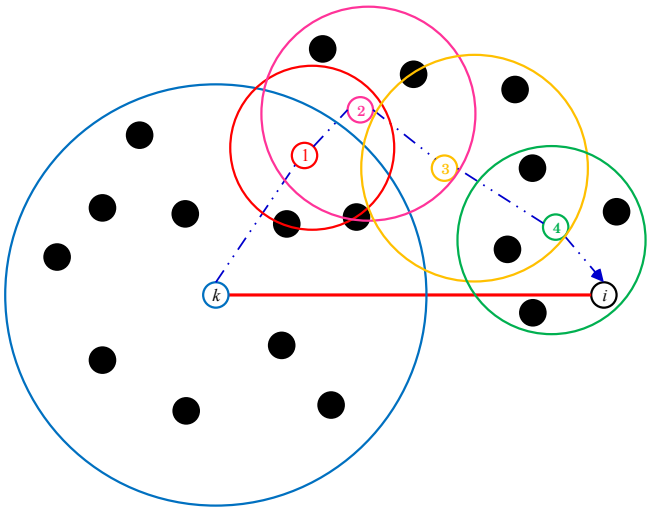

FIGURE 2.2 – Multi-hop transmission.

between the k-th anchor and the i-th node is necessary (i.e., two-hop transmission). Assuming a high node density in the network, the distance d_{k-i} between the two nodes can be accurately approximated as [13]-[30]

$$d_{k-i} \simeq d_{k-j} + d_{j-i}, \tag{2.1}$$

where d_{k-j} (d_{j-i}) is the effective distance between the k-th (i-th) and j-th nodes. Two methods have been so far developed to analytically estimate the distance d_{k-i} exploiting the aforementioned approximation [13]-[30]. In the first method, the j-th node estimates the distance d_{k-j}

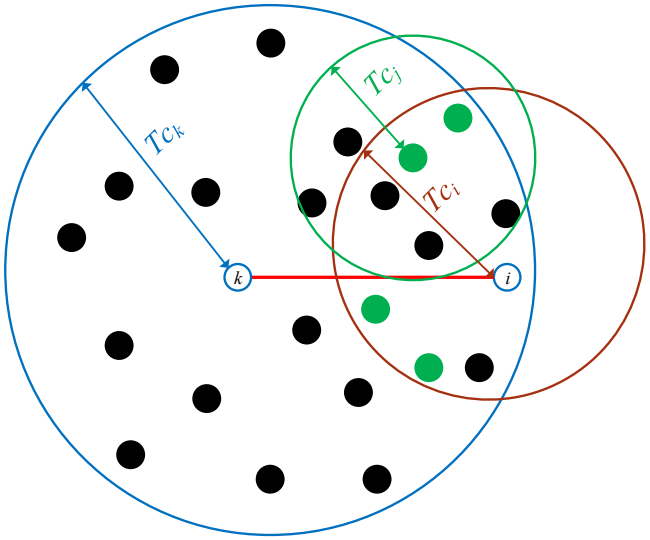

FIGURE 2.3 – Node's neighborhood in HWSN.

using the number of common neighbors with the k-th node. In fact, if n_{kj} common neighbors exist in the intersection area $I = D(k, Tc_k) \cap D(j, Tc_j)$, I could be approximated by $\hat{I} = n_{kj}\lambda^{-1}$ where $\lambda = N/S$ is the average node density in the network. Furthermore, using some geometrical properties, one can show that

$$\begin{aligned} I = f(d_{k-j}) &= Tc_j^2 \cos^{-1}\left(\frac{d_{k-j}^2 + Tc_j^2 - Tc_k^2}{2d_{k-j}Tc_j}\right) + Tc_k^2 \cos^{-1}\left(\frac{d_{k-j}^2 + Tc_k^2 - Tc_j^2}{2d_{k-j}Tc_k}\right) \\ &- \frac{1}{2}\sqrt{4d_{k-j}^2 Tc_k^2 - \left(d_{k-j}^2 - Tc_j^2 + Tc_k^2\right)^2}. \end{aligned} \tag{2.2}$$

d_{k-j} is then obtained as $d_{k-j} = f^{-1}(I) \simeq f^{-1}(n_{k-j}\lambda^{-1})$. Since it is impossible to derive f^{-1} in closed-form, d_{k-j} can be numerically derived using for instance the well-known secant method. The problem here is that the j-th node needs to be aware of n_{kj} to be able to estimate the area I. To this end, the k-th and j-th nodes broadcast a "Hello" message that will be sent back by their respective neighbors. Upon reception of the k-th node neighbors' list, the j-th node compares it with its own neighbors' list and, hence, n_{kj} is obtained. Unfortunately, it is no longer possible to get an exact knowledge of n_{kj} in HWSNs. Indeed, in such networks, it is very likely that the neighbor of a node has a different transmission capability from the latter. Thus, as shown in Fig. 2.3, some "Hello" messages sent back by some respective neighbors of the k-th and j-th node would not reach the latter nodes, due to their weaker capabilities. Consequently, the j-th node obtains $\hat{n}_{kj} \leq n_{kj}$ leading, hence, to inaccurate distance estimation. Note that this discussion also holds for d_{j-i}. This proves that this first analytical method is not suitable for HWSNs.

The second method uses the fact that the minimum mean square error (MMSE) of the distance estimation is obtained if $\hat{d} = E(d)$ and, hence,

$$\hat{d}_{k-i} \simeq \bar{d}_{k-j} + \bar{d}_{j-i}, \tag{2.3}$$

where $\bar{d}_{k-j} = \mathrm{E}\{d_{k-j}\}$ is the expected hop progress (EHP) and $\bar{d}_{j-i} = \mathrm{E}\{d_{j-i}\}$ is the mean last hop (MLH). One of the well-known analytical expressions of EHP is the one developed in [13] as follows :

$$\bar{d}_{k-j} = \sqrt{3}\lambda \int_0^{Tc_k} x^2 e^{-\frac{1}{3}\lambda\pi\left(Tc_k^2 - x^2\right)} dx, \tag{2.4}$$

where λ is the node density, and x is the distance between the k-th and the i-th node. From (2.4), the EHP a priori depends only on the k-th node transmission capability Tc_k and, therefore, its computation does not supposedly require any knowledge of the j-th node transmission capability

Tc_j. In what follows, and in contrast to (2.4), we will prove the EHP expression to be dependent on both Tc_k and Tc_j thereby revealing the expression derived in [13], as one example among too many others [16]-[25] whose approaches are similar to the above but not discussed here for lack of space, to lack accuracy.

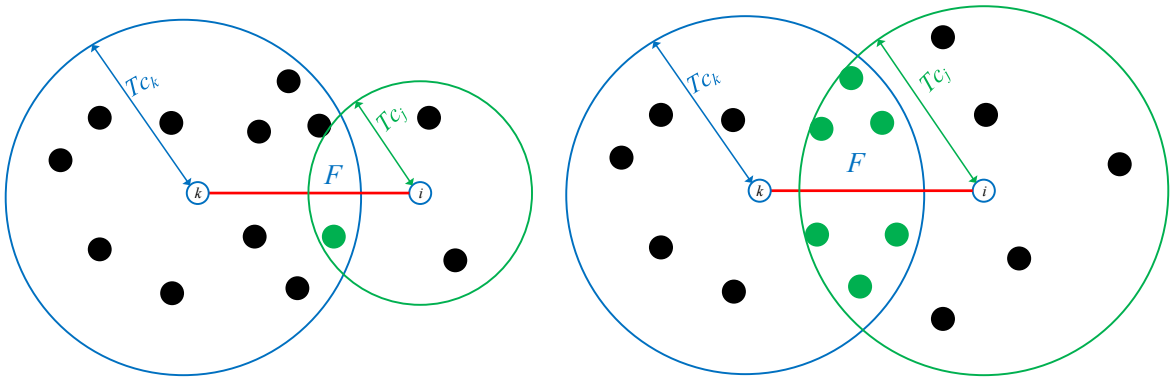

(a) Small Tc_j (b) Large Tc_j

FIGURE 2.4 – Effect of the intermediate node transmission capability.

Let F be the potential forwarding area wherein the intermediate node j could be located. Since this node should, at the same time, be located in the k-th node coverage area and communicate directly with the i-th node using its transmission capability Tc_j, F is given by

$$F = D(k, Tc_k) \cap D(i, Tc_j). \tag{2.5}$$

It is noteworthy that the EHP is nothing but the mean of all distances between the k-th node and all the potential intermediate nodes located in F and, hence, the EHP strongly depends on F. As can be observed from Fig. 2.4, if the intermediate node transmission capability Tc_j increases, the potential forwarding area F increases to include potential intermediate nodes closer to the k-th anchor, thereby decreasing the EHP. Likewise, if Tc_j decreases, F decreases to exclude potential intermediate nodes closer to the k-th anchor and, hence, the EHP increases. Consequently, the EHP depends not only on Tc_k, but also on Tc_j. Let us now turn our attention to the MLH. It is obvious that the transmission capability of the i-th node does not have any effects on the last hop size d_{j-i}. Therefore, in contrast with the EHP, the MLH depends only on the transmission capability of the transmitting node j. In the next section, novel approaches are developed to accurately derive the expressions of both the MLH and the EHP. These results will be exploited in Section 5.4 to propose a low-cost localization algorithm that complies with the heterogeneous

nature of WSNs.

2.3 Analytical evaluation of the MLH and EHP

In this section, expressions of both the MLH and the EHP are accurately derived. To this end, we consider the same scenario described in Section 4.2. For the sake of clarity, in what follows, we denote by X, Y, and Z the random variables that represent d_{k-i}, d_{j-i}, and d_{k-j}, respectively.

2.3.1 MLH derivation

Since the i-th regular node could be located anywhere in $D(j, Tc_j)$ (the j-th node's coverage area) with the same probability, Y can be considered as a uniformly distributed random variable on $[0, Tc_j]$. Therefore, the MLH denoted hereafter by $h_{\text{last}}(Tc_j)$ is given by

$$h_{\text{last}}(Tc_j) = \int_0^{Tc_j} y f_Y(y) dy = \int_0^{Tc_j} \frac{y}{Tc_j} dy = \frac{Tc_j}{2}, \tag{2.6}$$

where $f_Y(y) = 1/Tc_j$ is the probability density function (pdf) of Y.

2.3.2 EHP derivation

In order to derive the EHP, one should first compute the conditional cumulative distribution function (CDF) $F_{Z|X}(z) = P(Z \leq z|x)$ of Z with respect to the random variable X. In the following, two approaches are proposed to derive this CDF.

2.3.2.1 Approach 1

As can be shown from Fig. 3.4, $Z \leq z$ is guaranteed only if there are no nodes in the dashed area A. Therefore, the conditional CDF $F_{Z|X}(z)$ can be defined as

$$F_{Z|X}(z) = P(Z \leq z|x) = P(\mathrm{A}_0|F_1), \tag{2.7}$$

where $P(A_0|F_1)$ is the probability that the event $A_0 = \{\text{no nodes in the dashed area } A\}$ given $F_1 = \{\text{at least one node in the potential forwarding area }\}$ occurs. Since the nodes are uniformly deployed in S, the probability of having K nodes in F follows a Binomial distribution $\text{Bin}(N, p)$

where $p = \frac{F}{S}$. For relatively large N and small p, it can be readily shown that Bin (N, p) can be accurately approximated by a Poisson distribution Pois(λF). Using the Bayes' theorem, $F_{Z|X}(z)$ could be rewritten as

$$F_{Z|X}(z) = \frac{P(\mathrm{F}_1|A_0)\, P(\mathrm{A}_0)}{P(F_1)}, \tag{2.8}$$

and, hence, for a large number of nodes N and small p, we have

$$F_{Z|X}(z) = \frac{e^{-\lambda A}\left(1 - e^{-\lambda B}\right)}{\left(1 - e^{-\lambda F}\right)}, \tag{2.9}$$

where $B = F - A$. In the equation above, note that we use the fact that $P(\mathrm{F}_1|A_0)$ is the probability that at least one node is in B. As can be observed from (2.9), when $z = \alpha$ where $\alpha = x - Tc_j$, we have $B = 0$ and $A = F$ and, therefore, $F_{Z|X}(z) = 0$. This is expected since all potential intermediate nodes are located in the forwarding zone F where any node is at least at distance α from the k-th node (i.e., $P(Z \leq \alpha) = 0$). Furthermore, if $z = Tc_k$, it holds that $B = F$ and $A = 0$ and, hence, $P(Z \leq Tc_k) = 1$. This is also expected since all potential intermediate nodes are located in the k-th node's coverage area at distance Tc_k at most from the latter (i.e., $P(Z \leq Tc_k) = 1$). It should be noticed here that the properties above are not satisfied by any previously developed CDF expressions such as those in [13]-[20].

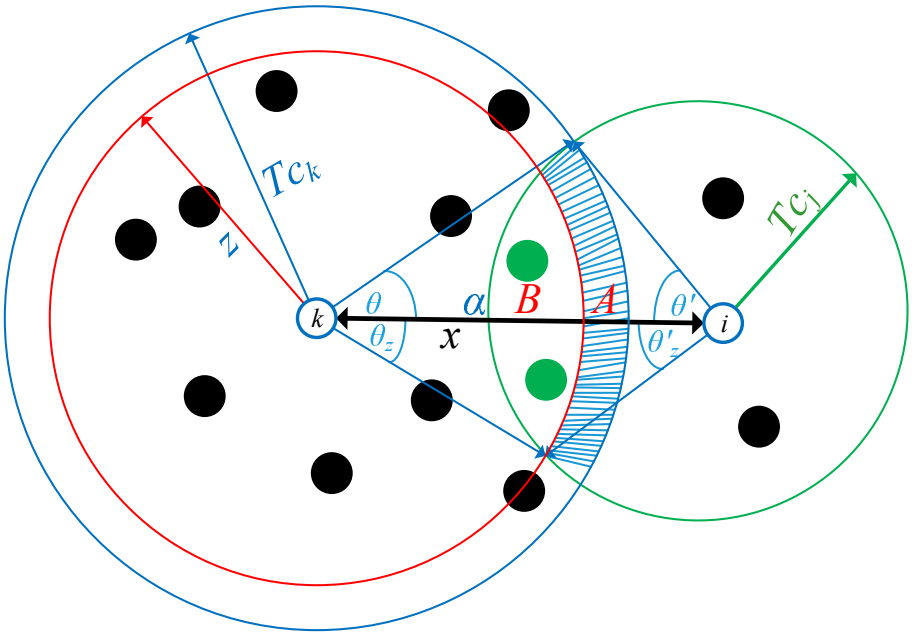

FIGURE 2.5 – EHP analysis.

Using some geometrical properties and trigonometric transformations, one can readily show

that

$$F = Tc_k^2 \left(\theta - \frac{\sin(2\theta)}{2}\right) + Tc_j^2 \left(\theta' - \frac{\sin(2\theta')}{2}\right), \tag{2.10}$$

$$B = z^2 \left(\theta_z - \frac{\sin(2\theta_z)}{2}\right) + Tc_j^2 \left(\theta'_z - \frac{\sin(2\theta'_z)}{2}\right), \tag{2.11}$$

where $\theta = \arccos\left(\frac{Tc_k^2 - Tc_j^2 + x^2}{2Tc_k x}\right)$, $\theta' = \arccos\left(\frac{Tc_j^2 - Tc_k^2 + x^2}{2Tc_j x}\right)$, $\theta_z = \arccos\left(\frac{z^2 - Tc_j^2 + x^2}{2zx}\right)$, and $\theta'_z = \arccos\left(\frac{Tc_j^2 - z^2 + x^2}{2Tc_j x}\right)$. Finally, the EHP $h(Tc_k, Tc_j)$ between the k-th and j-th nodes can be derived as

$$\begin{aligned} h(Tc_k, Tc_j) &= \mathrm{E}_x\left(\alpha H_{Z|X}(\alpha) + \int_{\alpha}^{Tc_k} H_{Z|X}(z)dz\right) \\ &= \int_{Tc_k}^{Tc_k+Tc_j} \left(\alpha H_{Z|X}(\alpha) + \int_{\alpha}^{Tc_k} H_{Z|X}(z)dz\right) f_X(x)\, dx, \end{aligned} \tag{2.12}$$

where $H_{Z|X}(z) = 1 - F_{Z|X}(z)$ and $f_X(x)$ is the pdf of X. Note that the latter can be considered as a uniform random variable over $[Tc_k, Tc_k + Tc_j]$ and, hence, $f_X(x)$ can be substituted there by $1/Tc_j$. To the best of our knowledge, a closed-form expression for the EHP in (2.12) does not exist. However, $h(Tc_k, Tc_j)$ can be easily implemented since it depends on finite integrals. As can be observed from (2.12), the proposed EHP depends on both Tc_k and Tc_j. Such extremely important and crucial features in HWSNs no longer hold true for the previously proposed EHPs, such as in (2.4), which are only dependent on the sender node's transmission capability. It can be shown from Figs. 2.6 and 2.7 that the so-obtained EHP decreases if Tc_j increases while it increases when Tc_k increases. This collaborates the discussion made above. These figures also show that the proposed EHP above increases with the node density. This is expected since it is very likely that the per-hop distance increases when the number of nodes located in F increases if, of course, both Tc_k and Tc_j are fixed. Therefore, the so-obtained EHP expression is more accurate than those developed so far and, hence, should allow more accurate distance estimation and more reliable localization as will be shown next.

2.3.2.2 Approach 2

The main issue with the approach developed above is that it holds only when the number of nodes N is sufficiently large and the area F is much smaller than the network size. Since N is typically large in the context of WSNs, the first condition is very likely to be satisfied. Unfortunately, the second condition cannot be always guaranteed, especially when the transmission

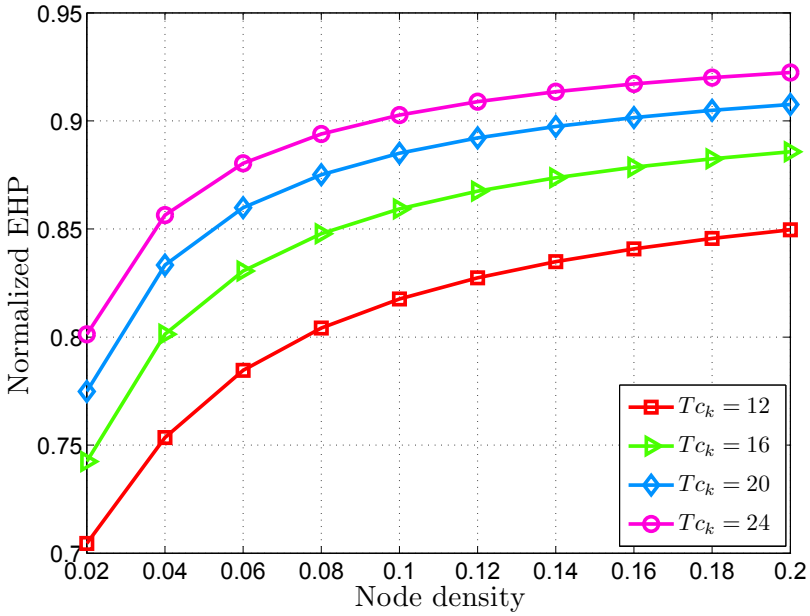

FIGURE 2.6 – Effect of the k-th node transmission capability on the EHP.

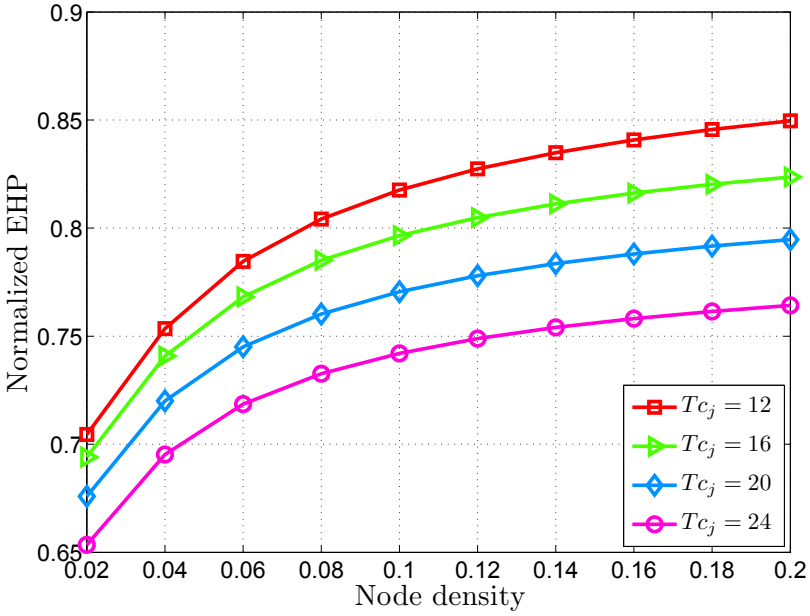

FIGURE 2.7 – Effect of the intermediate node transmission capability on the EHP.

capabilities Tc_k and Tc_j are not small enough. Indeed, in such a case F is very likely to be large and, hence, the EHP derived using the above CDF is no longer accurate. In this section, we propose another approach aiming to derive this CDF for any N, Tc_k and Tc_j.

Let us assume that M potential intermediate nodes exist between the i-th and k-th nodes,

or, in other words, M potential positions of the intermediate node j exist in F. Let Z_m be the random variable that represents the distance between the k-th node and the m-th potential intermediate node. Thus, one can define $F_{Z|X}(z)$ as follows

$$F_{Z|X}(z) = P\left(Z_1 \leq z \cap Z_2 \leq z, \ldots, \cap Z_M \leq z\right). \tag{2.13}$$

Using the fact that $Z_m, m = 1, \ldots, M$ are independently and identically distributed (i.i.d) random variables, we obtain

$$F_{Z|X}(z) = P\left(Z_m \leq z\right)^M. \tag{2.14}$$

As can be observed from Fig. 3.4, in order to satisfy $Z_m \leq z$, the m-th intermediate node should be located in the area B and, hence,

$$F_{Z_m|X}\left(z\right) = P\left(Z_m \leq z|x\right) = P\left(\mathrm{E}_2\right), \tag{2.15}$$

where $P(\mathrm{E}_2)$ is the probability that the event $\mathrm{E}_2 = \{$the m-th intermediate node is located in $B\}$ occurs. Since the nodes distribution is assumed to be uniform, the m-th intermediate node could be located anywhere in F with the same probability. Therefore, the probability that this node is located in any area $\Omega \subset F$ is nothing but the ratio of Ω to F. Consequently, $F_{Z|X}(z)$ is given by

$$F_{Z|X}\left(z\right) = \left(1 - \frac{A}{F}\right)^M. \tag{2.16}$$

Using similar steps to derive A, it can be shown that

$$F = Tc_k^2\left(\theta - \frac{\sin(2\theta)}{2}\right) + Tc_j^2\left(\theta' - \frac{\sin(2\theta')}{2}\right), \tag{2.17}$$

where A is obtained by subtracting (3.12) from (3.8). Finally, the EHP is derived by substituting (2.16) in (2.12). By avoiding the Binomial-to-Poisson approximation exploited in Approach 1, the obtained EHP using Approach 2 is then valid for any N, Tc_k and Tc_j and, hence, it is more likely to be accurate than that developed in Section 2.3.2.1. However, the main drawback of Approach 2 is that the EHP depends on the number of potential intermediate nodes M which should be determined by training, i.e., at additional overhead and power costs with respect to Approach 1. Therefore, Approach 1 is favored when restrictions on power and overhead costs are severe while Approach 2, which performs better as will be verified later by simulations in Section 3.8, is favored when these restrictions are milder.

In the next section, based on the so-obtained EHP and MLH expressions, we propose a novel localization algorithm suitable for HWSNs where nodes have different range capabilities.

2.4 Proposed localization for HWSNs

In this section, we propose a novel three-step localization algorithm for HWSNs. In the first step, the regular nodes receive in a multi-hop fashion all the information required to estimate their respective positions while, in the second step, they compute an initial guess exploiting one of the two EHP expressions developed above. In the third and last step, a correction mechanism is locally performed at each node, in order to further minimize the incurred localization errors. These three steps will be further detailed in the sequel.

2.4.1 Initialization

In this step, the k-th anchor starts by broadcasting through the network a packet which consists of a header followed by a data payload. The packet header contains the anchor position (x_k, y_k), while the data payload contains $(Tc_k, \hat{d}_k)$, where Tc_k is the transmission capability of the k-th anchor and $\hat{d}_k$ is the estimated distance initialized to zero. If the packet is successfully received by a node, the latter estimates the EHP using either Approach 1 or 2 above, adds it to $\hat{d}_k$, stores the resulting value in its database and then, rebroadcasts the resulting packet after substituting Tc_k by its own transmission capability. Once this packet is received by another node, its database information is checked. If the k-th anchor information exists and the stored estimated distance is larger than that of the received one, the node updates the k-th anchor's information, then broadcasts the resulting packet after substituting the received transmission capability by its own. Otherwise, the node discards the received packet. However, when the node is oblivious to the k-th anchor position, it adds this information to its database and forwards the received packet after substituting the received transmission capability by its own. This mechanism will continue until each regular node in the network becomes aware of each anchor position as well as the distance from the latter to the last intermediate node before reaching that node. Note that the implementation of the proposed algorithm requires that each node broadcasts the anchor information not only with its estimated distance but also its transmission capability to allow the EHP computation at the next receiving node. In contrast, the implementation of existing algorithms in HWSNs requires the broadcast of the anchor information and the estimated distance only. Yet we will prove next in Section 2.6 that the additional power cost that could be incurred a priori when broadcasting the transmission capabilities can be easily avoided by the

proposed algorithm.

2.4.2 Positions' computation

In this section, we will show how the so-received information can be exploited to get an initial guess of each regular node position. Using its available information, the $(i-N_a)$-th regular node (or the i-th node) computes an estimate of its distance to the k-th anchor as

$$\hat{d}_{k-i} = \hat{d}_k + h_{\text{last}}(Tc_{k+L}), \tag{2.18}$$

where

$$\hat{d}_k = \sum_{l=k}^{k+L-1} h\left(Tc_l, Tc_{l+1}\right), \tag{2.19}$$

is the distance from the k-th anchor to the last intermediate node. In (2.18) and (2.19), we assume for simplicity, yet without loss of generality, that L intermediate nodes exist over the shortest path between the k-th anchor and the $(i-N_a)$-th regular node and that the l-th intermediate node is the $(k+l)$-th node. Using its estimated distances to the N_a anchors as well as the latters' coordinates, the position of the $(i-N_a)$-th regular node could be obtained by multilateration as [35]

$$[\hat{x}_i, \hat{y}_i]^T = -\frac{1}{2}\left(\boldsymbol{\Upsilon}\boldsymbol{\Upsilon}^T\right)^{-1}\boldsymbol{\Upsilon}^T\boldsymbol{\kappa_i}, \tag{2.20}$$

where $(\hat{x}_i, \hat{y}_i)$ are the biased initial guesses of the $(i-N_a)$-th regular node's coordinates,

$$\boldsymbol{\Upsilon} = \begin{bmatrix} x_1 - x_{N_a} & y_1 - y_{N_a} \\ x_2 - x_{N_a} & y_2 - y_{N_a} \\ \vdots & \vdots \\ x_{(N_a-1)} - x_{N_a} & y_{(N_a-1)} - y_{N_a} \end{bmatrix}, \tag{2.21}$$

and

$$\boldsymbol{\kappa_i} = \begin{bmatrix} \hat{d}_{1-i}^2 - \hat{d}_{N_a-i}^2 + x_{N_a}^2 - x_1^2 + y_{N_a}^2 - y_1^2 \\ \hat{d}_{2-i}^2 - \hat{d}_{N_a-i}^2 + x_{N_a}^2 - x_2^2 + y_{N_a}^2 - y_2^2 \\ \vdots \\ \hat{d}_{(N_a-1)-i}^2 - \hat{d}_{N_a-i}^2 + x_{N_a}^2 - x_{(N_a-1)}^2 + y_{N_a}^2 - y_{(N_a-1)}^2 \end{bmatrix}. \tag{2.22}$$

It is noteworthy from (6.3) and (6.4) that $\hat{x}_i$ and $\hat{y}_i$ are solely dependant on the anchors' coordinates $(x_k, y_k), k = 1, \ldots, N_a$ and the estimated distances $\hat{d}_{k-i}, , k = 1, \ldots, N_a$ which are all locally available at the $(i-N_a)$-th regular node.

Unfortunately, errors are expected to occur when estimating the distance between each regular node-anchor pair, thereby hindering localization accuracy. As a third step of our proposed algorithm, we propose a correction mechanism aiming to reduce this error.

2.4.3 Correction mechanism

Let ϵ_{ki} denote the estimation error of the distance between the k-th anchor and the i-th regular node as

$$\epsilon_{ki} = \hat{d}_{k-i} - d_{k-i}, \tag{2.23}$$

where d_{k-i} is the true distance between the two nodes. As discussed above, this error hinders localization accuracy. As such, we have

$$\begin{cases} x_i = \hat{x}_i + \delta_{x_i} \\ y_i = \hat{y}_i + \delta_{y_i} \end{cases}, \tag{2.24}$$

where δ_{x_i} and δ_{y_i} are the location coordinates' errors to be determined. Exploiting the Taylor series expansion and retaining the first two terms, the following approximation holds :

$$d_{k-i} \simeq \tilde{d}_{k-i} + \psi_{ki}\delta_{x_i} + \phi_{ki}\delta_{y_i}, \tag{2.25}$$

where

$$\tilde{d}_{k-i} = \sqrt{(\hat{x}_i - x_k)^2 - (\hat{y}_i - y_k)^2}, \tag{2.26}$$

and

$$\psi_{ki} = \left.\frac{\partial \tilde{d}_{k-i}}{\partial x}\right|_{\hat{x}_i,\hat{y}_i} = \frac{\hat{x}_i - x_k}{\sqrt{(\hat{x}_i - x_k)^2 - (\hat{y}_i - y_k)^2}} = \frac{\hat{x}_i - x_k}{\tilde{d}_{k-i}}, \tag{2.27}$$

$$\phi_{ki} = \left.\frac{\partial \tilde{d}_{k-i}}{\partial y}\right|_{\hat{x}_i,\hat{y}_i} = \frac{\hat{y}_i - y_k}{\sqrt{(\hat{x}_i - x_k)^2 - (\hat{y}_i - y_k)^2}} = \frac{\hat{y}_i - y_k}{\tilde{d}_{k-i}}, \tag{2.28}$$

for $k = 1, 2, \ldots, N_a$. Note that $\tilde{d}_{k-i}$ is different from $\hat{d}_{k-i}$ due to the error incurred by multilateration [35]. Therefore, rewriting (2.25) in a matrix form yields

$$\mathbf{\Gamma}_i \boldsymbol{\delta}_i = \boldsymbol{\zeta}_i - \boldsymbol{\epsilon}_i, \tag{2.29}$$

where $\mathbf{\Gamma}$ is a $N_a \times 2$ matrix with

$$[\mathbf{\Gamma_i}]_{k1} = \psi_{ki}, [\mathbf{\Gamma_i}]_{k2} = \phi_{ki}, \tag{2.30}$$

and

$$\boldsymbol{\zeta}_i = \left[\begin{array}{cccc} \hat{d}_{1-i} - \tilde{d}_{1-i} & \hat{d}_{2-i} - \tilde{d}_{2-i} & \ldots & \hat{d}_{N_a-i} - \tilde{d}_{N_a-i} \end{array} \right]^T, \tag{2.31}$$

$\boldsymbol{\epsilon}_i = [\epsilon_{1i}, \epsilon_{2i}, \ldots, \epsilon_{N_a i}]^T$, and $\boldsymbol{\delta}_i = [\delta_{x_i}, \delta_{y_i}]^T$. Many methods such as the weighted least squares

Algorithm 1 Proposed algorithm for every nodes

Input : Number of anchors N_a, and their positions (x_k, y_k), where $k = 1, \ldots, N_a$, as well as their transmission capabilites

for $i = 1 \rightarrow N_a$ **do**

$\hat{d}_{k-i} \leftarrow$ using Approach 1 or 2 (Section 2.3)

end for

$\hat{x}_i, \hat{y}_i \leftarrow$ Eq. (6.5) in the section 5.4

$\boldsymbol{\delta}_i = \left(\boldsymbol{\Gamma}_i^T \mathbf{P}_i^{-1} \boldsymbol{\Gamma}_i\right)^{-1} \boldsymbol{\Gamma}_i^T \mathbf{P}_i^{-1} \boldsymbol{\zeta}_i \leftarrow$ Eq. (2.32)

$x_i \leftarrow \hat{x}_i + \delta_x$;

$y_i \leftarrow \hat{y}_i + \delta_y$;

while $\boldsymbol{\delta}_i \geq 0$ **do**

$\hat{x}_i \leftarrow x_i$;

$\hat{y}_i \leftarrow y_i$;

Recalculate $\|\boldsymbol{\delta}_i\| \leftarrow$ Eq. (2.32)

$x_i \leftarrow \hat{x}_i + \delta_x$;

$y_i \leftarrow \hat{y}_i + \delta_y$;

end while

Output (x_i, y_i) ▷ Estimated position of the i-th node

(WLS) might be used to properly derive $\boldsymbol{\delta}_i$. Using WLS, the solution of (2.29) is given by :

$$\boldsymbol{\delta}_i = \left(\boldsymbol{\Gamma}_i^T \mathbf{P}_i^{-1} \boldsymbol{\Gamma}_i\right)^{-1} \boldsymbol{\Gamma}_i^T \mathbf{P}_i^{-1} \boldsymbol{\zeta}_i, \tag{2.32}$$

where $\mathbf{P}_i$ is the covariance matrix of $\boldsymbol{\epsilon}_i$. Since ϵ_{ki} $k = 1, \ldots, N_a$ are independent random variables, $\mathbf{P}_i$ boils down to diag $\left\{\sigma_{1i}^2, \ldots, \sigma_{N_a i}^2\right\}$ where σ_{ki}^2 is the variance of ϵ_{ki}. A straightforward inspection of (2.32) reveals that $\boldsymbol{\delta}_i$ depends on some locally available information as well as all $\sigma_{ki}^2, k = 1, \ldots, N_a$. Yet we will show in what follows that the derivation of $\sigma_{ki}^2, k = 1, \ldots, N_a$ requires a negligible additional power cost that could be easily avoided. Once we get $\boldsymbol{\delta}_i$, the value of $(\hat{x}_i, \hat{y}_i)$ is updated as $\hat{x}_i = \hat{x}_i + \delta_{x_i}$ and $\hat{y}_i = \hat{y}_i + \delta_{y_i}$. The computations are repeated until $\|\boldsymbol{\delta}_i\|$ approaches

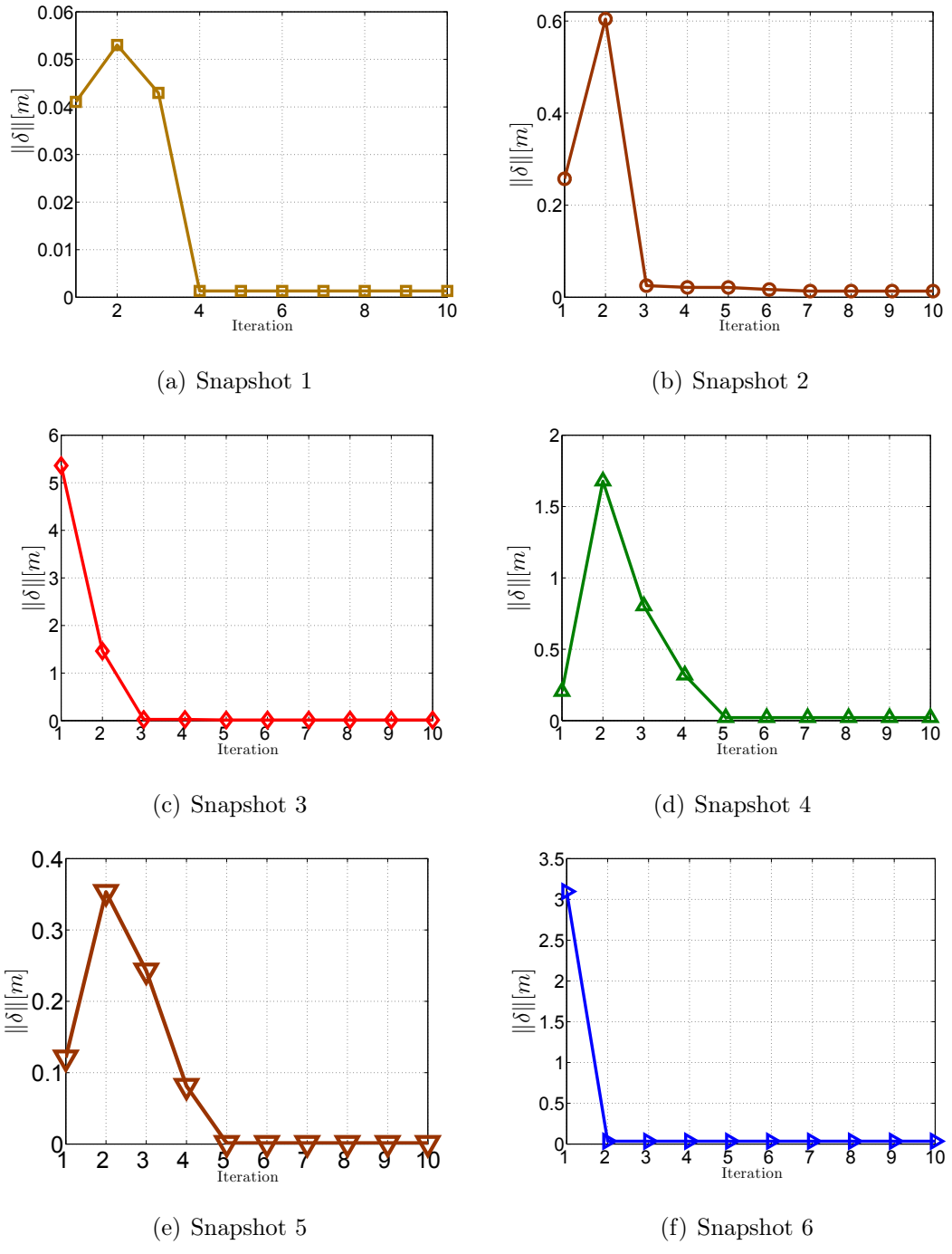

(a) Snapshot 1

(b) Snapshot 2

(c) Snapshot 3

(d) Snapshot 4

(e) Snapshot 5

(f) Snapshot 6

FIGURE 2.8 – Convergence of $\|\boldsymbol{\delta}\|$ vs. the number of iterations.

zero. In such a case, we have from (2.24) that $x_i \simeq \hat{x}_i$ and $y_i \simeq \hat{y}_i$ and, hence, more accurate localization is performed. As can be observed from Fig. 2.8, the proposed correction mechanism converges after 5 iterations at most. Nevertheless, we will prove in Section 2.6 that the proposed algorithm perfectly tailored for HWSNs, and whose pseudocode implementable at each node is

summarized in Algorithm 1, does not burden the overall cost of the WSN.

2.5 Variance evaluation

This section aims to derive the expression of the variances $\sigma_{ki}^2,\ k = 1, \ldots, N_a$ which are required for the proposed algorithm's implementation. As such, two different methods, analytical and non-parametric, are proposed.

2.5.1 Analytical method

Assuming a high node density in the network, the distance d_{k-i} between two nodes can be rewritten as

$$d_{k-i} \simeq \sum_{l=k}^{k+L} d_{l-(l+1)}, \tag{2.33}$$

where L is the number of intermediate nodes over the shortest path and $d_{l-(l+1)}$ is the distance between the l-th and $(l+1)$-th intermediate node. It follows from (2.18) and (2.33) that the distance estimation error (DER) ε_{ki} is given by

$$\varepsilon_{ki} \simeq \sum_{l=k}^{k+L-1} e_l + e_{\text{last}}, \tag{2.34}$$

with $e_l = h\left(Tc_l, Tc_{l+1}\right) - d_{l-(l+1)}$ being the error incurred during the $(l-k+1)$-th hop and $e_{\text{last}} = h_{\text{last}}(Tc_{k+L}) - d_{(k+L)-i}$ the error incurred at the last hop. It can be readily shown from (2.34) that $\sigma_{ki}^2 = \sum_{l=k}^{k+L-1} \sigma_l^2 + {\sigma_{\text{last}}}^2$ where σ_l^2 and ${\sigma_{\text{last}}}^2$ are the variances of e_l and e_{last}, respectively. Using the results developed in Section 2.3, we obtain

$${\sigma_{\text{last}}}^2 = \frac{Tc_{(k+L)}^2}{12}, \tag{2.35}$$

and

$$\begin{aligned} {\sigma_l}^2 = &\int_{Tc_l}^{Tc_l+Tc_{l+1}} \left(\alpha^2 H(\alpha) + 2\int_{\alpha}^{Tc_l} zH(z)dz\right) f_X\left(x\right) dx - \\ &\left(\int_{Tc_l}^{Tc_l+Tc_{l+1}} \left(\alpha H(\alpha) + \int_{\alpha}^{Tc_l} H(z)dz\right) f_X\left(x\right) dx\right)^2. \end{aligned} \tag{2.36}$$

Note that ${\sigma_l}^2$ could be obtained using any of the CDFs developed in Section 2.3.2. As can be observed from (2.35) and (2.36), ${\sigma_{\text{last}}}^2$ is locally computable by the i-th node while ${\sigma_l}^2$ should be

computed at the $(l+1)$-th intermediate node, added to the term $\sum_{m=k}^{l-1} \sigma_m^2$, then forwarded to the next intermediate node. This results in additional few bits that must be transmitted by each node in the network. In what follows, we will prove that the additional power cost that could be incurred a priori when transmitting σ_l can be easily avoided by the proposed algorithm.

2.5.2 Non-parametric method

In the previous section, the analytical expression of σ_{ki}^2 was derived using the approximation in (2.33) which holds only for highly dense networks. However, if this assumption is not satisfied (i.e., lowly dense network), (2.33) would no longer be valid and, hence, σ_{ki}^2's expression would no longer be accurate enough. In such a case, to properly derive σ_{ki}^2, we propose to exploit the PDF of the DER ε_{ki} denoted by $f(\varepsilon)$. Unfortunately, to the best of our knowledge, there is no closed form solution for such a PDF. In this work, we propose to use a non-parametric technique to estimate it owing to some potential observations available at anchors. So far, many non-parametric techniques have been proposed in the literature such as the histogram [39] and the well-known kernel density estimation (KDE) [40] techniques. In this paper, we are only concerned by the latter which can estimate an arbitrary distribution without much observations. Such observations can in fact be easily obtained at the k-th anchor. Indeed, since this anchor is aware of all other anchor positions, it is able to derive the actual distances between it and the latters. Using (2.18), the k-th anchor could also obtain the estimated distances between it and the other anchors and, therefore, derive ε_{ki}. Hence, if N_a anchors exist in the network, the total number of available observations is $n_o = N_a(N_a - 1)$. Let $\varepsilon_1, \varepsilon_2, \ldots, \varepsilon_{n_o}$ denote such observations. Using the KDE technique, $f(\varepsilon)$ can be then approximated by

$$\hat{f}(\varepsilon) = \frac{1}{p s_\varepsilon} \sum_{t=1}^{n_o} K\left(\frac{\varepsilon - \varepsilon_t}{s_\varepsilon}\right), \tag{2.37}$$

where s_ε is a smoothing parameter determined using the method in [41] and $K(\varepsilon)$ is the Gaussian kernel given by

$$K(\varepsilon) = \frac{1}{\sqrt{2\pi}} \exp(-\frac{1}{2}\varepsilon^2). \tag{2.38}$$

As can be noticed from (2.37) and (2.38), the estimated PDF is computed by averaging the Gaussian density over all observations. Substituting (2.38) in (2.37) and using the resulting

PDF to compute σ_{ki}^2 yields

$$\sigma_{ki}^2 = \frac{\sum_{t=1}^{n_o}\left(X_t G_t - Y_t^2\right)}{\sum_{t=1}^{n_o} G_t^2}, \tag{2.39}$$

where

$$X_t = \left(s_\varepsilon^2 + \varepsilon_t^2\right) G_t - s_\varepsilon^2 \left(\left(\varepsilon_t + 1\right) e^{-\frac{(1-\varepsilon_t)^2}{2s_\varepsilon^2}} + \left(\varepsilon_t - 1\right) e^{-\frac{(1+\varepsilon_t)^2}{2s_\varepsilon^2}} \right), \tag{2.40}$$

$$G_t = s_\varepsilon \sqrt{2\pi} \left(Q\left(\frac{\varepsilon_t - 1}{s_\varepsilon}\right) - Q\left(\frac{\varepsilon_t + 1}{s_\varepsilon}\right) \right), \tag{2.41}$$

and

$$Y_t = \varepsilon_t G_t - s_\varepsilon^2 \left[e^{-\frac{(1-\varepsilon_t)^2}{2s_\varepsilon^2}} - e^{-\frac{(1+\varepsilon_t)^2}{2s_\varepsilon^2}} \right], \tag{2.42}$$

with $Q(x)$ being the Q-function.

Fig. 2.9 plots the empirical $f\left(\varepsilon\right)$ as well as $\hat{f}\left(\varepsilon\right)$ for different numbers of anchors. We see there that only a few anchors (i.e., few observations) are required to accurately estimate the localization errors' PDF. Furthermore, from Fig. 2.9, the estimated PDF approaches the empirical one, as N_a increases. This gives a sanity check for the proposed nonparametric method.

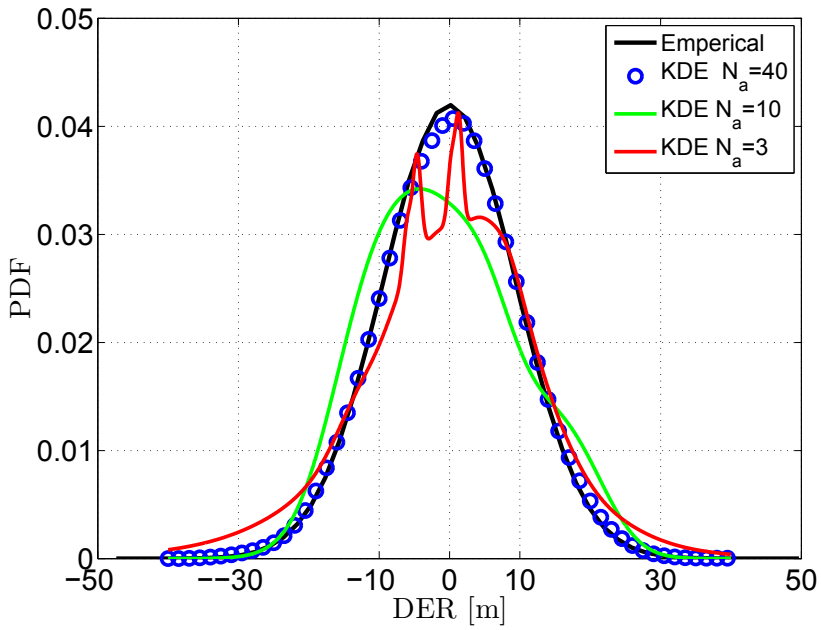

FIGURE 2.9 – Estimated DER's PDF using KDE.

Nevertheless, in order to derive σ_{ki}^2 using this approach, each regular node needs to be aware of all observations. If this is not properly done, it will be very expensive in terms of power

consumption, since each anchor would recur to a second broadcast to share its observations with the regular nodes. In order to circumvent this problem, we propose in what follows a power-efficient observation sharing protocol where anchors periodically broadcast their information. In fact, during the first time slot, only the first anchor should broadcast its own information while the $(N_a - 1)$ other anchors only execute the tasks described in Section 2.4.1. At the second time slot, the second anchor derives an estimation error observation using the information received from the first anchor, adds it to its packet and broadcasts the resulting packet in the network. Upon reception of this information, the rest of anchors derive and store a second observation. Two observations are then available at the third anchor which also broadcasts them in the network. This process will continue until each regular node becomes aware of a sufficient number of observations. Note that if N_a is large enough so that $(N_a - 1)$ observations are sufficient to accurately derive the PDF, only two time slots are required. Indeed, after the first time slot, $(N_a - 1)$ observations are available and can be simultaneously broadcasted by the $(N_a - 1)$ anchors in the network. In the next section, we will prove that each anchor could transmit few observations without incurring any power cost. Fig. 2.10 plots the error variance for different node

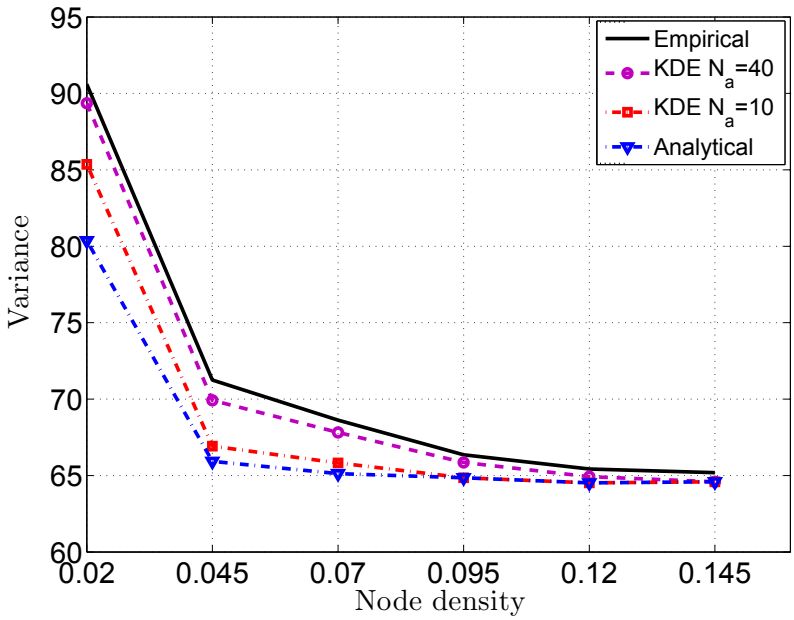

FIGURE 2.10 – Global variance for different node densities.

densities. It shows, as expected, that the variance decreases when the node density increases. Beyond a node density threshold of less than 0.1, both the analytical and the non-parametric

methods start to yield about the same variance as the empirical one. Furthermore, when N_a increases, more so at large enough values, the efficiency of the non-parametric method increases even at low node densities. Note that increasing the number of anchors N_a does not only result in a more accurate variance, but also in a more reliable localization [4].

2.6 Proposed algorithm's implementation cost

As discussed in Section 5.4, the Proposed algorithm's implementation requires the $(i-N_a)$-th regular node to be able to compute its coordinates' initial guess $(\hat{x}_i, \hat{y}_i)$ as well as $\boldsymbol{\delta}_i$ which is used at the position correction step. As discussed above, since these quantities depend solely on the information locally available at the $(i - N_a)$-th regular node, their computation does not require any additional overhead or power cost. Furthermore, from (6.5) and (2.32), this node must perform matrix-inversion operations to the matrices $\boldsymbol{\Upsilon}\boldsymbol{\Upsilon}^T$ and $\boldsymbol{\Gamma}_i^T\mathbf{P}_i^{-1}\boldsymbol{\Gamma}_i$ in order to derive $(\hat{x}_i, \hat{y}_i)$ and $\boldsymbol{\delta}_i$, respectively. This kind of operations which is often highly computationally demanding may significatively increase the overall cost of the WSN. Nevertheless, since these matrices are 2-by-2, the entries of their inverses can be analytically and easily derived using the locally available information at the $(i - N_a)$-th regular. This proves that the computation of $(\hat{x}_i, \hat{y}_i)$ and $\boldsymbol{\delta}_i$ does not burden neither the implementation complexity of the proposed algorithm nor the overall cost of the WSN. Moreover, some iterations should be repeated, at most 5 times as shown in Fig. 2.8, to ensure the convergence of the proposed correction mechanism. Knowing that the required power to execute one instruction is in the range of 10^{-4} of the power consumed per transmitted bit [33]-[34], the power needed to execute this mechanism is then very negligible with respect to the overall power consumed by each node. On the other hand, as discussed in Sections 5.4 and 2.5, the proposed algorithm's implementation requires that each node transmits, upon reception a message from an anchor, its transmission capability and variance besides to the latter's coordinates and the distance between the two nodes. This results in additional few bits, with respect to the existent algorithms, thereby causing an additional power cost. We will shortly see below that this cost could be easily avoided.

Let p_i be the available power at the i-th node, b_i be the length in bits of the original packet sent when the existing algorithms are implemented (i.e., packet includes only the anchor's coordinates and its distance to the i-th node), and a_i be the cost in bits if Tc_i and ${\sigma_i}^2$ are added to the

packet. If the power p_i allows the i-th node to transmit b_i bits over a Tc_i coverage distance, this power will also allow the latter node to transmit $b_i + a_i$ bits but over a coverage distance $\tilde{T}c_i < Tc_i$, where $\tilde{T}c_l$ is the new transmission capability of the i-th node. Since no matter are the transmission capabilities of the i-th node and the previous intermediate node, this node is always able to compute the EHP, the fact that Tc_i decreases to $\tilde{T}c_i$ does not affect the performance of the proposed localization algorithm. Therefore, the additional bits a_i could be broadcasted without any additional power cost.

All the above discussion proves that the proposed localization algorithm can be implemented at a low cost. Furthermore, since it complies with the heterogeneous nature of WSNs and, further, is power efficient, it could easily find application in EH-WSNs where the power is considered as a scarce resource.

2.7 Simulations results

In this section, we evaluate the performance of the proposed algorithm in terms of localization accuracy by simulations using Matlab. These simulations are conducted to compare, under the same network settings, the proposed algorithm with some of the best representative localization algorithms currently available in the literature, i.e., DV-Hop [4], LAEP [13] and EPHP [20]. All simulation results are obtained by averaging over 100 trials. In the simulations, nodes are uniformly deployed in a 2-D square area $S = 100 \times 100\ m^2$. We always assume that $Tc_i \neq Tc_j$ if $i \neq j$ and that all transmission capabilities are set between 5 and 30 meters, except in Fig. 2.12(b) where the transmission capability $T_c = 20$ meters is the same across the network (i.e., homogenous WSN). We also assume that the number of anchors N_a is set to 20.

Parameter	**Value**
λ	$0.02 : 0.025 : 0.145$
Transmission capabilities	$5 - 30$ m
S	$10^4\ m^2$
N_a	20

TABLE 2.1 – Simulation parameters.

As a performance metric, we propose to adopt both the distance DER and the normalized

root mean square error (NRMSE) which is defined as and

$$\text{NRMSE} = \frac{1}{N_u} \sum_{i=1}^{N_u} \frac{\sqrt{(x_i - \hat{x}_i)^2 + (y_i - \hat{y}_i)^2}}{Tc_i}. \tag{2.43}$$

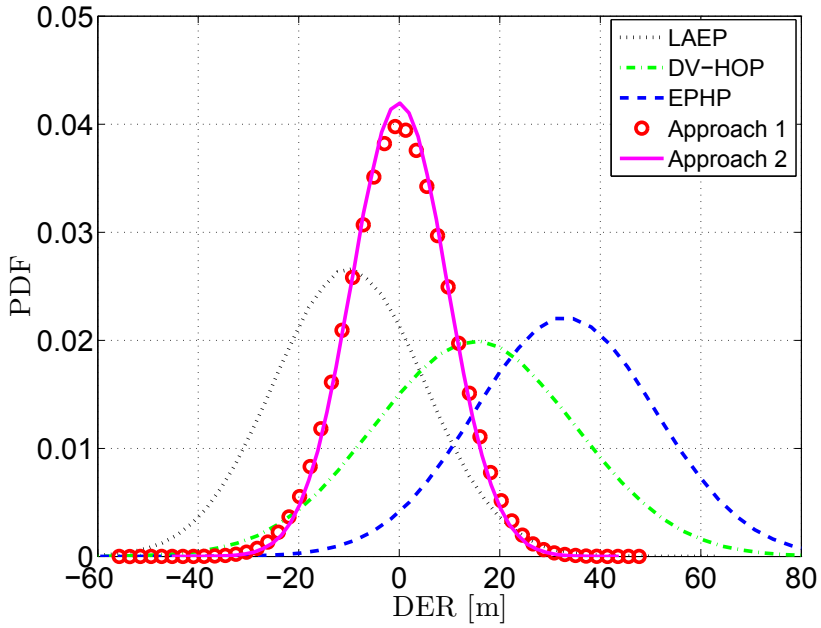

FIGURE 2.11 – Empirical PDFs of the DERs achieved by different localization algorithms.

Fig. 2.11 illustrates the empirical DER's PDF achieved by our proposed localization algorithm as well as those achieved by other well-known algorithms. Since these localization algorithms exploit the distance between each regular node and all anchors to estimate the coordinates of the latter, the better is the distance estimation, the more accurate are these localization algorithms. As can be shown from this figure, when using Approaches 1 or 2, we are able to achieve a narrower PDF centered around 0, thereby offering unbiased and far-more accurate distance estimation. This is expected since in contrast to the previous works, both Approaches 1 and 2 take into account the fact that different transmission capabilities may coexist as it is the case in HWSNs.

Fig. 2.12 plots the localization NRMSE achieved by DV-Hop, EPHP, LAEP and the proposed algorithm for different node densities λ in (a) HWSN and (b) Homogenous WSN. From Fig. 2.12(a), the proposed algorithm, with or without localization correction, always outperforms its counterparts. Indeed, our proposed algorithm turns out to be until about two, three and four times more accurate than LAEP, DV-Hop, and EPHP, respectively. Furthermore, as

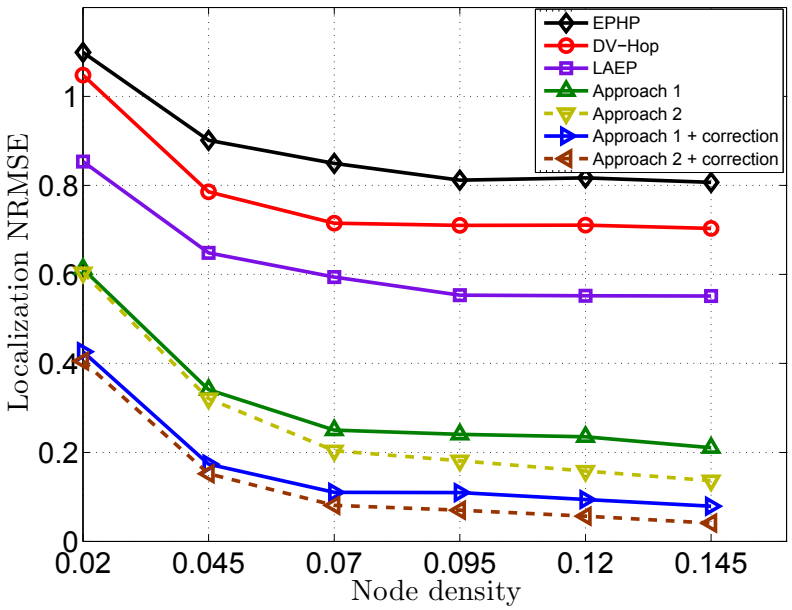

(a)

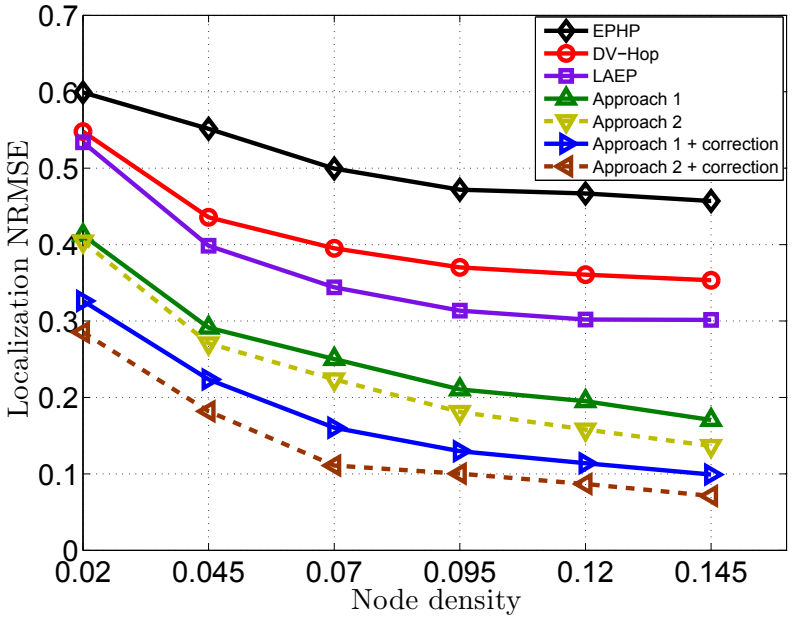

(b)

FIGURE 2.12 – Localization NRMSE vs. node density in : (a) a heterogenous, and (b) a homogenous WSN.

can be observed from this figure, the NRMSE achieved by the proposed algorithm significantly decreases when the node density λ increases while those achieved by its counterparts slightly

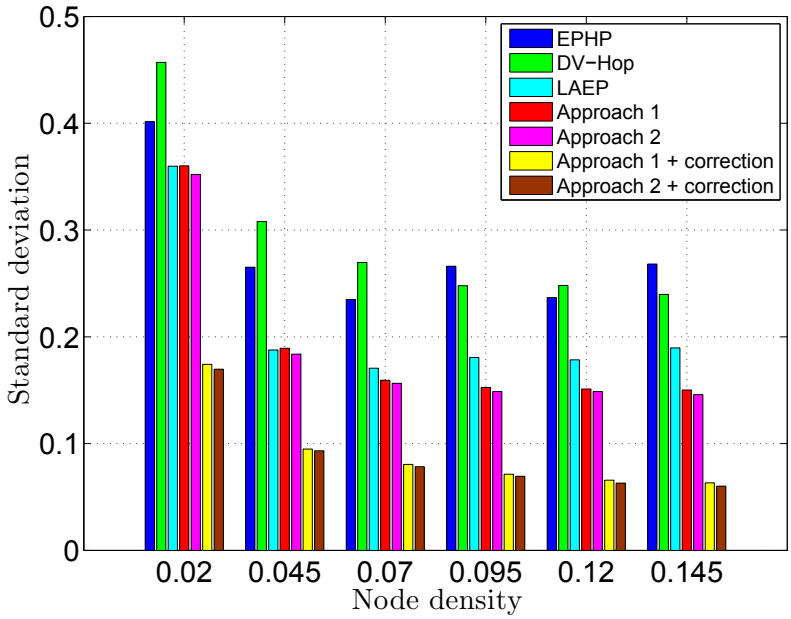

FIGURE 2.13 – Standard deviation vs. node density.

decrease then quickly saturate. This is expected since two conflicting phenomena arise when λ grows large. The first is that the approximation in (2.33) becomes more realistic and, hence, more accurate localization is performed. The second is the increase of the number of different transmission capabilities due to the heterogeneous nature of WSNs when the node density increases. Since more different are the transmission capabilities in the network, worse is the accuracy of the former algorithms. This explains why their performance quickly saturates when the node density increases. The proposed algorithm's accuracy, in contrast, increases with λ since it takes into account the difference between the transmission capabilities that is typical of HWSNs. This further proves the efficiency and suitability of the proposed localization algorithm to HWSNs. Moreover, from Fig. 2.12(b), our algorithm is also the most accurate in homogenous WSNs where the transmission capability is the same across the network. As could be seen from this figure, although all algorithms' accuracy improve as expected in homogenous WSN with respect to the heterogenous case, our proposed algorithm remains the best algorithm. This is due to the fact that our EHP accounts for the transmission capabilities of the sender and receiver nodes, leading thereby to a more accurate localization. This is in contrast with DV-Hop, EPHP ans LAEP whose respective EHPs are derived accounting only for the sender node's transmission capability. The last result further proves the efficiency of our proposed algorithm.

Fig. 2.13 plots the NRMSE's standard deviation achieved by all localization algorithms. As can be observed from this figure, the one achieved by the proposed algorithm substantially decreases when the node density increases while those achieved by the other algorithms slightly decrease. This is due once again to the fact that the proposed algorithm complies with the heterogeneous nature of the WSNs when the former algorithms do not. Furthermore, the NRMSE standard deviation achieved by the proposed algorithm using either Approach 1 or 2 approaches zero. This means that implementing our algorithm in HWSNs guarantees a very accurate localization for any given realization. This result is very interesting in terms of implementation strategy, since it proves that the result in Fig. 2.12 becomes more and more meaningful as λ grows large.

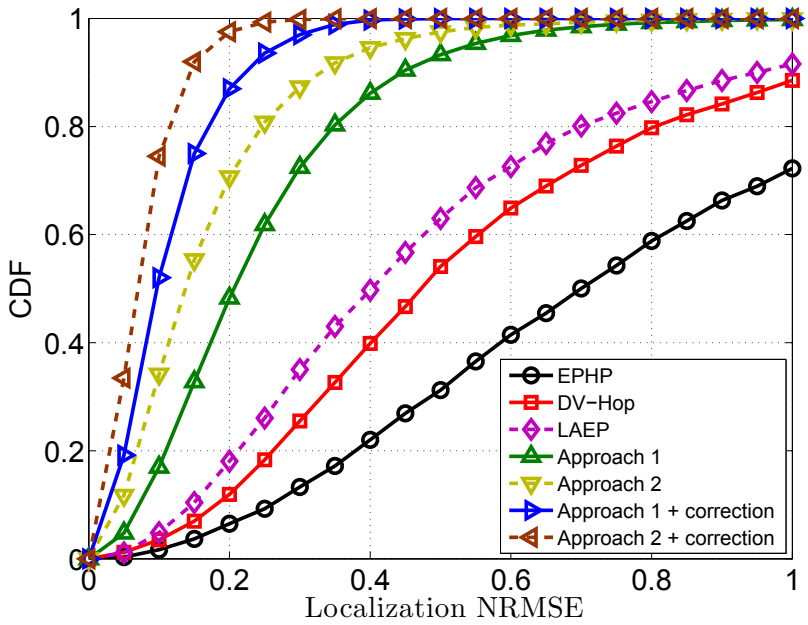

FIGURE 2.14 – Localization NRMSE's CDF.

Fig. 2.14 illustrates the localization NRMSE's CDF. Using the proposed algorithm, 90% (99.5% with Approach 2) of the regular nodes could estimate their position within almost the fifth of their transmission capabilities. In contrast, 20% of the nodes achieve the same accuracy with LAEP, about 14% with DV-Hop, and only 9% with EPHP. This further proves the efficiency of the proposed localization algorithm.

Fig. 2.15 plots the localization NRMSE achieved by DV-Hop, EPHP, LAEP and the proposed algorithm versus the degree of irregularity (DoI) of the transmission capabilities, when $\lambda = 0.045$.

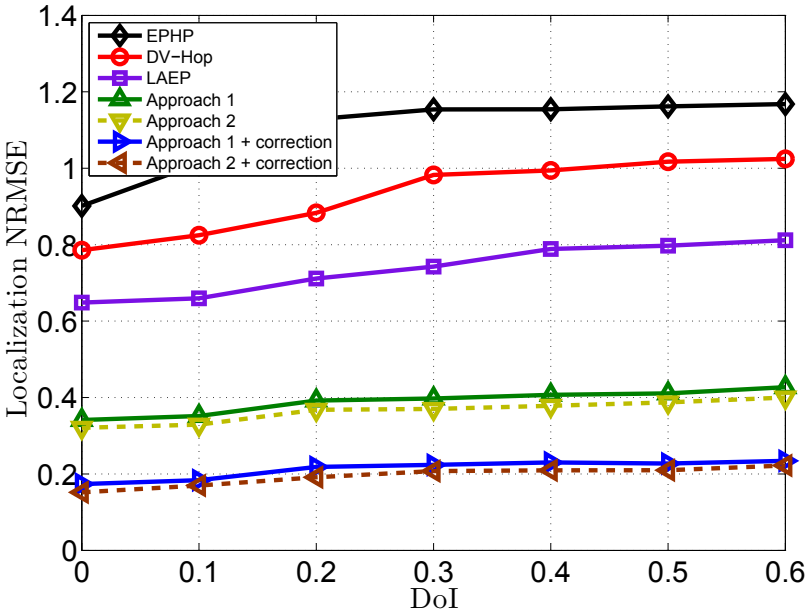

FIGURE 2.15 – Localization NRMSE vs. DOI with $\lambda = 0.045$.

The adopted transmission model in this figure is the same as in [38]. As could be shown from Fig. 2.15, the accuracy of all algorithms deteriorate, as expected, when DoI increases. However, from this figure, the proposed algorithm still outperforms its counterparts even in more adverse conditions. Furthermore, from Fig. 2.15, our algorithm accuracy slowly deteriorates with DoI, in contrast with its counterparts. This makes it more robust against such a phenomenon.

Fig. 4.18 shows the total number of exchanged packets N_{packets} using by the proposed algorithm and its counterparts versus the node density. As could be seen from this figure, the proposed algorithm requires the same number of exchanged packets as LAEP and EPHP while it requires half the packets exchanged with DV-Hop. This is expected since the three first are analytical algorithms where the EHP evaluation and, hence, the position estimation are locally performed at each node after the initialization step, without requiring any additional information exchange. This is in contrast with DV-hop whose heuristical nature imposes a second broadcast from the anchors to assist regular nodes' self-localization. This implies that the overall power required by our algorithm to transmit and receive the exchanged packets is the same as that required by LAEP and EPHP while it is the half of that needed by DV-Hop. On the other hand, the additional power cost incurred by the proposed algorithm due to the correction mechanism's instructions is negligible and to the few extra bits in each packet is easily avoidable, as discussed

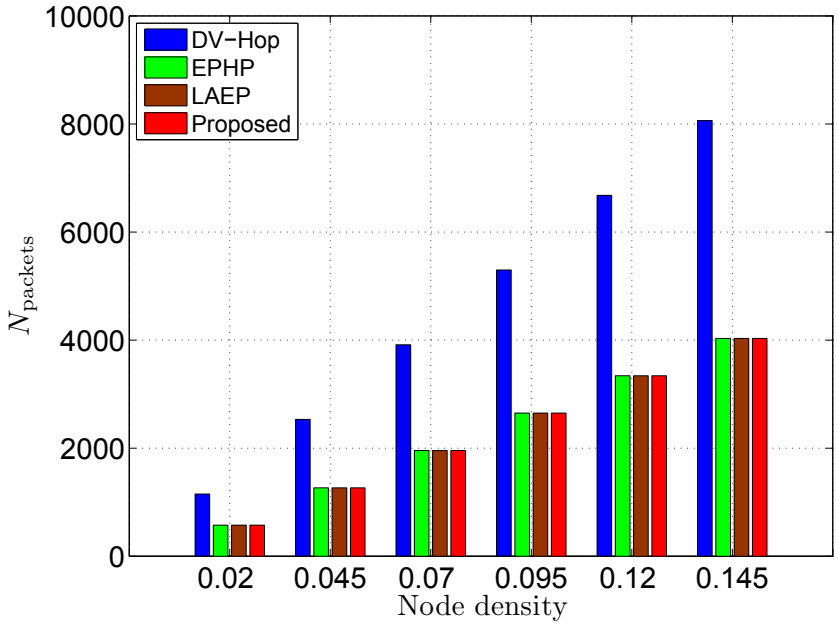

FIGURE 2.16 – The total number of exchanged packets N_{packets} versus the node density.

in Section 2.6. Therefore, our proposed algorithm incurs almost the same power cost as LAEP and EPHP while it incurs the half cost of DV-hop. This proves that the proposed algorithm outperforms in accuracy all its counterparts, yet a no extra power cost, thereby highlighting its superiority.

2.8 Conclusion

In this paper, a novel low-cost localization algorithm which accounts for the heterogeneous nature of WSNs was proposed. Two different approaches were developed to accurately derive the EHP. Using the latter, the proposed algorithm is able to accurately locate the sensor nodes owing to a new low-cost implementation that avoids any additional power consumption. Furthermore, a correction mechanism which complies with the heterogeneous nature of WSNs was developed to further improve localization accuracy without incurring any additional costs. The proposed algorithm, whether applied with or without correction, is shown to outperform in accuracy the most representative WSN localization algorithms.

Bibliographie

[1] D.P. Agrawal and Q.-A. Zeng, *Introduction to Wireless and Mobile Systems,* 3^{rd} edition Cengage Learning, USA, 2010.

[2] F. Akyildiz, W. Su, Y. Sankarasubramaniam, and E. Cayirci, "A survey on sensor networks," *IEEE Commun. Mag.,* vol. 40, no. 8, pp. 102-114, August 2002.

[3] J.N. Al-Karaki and A.E. Kamal, "Routing techniques in wireless sensor networks : a survey," *IEEE Wireless Commun.* vol. 11, no. 6, pp. 6-8, December 2004.

[4] F. Gustafsson and F. Gunnarsson, "Mobile Positioning Using Wireless Networks : Possibilities and Fundamental Limitations Based on Available Wireless Network Measurements," *IEEE Signal Process. Mag.,* vol. 22, no. 4, pp. 41-53, July 2005.

[5] V. Lakafosis and M.M. Tentzeris, "From single-to multihop : The status of wireless localization," *IEEE Microw. Mag.,* vol. 10 , no. 7, pp. 34-41, December 2009.

[6] W. Zhang and G. Cao, "DCTC : Dynamic Convoy Tree-Based Collaboration for Target Tracking in Sensor Networks," *IEEE Trans. Wireless Commun,* vol. 3, no. 5, pp. 1689-1701, September 2004.

[7] H. Ren and M. Q-H. Meng, "Power Adaptive Localization Algorithm for Wireless Sensor Networks Using Particle Filter," *IEEE Trans. Veh Techno.,* vol. 58, no. 5, pp. 2498-2508, June 2009.

[8] J. Rezazadeh, M. Moradi, A.S. Ismail and E. Dutkiewicz, "Superior Path Planning Mechanism for Mobile Beacon-Assisted Localization in Wireless Sensor Networks," *IEEE Sensors J.,* vol. 14, no. 9, pp. 3052-3064, May 2014.

[9] J. Lee, Y. Kim, J. Lee, and S. Kim , "An Efficient Three-Dimensional Localization Scheme Using Trilateration in Wireless Sensor Networks," *IEEE Commun. Lett.,* vol. 18, no. 9, pp. 1591-1594, September 2014.

[10] S. Hong, D. Zhi, S. Dasgupta, and Z. Chunming, "Multiple Source Localization in Wireless Sensor Networks Based on Time of Arrival Measurement," *IEEE Trans. Signal Process.,* vol. 62, no. 8, pp. 1938-1949, February 2014.

[11] D. Niculescu and B. Nath, "Ad hoc positioning system (APS)," *Proc. IEEE GLOBECOM'2001,* San Antonio, TX, USA, November 25-29, 2001.

[12] A. Boukerche, H.A.B.F. Oliveira, E.F. Nakamura, A.A.F. Loureiro, "DV-Loc : a scalable localization protocol using Voronoi diagrams for wireless sensor networks," *IEEE Wireless. Commun. Mag.,* vol. 16, no. 2, pp. 50-55, April 2009.

[13] L. Gui, T. Val, A. Wei, "Improving Localization Accuracy Using Selective 3-Anchor DV-Hop Algorithm," *Proc. IEEE VTC'2011,* San Francisco, CA, USA, Septembre 5-8, 2011.

[14] C. Bettstetter, J. Eberspacher , "Hop distances in homogeneous ad hoc networks," *Proc. IEEE VTC'2003,* Jeju Island, Korea, April 22-25, 2003.

[15] D. Ma, MJ. Er, B. Wang , "Analysis of Hop-Count-Based Source-to-Destination Distance Estimation in Wireless Sensor Networks With Applications in Localization," *IEEE Trans. Veh. Technol.,* vol. 59, no. 6, pp. 2998-3011, July 2010.

[16] D. Ma, MJ. Er, B. Wang , "A novel approach toward source-to-sink distance estimation in wireless sensor networks," *IEEE Commun. Lett.,* vol. 14, no. 5, pp. 384-386, May 2010.

[17] X. Ta, G. Mao, and B. D. Anderson, "On the probability of k-hop connection in wireless sensor networks," *IEEE Commun. Lett.,* vol. 11, no. 9, pp. 662-664, August 2007.

[18] R. Yates and D. Goodman, *Probability and Stochastic Process,* 2^{nd} edition Wiley, New York, USA, 2004.

[19] X. Ta, G. Mao, and B. D. Anderson, "Evaluation of the probability of k-hop connection in homogeneous wireless sensor networks," *Proc. IEEE GLOBECOM'2007,* Washington, DC, USA, November 26-30, 2007.

[20] Y. Wang, X. Wang, D. Wang, and D. P. Agrawal, "Range-Free Localization Using Expected Hop Progress in Wireless Sensor Networks," *IEEE Trans. Parallel Distrib. Syst.,* vol. 25, no. 10, pp. 1540-1552, October 2009.

[21] L. Kleinrock and J. Silvester, "Optimum Transmission Radii for Packet Radio Networks or Why Six is a Magic Number," *in Proc. IEEE NTC '1978,* Birmingham, AL, Alabama, December 4-6, 1978.

[22] S. Vural and E. Ekici, "On Multihop Distances in Wireless Sensor Networks with Random Node Locations," *IEEE Trans. Mobile Comput.,* vol. 9, no. 4, pp. 540-552, April 2010.

[23] A. El Assaf, S. Zaidi, S. Affes, and N. Kandil, "Efficient Range-Free Localization Algorithm for Randomly Distributed Wireless Sensor Networks," *IEEE GLOBECOM'2013,* Atlanta, GA, December 9-13, 2013.

[24] M. Haenggi, "On distances in uniformly random networks," *IEEE Trans. Inf. Theory,* vol. 51 , no. 10 , pp. 3584-3586, October 2005.

[25] JC. Kuo, W. Liao, "Hop Count Distribution of Multihop Paths in Wireless Networks With Arbitrary Node Density : Modeling and Its Applications," *IEEE Trans. Veh. Technol.,* vol. 56, no. 4, pp. 2321-2331, July 2007.

[26] M. Li and Y. Liu,, "Rendered path : Range-free localization in anisotropic sensor networks with holes," *IEEE/ACM Trans. Netw.,* vol. 18, no. 1, pp. 320-332, February 2010.

[27] B. Xiao, L. Chen, Q. Xiao, M. Li , "Reliable Anchor-Based Sensor Localization in Irregular Areas," *IEEE Trans. Mobile Comput.,* vol. 9, no. 1, pp. 60-72, January 2010.

[28] Z. Shigeng, C. Jiannong, L.-J. Chen , C. Daoxu Chen, "Accurate and Energy-Efficient Range-Free Localization for Mobile Sensor Networks," *IEEE Trans. Mobile Comput.,* vol. 9, no. 6, pp. 897-910, June 2010.

[29] Q. Xiao, B. Xiao, J. Cao, J. Wang, "Multihop Range-Free Localization in Anisotropic Wireless Sensor Networks : A Pattern-Driven Scheme," *IEEE Trans. Mobile Comput.,* vol. 9, no. 11, pp. 1592-1607, November 2010.

[30] A. Kansal, J. Hsu, S. Zahedi, and M. B. Srivastava, "Power Management in Energy Harvesting Sensor Networks," *ACM Trans. Embedded Computing Systems,* vol. 6, no. 4, pp. 1-38, September 2007.

[31] A. P. Sample, D. J. Yeager, P. S. Powledge, A. V. Mamishev, and J. R. Smith, "Design of an RFID-Based Battery-Free Programmable Sensing Platform," *IEEE Trans. Instrum. Meas.,* vol. 57, no. 11, pp. 2608-2615, November 2008.

[32] Y. Luo, J. Zhang, and K. B. Letaief, "Optimal Scheduling and Power Allocation for Two-Hop Energy Harvesting Communication Systems," *IEEE Trans. Wireless Commun.,* vol. 12, no. 9, pp. 4729-4741, September 2013.

[33] S. Sudevalayam and P. Kulkarni, "Energy Harvesting Sensor Nodes : Survey and Implications," *IEEE Commun. Survey and tutorials,* vol. 13, no. 3, pp. 443-461, Third Quarter 2011.

[34] A. El Assaf, S. Zaidi, S. Affes, and N. Kandil, "Range-free localization algorithm for heterogeneous wireless sensors networks," *Proc. IEEE WCNC'2014,* Istanbul, Turkey, April 6-9, 2014.

[35] W. Dargie and C. Poellabauer, *Fundamentals of Wireless Sensor Networks : Theory and Practice,* 1^{st} edition Wiley, New York, USA, 2010.

[36] N. Patwari, J.N. Ash, S. Kyperountas, A.O. Hero, R.L. Moses and N.S. Correal, "Locating the nodes : cooperative localization in wireless sensor networks," *IEEE Signal Process. Mag.,* vol. 22, no. 4, pp. 54-69, July 2005.

[37] J.C. Chen, K. Yao, and R.E. Hudson, "Source localization and beamforming," *IEEE Signal Process. Mag.,* vol. 19, no. 2, pp. 30-39, March 2002.

[38] G. Zhou, T. He, S. Krishnamurthy, and J.A. Stankovic, "Impact of Radio Irregularity on Wireless Sensor Networks," *ACM MobiSys,* pp. 125-138, June 2004.

[39] B. W. Silverman, *Density Estimation for Statistics and Data Analysis,* 1^{st} edition Chapman and Hall, London, 1986.

[40] A.R. Webb and K.D. Copsey, *Statistical Pattern Recognition,* 3^{rd} edition Wiley, USA, 2011.

[41] A.W. Bowman ; A. Azzalini, *Applied Smoothing Techniques for Data Analysis : The Kernel Approach with S-Plus Illustrations : The Kernel Approach with S-Plus Illustrations,* Oxford University Press, Oxford, USA, 1997.

Chapitre 3

Accurate Nodes Localization in Anisotropic Wireless Sensor Networks

Ahmad El Assaf, Slim Zaidi, Sofiène Affes and Nahi Kandil

International Journal of Distributed Sensor Networks, vol. 2015, pp. 1-17, April 2015. **Invited Paper**.

Résumé : Ce chapitre propose un algorithme de localisation précise adapté pour les réseaux de capteurs sans fil distribués dans des environnements anisotropes (AWSNs). En utilisant l'algorithme proposé, chaque nœud régulier estime les distances lui séparant de tous nœuds d'ancres fiables. Ces derniers sont bien choisis suite à une nouvelle stratégie de sélection d'ancre fiable qui assure une estimation précise de la distance rendant ainsi notre algorithme de localisation plus précise. Il est prouvé que l'algorithme proposé est réalisable dans les deux scénarios : deux et trois dimensionnel (2-D et 3-D). Un mécanisme d'économie d'énergie visant à améliorer la durée de vie de WSN est également envisagé dans ce chapitre. Il est prouvé que l'algorithme proposé pourrait facilement intégrer un tel mécanisme. Il est aussi montre que notre algorithme, qu'il soit combiné ou non avec le mécanisme d'économie d'énergie, surpasse constamment les meilleurs algorithmes de localisation représentatifs actuellement disponibles dans la littérature en ce qui concerne la précision, même dans le cas de distribution non uniforme des nœuds ou avec la présence de la phénomène de irrégularité de portée de transmission.

Abstract

An accurate localization algorithm tailored for anisotropic wireless sensors networks (WSN)s is proposed in this paper. Using the proposed algorithm, each regular or position-unaware node estimates its distances only to reliable anchors or position-aware nodes. The latter are properly chosen following a new reliable anchor selection strategy that ensures an accurate distance estimation making thereby our localization algorithm more precise. It is shown that the proposed algorithm is implementable in both 2-dimensional (2-D) and 3-dimensional (3-D) scenarios. A power saving mechanism aiming to enhance the WSN lifetime is also envisaged in this paper. It is proven that the proposed algorithm could easily incorporate such a mechanism. Simulations show that our algorithm, whether combined or not with for the power saving mechanism, consistently outperforms the best representative localization algorithms currently available in the literature in terms of accuracy, even with the presence of non-uniform node distribution or radiation irregularities.

3.1 Introduction

Due to their reliability, low cost, and ease of deployment, wireless sensor networks (WSNs) are emerging as a key tool for many applications such as environment monitoring, disaster relief, and target tracking [3]- [2]. A WSN is a set of small and low-cost sensor nodes with limited communication capabilities. The latter are often deployed in a random fashion to collect some physical phenomena from the surrounding environments such as temperature, light, pressure, etc. [2]. Due to their limited transmission ranges, the sensor nodes are often unable to directly communicate with a remote access point (AP). For this reason, they recur to multi-hop communication through several intermediate nodes that successively forward their gathered data to the AP. However, the sensing data are very often meaningless if the location from where they have been measured is unknown ; which makes their localization a fundamental and essential issue in WSNs. So far, many localization algorithms have been proposed in the literature and mainly fall into two categories : range-based and range-free.

To properly localize the regular or position-unaware nodes, range-based algorithms exploit the measurements of the received signal characteristics such as the time of arrival (TOA), the angle of

arrival (AOA), or the received signal strength (RSS) [6]-[6]. These signals are, in fact, transmitted by nodes having prior knowledge of their positions, called anchors (or landmarks). Although the range-based algorithms stand to be very accurate, they are unsuitable for WSNs. Indeed, these algorithms require high power to ensure communication between anchors and regular nodes which are small battery-powered units. Furthermore, additional hardware is usually required at both anchors and regular nodes, thereby increasing the overall cost of the network. Moreover, the performance of these algorithms can be severely affected by noise, interference, and/or fading. Unlike range-based algorithms, range-free algorithms, which rely on the network connectivity to estimate the regular node positions, are more power-efficient and do not require any additional hardware and, hence, are suitable for WSNs [4]-[29]. Due to these practical merits, range-free localization algorithms have garnered the attention of the research community. Unfortunately, in anisotropic environments where obstacles and/or holes may exist, range-free algorithms do not provide sufficient accuracy due to large errors occurring when mapping the hops into distance units. Indeed, in such environments, it is very likely that the shortest path between an anchor and a regular node is curved, thereby resulting in overestimation of the distance between these two nodes. The more obstacles and/or holes there are, the larger are distance estimation errors and, consequently, less accurate is localization.

In this paper, we propose a novel range-free localization algorithm tailored for anisotropic WSNs. Using the proposed algorithm, each regular node estimates its distances only to reliable anchors. The latter are properly chosen following a new reliable anchor selection strategy that ensures an accurate distance estimation thereby making our localization algorithm more precise. New average hop sizes' expressions are also developed in this paper for both 2-D and 3-D scenarios. We show that the obtained expressions are very accurate especially for high nodes densities. Furthermore, a power saving mechanism aiming to enhance the WSN lifetime is envisaged. We prove that our proposed algorithm could easily incorporate such a mechanism. Simulations show that our algorithm, whether combined or not with the power saving mechanism, consistently outperforms the best representative range-free localization algorithms currently available in the literature in terms of accuracy, even with the presence of non-uniform node distribution or radiation irregularities.

The rest of this paper is organized as follows : Section 4.2 describes the network model. Section 3.3 presents the related works and defines the motivation scenario. Section 3.4 proposes

a novel localization algorithm while Section 3.5 and 3.6 introduce a new reliable anchor selection strategy and a novel distance estimation technique, respectively. A power saving mechanism aiming to enhance the WSN lifetime is envisaged in Section 3.7. Simulation results are discussed in Section 3.8 and concluding remarks are made in section 5.6.

3.2 Network model

Fig. 6.1 illustrates the system model of N WSN nodes uniformly deployed in a 2-D square area S in the presence of a rectangle obstacle which makes the network topology C-shaped. All nodes are assumed to have the same transmission capability (i.e., range) denoted by R. Each node is able to directly communicate with any other node located in the disc having that node as a center and R as a radius, while it communicates in a multi-hop fashion with the nodes located outside. Due to the high cost of the global positioning system (GPS) technology, only a few nodes commonly known as anchors are equipped with it and, hence, are aware of their positions. The other nodes, called hereafter position-unaware or regular nodes for the sake of simplicity, are oblivious to this information. As shown in Fig. 6.1, the anchor nodes are marked with red triangles and the regular ones are marked with blue circles. If two nodes are able to directly communicate, they are linked with a dashed line that represents one hop. Let N_a and $N_u = N - N_a$ denote the number of anchors and regular nodes, respectively. Without loss of generality, let $(x_i, y_i)\,,\ i = 1, \ldots, N_a$ be the coordinates of the anchor nodes and $(x_i, y_i)\,,\ i = N_a + 1, \ldots, N$ those of the regular ones.

3.3 Related works and motivation

In order to localize the i-th regular node (i.e., $(N_a + i)$-th node), the distances between it and at least 3 anchors are usually required. The k-th anchor should then broadcast its coordinates (x_k, y_k) through the network. If the i-th regular node is located in the coverage area of this anchor (i.e., the disc $D(k, R)$ having the k-th anchor as center and R as radius), it receives the coordinates in $n_k = 1$ hop. Otherwise, it receives them after $n_k > 1$ hops. So far, in most previous algorithms, the i-th regular node estimates its distance to the k-th anchor $d_{k-(N_a+i)}$ using only

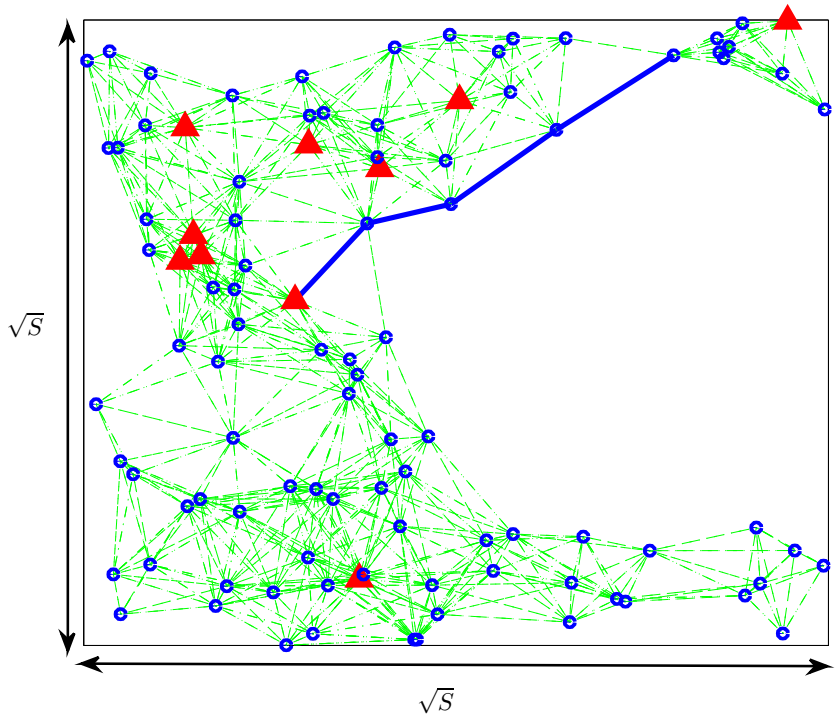

FIGURE 3.1 – Network model (C-shaped topology).

the information n_k as

$$\hat{d}_{k-(N_a+i)} = n_k \bar{h}_s \tag{3.1}$$

where $\bar{h}_s$ is a predefined average hop size. Note that this distance estimation approach relies on the fact that in highly dense WSNs,

$$d_{k-(N_a+i)} \approx \sum_{l=1}^{n_k} h_l, \tag{3.2}$$

holds. In (4.2), h_l is the l-th hop's distance. $\bar{h}_s$ is usually derived either analytically (i.e., $\bar{h}_s = \mathrm{E}\{h_l\}$) as with LAEP [13] or heuristically as with DV-Hop [4] by computing the mean hop size of all the shortest paths between anchors as follows

$$\bar{h}_s = \frac{1}{N_a(N_a-1)} \sum_{k=1}^{N_a} \sum_{j=1}^{N_a} \frac{d_{k-j}}{n_{k,j}} \tag{3.3}$$

where $n_{k,j}$ is the number of hops between the k-th and j-th anchors. Although heuristical and analytical algorithms are proven to be sufficiently accurate in isotropic WSNs (i.e., where obstacles do not exist), their accuracies substantially deteriorate in anisotropic WSNs (AWSN)s. Indeed, in such type of networks, it is very likely that the shortest paths between one regular

node and some anchors are not straight lines due to the presence of an obstacle, as can be observed from Fig. 3.2. This unfortunately causes an overestimation of the distances between the regular node and these anchors, when mapping the number of hops into distance, thereby hindering localization accuracy. In the example of Fig. 3.2, the regular node 1 communicates with the anchor node A_1 through $n_1 = 6$ hops. Its distance estimate to this anchor $\hat{d}_{k-(N_a+1)}$ is derived using (3.1). As can be seen from Fig. 3.2, if the blue obstacle does not exist, n_1 would be much less than 6 and, hence, the distance from i to A_1 is overestimated. Thus, using $\hat{d}_{k-(N_a+i)}$ when performing multilateration will undoubtedly result in an imprecise localization. An interesting approach to circumvent this issue is to properly select the anchors so that overestimation stemming from situations similar to the one illustrated in Fig. 3.2 is avoided or minimized. Based on this reliable anchor selection, several localization algorithms for AWSNs have been so far proposed such as pattern-driven in [20] and RAL in [29]. Despite their valuables to the advancement of knowledge and know-how in this key topic, we will later see that they still leave room for significant additional accuracy improvements in AWSNs.

In the following, we develop a novel localization algorithm based on new reliable anchor selection strategy and prove that it outperforms all the aforementioned algorithms.

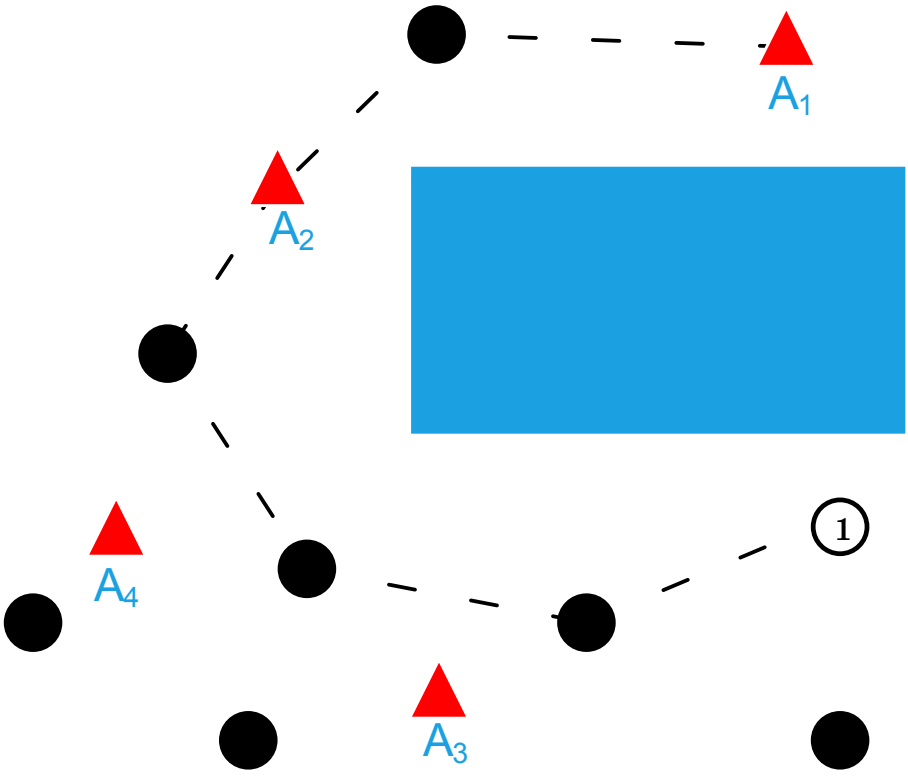

FIGURE 3.2 – Motivation scenario.

3.4 Proposed localization algorithm

As a first step of any anchor-based localization algorithm, the k-th anchor broadcasts through the network a message containing (x_k, y_k, n) where n is the hop-count value initialized to one. When a node receives this message, it stores the k-th anchor position as well as the received hop-count $n_k = n$ in its database, adds one to the hop-count value and broadcasts the resulting message. Once this message is received by an another node, its database information is checked. If the k-th anchor information exists and the received hop-count value n is smaller than the stored one n_k, the node updates n_k to n, increases it by 1, then broadcasts the resulting message. If n_k is smaller than n, the node discards the received message. However, when the node is oblivious to the k-th anchor position, it adds this information to its database and forwards the received message after increasing n by 1. This mechanism will continue until all nodes become aware of all anchors' positions and their corresponding minimum hop counts. In order to avoid the situation illustrated in Fig. 3.2, we propose a reliable anchor selection phase in the second step of our algorithm. In the next section, we introduce a new selection strategy where the k-th anchor properly selects a set of reliable anchors among all of those in the network denoted by s_k. The k-th anchor then broadcasts s_k over the network. Upon reception of all $(x_k, y_k, n_k, s_k),\ k = 1, \ldots, N_a$, each regular node estimates its distance only to its nearest anchor (i.e, $k_0 = \arg\min_k n_k$) and to the reliable anchors in the set s_{k_0}. The regular nodes finally compute their own positions exploiting their available distances' estimates by performing multilateration [22].

In what follows, we develop our proposed reliable anchor selection strategy as well as our distance estimation technique.

3.5 Reliable anchor selection strategy

After receiving all anchors' information, the k-th anchor becomes aware of its own position as well as those of all other anchors in the network and, hence, is able to compute all true distances separating it from the latter. On the other hand, this anchor could also compute the estimate of the distance to any other anchor j and the corresponding estimation error e_{k-j} stemming from the use of (3.1). Nevertheless, due to the anisotropic topology of the WSN considered here, errors could be too large if we fall in a situation such as in Fig. 3.2. Consequently, a threshold on

e_{k-j} is required to guarantee some reliability of the j-th anchor with respect to the k-th anchor. If the topology of the WSN were isotropic, the estimation error of the distance between these anchors would be

$$\begin{aligned} T_1 &= \hat{d}_{k-j} - d_{k-j} \\ &= \lceil \frac{d_{k-j}}{\bar{h}_s} \rceil \bar{h}_s - d_{k-j}, \end{aligned} \tag{3.4}$$

where the second line is due to the fact that $\hat{d}_{k-j}$ is obtained using (3.1). In (3.4), $\lceil x \rceil$ refers to the ceiling function. Thus, a distance estimation error higher than T_1 occurs only if the shortest path between the k-th and the j-th anchors is curved due to the presence of obstacles between the two nodes. In such a case, the number of hops between the latter is much larger than $d_{k-j}/\bar{h}_s$ and, hence, we should have $e_{k-j} \gg T_1$. Therefore, we chose T_1 as a threshold below/above which an anchor is deemed reliable or not, respectively. Finally, in order to ensure an accurate distance estimation, each regular node will estimate its distance only to the nearest anchor and to those rated reliable by the latter.

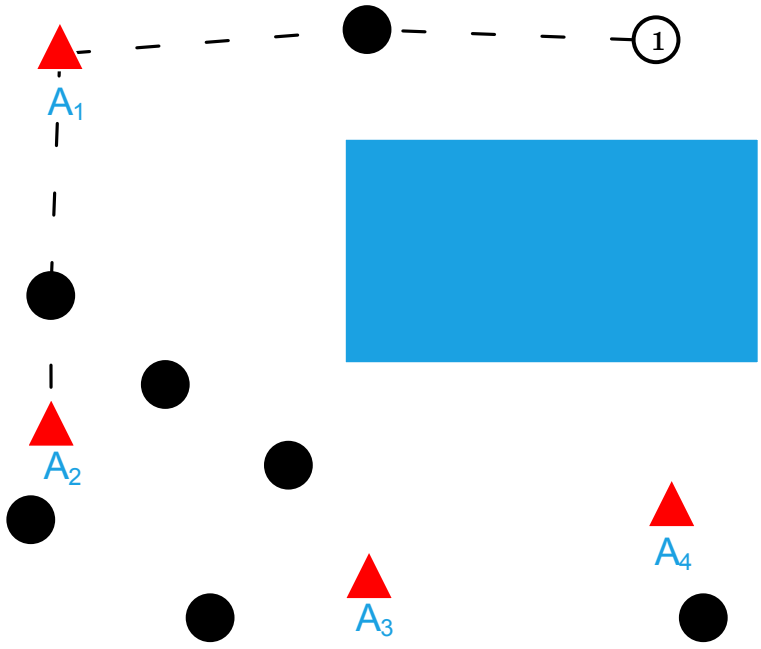

FIGURE 3.3 – Reliable anchors.

However, some anchors deemed reliable by the nearest anchor could be found unreliable by the regular node, since the shortest path from the latter to these anchors may be curved as shown in Fig. 3.3. To circumvent this issue, we implement a finer selection at the regular node that discards each anchor having a number of hops larger than $T_2 = \lceil \sqrt{2S}/R \rceil$. Note that T_2

Algorithm 2 Localization algorithm for anchor nodes

% k refers to the k-th anchor node %

$s_k = \{\}$

for j=1 to N_a and $j \neq k$ **do**

$\hat{d}_{k-j} = n_k \times \bar{h}_s$

$e_{k-j} = \hat{d}_{k-j} - d_{k-j}$

if $e_{k-j} \leq T_1$ **then**

$s_k = s_k \cup \{j\}$

end if

end for

Broadcast the set s_k of reliable anchors

Algorithm 3 Localization algorithm for regular nodes

% i refers to the i-th regular node %

% s_{k_i} is the set of the reliable anchors at the nearest anchor node from the i-th regular node%

% s_i is the new set of reliable anchors at the i-th regular node %

$s_i = \{\}$

$c = 0$

for $k \in s_{k_i}$ **do**

if $h_{i-k} \leq T_2$ **then**

$s_i = s_i \cup \{k\}$

$c = c + 1$

end if

end for

for $j = 1 \rightarrow c$ **do**

$\hat{d}_{j_i} = n_{j_i} \times \bar{h}_s$

end for

% j_i denotes the j-th reliable anchor node index in the set s_i %

% $\hat{x}_i$, and $\hat{y}_i$ can be estimated using multilateration. %.

is the maximum number of hops that may occur if the shortest path is not curved. Processing steps at the anchors and regular nodes are summarized by localization algorithms 2 and 3 listed in Algorithms 1 and 2, respectively.

3.6 Distance estimation technique

We propose in this work to estimate each regular-anchor distance using (3.1). To this end, one should accurately derive the average hop size $\bar{h}_s$ between any two consecutive nodes on the shortest path between any regular and anchor nodes. Let us consider a two-hop scenario where the k-th node communicates with the i-th node through an intermediate node j. In what follows, we denote by Z and X the random variables that represent the distances d_{k-j} and d_{k-i}, respectively. In order to derive

$$\bar{h}_s = \mathrm{E}\left\{Z\right\}, \tag{3.5}$$

we start by deriving the conditional cumulative distribution function (CDF) $F_{Z|X}(z)$ of Z with respect to X.

3.6.1 Two-dimensional (2-D) case

As can be shown from Fig. 3.4, $Z \leq z$ is guaranteed only if there are no nodes in the area $B_z = F - A_z$ where $F = D(k,R) \cap D(i,R)$, $A_z = F \cap D(k,z)$ and $D(\cdot,\star)$ is the disc having the $\cdot$-th node as a center and $\star$ as a radius. It is noteworthy that F is nothing but the forwarding zone area where any potential intermediate node must exist. $F_Z(z)$ can be then defined as

$$F_{Z|X}(z)(z) = P\left(Z \leq z|x\right) = P\left(\mathrm{E}_0\right), \tag{3.6}$$

where $P(\mathrm{E}_0)$ is the probability that the event $\mathrm{E}_0 = \{\text{no nodes in the area } B_Z\}$ occurs. Since the nodes are uniformly deployed in S, the probability of having K nodes in B_z follows a Binomial distribution $\mathrm{Bin}(N,p)$ where $p = \frac{B_z}{S}$. For relatively large N and small p, it can be readily shown that $\mathrm{Bin}(N,p)$ can be accurately approximated by a Poisson distribution $\mathrm{Pois}(\lambda B_z)$ where $\lambda = N/S$ is the average nodes density in the network. Consequently, for a large number of nodes N and small p, we have

$$F_{Z|X}(z) = e^{-\lambda B_z}. \tag{3.7}$$

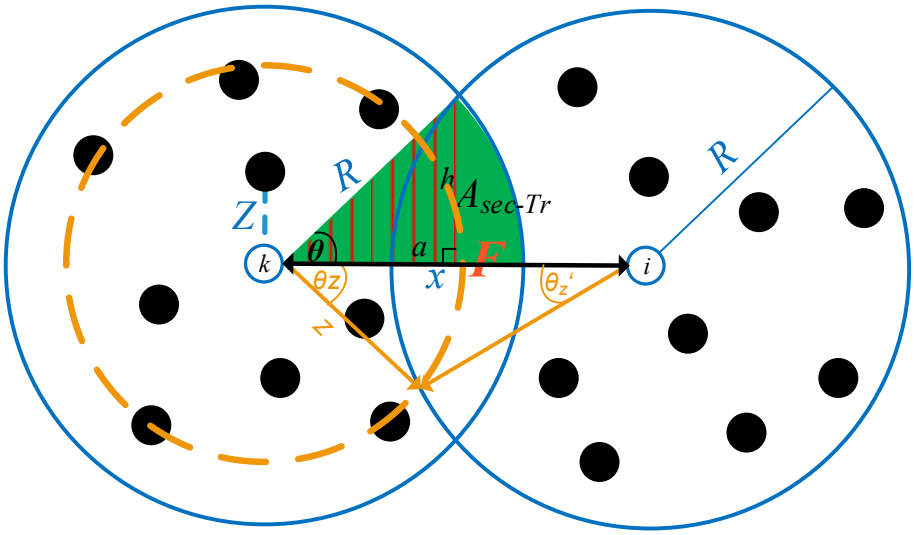

FIGURE 3.4 – 2-D distance analysis.

As can be seen from Fig. 3.4, $F = 4A_{\text{Sec}-\text{Tr}}$ where $A_{\text{Sec}-\text{Tr}}$ is the green sector area minus the dashed triangle area. Please note that this equality holds only when the two circles have the same radius R (i.e., the k-th and j-th nodes have the same transmission capability). F is then given by

$$\begin{aligned} F &= 2(R^2\theta - a \times h) \\ &= 2R^2\left(\theta - \frac{\sin(2\theta)}{2}\right). \end{aligned} \tag{3.8}$$

Following the same approach as above, A_z can be obtained as

$$A_z = z^2\left(\theta_z - \frac{\sin(2\theta_z)}{2}\right) + R^2\left(\theta_z' - \frac{\sin(2\theta_z')}{2}\right). \tag{3.9}$$

Furthermore, using some geometrical properties, we easily show that

$$\theta_z = \sqrt{\frac{z + R\left(1 - 2\cos\left(\theta\right)\right)}{2R\left(1 - \cos\left(\theta\right)\right)}}\theta, \tag{3.10}$$

and

$$\theta_z' = \sqrt{\frac{R - z}{2R\left(1 - \cos\left(\theta\right)\right)}}\theta. \tag{3.11}$$

Substituting (3.10) and (3.11) in (3.9) and using (3.8), we have

$$B_z = R^2\left(2\theta - \sin\left(2\theta\right) - \theta_z' + \frac{\sin(2\theta_z')}{2}\right) - z^2\left(\theta_z - \frac{\sin(2\theta_z)}{2}\right). \tag{3.12}$$

Substituting (3.12) in (3.7) and using the resulting CDF to compute the mean of the random variable Z yields to

$$\bar{h}_s^{2D} = R - \frac{3}{\pi}\int_0^{\frac{\pi}{3}}\int_0^R e^{-\lambda B_z} dz d\theta. \tag{3.13}$$

Note in (3.13) that we use the fact that $\theta \in [0, \pi/3]$ since $\theta = \arccos(x/2R)$ where $x \in]R, 2R]$. It follows from (3.13) that $\bar{h}_s^{2D}$ increases with the nodes density λ. This is expected since it is very likely that the per-hop distance increases when the number of nodes located inside F increases if, of course, R is fixed. From (3.13), $\bar{h}_s^{2D}$ is also an increasing function of R. Fig. 3.5

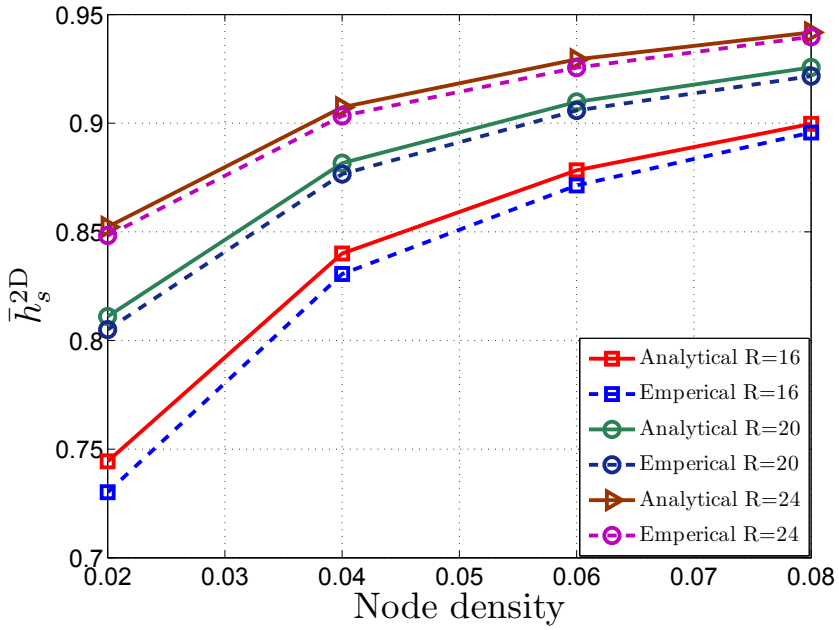

FIGURE 3.5 – Analytical and empirical results of $\bar{h}_s^{2D}$.

plots $\bar{h}_s^{2D}$ versus λ for different values of R. From this figure, the analytical $\bar{h}_s^{2D}$ approaches its empirical counterpart for small λ while the two curves almost coincide when the latter is large. This is expected since the approximation of Bin (N, p) by Pois (λF) becomes more accurate as λ grows large. Fig. 3.5 also shows that $\bar{h}_s^{2D}$ increases with λ and R, which corroborates the above discussion.

3.6.2 Three-dimensional (3-D) case

Since each node is able to communicate with any other node located at most at R meters from it, its transmission coverage in the 3-D case is spherical. Let us denote by V the forwarding

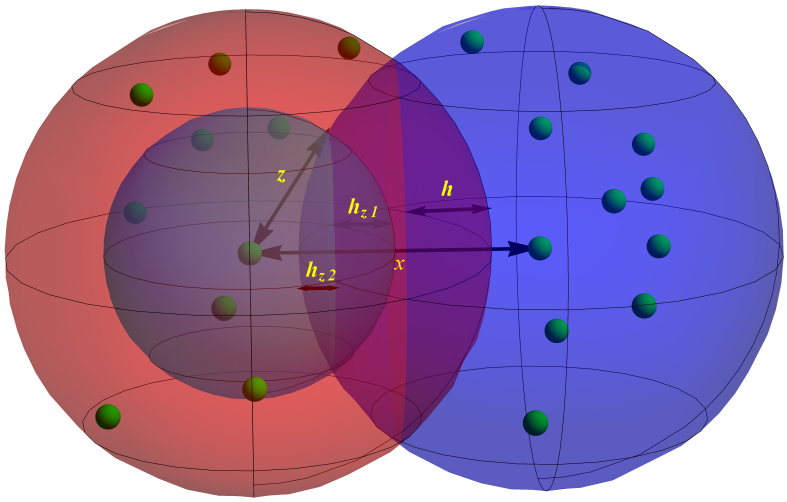

FIGURE 3.6 – 3-D distance analysis.

zone defined as $V = S(k,R) \cap S(i,R)$ where $S(\cdot,\star)$ is the sphere having the $\cdot$-th node as a center and $\star$ as a radius. In 3-D case, the CDF $F_{Z|X}(z)$ is then given by

$$F_{Z|X}(z) = e^{-\lambda_v (V - V_z)}, \tag{3.14}$$

where $V_z = S(k,z) \cap S(i,R)$, $\lambda_v = N/V_{\mathrm{T}}$, and V_{T} is the total volume where the WSN is deployed. As can be shown from Fig. 3.6, $V = 2V_{\mathrm{c}}$ where V_{c} is the volume of the spherical cap with height

$$h = \frac{2R - x}{2}. \tag{3.15}$$

Therefore, V is given by

$$V = \frac{1}{12}\pi (2R - x)^2 (4R + x). \tag{3.16}$$

As far as V_z is concerned, from Fig. 3.6, it is the sum of the volumes of two spherical caps with heights

$$h_{z1} = \frac{(R - z + x)(R + z - x)}{2x} \tag{3.17}$$

$$h_{z2} = \frac{(R - x + z)(-R + x + z)}{2x}. \tag{3.18}$$

V_z is then given by

$$V_z = \frac{\pi (R - x + z)^2 ((x - z)(x + 3z) + 2R(x + 3z) - 3R^2)}{12x}. \tag{3.19}$$

Substituting (3.16) and (3.19) in (3.14) and using the resulting CDF, we obtain

$$\bar{h}_s^{3\mathrm{D}} = R - \frac{1}{R} \int_R^{2R} \int_0^R e^{-\lambda_v (V - V_z)} dz dx. \tag{3.20}$$

From (3.20), $\bar{h}_s^{3D}$ is an increasing function of λ_v and R. This observation is further verified by the empirical results in Fig. 3.7.

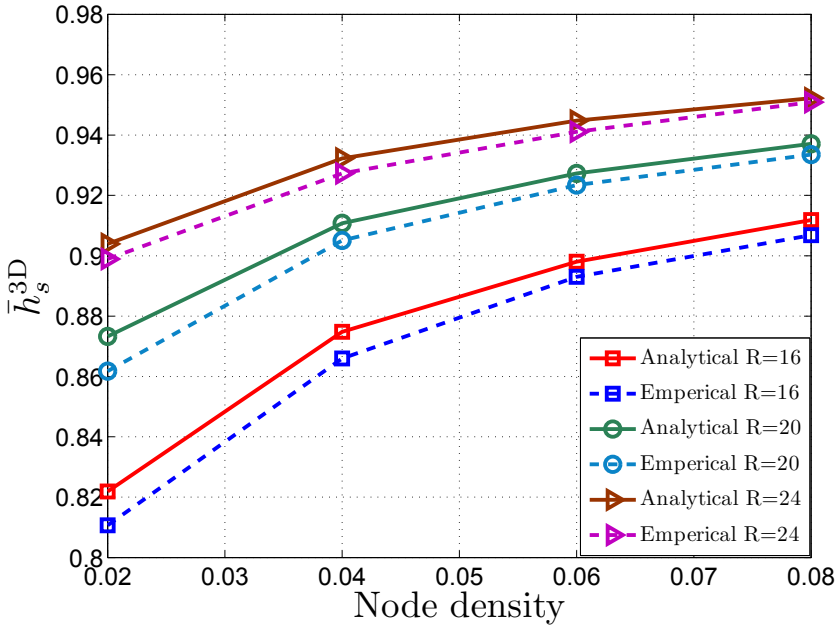

FIGURE 3.7 – Analytical and empirical results of $\bar{h}_s^{3D}$.

3.7 Power saving mechanism

In order to provide the required operational power, WSN nodes are usually equipped with batteries or energy harvesting devices. However, the batteries have a very limited capacity while energy harvesting using the technologies so far developed is not only very expensive, especially if embedded in large scale WSNs, but also unable to provide the sufficient amount of energy. This makes power saving a crucial mechanism in WSNs. If such a mechanism is not taken into account during the localization process, it may hinder localization accuracy. In what follows, we will show how a power saving mechanism could be easily incorporated in our proposed localization algorithm. Although several power saving mechanisms exist in the literature, we are only concerned in this paper by the most basic mechanism which consists on switching periodically each node between the awake (i.e.,power on) and the sleep (i.e., power off) states to save power and, hence, increase the WSN lifetime. Using this mechanism, the time is equally divided into cycles where each node independently decides whether to be awake or sleep. This

causes the randomization of the number of available (i.e, in the awake state) nodes assumed to be equal to N in (3.13) and (3.20) may hinder localization accuracy. To circumvent this issue, we propose to substitute N in these two equations by the average number of available nodes N_{av}. Assuming that the time required to perform the proposed algorithm does not exceed one cycle, N_{av} is given by

$$N_{\text{av}} = \sum_{i=1}^{N} p_i^{\text{aw}}, \tag{3.21}$$

where p_i^{aw} is the probability that the i-th node is in the awake state. If this probability is the same across the network (i.e., $p_i^{\text{aw}} = p^{\text{aw}},\ i = 1, \ldots, N$), N_{av} would be reduced to Np_i^{aw}. Using the latter result in (3.13) and (3.20) yields to

$$\bar{h}_s^{\text{2D}} = R - \tfrac{3}{\pi} \int_0^{\frac{\pi}{3}} \int_0^R e^{-\lambda p^{\text{aw}} B_z} dz d\theta, \tag{3.22}$$

and

$$\bar{h}_s^{\text{3D}} = R - \frac{1}{R} \int_R^{2R} \int_0^R e^{-\lambda_v p^{\text{aw}} (V - V_z)} dz dx, \tag{3.23}$$

respectively.

3.8 Simulations results

In this section, we evaluate by simulations the performance of the proposed algorithm in terms of localization accuracy using Matlab. These simulations are conducted to compare, under the same network settings, the proposed algorithm with some of the best representative localization algorithms currently available in the literature, i.e., DV-Hop [4], RAL [29], and pattern-driven [20]. Simulations are run both in 2-D and 3-D cases. In the 2-D case, nodes are assumed to be uniformly deployed in a square area $S = 10^4\ m^2$ and in a cubic volume $V = 10^4 m^3$ in the 2-D and 3-D cases, respectively. Besides to the C-shaped network topology in Fig. 6.1, we consider two other anisotropic topologies commonly used in the context of WSN : W-shaped and S-shaped topologies as depicted in Fig. 3.8(a) and Fig. 3.8(b), respectively.

As an evaluation criterion, we propose to use the normalized root mean square error (NRMSE) defined as follows

$$e = \frac{\sum_{i=1}^{N_u} \sqrt{(x_i - \hat{x}_i)^2 + (y_i - \hat{y}_i)^2}}{N_u R}. \tag{3.24}$$

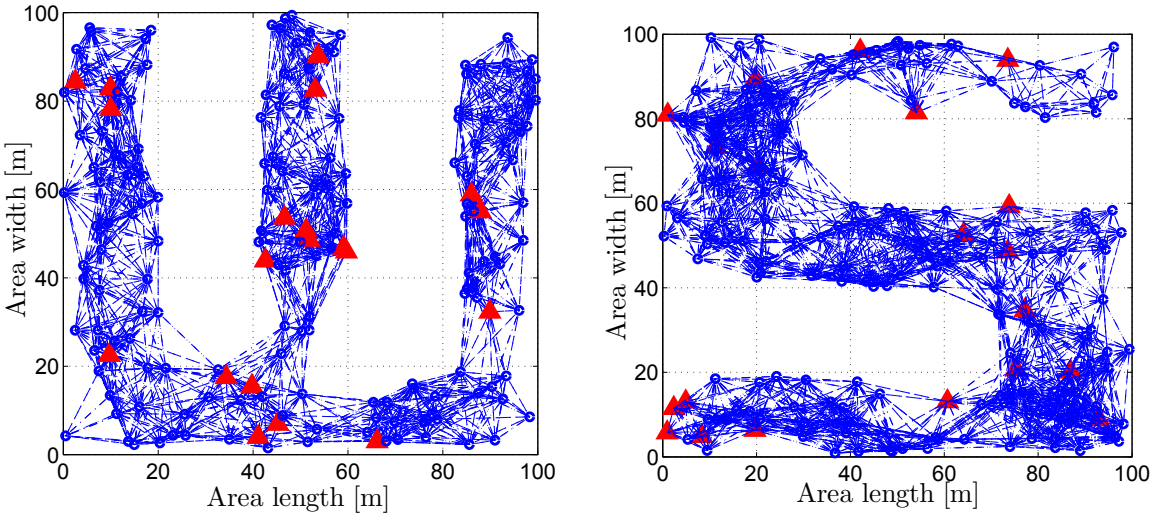

(a) W-Shaped network topology

(b) S-shaped network topology

FIGURE 3.8 – Anisotropic WSN topologies.

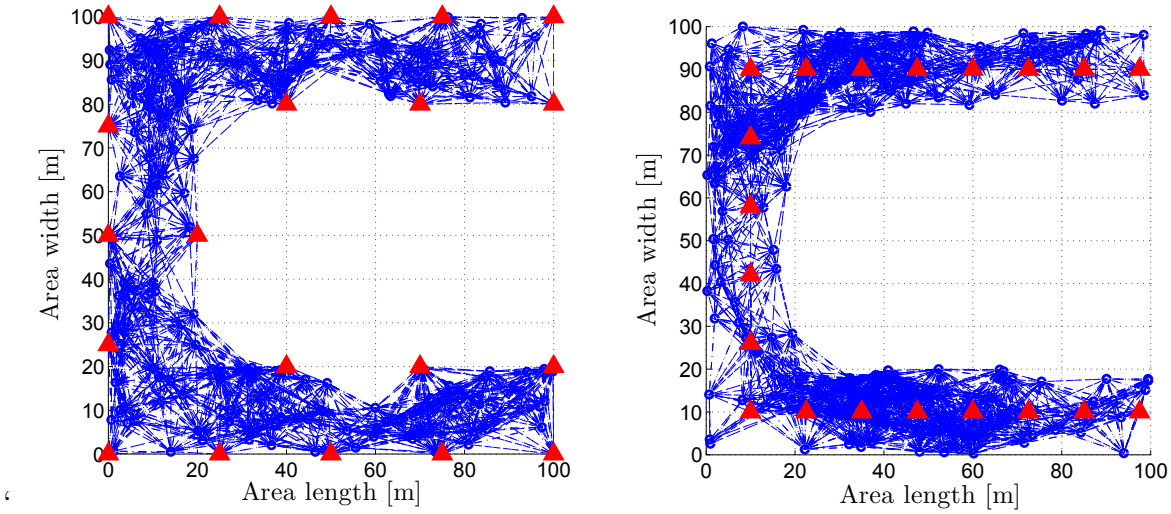

(a) Perimeter.

(b) Grid.

FIGURE 3.9 – Anchors' placements illustrated C-Shape topology.

All the following results are obtained by averaging over 100 trials.

Fig. 3.10 plots the localization NRMSE achieved by DV-Hop, RAL, pattern-driven, and our proposed algorithm versus the node density with a constant number of anchors set to be 20 in C-, W-, and S-shaped network topologies. Figs. 3.10(a), 3.10(c), and 3.10(e) provide the results of the 2-D case, while Figs. 3.10(b), 3.10(d), and 3.10(f) provide those of the 3-D case. As

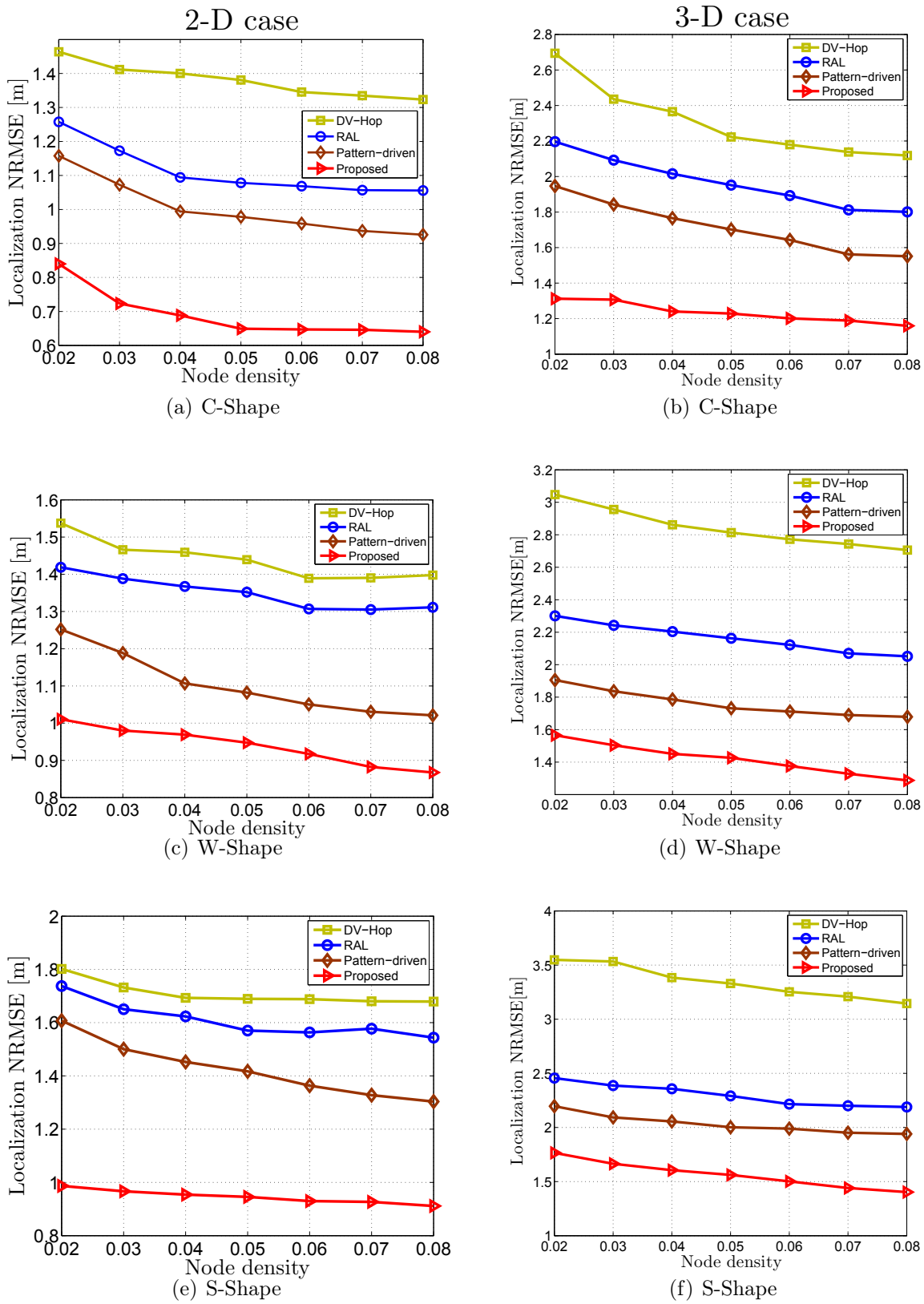

FIGURE 3.10 – Localization NRMSE vs. node density with $N_a = 20$ in C-, W-, and S-shaped network topologies in 2-D and 3-D cases.

can be shown from these figures, the proposed algorithm always outperforms its counterparts. Indeed, in the 2-D case (3-D case), it is until about 80% (180%), 70% (100%), and 60% (60%) more accurate than DV-Hop, RAL, and pattern-driven, respectively. Furthermore, our algorithm achieves almost the same performance in the three network topologies while DV-Hop's, RAL's, and driven-pattern's performance, which are already poor in the C-shaped topology, severely deteriorate in the W-shaped topology, more so in the S-shaped topology.

Fig. 3.11 shows the NRMSEs' standard deviations achieved by all localization algorithms for different node densities in the C-, W-, and S-shaped network topologies. Figs. 3.11(a), 3.11(c), and 3.11(e) provide the results of the 2-D case, while Figs. 3.11(b), 3.11(d), and 3.11(f) provide those of the 3-D case. As can be seen from these figures, the NRMSEs' standard deviations achieved by DV-Hop, RAL, and driven-pattern slightly decrease when the node density increases while the one achieved by the proposed algorithm substantially decreases. This means that implementing our algorithm in any network topology guarantees an accurate localization for any given realization. This result is very interesting in terms of implementation strategy, since it proves that the result in Fig. 3.10 becomes more and more meaningful as λ grows large.

Fig. 3.12 illustrates the localization NRMSE's CDF achieved by DV-Hop, RAL, pattern-driven, and our proposed algorithm with $N = 200$ and $N_a = 20$ in the C-, W-, and S-shaped network topologies. Figs. 3.12(a), 3.12(c), and 3.12(e) provide the results of the 2-D case, while Figs. 3.12(b), 3.12(d), and 3.12(f) provide those of the 3-D case. Using the proposed algorithm, until 80% (90%) of the regular nodes could estimate their position within twice the transmission range in the 2-D case (3-D case). In contrast, until 38% (10%) and 42% (60%) of the nodes achieve the same accuracy with RAL and pattern-driven, respectively, and about 0% (10%) with DV-Hop. This further proves the efficiency of our new algorithm.

Fig. 3.13 plots the localization NRMSEs achieved by our proposed algorithm and its counterparts versus the anchors number with $N = 200$ in the C-, W-, and S-shaped network topologies in both 2-D and 3-D cases. As can be observed from this figure, all algorithms become more accurate as the number of anchors in the network increases. From Fig. 3.13, the NRMSE achieved by the proposed algorithm decreases more rapidly than those achieved by DV-Hop, RAL and pattern-driven. This is expected since the number of potentially reliable anchors increases with the total number of anchors and, hence, localization is more accurate. This is in contrast with DV-Hop in which each regular node estimates its distance to all anchors (i.e., even those

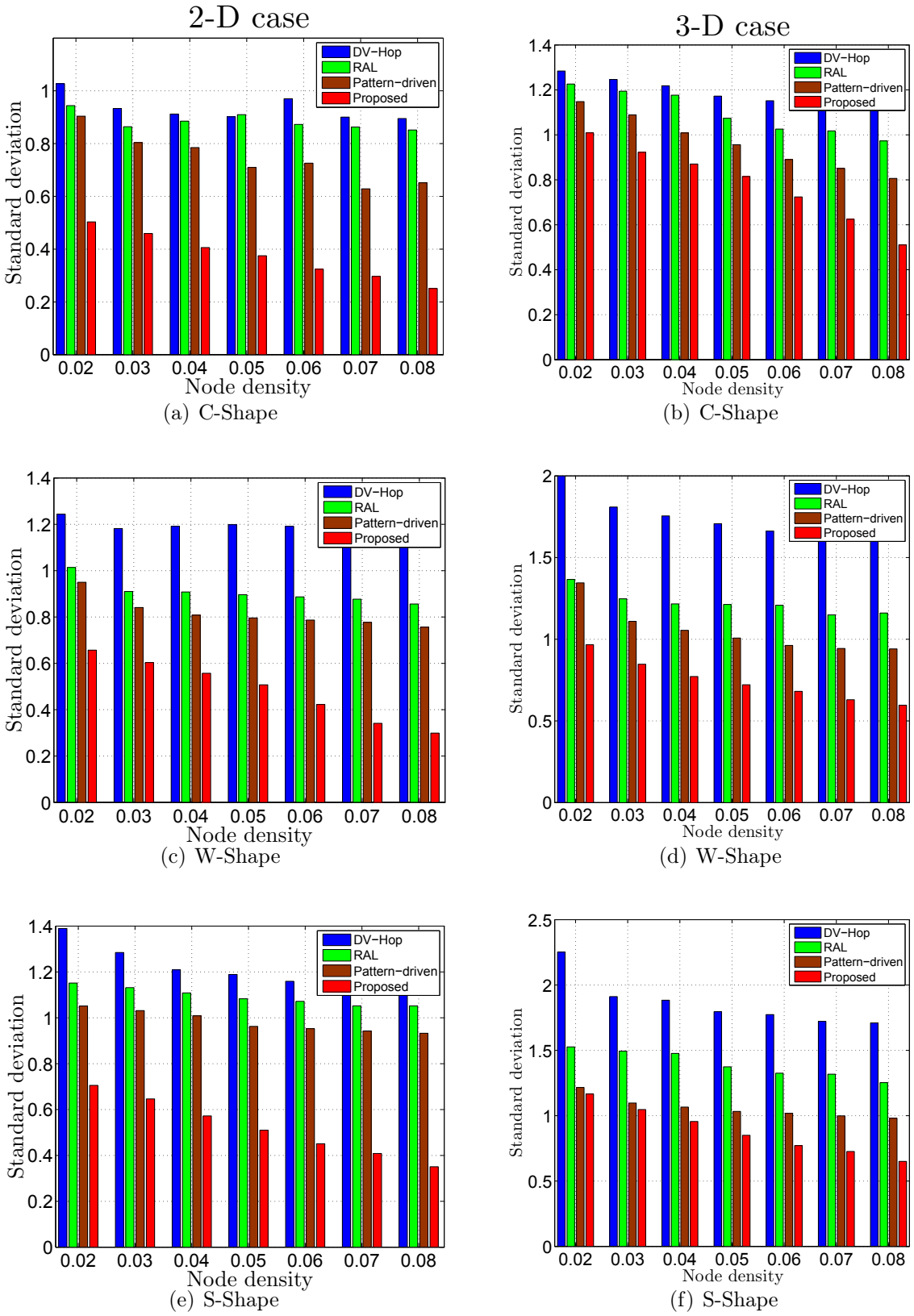

FIGURE 3.11 – Localization NRMSE's standard deviation vs. node density with $N_a = 20$ in C-, W-, and S-shaped network topologies for 2-D and 3-D cases.

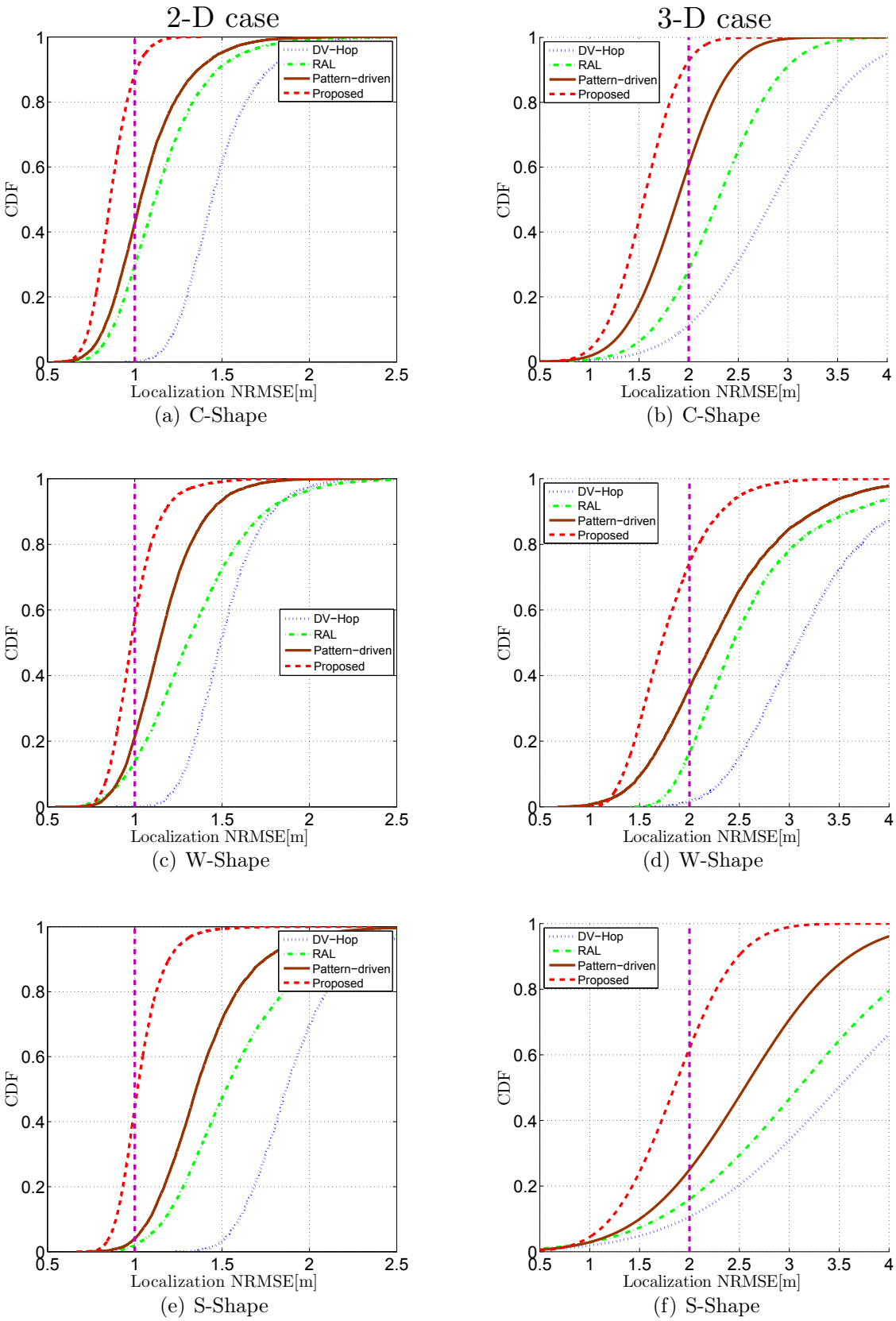

FIGURE 3.12 – Localization NRMSE's CDF with $N = 200$ and $N_a = 20$ in C-, W-, and S-shaped network topologies in 2-D and 3-D cases.

with curved shortest path) in the network, thereby hindering localization accuracy. The fact that the NRMSE achieved by the proposed algorithm decreases more rapidly than that achieved by pattern-driven an RAL proves that our anchors selection strategy is more reliable and efficient than that in [20] and [29].

Fig. 3.14 displays the localization NRMSEs achieved by the proposed algorithm and its counterparts versus p^{aw} in the C-, W-, and S-shaped network topologies in both 2-D and 3-D cases. As can be observed from this figure, localization accuracy of each algorithm improves when p^{aw} increases. This is expected since the number of potentially available nodes increases with p^{aw} and, hence, the nodes density increases. Furthermore, from Fig. 3.14, if the proposed algorithm accounts for the power saving mechanism, its achieved NRMSE remains almost constant when p^{aw} increases. This highlights another advantage of our algorithm over its counterparts, namely its ability to efficiently incorporate a power saving mechanism.

Fig. 3.15 plots the localization NRMSEs achieved by the proposed algorithm and its counterparts versus the nodes density with different anchors placement strategies : perimeter, grid and random as depicted in Figs. 3.9(a), 3.9(b), and 3.8, respectively. This figure shows that the grid anchors' placement is the most efficient strategy in W- and S-shaped topology while the random anchors' placement is best in the C-shaped topologies. This result is very interesting since it proves that the performance of each strategy is closely related to the network topology. In other words, if the latter is known beforehand, we will be able to select the appropriate strategy when deploying the WSN.

Figs. 3.16 and 3.17 plot the localization NRMSEs achieved by the proposed algorithm and its counterparts versus the nodes density and the degree of range irregularity (DoI), respectively. In Fig. 3.16, a non-uniform nodes' deployment is assumed while, in Fig. 3.17, the transmission range is no longer assumed circular. A range irregularity model similar to that in [8] was implemented instead. From these figures, the localization NRMSEs achieved by all algorithms deteriorate due to both non-uniform nodes' deployment and range irregularity. This is expected since these phenomena are not taken into account when designing the proposed algorithm and its counterparts. However, as could be observed from Figs. 3.16 and 3.17, the proposed algorithm remains more accurate than its counterparts. This further proves the increased robustness of our proposed algorithm to model imperfections.

3.9 Conclusion

In this paper, we proposed a novel range-free localization algorithm tailored for anisotropic WSNs. Using the proposed algorithm, each regular node estimates its distances to reliable anchors only. The latter are properly chosen following a new reliable anchor selection strategy that ensures an accurate distance estimation thereby making our localization algorithm more precise. New average hop sizes' expressions were also developed in this paper for both 2-D and 3-D scenarios. We showed that the obtained expressions are very accurate especially for high nodes densities. Furthermore, a power saving mechanism aiming to enhance the WSN lifetime was envisaged. We proved that our proposed algorithm could easily incorporate such a mechanism. Simulations showed that our algorithm, whether combined or not with the power saving mechanism, consistently outperforms the best representative range-free localization algorithms currently available in the literature in terms of accuracy, even with the presence of non-uniform node distribution or radiation irregularities.

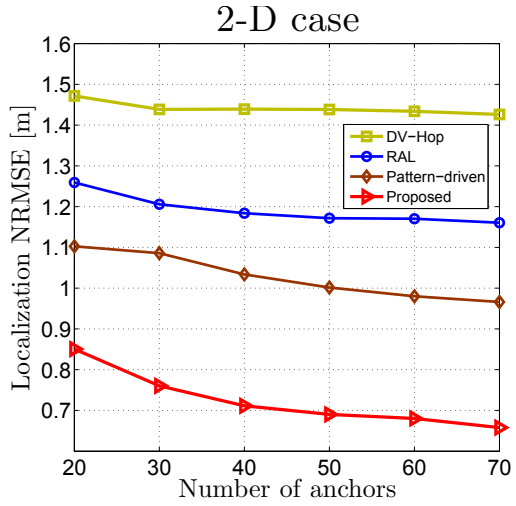

(a) C-Shape

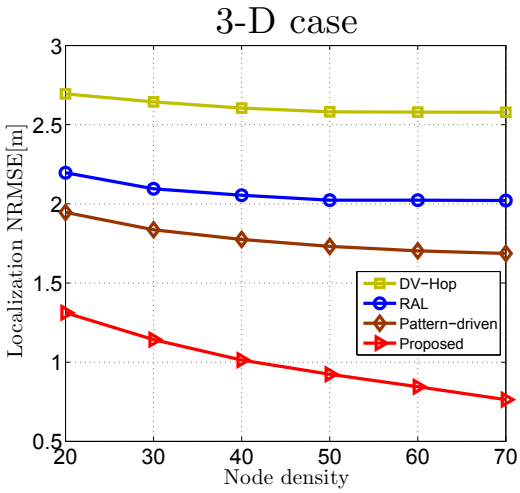

(b) C-Shape

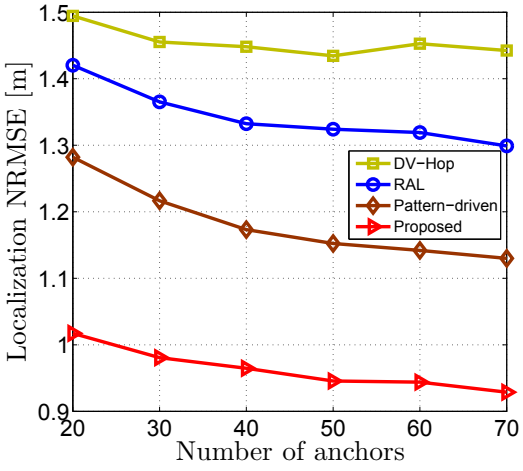

(c) W-Shape

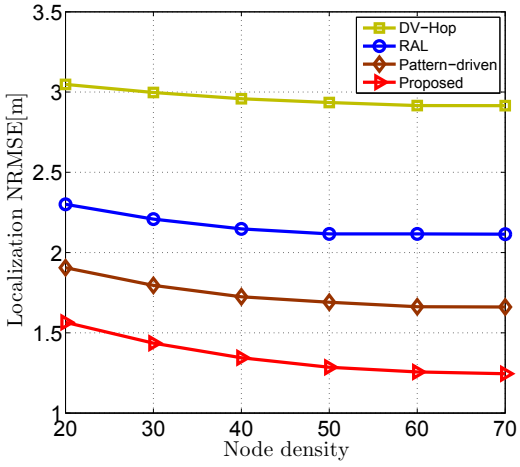

(d) W-Shape

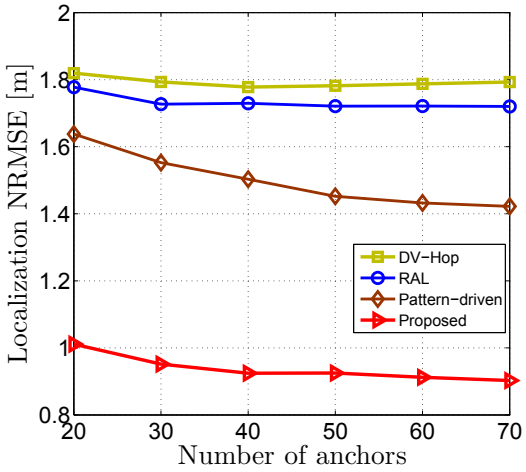

(e) S-Shape

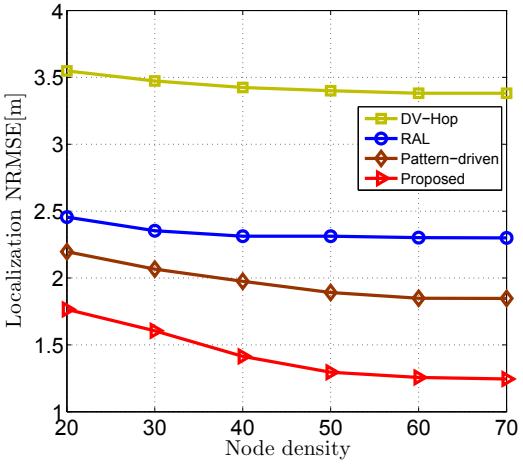

(f) S-Shape

FIGURE 3.13 – Localization NRMSE vs. anchors number with $N = 200$ in C-, W-, and S-shaped network topologies in 2-D and 3-D cases.

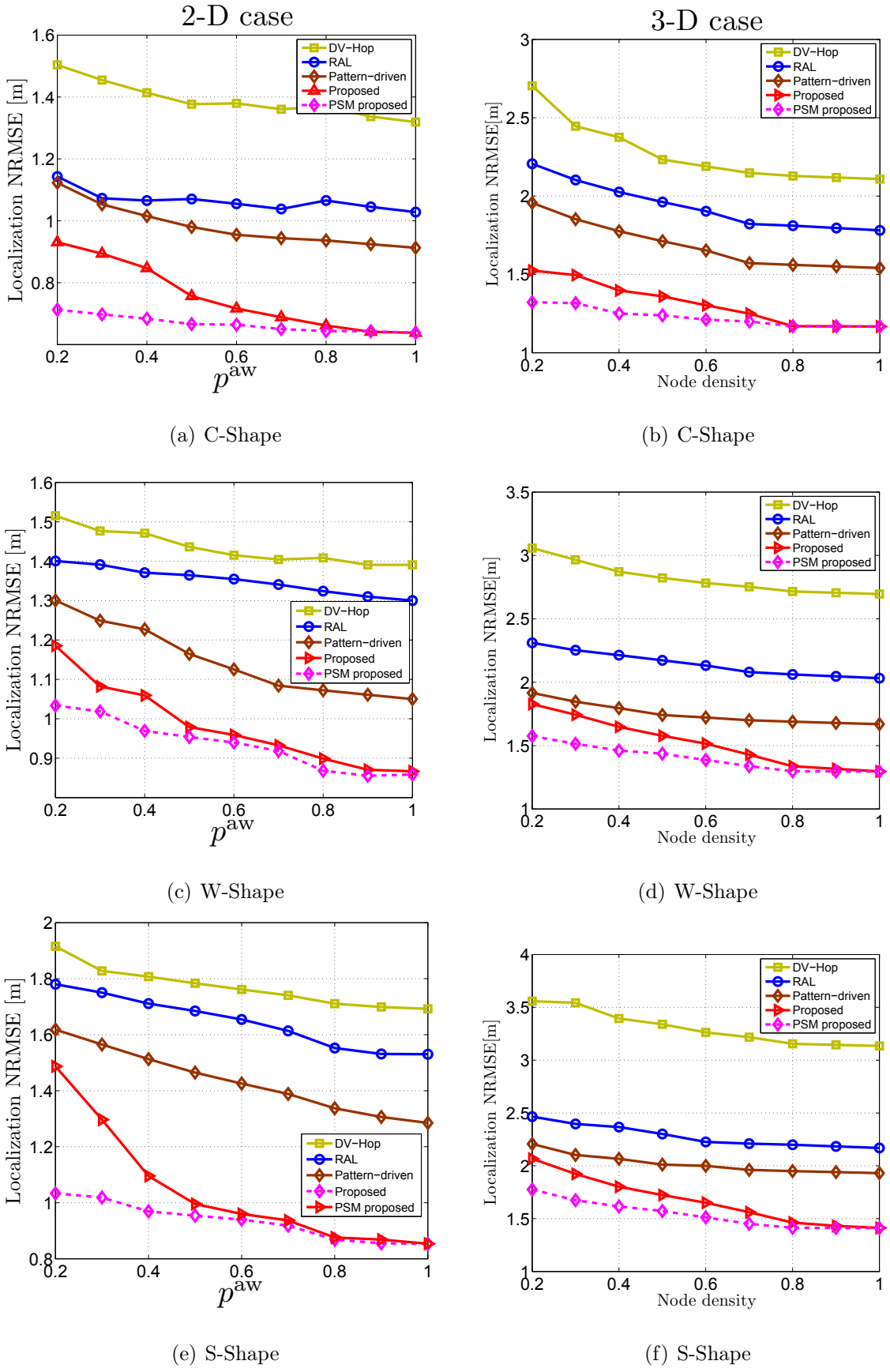

(a) C-Shape

(b) C-Shape

(c) W-Shape

(d) W-Shape

(e) S-Shape

(f) S-Shape

FIGURE 3.14 – Localization NRMSE vs. p^{aw} in C-, W-, and S-shaped network topologies in 2-D and 3-D cases.

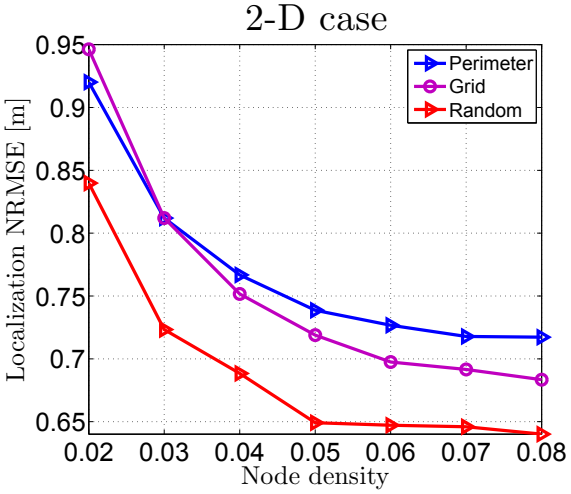

(a) C-Shape.

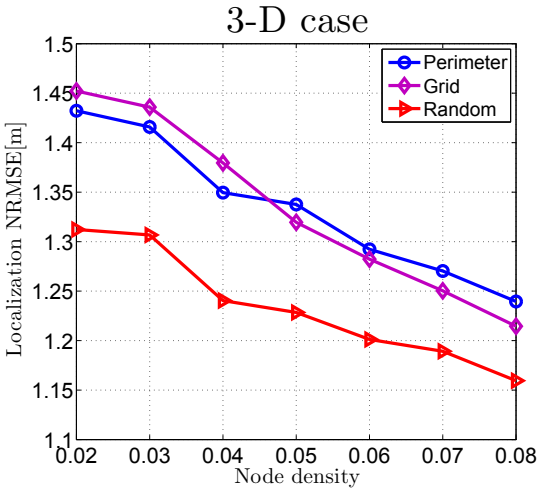

(b) C-Shape.

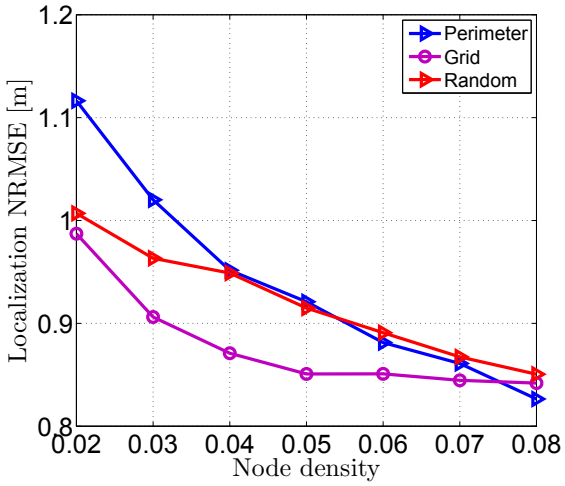

(c) W-Shape.

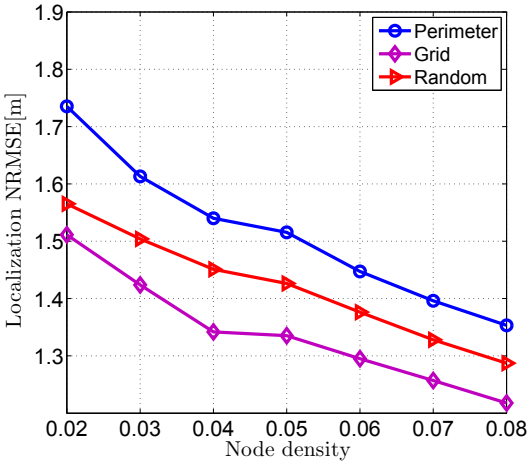

(d) W-Shape.

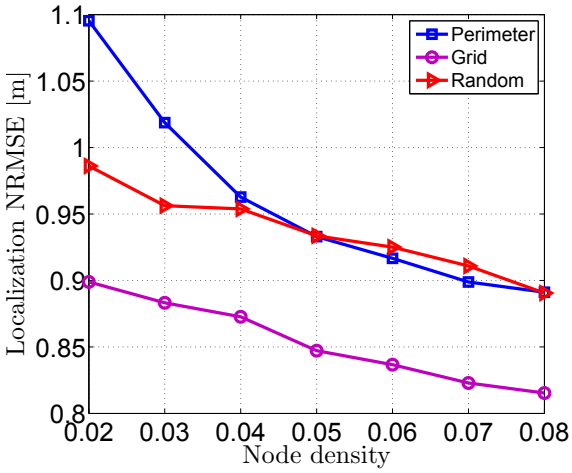

(e) S-Shape.

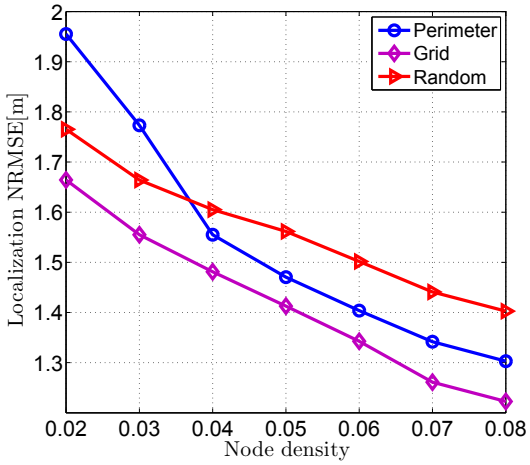

(f) S-Shape.

FIGURE 3.15 – Proposed algorithm's NRMSE vs. anchors' placements in C-, W-, and S-shaped network topologies in 2-D and 3-D cases.

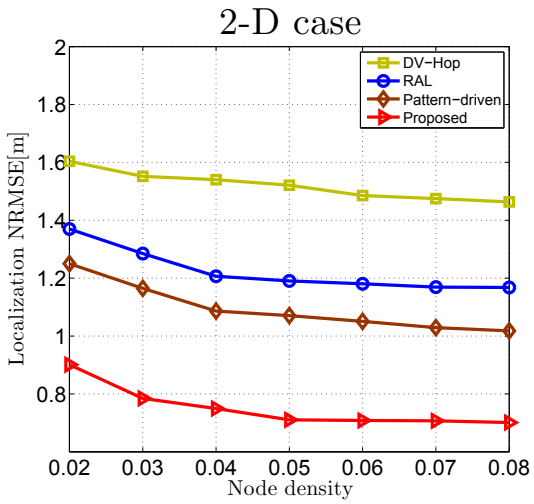

(a) C-Shape

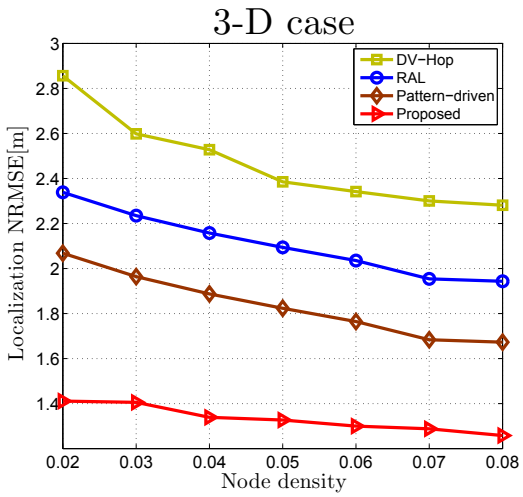

(b) C-Shape

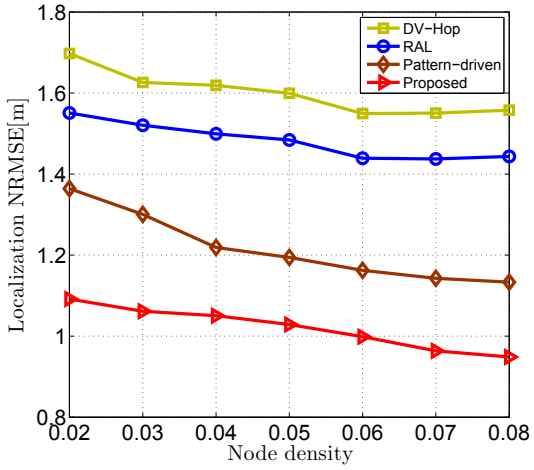

(c) W-Shape

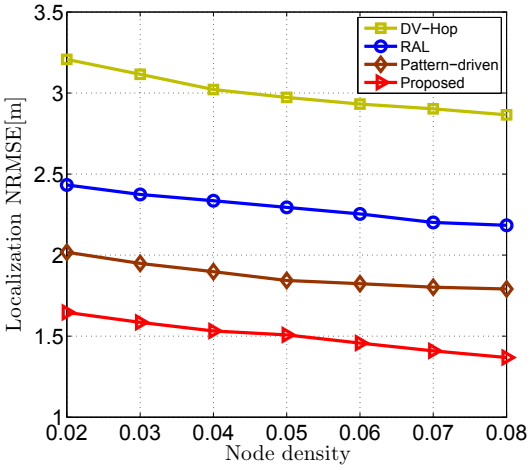

(d) W-Shape

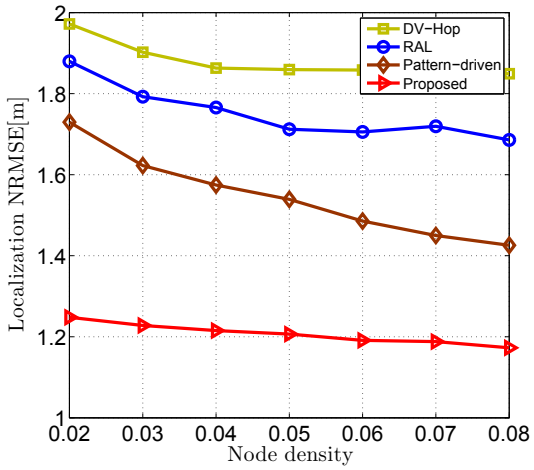

(e) S-Shape

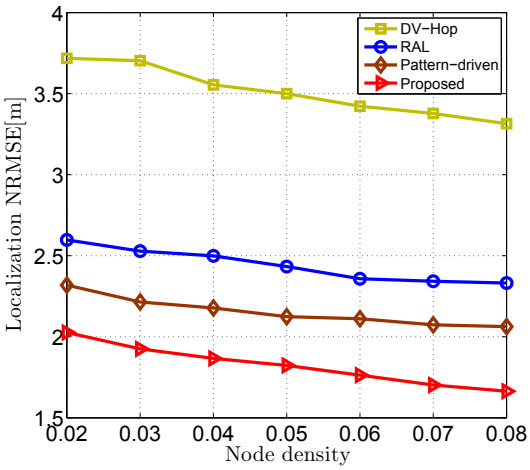

(f) S-Shape

FIGURE 3.16 – Localization NRMSE with $N_a = 20$ assuming non-uniform nodes' deployment in C-, W-, and S-shaped network topologies in 2-D and 3-D cases.

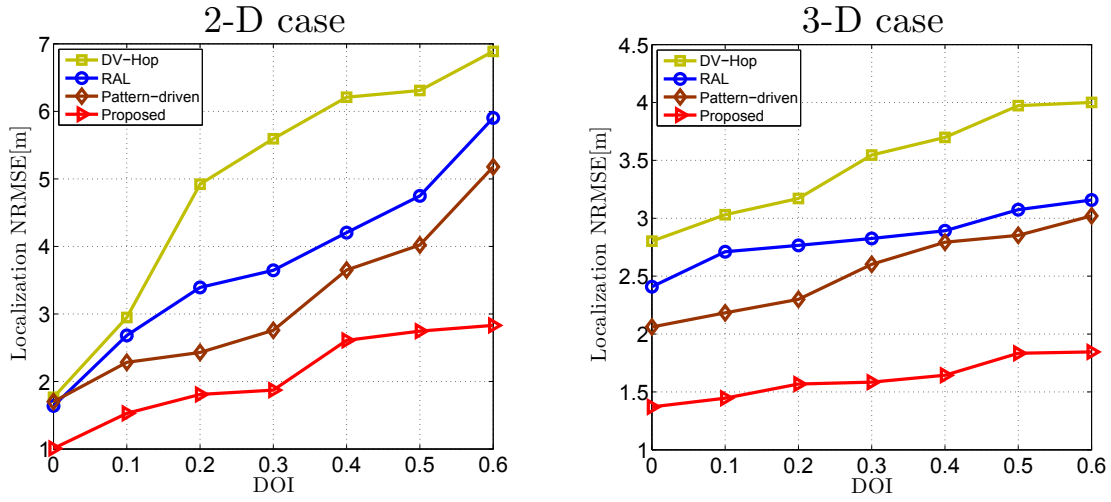

(a) C-Shape (b) C-Shape

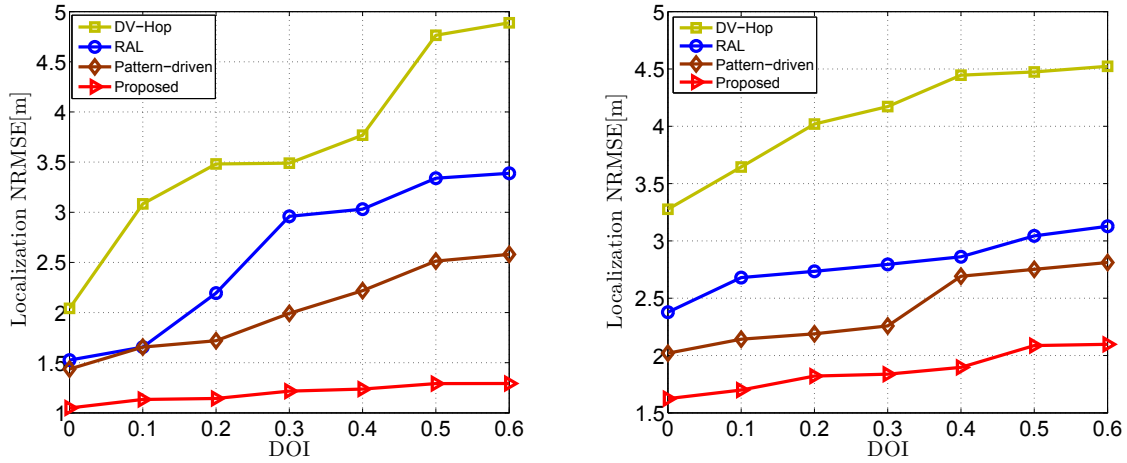

(c) W-Shape (d) W-Shape

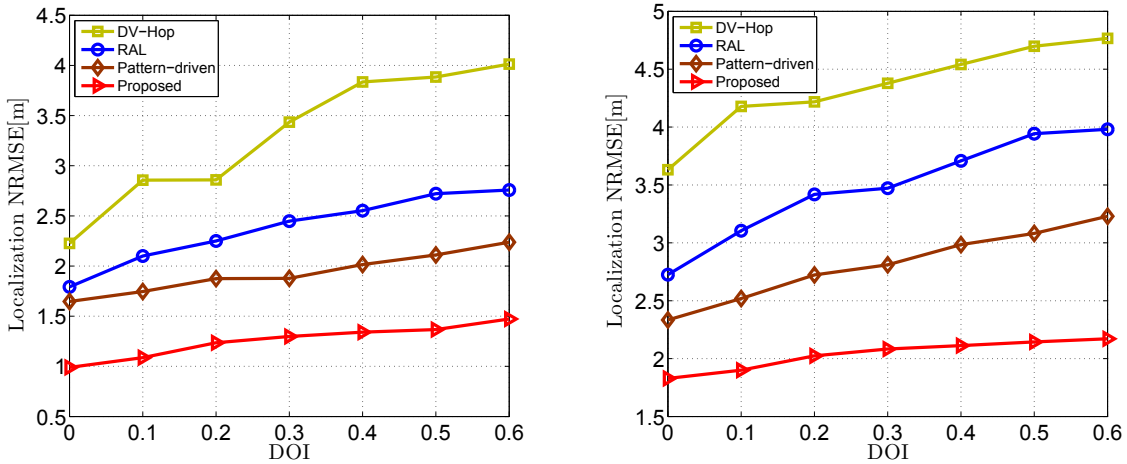

(e) S-Shape (f) S-Shape

FIGURE 3.17 – Localization NRMSE vs. DOI with $N = 200$ and $N_a = 20$ in C-, W-, and S-shaped network topologies in 2-D and 3-D cases.

Bibliographie

[1] F. Gustafsson and F. Gunnarsson, "Mobile Positioning Using Wireless Networks : Possibilities and Fundamental Limitations Based on Available Wireless Network Measurements," *IEEE Signal Process. Mag.,* vol. 22, no. 4, pp. 41-53, July 2005.

[2] W. Zhang and G. Cao, "DCTC : Dynamic Convoy Tree-Based Collaboration for Target Tracking in Sensor Networks," *IEEE Trans. Wireless Commun.* vol. 3, no. 5, pp. 1689-1701, September 2004.

[3] F. Akyildiz, W. Su, Y. Sankarasubramaniam, and E. Cayirci, "A Survey on Sensor Networks," *IEEE Commun. Mag.,* vol. 40, no. 8, pp. 102-114, August 2002.

[4] N. Patwari, A. O. Hero III, M. Perkins, N. S. Correal and R. J. O'Dea, "Relative Location Estimation in Wireless Sensor Networks," *IEEE Trans. Signal Process.,* vol. 51, no. 8, pp. 2137-2148, August 2003.

[5] D. Niculescu and B. Nath, "Ad Hoc Positioning System (APS) Using AOA," *IEEE INFOCOM'2003,* vol. 3, pp. 1734-1743, 2003.

[6] H. Ren and M. Q.-H. Meng, "Power Adaptive Localization Algorithm for Wireless Sensor Networks Using Particle Filter," *IEEE Trans. Veh. Techno.,* vol. 58, no. 5, pp. 2498-2508, June 2009.

[7] D. Niculescu and B. Nath, "Ad hoc Positioning System (APS)," *Proc. IEEE GlobeCom'2001,* Nov. 25-29, 2001.

[8] A. El Assaf, S. Zaidi, S. Affes, and N. Kandil, "Efficient Range-Free Localization Algorithm for Randomly Distributed Wireless Sensor Networks," *IEEE GLOBECOM'2013,* Atlanta, USA, Dec. 9-13 2013.

[9] L. Gui, T. Val, A. Wei, "Improving Localization Accuracy Using Selective 3-Anchor DV-Hop Algorithm," *Proc. IEEE VTC'2011,* San Francisco, USA, Septembre 5-8, 2011.

[10] A. Boukerche, H. A. B. F. Oliveira, E. F. Nakamura, A. A. F. Loureiro,"DV-Loc : a Scalable Localization Protocol using Voronoi Diagrams for Wireless Sensor Networks," *IEEE Wireless. Commun. Mag.,* vol. 16, no. 2, pp. 50-55, April 2009.

[11] D. Ma, M.J. Er, B. Wang , "Analysis of Hop-Count-Based Source-to-Destination Distance Estimation in Wireless Sensor Networks with Applications in Localization," *IEEE Trans. Veh. Techno.,* vol. 59, no. 6, pp. 2998-3011, July 2010.

[12] A. El Assaf, S. Zaidi, S. Affes, and N. Kandil, "Range-Free Localization Algorithm for Heterogeneous Wireless Sensors Networks," *IEEE WCNC'2014,* Istanbul, Turkey, Apr. 6-9, 2014.

[13] Y. Wang, X. Wang, D. Wang, and D. P. Agrawal, "Range-Free Localization Using Expected Hop Progress in Wireless Sensor Networks," *IEEE Trans. Parallel Distrib. Syst.,* vol. 25, no. 10, pp. 1540-1552, October 2009.

[14] L. Kleinrock and J. Silvester, "Optimum Transmission Radii for Packet Radio Networks or Why Six is a Magic Number," *Proc. IEEE NTC '1978,* Dec. 4-6, 1978.

[15] H. Takagi and L. Kleinrock, "Optimal Transmission Ranges for Randomly Distributed Packet Radio Terminals," *IEEE Trans. Commun.,* vol. 32, no. 3, pp. 246-257, March 1984.

[16] J. C. Ku and W. Liao, "Hop Count Distribution of Multihop Paths in Wireless Networks with Arbitrary Node Density : Modeling and its Applications," *IEEE Trans. Veh. Techno.,* vol. 56, no. 4, pp. 2321-2331, July 2007.

[17] M. Li and Y. Liu,, "Rendered Path : Range-Free Localization in Anisotropic Sensor Networks with Holes," *IEEE/ACM Trans. Netw.,* vol. 18, no. 1, pp. 320-332, February 2010.

[18] S. Zhang, J. Wang, X. Liu, J. Cao, "Range-free selective multilateration for anisotropic wireless sensor networks," *IEEE SECON'2012,* Seoul, South Korea, June 18-21 2012.

[19] S. Lee, B. Koo, S. Kim, "RAPS : Reliable Anchor Pair Selection for Range-Free Localization in Anisotropic Networks," *IEEE Commun. Lett.,* vol. 18, no. 8, pp. 1403-1406, July 2014.

[20] Q. Xiao, B. Xiao, J. Cao, J. Wang, "Multihop Range-Free Localization in Anisotropic Wireless Sensor Networks : A Pattern-Driven Scheme," *IEEE Trans. Mobile Comput.,* vol. 9, no. 11, pp. 1592-1607, November 2010.

[21] B. Xiao, L. Chen, Q. Xiao, and M. Li , "Reliable Anchor-Based Sensor Localization in Irregular Areas," *IEEE Trans. Mobile Comput.,* vol. 9, no. 1, pp. 60-72, January 2010.

[22] D. E. Manolakis, “Efficient Solution and Performance Analysis of 3-D Position Estimation by Trilateration,” *IEEE Trans. Aerosp. Electron. Syst.,* vol. 32, no. 4, pp. 1239-1248, October 1996.

[23] S. Biaz, Ji. Yiming, Q. Bing, Wu. Shaoen, “Realistic radio range irregularity model and its impact on localization for wireless sensor networks," *IEEE WiCOM'2005,* Wuhan, China, Sept. 23-26 2005.

[24] C. Bettstetter, “On the Connectivity of Ad Hoc Networks," *The Computer Journal,* vol. 47, no. 4, pp. 432-447, July 2004.

[25] C. Bettstetter, “On the Connectivity of Wireless Multihop Networks with Homogeneous and Inhomogeneous Range Assignment," *IEEE VTC'2002-Fall,* Vancouver, Canada, Sept. 24-28, 2002.

Chapitre 4

Accurate Range-Free Localization in Multi-Hop Wireless Sensor Networks

Slim Zaidi, Ahmad El Assaf, Sofiène Affes and Nahi Kandil

Accepted for publication in *IEEE Transactions on Communications,* July 2016.

Résumé : Jusqu'à présent, tous les algorithmes de localisation de type *range-free* exploitent une seule information (i.e., nombre de saut, taille moyenne de saut, etc.) pour localiser les capteurs. Afin de pousser la précision de localisation, ce chapitre propose un nouvel algorithme de localisation qui prend en compte non seulement l'information de nombre de sauts entre les nœuds réguliers et les nœuds des ancres mais aussi des informations déjà fournies par les nœuds intermédiaire (à savoir, relais) entre chaque ancre et nœud régulier. En tant que tel, nous développons un nouvel algorithme de localisation *range-free*. En tenant compte les positions des nœuds d'ancre l'expression analytiquement exacte de la moyenne de l'erreur de l'estimation de positon (LEE) a été calculée pour la première fois en *closed-form* dans ce chapitre. Il est démontré que la performance de notre algorithme proposé surpasse les meilleurs algorithmes représentatifs de la littérature en termes de précision. Contrairement à ce dernier, nous montrons en outre qu'il est en mesure d'atteindre une moyenne et une variance de LEE autour de 0 dans les réseaux très denses, réalisant ainsi une précision sans précédent parmi les techniques *range-free*.

Abstract

To localize wireless sensor networks (WSN)s nodes, only the hop-based information (i.e., hops' number, average hop size, etc.) have been so far exploited by range-free techniques, with poor-accuracy, however. In this paper, we show that localization accuracy may greatly benefit from joint exploitation, at no cost, of the information already provided by the forwarding nodes (i.e., relays) between each anchor (i.e., position-aware) and sensor nodes pair. As such, we develop a novel range-free localization algorithm, derive its average location estimation error (LEE) in closed-form, and compare it in LEE performance with the best representative algorithms in the literature. We show that the proposed algorithm outperforms them in accuracy. In contrast to the latter, we further prove that it is able to achieve a LEE average and variance of about 0 when the number of sensors is large enough, thereby achieving an unprecedented accuracy performance among range-free techniques.

4.1 Introduction

Recent advances in wireless communications and low-power circuits technologies have led to proliferation of wireless sensor networks (WSNs). A WSN is a set of small and low-cost sensor nodes often equipped with small batteries. The latter are often deployed in a random fashion to sense or collect from the surrounding environments some physical phenomena such as temperature, light, pressure, etc. [1]-[3]. Since power is a scarce resource in such networks, sensors usually recur to multi-hop transmission in order to send their gathered data to an access point (AP). However, the received data at the latter are often fully or partially meaningless if the location from where they have been measured is unknown [4], making the sensors' localization an essential task in multi-hop WSNs. Designed to comply with such networks, many localization algorithms exist in the literature [5]-[30]. To properly localize each sensor, most of these algorithms require the distance between the latter and at least three position-aware nodes called hereafter anchors [1]. Since it is very likely in multi-hop WSNs that some sensors be unable to

1. In practice, an anchor node refers to a sensor, base station, or a nearby access point (AP) with known position. This information is usually acquired using global positioning system (GPS) technology, configured or manually entered into the node memory prior to deployment.

directly communicate with all anchors, the distance between each anchor-sensor pair is usually estimated using their shortest path. This distance is in fact approximated by the sum of the distances between any consecutive intermediate nodes located on the shortest path between the two nodes. The localization algorithms based on such an approximation are commonly known in the literature as connectivity-based or range-free algorithms [5]-[30]. Depending on the process used to estimate the distances between the intermediate nodes, range-free algorithms may fall into three categories : measurement-based, heuristic, and analytical [5]-[30].

Measurement-based algorithms exploit the measurements of the received signals' characteristics such as the received signal strength (RSS) [5] or the time of arrival (ToA) [6], etc. Using the RSS measurement, the distance between any sensors' pair could be obtained by converting the power loss due to propagation from a sensor to another based on some propagation laws. Unfortunately, due to the likely presence of noise and interference, the distance's estimate would be far from being accurate, thereby leading to unreliable sensor localization accuracy. Using the ToA measurement, both sensor and anchor nodes require high-resolution clocks and extremely accurate synchronization between them [2]. While the first requirement may dramatically increase the cost and the size of every node, the second results in severe depletion of their power due to the additional overhead required by such a process. Furthermore, in the presence of noise and/or multipath, the ToA measurement is severely affected thereby hindering sensors' localization accuracy.

As far as heuristic algorithms [4]-[12] are concerned, most of them are based on variations of the DV-HOP technique [4], whose implementation in multi-hop WSNs requires the computation of the average hop size (i.e., average distance between any two consecutive intermediate nodes) h_{av} to estimate the distance between a sensor and an anchor as $n_h h_{\text{av}}$ where n_h is the number of hops between the two nodes. Such algorithms have, however, a major drawback. Indeed, h_{av} is computed in a non-localized manner and broadcasted in the network by each anchor. This incurs undesired prohibitive overhead and power consumption, thereby increasing the overall cost of the localization process.

More popular alternatives suitable for multi-hop WSNs are the analytical algorithms [13]-[30]

2. Please note that advanced ToA-based algorithms known as round-trip (i.e., two-way) ToA algorithms do not require any synchronization between nodes [31], [32]. However, this advantage comes at the cost of additional overhead which becomes prohibitive especially in multi-hop WSNs, making the round-trip ToA algorithms unsuitable for such networks.

which evaluate theoretically h_{av} using the statistical characteristics of the network deployment. The obtained h_{av} is actually locally computable at each regular node, thereby avoiding the unnecessary overhead and power consumption incurred by heuristic techniques if, likewise, it had to be broadcasted in the network. In spite of their valuable contributions, the localization algorithms developed so far in [13]-[30] do not provide unfortunately sufficient accuracy, due to large errors occurred when mapping n_h into distance units. This is primarily caused by the lack of information provided by both h_{av} and n_h. Actually, the distance between an anchor-sensor pair depends not only on the latter hop-based information, but also on the number m of forwarding [3] nodes (i.e., which forward any data between the two nodes). Indeed, when n_h and the total nodes' number are fixed, the distance increases (decreases) if m increases (decreases). Consequently, if this easily-obtained information is taken into account when designing a localization algorithm, its accuracy would definitely be improved.

Hence we propose in this paper, a novel analytical localization algorithm that properly exploits m alongside the hop-based information, derive its average location estimation error (LEE) in closed-form, and compare it in LEE performance with the best representative algorithms in the literature. We show that the proposed algorithm outperforms them in accuracy. In contrast to the latter, we further prove that it is able to achieve a LEE average and variance of about 0 when the number of sensors is large enough, thereby achieving an unprecedented accuracy performance among range-free techniques.

The rest of this paper is organized as follows : Section 4.2 describes the system model and discusses the motivation for this work. Section 4.3 proposes a new approach aiming to estimate the distance between any anchor-sensor pair. A novel localization algorithm for multi-hop WSNs is introduced in section 5.4. Its accuracy is analyzed in Section 4.5. Simulation results are discussed in Section 5.5 and concluding remarks are made in Section 5.6.

4.2 Network model and motivation

Fig. 4.1 displays the system model of M anchor and N sensor nodes deployed in a 2-D square area S. The anchors[1] are aware of their positions while the sensors are oblivious to this

3. Note that a forwarding node between an anchor-sensor pair is a node able to forward any data between the two nodes without being necessary on the shortest path. An intermediate node on this path is then a forwarding node but the reciprocal does not hold true.

information. These sensors are assumed to be uniformly distributed in S. All anchor and sensor

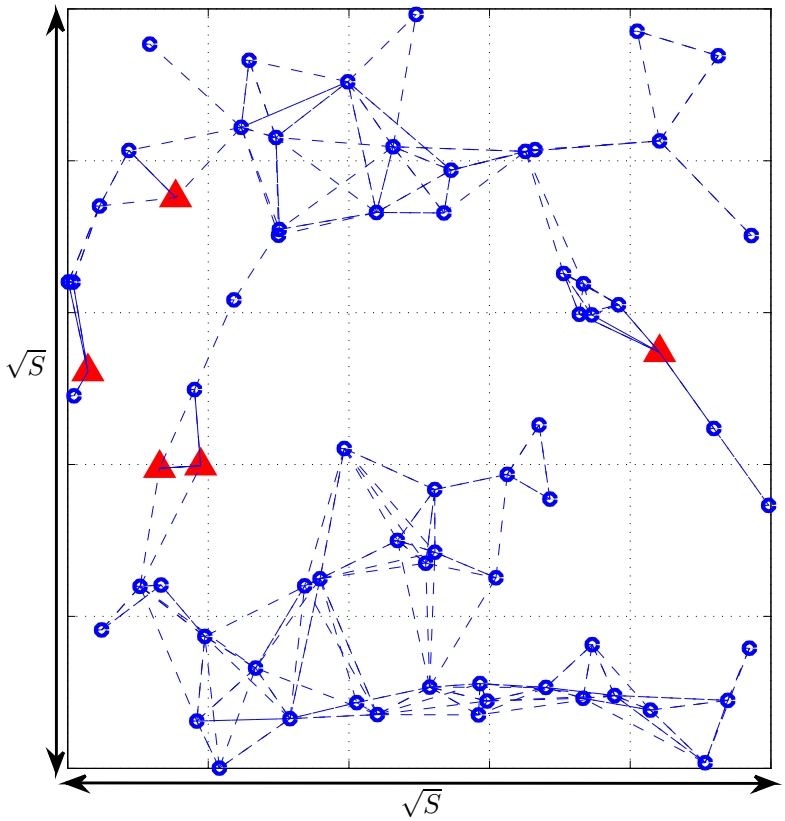

FIGURE 4.1 – Network model.

nodes are assumed to have the same range (i.e., transmission capability) denoted by R. Each node is then able to directly communicate with any other node located in the disc having that node as a center and R as a radius, while it communicates in a multi-hop fashion with the nodes located outside it. As shown in Fig. 4.1, the anchors are marked with red triangles and the sensors are marked with blue circles. If two nodes are able to communicate directly, they are linked with a dashed line that represents one hop. Let $(x_i, y_i)\,,\ i = 1, \ldots, N$ be the coordinates of the sensors and $(a_k, b_k)\,,\ k = 1, \ldots, M$ be those of the anchors.

In what follows, we propose an efficient anchor-based localization algorithm aiming to accurately estimate the sensors' positions. Such an algorithm requires that the latter estimate their distances to at least 3 anchors and be aware of their coordinates. The k-th anchor should then broadcast its coordinates (a_k, b_k) through the network. If the i-th sensor is located at a distance less than or equal to R from that anchor, it receives the coordinates in $n_h = 1$ hop. Otherwise,

it receives them after $n_h > 1$ hops. So far, in most previous algorithms, the i-th sensor estimates its distance to the k-th anchor d_{i-k} using only the information n_h as

$$\hat{d}_{i-k} = n_h h_{\text{av}}, \tag{4.1}$$

where h_{av} is a predefined average hop size. Note that this distance estimation (DE) approach relies on the fact that in highly dense WSNs,

$$d_{i-k} \approx \sum_{l=1}^{n_h} h_l, \tag{4.2}$$

holds. In (4.2), h_l is the l-th hop's distance. Unfortunately, this approach exhibits a major drawback. Indeed, h_{av} is usually derived either analytically (i.e., $h_{\text{av}} = \mathrm{E}\{h_l\}$) by exploiting the Poisson Limit Theorem valid for high nodes densities [13]-[30] or heuristically by computing the mean hop size of all the shortest paths between anchors as in [4]

$$h_{\text{av}} = \frac{1}{M(M-1)} \sum_{k=1}^{M} \sum_{l=1}^{M} \frac{\sqrt{(a_k - a_l)^2 + (b_k - b_l)^2}}{n_{k,l}}, \tag{4.3}$$

where $n_{k,l}$ is the number of hops between the k-th and l-th anchors. It is then very likely that h_{av} be different from the mean hop size of the shortest path between the k-th anchor and the i-th sensor (i.e., $h_{\text{av}} \neq \left(\sum_{l=1}^{n_h} h_l\right)/n_h$ and, hence, large DE errors may occur, thereby hindering the i-th sensor's localization accuracy. This motivates us to seek for more efficient DE approach for exploitation by our localization algorithm.

4.3 Proposed DE approach

In this work, we propose to exploit, in addition to n_h, another easily obtained information, in order to reduce the distance estimation error, thereby improving the localization accuracy. According to the parity of n_h, we distinguish below between two cases and develop two different approaches suitable for each case.

4.3.1 n_h is even

For simplicity, let us first assume that $n_h = 2$. Let $D_k(R)$ and $D_i(R)$ be the discs with radius R and having, respectively, the k-th anchor and the i-th sensor as centers. $F = D_k(R) \cap D_i(R)$

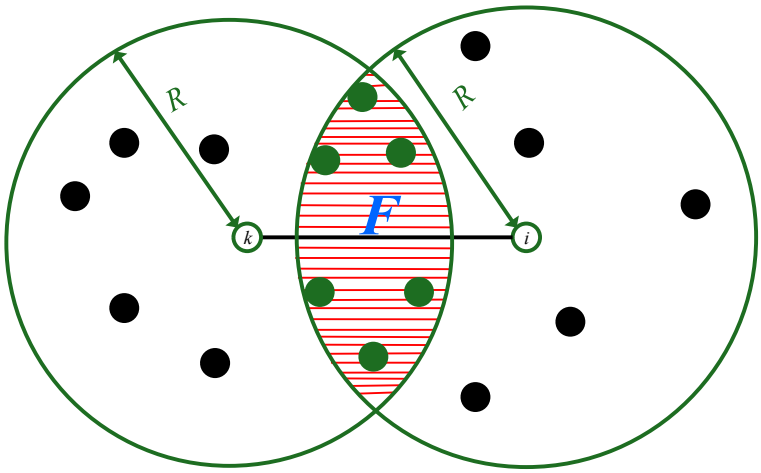

(a) Small distance.

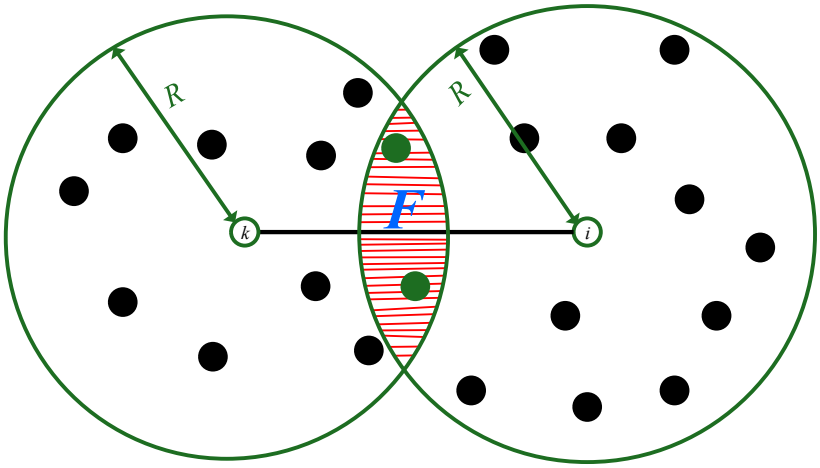

(b) Large distance.

FIGURE 4.2 – Effect of the distance d_{i-k} on the forwarding area F.

is then the forwarding area wherein the forwarding nodes [4], which forward the messages sent from the k-th anchor to the i-th sensor, are located. An in depth look at this area reveals that it is strongly dependant on d_{i-k} ; a fact that could be exploited to estimate the latter. Indeed, as can be observed from Fig. 4.2, if d_{i-k} increases (decreases). then F decreases (increases). Using some geometrical properties and trigonometric transformations, one can even show that

$$F = \Phi\left(d\right) = 2R^2 \cos^{-1}\left(\frac{d_{ki}}{2R}\right) - \frac{1}{2} d_{ki} \sqrt{4R^2 - d_{ki}^2}. \tag{4.4}$$

4. A forwarding node refers to a sensor located in the forwarding area F. Please note that we consider, in this work, that an anchor assists the sensors' localization by only broadcasting its information across the WSN. It is then not involved in forwarding the messages of other anchors.

It follows from (4.4) that $\Phi(d)$ is a decreasing function of d, which confirms the above observation. As such, computing F is crucial in order to estimate the distance between the k-th anchor and the i-th sensor. From Fig. 4.3, the latter receives m times the k-th anchor' coordinates, each

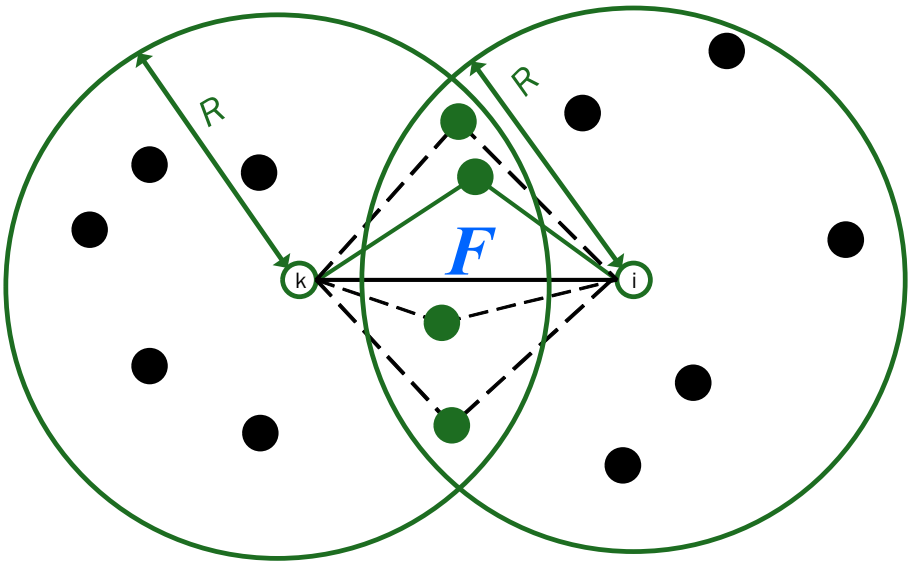

FIGURE 4.3 – Two-hop communication.

from a distinct forwarding node. Since nodes are uniformly distributed in S, knowing m, the i-th sensor is able to locally approximate F as $\hat{F} = m/\lambda$ where $\lambda = N/S$ is the WSN density. $\hat{d}_{i-k}$ could then be obtained as

$$\hat{d}_{i-k} = \Psi(\hat{F}), \tag{4.5}$$

where $\Psi(x) = \Phi^{-1}(x)$ is the inverse function of Φ. Unfortunately, to the best of our knowledge, there is no closed-form expression for $\Psi(x)$. It is then impossible to obtain $\hat{d}_{i-k}$ using (4.5). In order to circumvent this impediment, a look-up table may be envisaged at each sensor. However, such a table usually requires a large memory space; a scarce resource for these often-primitive devices. Even if it is possible to implement an additional memory space at each node, this would substantially increase the overall cost of the network, especially for large-scale WSNs. Alternatively, one may numerically compute $\hat{d}_{i-k}$. To this end, we propose to equivalently reformulate this problem as a root-finding problem of the function $\widetilde{\Phi}(x) = \Phi(x) - \hat{F}$. Many root-finding iterative algorithms already exist in the literature such as Newton-Raphson method, Brent's method, Secant method, etc.. Due to its simplicity, only the latter is of concern in this work.

Using the Secant method, $\hat{d}_{i-k}$ is derived by iteratively executing the following instruction :

$$\hat{d}_{i-k}^{p+1} = \hat{d}_{i-k}^{p} - \tilde{\Phi}\left(d_{i-k}^{p}\right) \frac{d_{i-k}^{p} - d_{i-k}^{p-1}}{\Phi\left(d_{i-k}^{p}\right) - \Phi\left(d_{i-k}^{p-1}\right)}, \tag{4.6}$$

where p refers to the p-th iterations, until convergence (i.e., $p = p^{\max} = \inf_p\{\hat{d}_{i-k}^{p} = \hat{d}_{i-k}^{p+s}, \quad \forall s \in \mathbb{N}^{\star}\}$). From (4.6), two initial values $\hat{d}_{i-k}^{0}$ and $\hat{d}_{i-k}^{1}$ are required to properly compute $\hat{d}_{i-k} = \hat{d}_{i-k}^{p^{\max}}$. To guarantee fast convergence of the Secant method, $\hat{d}_{i-k}^{0}$ and $\hat{d}_{i-k}^{1}$ must be chosen among the range of possible values of $\hat{d}_{i-k}$ (i.e., [R,2R]). In this work, we opt for $\hat{d}_{i-k}^{0} = R$ and $\hat{d}_{i-k}^{1} = 2R$. As

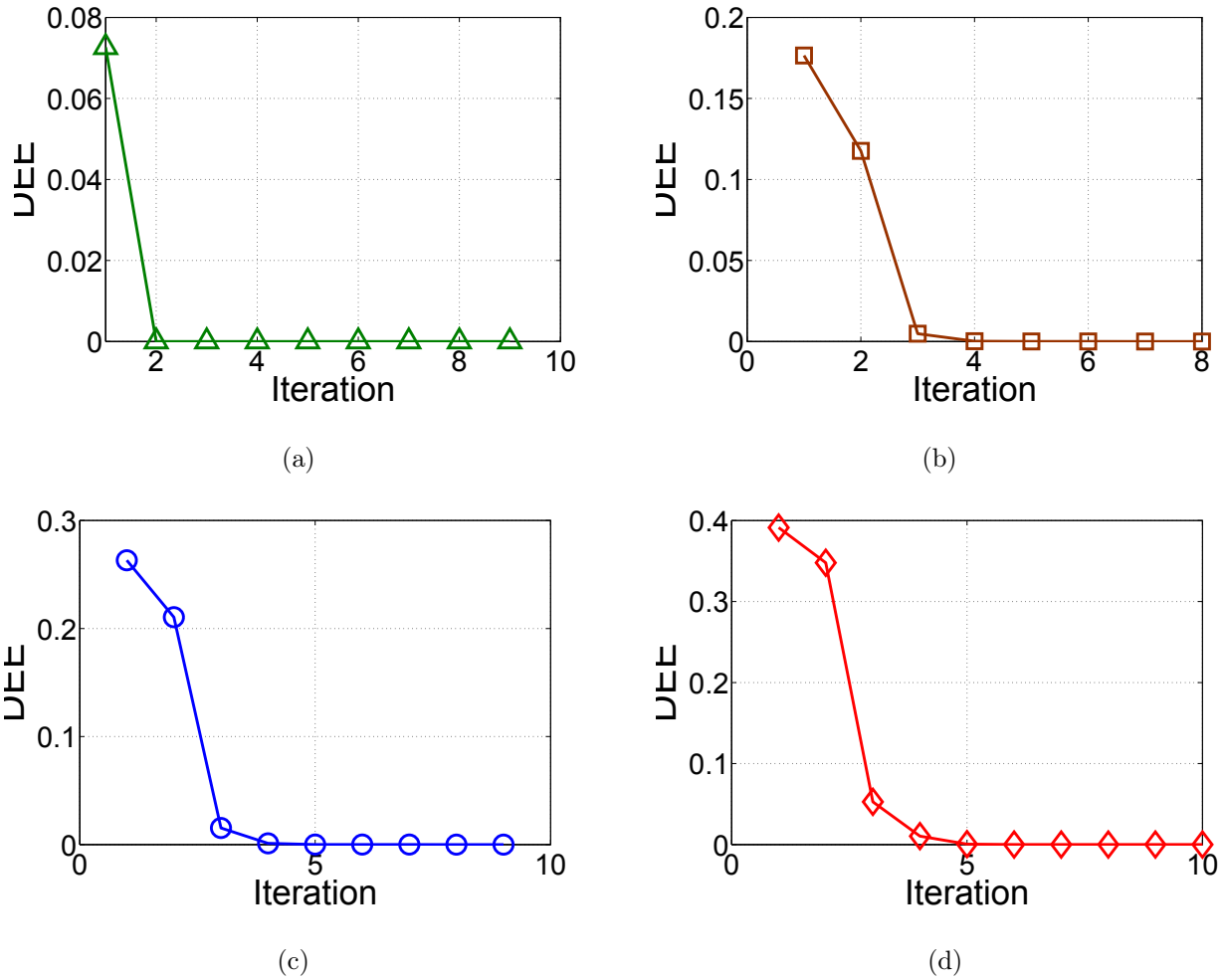

FIGURE 4.4 – Distance estimation error (DEE) vs. the number of iterations.

can be observed from Fig. 4.4, using these values, $p^{\max}$ does not exceed 5 iterations. Knowing that the required power to execute one instruction is in the range of 10^{-4} of the power consumed per transmitted bit [33]-[34], the power needed to execute the Secant method is then very negligible with respect to the overall power consumed by each sensor. Consequently, the proposed DE approach complies with WSNs where the power is considered as a scarce resource.

Now, let us generalize the proposed DE approach by considering $n_h > 2$. In such a case, d_{i-k} would simply be, as could be observed from Fig. 4.5, the summation of $n_h/2$ two-hop distances between the k-th anchor and the i-th sensor. $\hat{d}_{i-k}$ is then given by

$$\hat{d}_{i-k} = \sum_{l=1}^{n_h/2} \Psi\left(\frac{m_l}{\lambda}\right), \tag{4.7}$$

where m_l is the number of forwarding nodes at the l-th 2-hop distance.

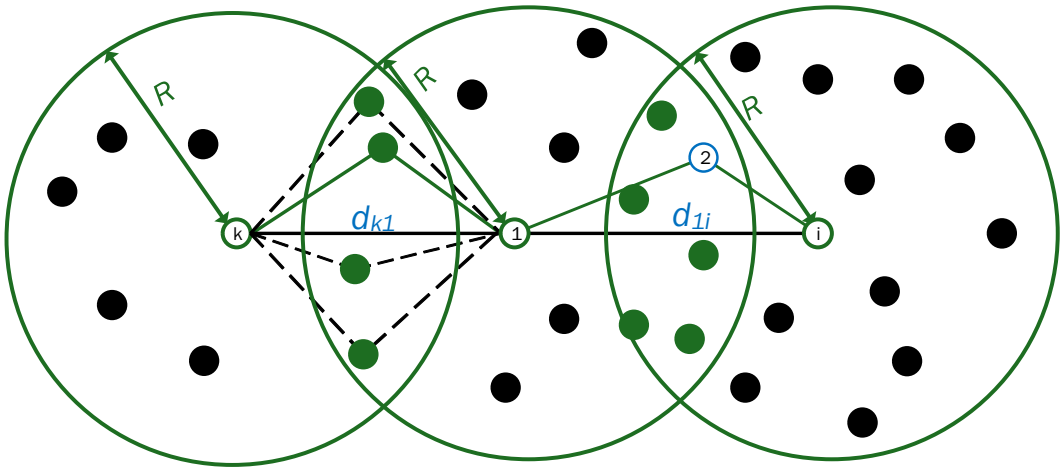

FIGURE 4.5 – Four-hop communication.

4.3.2 n_h is odd

If n_h is odd, d_{i-k} would be the summation of $(n_h - 1)/2$ 2-hop distances plus the last-hop distance d^{Last}. Using the fact that the minimum square error (MMSE) of the last-hop distance estimation is obtained as $d_{\text{av}}^{\text{Last}} = \text{E}\{d^{\text{Last}}\}$, $\hat{d}_{i-k}$ is given by

$$\hat{d}_{i-k} = \sum_{l=1}^{(n_h-1)/2} \Psi\left(\frac{m_l}{\lambda}\right) + d_{\text{av}}^{\text{Last}}. \tag{4.8}$$

Now, let us focus on $d_{\text{av}}^{\text{Last}}$. In order to derive it, one should compute the conditional cumulative distribution function (CDF) $F_Z(z) = P\left(Z \leq z / Z \leq R\right)$ where, for the sake of clarity, Z refers to the random variable d^{Last}. Actually, as shown in Fig. 4.6, the probability that the event $\{Z \leq z\}$ occurs is the probability that the i-th sensor be in the disc $D_j(z)$ having the j-th sensor as center and z as radius. Therefore, $F_Z(z)$ can be defined as

$$F_Z\left(z\right) = P\left(\mathcal{A}|\mathcal{B}\right) = \frac{P\left(\mathcal{A}\right)}{P\left(\mathcal{B}\right)}, \tag{4.9}$$

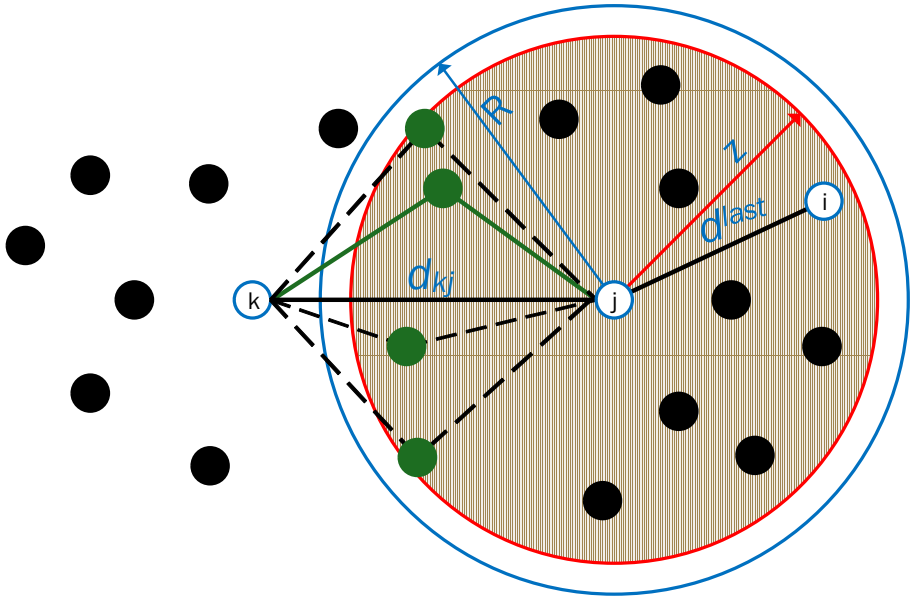

FIGURE 4.6 – Last-hop distance estimation.

where $P(\mathcal{A}|\mathcal{B})$ is the probability that the event $\mathcal{A} = \{\text{the } i\text{-th sensor is in the dashed disc } D_j(z)\}$ given $\mathcal{B} = \{\text{the } i\text{-th sensor is in } D_j(R)\}$ occurs. Since the nodes are uniformly distributed in S, we have

$$P(\mathcal{A}) = \frac{\pi z^2}{S}, \tag{4.10}$$

$$P(\mathcal{B}) = \frac{\pi R^2}{S}. \tag{4.11}$$

It follows from (4.10) and (4.11) that $F_Z(z) = (z/R)^2$ and, hence, the probability density function (PDF) $f_Z(z)$ of Z is given by

$$f_Z(z) = \frac{2z}{R^2}. \tag{4.12}$$

Exploiting (4.12), we easily show that

$$\hat{d}^{\text{Last}} = \frac{2R}{3}. \tag{4.13}$$

In what follows, we introduce a new localization algorithm for multi-hop WSN that exploits the proposed DE approach and analytically prove its accuracy. The obtained results will be further verified using Monte Carlo simulations.

4.4 Proposed localization algorithm

4.4.1 Initialization

As a first step of any anchor-based localization algorithm, the k-th anchor broadcasts through the network a packet which consists of a header followed by a data payload. The packet header contains the anchor position (a_k, b_k), while the data payload contains $(n, \hat{d})$, where n is the hop-count value initialized to one and $\hat{d}$ is the estimated distance initialized to zero. If the packet is successfully received by a node, it stores the k-th anchor position as well as the received hop-count $n_k = n$ in its database, adds one to the hop-count value and broadcasts the resulting message. Once this message is received by the another node, its database information is checked. If the k-th anchor's position does not exist, the node adds the received information to its database and checks the parity of n. If it is odd, the message is broadcasted after incrementing it by 1. Otherwise, the node creates a variable m_k, which represents the number of received packets from the k-th anchor with the same data payload, and initializes it to one. However, if the node is aware of the k-th anchor's coordinates, it compares n and $\hat{d}$ with the stored ones n_k and $\hat{d}_k$, respectively. If $n > n_k$ or $n = n_k$ but $\hat{d} > \hat{d}_k$, the packet is immediately discarded. If $n < n_k$ or $n = n_k$ and $\hat{d} < \hat{d}_k$, the node updates n_k to n and $\hat{d}_k$ to $\hat{d}$. Otherwise, the parity of n is checked. If it is odd, the packet is broadcasted after incrementing it by 1. If not, m_k is incremented by 1. At this stage, a waiting-time τ, before transmitting the k-th anchor information, is envisaged to ensure that all similar packets are received. Afterwards, using m_k and the approach in Section 4.3.1, the node estimates the last two-hop distance, adds the estimate to $\hat{d}_k$ and broadcasts the resulting packet in the network. This process will continue until each sensor in the network becomes aware of all anchors' position. It is noteworthy that, at this stage, if n_k is even, the sensor is already aware of its distance to the k-th anchor. Otherwise, it is obtained by adding, as discussed in Section 4.3.2, $2/3$ to the stored $\hat{d}_k$. Fig. 4.7 summarizes our algorithm's pseudocode implementable at each sensor.

4.4.2 Positions' computation

Once the i-th sensor obtains all the anchors' coordinates and their corresponding distances, it computes its position by solving the following nonlinear equations system :

$$\begin{cases} (a_1 - \hat{x}_i)^2 + (b_1 - \hat{y}_i)^2 = & \hat{d}_{i-1}^2 \\ (a_2 - \hat{x}_i)^2 + (b_2 - \hat{y}_i)^2 = & \hat{d}_{i-2}^2 \\ \vdots & \vdots \\ (a_M - \hat{x}_i)^2 + (b_M - \hat{y}_i)^2 = & \hat{d}_{i-M}^2 \end{cases}, \tag{4.14}$$

where $(\hat{x}_i, \hat{y}_i)$ are the estimated i-th sensor's coordinates. After some rearrangements aiming to linearize the system above, we obtain

$$\boldsymbol{\Upsilon}\hat{\boldsymbol{\alpha}}_i = -\frac{1}{2}\boldsymbol{\kappa_i}, \tag{4.15}$$

where $\hat{\boldsymbol{\alpha}}_i = [\hat{x}_i, \hat{y}_i]^T$,

$$\boldsymbol{\Upsilon} = \begin{bmatrix} a_1 - a_M & b_1 - b_M \\ a_2 - a_M & b_2 - b_M \\ \vdots & \vdots \\ a_{(M-1)} - a_M & b_{(M-1)} - b_M \end{bmatrix}, \tag{4.16}$$

and

$$\boldsymbol{\kappa_i} = \begin{bmatrix} \hat{d}_{i-1}^2 - \hat{d}_{i-M}^2 + a_M^2 - a_1^2 + b_M^2 - b_1^2 \\ \hat{d}_{i-2}^2 - \hat{d}_{i-M}^2 + a_M^2 - a_2^2 + b_M^2 - b_2^2 \\ \vdots \\ \hat{d}_{i-(M-1)}^2 - \hat{d}_{i-M}^2 + a_M^2 - a_{(M-1)}^2 + b_M^2 - b_{(M-1)}^2 \end{bmatrix}. \tag{4.17}$$

Since $\boldsymbol{\Upsilon}$ is a non-invertible matrix, $\hat{\boldsymbol{\alpha}}_i$ could be estimated with the pseudo-inverse of $\boldsymbol{\Upsilon}$ as follows :

$$\hat{\boldsymbol{\alpha}}_i = -\frac{1}{2}\left(\boldsymbol{\Upsilon}\boldsymbol{\Upsilon}^T\right)^{-1}\boldsymbol{\Upsilon}^T\boldsymbol{\kappa_i}. \tag{4.18}$$

Therefore, the i-th sensor is able to obtain an estimate of its coordinates as $\hat{x}_i = [\hat{\boldsymbol{\alpha}}_i]_1$, and $\hat{y}_i = [\hat{\boldsymbol{\alpha}}_i]_2$. It is also noteworthy from (6.3) and (6.4) that $\hat{x}_i$ and $\hat{y}_i$ are solely dependent on the anchors' coordinates $(a_k, b_k), k = 1, \ldots, M$ and the estimated distances $\hat{d}_{k-i}, k = 1, \ldots, M$ which are all locally available at the i-th sensor. Therefore, their computation does not require any additional overhead (i.e., additional power cost), making our algorithm compliant with WSNs' power restrictions.

Input : Number of anchors M, and their positions (x_k, y_k), as well as the received hop-count n_k, and the number of received packets m initialized to zero, where $k = 1, \ldots, M$

for $k = 1 \rightarrow M$ **do**

Check database

if Data$\{k\}= \emptyset$ **then**

Save Data$\{k\}$

$n_k = n_k + 1$

Broadcast updated Data$\{k\}$

else if $n \geq n_k$ and $\hat{d} \geq \hat{d}_k$ **then**

Discard received data

else if $n \leq n_k$ and $\hat{d} \leq \hat{d}_k$ **then**

$n_k = n$

$\hat{d}_k = \hat{d}$

else if $(n_k \mod 2) = 0$ **then**

$m = m + 1$

Wait τ

$\hat{d}_{k-(n_k-2)} \leftarrow$ Eq. (6.2) in section 5.4

else

$n_k = n_k + 1$

Broadcast updated Data$\{k\}$

end if

end for

$\hat{x}_i, \hat{y}_i \leftarrow$ Eq. (6.5) in section 6.1

Output (x_i, y_i) ▷ Estimated position of the i-th node

FIGURE 4.7 – Proposed algorithm for sensors.

In what follows, the performance of the proposed localization algorithm is analyzed and compared to the most representative benchmarks in the literature.

4.5 Performance analysis of the proposed algorithm

4.5.1 Performance metrics

One way to prove the efficiency of the proposed localization algorithm is undoubtedly analyzing its accuracy. To this end, we introduce the following performance metric :

$$\mathcal{E}_{\mathrm{P},i} = \left\| \boldsymbol{\alpha}_i - \hat{\boldsymbol{\alpha}}_i \right\|^2, \tag{4.19}$$

where $\mathcal{E}_{\mathrm{P},i}$ denotes the i-th sensor's location estimation error (LEE) and $\boldsymbol{\alpha}_i = [x_i, y_i]^T$ is a vector whose entries are the true i-th sensor coordinates. From (6.6), $\mathcal{E}_{\mathrm{P},i}$ is an excessively complex function of the random variables $(x_i, y_i), i = 1, \ldots, N$, d_{i-k} and $\hat{d}_{i-k}, k = 1, \ldots, M$ and, hence, a random quantity of its own. Therefore, it is practically more appealing to investigate the behavior and the properties of the average LEE $\bar{\mathcal{E}}_{\mathrm{P}}(N) = \mathrm{E}\{\mathcal{E}_{\mathrm{P},i}\}$ achieved using the proposed algorithm. Actually, $\bar{\mathcal{E}}_{\mathrm{P}}(N)$ could be differently defined as

$$\bar{\mathcal{E}}_{\mathrm{P}}(N) = \mathrm{E}\left\{\mathcal{G}_{\mathrm{P}}^{\mathrm{Net}}(N)\right\}, \tag{4.20}$$

where

$$\mathcal{G}_{\mathrm{P}}^{\mathrm{Net}}(N) = \frac{1}{N}\sum_{i=1}^{N} \mathcal{E}_{\mathrm{P},i}, \tag{4.21}$$

refers to the global LEE through the network, which is commonly used as a performance metric in the context of localization in WSNs [4]- [7]. Furthermore, using the strong law of large numbers, we show for large N that we have

$$\mathcal{G}_{\mathrm{P}}^{\mathrm{Net}}(N) \xrightarrow{p1} \bar{\mathcal{E}}_{\mathrm{P}}(N), \tag{4.22}$$

where $\xrightarrow{p1}$ stands for convergence with probability one. From (6.9), $\bar{\mathcal{E}}_{\mathrm{P}}(N)$ is not only the statistical average of $\mathcal{G}_{\mathrm{P}}^{\mathrm{Net}}(N)$, but also it approaches the latter for any given realization (i.e., any given $(x_i, y_i), i = 1, \ldots, N$). All this proves that $\bar{\mathcal{E}}_{\mathrm{P}}(N)$ is a meaningful and useful performance metric.

In the next section, the average LEE $\bar{\mathcal{E}}_{\mathrm{P}}(N)$ achieved using the proposed algorithm is derived in closed -form and its behavior is analyzed.

4.5.2 Proposed algorithm's average LEE

It follows from (6.5) that

$$\mathcal{E}_{\mathrm{P},i} \;=\; \frac{1}{4}\left\|\left(\boldsymbol{\Upsilon}\boldsymbol{\Upsilon}^T\right)^{-1}\boldsymbol{\Upsilon}^T\boldsymbol{\delta}_i\right\|^2, \tag{4.23}$$

where $[\boldsymbol{\delta}_i] = [\epsilon_1 - \epsilon_M, \ldots, \epsilon_{M-1} - \epsilon_M]^T$ with $\epsilon_k = \hat{d}_{i-k}^2 - d_{i-k}^2$ being the squared-distance estimation error. $\mathcal{E}_{\mathrm{P},i}$ is then given by

$$\begin{aligned}\mathcal{E}_{\mathrm{P},i} &= \mathrm{Tr}\left(\left(\boldsymbol{\Upsilon}\boldsymbol{\Upsilon}^T\right)^{-1}\boldsymbol{\Upsilon}^T\boldsymbol{\delta}_i\boldsymbol{\delta}_i^T\boldsymbol{\Upsilon}\left(\boldsymbol{\Upsilon}\boldsymbol{\Upsilon}^T\right)^{-1}\right)\\ &= \mathrm{Tr}\left(\boldsymbol{\Omega}\boldsymbol{\delta}_i\boldsymbol{\delta}_i^T\right) = \sum_{k=1}^{M-1}\boldsymbol{\Omega}_{kk}\left([\boldsymbol{\delta}_i]_k\right)^2 + \sum_{k=1}^{M-1}\sum_{l=1,l\neq k}^{M-1}\boldsymbol{\Omega}_{kl}[\boldsymbol{\delta}_i]_l[\boldsymbol{\delta}_i]_k,\end{aligned} \tag{4.24}$$

where $\mathrm{Tr}\left(\mathbf{X}\right)$ is the trace of the matrix $\mathbf{X}$ and $\boldsymbol{\Omega} = \boldsymbol{\Upsilon}\left(\boldsymbol{\Upsilon}\boldsymbol{\Upsilon}^T\right)^{-2}\boldsymbol{\Upsilon}^T$. Note in the second line of (6.11) that we exploit the cyclic property of the trace. Since $\epsilon_k, k = 1, \ldots, M$ are i.i.d random variables, we have from (6.11) the following

$$\bar{\mathcal{E}}_{\mathrm{P}}(N) \;=\; \sigma_\epsilon^2\left(2\mathrm{Tr}\left(\boldsymbol{\Omega}\right) + \sum_{k=1}^{M-1}\sum_{l=1,l\neq k}^{M-1}\boldsymbol{\Omega}_{kl}\right). \tag{4.25}$$

Now let us turn our attention to σ_ϵ^2. For the sake of clarity, we first assume that there are exactly two hops between the i-th sensor and each anchor. The obtained results will be thereafter generalized. In such a case, from (4.4) and (4.5), the Taylor series expansion of $\Psi(x)$ at F_k yields

$$\hat{d}_{i-k} \;=\; d_{i-k} + \sum_{n=1}^{\infty}\frac{\Psi^{(n)}\left(F_k\right)}{n!}\Delta F^n, \tag{4.26}$$

where $\Psi^{(n)}(x)$ is the n-th derivative of $\Psi(x)$ and $\Delta F = m_k/\lambda - F_k$. Assuming that ΔF is small enough to allow approximation of $\hat{d}_{k-i}$ by the first three non-zero terms of the right-hand-side (RHS) of (4.26), we obtain

$$\epsilon_k \simeq\; 2d_{i-k}\Psi^{(1)}(F_k)\Delta F + \left(\left(\Psi^{(1)}(F_k)\right)^2 + d_{i-k}\Psi^{(2)}(F_k)\right)\Delta F^2, \tag{4.27}$$

where $\Psi^{(1)}\left(x\right) = \left(4R^2 - \Psi(x)^2\right)^{-1/2}$ and $\Psi^{(2)}\left(x\right) = \Psi\left(x\right)/\left(4R^2 - \Psi\left(x\right)^2\right)^2$. Since the nodes are uniformly deployed in S, the probability of having m_k nodes in F_k follows a Binomial distribution $\mathrm{Bin}\left(N, p\right)$ where $p = \frac{F_k}{S}$ and, therefore, the first and second order statistics of m_k are $\mathrm{E}\{m_k\} = \lambda F_k$ and $\mathrm{E}\{m_k^2\} = \lambda F_k\left(1 - \frac{F_k}{S} + \lambda F_k\right)$, respectively. Using the latter along with (4.27) yields

$$\mathrm{E}_{m_k}\left\{\epsilon_k\right\} = \frac{4R^2\lambda^{-1}F_k\left(1 - \frac{F_k}{S}\right)}{\left(4R^2 - \Psi\left(F_k\right)^2\right)^2}, \tag{4.28}$$

where the expectation is taken with respect to m_k. As could be observed from (4.28), the probability density function $f_{F_k}(F)$ of F_k is crucial to derive σ_ϵ^2 in closed-form. For the sake of mathematical tractability, F_k is assumed to be Uniform in $[0, F_{\max}]$ where $F_{\max} = \Phi(R) = \left(-\frac{\sqrt{3}}{2} + \frac{2\pi}{3}\right) R^2$. Despite this simplifying assumption, we will shortly see in Section 5.5 that the obtained analytical results closely match those obtained empirically by Monte Carlo simulations. $\mathrm{E}\{\epsilon_k\}$ is then given by

$$\begin{aligned} \mathrm{E}\{\epsilon_k\} &= 4R^2\lambda^{-1}\int_R^{2R} \frac{\Phi(x)\left(1-\Phi(x)S\right)}{\left(4R^2-x^2\right)^2}dx = \frac{1}{9\left(3\sqrt{3}-4\pi\right)N}\Bigg(12\left(-9+\sqrt{3}\pi\right)S \\ &+ \left(27\sqrt{3}+4\pi\big(9-2\sqrt{3}\pi\big)\right)R^2\Bigg). \end{aligned} \tag{4.29}$$

In the first line of (4.29), please note that we resort to the variable change $F = \Phi(x)$. Following similar steps as above, we show that

$$\mathrm{E}\left\{\epsilon_k^2\right\} = \frac{\left(4\pi\left(4\pi\left(9\sqrt{3}+4\pi\right)-189\right)-1053\sqrt{3}\right)R^4 - 9\left(8\pi\left(3\sqrt{3}+2\pi\right)-243\right)R^2S}{27\left(3\sqrt{3}-4\pi\right)N}. \tag{4.30}$$

and, hence, σ_ϵ^2 is obtained. It can be then inferred from (6.12)-(4.30) that the achieved average LEE $\bar{\mathcal{E}}_{\mathrm{P}}(N)$ using the proposed algorithm linearly decreases with N when S and R are fixed. Furthermore, for sufficiently large N, we have $\bar{\mathcal{E}}_{\mathrm{P}}(N) \simeq 0$. This property is actually a desired feature for any sensor localization algorithm since WSNs are typically dense. It is noteworthy here that the best representative benchmarks in the literature lack such a feature [4], [13]. Recall, however, that the results in (4.29) and (4.30) were derived assuming that the number of hops between any anchor-sensor pair is $n_h = 2$ hops. For the sake of generalization, we consider in the sequel that n_h is a random variable with mean $\bar{n}_h$. In such a case, $\mathrm{E}\{\epsilon_k\}$ and $\mathrm{E}\{\epsilon_k^2\}$ could be expressed as

$$\begin{aligned} \mathrm{E}\{\epsilon_k\} &= R^2\Bigg(\frac{3\big(2\bar{n}_h-1\big)\big(\xi_{0,2}+2\xi_{1,1}\big)+\xi_{0,1}\Big(3\xi_{1,0}\Big(2\bar{n}_h\big(\bar{n}_h-3\big)+3\Big)+4\big(\bar{n}_h-1\big)\Big)}{12N} - \frac{1}{36} \\ &+ \frac{\xi_{0,1}^2\Big(2\bar{n}_h\big(\bar{n}_h-3\big)+3\Big)}{8N^2}\Bigg), \end{aligned} \tag{4.31}$$

$$\mathrm{E}\left\{\epsilon_k^2\right\} = \frac{R^2}{4N}\Bigg(\frac{16\xi_{0,2}}{9} - \frac{4\xi_{0,1}}{27} - \frac{(\bar{n}_h-1)}{72}\Big(2\big(\xi_{0,2}+2\xi_{1,1}\big)+\xi_{0,1}\big(\bar{n}_h-3\big)\big(\frac{\xi_{0,1}}{N}+2\xi_{1,0}\big)\Big)\Big(1 - \frac{12\xi_{0,1}\big(\bar{n}_h-1\big)}{N}\Big) + \big(\bar{n}_h-1\big)\Bigg(4\xi_{2,2} + \frac{\bar{n}_h-3}{2}\Big(\frac{3\xi_{0,2}^2}{N} + 8\big(\frac{\xi_{1,1}^2}{N}+\xi_{1,2}\xi_{1,0}\big) + \frac{2\xi_{0,1}}{N}\Big(6\xi_{1,2} + 4\xi_{2,1} + \big(3\xi_{0,2}+4\xi_{1,1}\big)\big(\bar{n}_h-5\big)\xi_{1,0}\Big) + \frac{6\xi_{0,1}^3\xi_{1,0}}{N^2}\big(\bar{n}_h-7\big)\big(\bar{n}_h-5\big) + \frac{2\xi_{0,2}\xi_{0,1}^2}{N^2}\Big(\big(\bar{n}_h-5\big)\xi_{1,0}^2 + 2\xi_{2,0}\Big)\Big(\frac{6\xi_{0,2}}{N} + \big(\bar{n}_h-5\big)\Big(\frac{12\xi_{1,1}}{N} + \big(\bar{n}_h-7\big)\xi_{1,0}^2 + \xi_{2,0}\Big)\Big)\Big)\Big) + \bar{n}_h\Bigg(4\xi_{2,2} + \big(\bar{n}_h-2\big)\Big(\frac{3\xi_{0,2}^2}{2N} + 4\big(\frac{\xi_{1,1}^2}{N} + \xi_{1,2}\xi_{1,0}\big) + \frac{\xi_{0,1}}{N}\Big(6\xi_{1,2} + 4\xi_{2,1} + \big(\bar{n}_h-4\big)\big(3\xi_{0,2}+4\xi_{1,1}\big)\xi_{1,0}\Big) + 3\frac{\xi_{0,1}^3}{N^2}\big(\bar{n}_h-6\big)\big(\bar{n}_h-4\big)\xi_{1,0} + \xi_{0,2}\Big(\big(\bar{n}_h-2\big)\xi_{1,0}^2 + \frac{\xi_{2,0}}{2}\Big) + \frac{\xi_{0,1}^2}{N}\Big(\frac{3\xi_{0,2}}{N} + \big(\bar{n}_h-4\big)\Big(\frac{6\xi_{1,1}}{N} + \big(\frac{\bar{n}_h-6}{2}\big)\xi_{1,0}^2 + \xi_{2,0}\Big)\Big)\Big)\Big)\Bigg) + R^2\Big(\frac{25R^2}{162} + \frac{2R\xi_{1,0}}{15} + \frac{\xi_{2,0}}{9}\Big), \tag{4.32}$$

respectively, where $\xi_{n,m}$ $n,m=0,1,2$ are parameter functions of R and S whose expressions are listed in TABLE 4.1.

Proof : See Appendix A.

It is noteworthy that the results in (4.31) and (4.32) are very interesting in terms of implementation strategy, since they allow, through (6.12), to easily find the smallest N that keeps $\bar{\mathcal{E}}_{\mathrm{P}}(N)$ below a certain level. They also allow to find the best anchor placement strategy that minimizes $\bar{\mathcal{E}}_{\mathrm{P}}(N)$ for a given N. Moreover, in contrast with the two-hop case, it follows from (4.31) and (4.32) that we have

$$\bar{\mathcal{E}}_{\mathrm{P}}(N) \simeq 0.16R^4 + \frac{2R^3}{15}\xi_{1,0} + \frac{R^2}{9}\xi_{2,0} \neq 0, \tag{4.33}$$

when N is large enough. Note that x is nothing but the error incurred when estimating the last hop of an odd distance between any anchor-sensor pair in the network. A proper anchor selection scheme should then be envisaged to make our proposed algorithm reach its optimal accuracy (i.e., $\bar{\mathcal{E}}_{\mathrm{P}}(N) \simeq 0$) at large N. Indeed, if each sensor selects among the list of anchors only those with an even number of hops, its achieved average LEE would approach 0 when N is large enough. This, of course, requires that at least 3 anchors comply with the above criterion. Please note that such a selection scheme could be easily implemented in each sensor without burdening neither the implementation complexity of the proposed localization algorithm nor the overall cost of the WSNs.

Parameter	Closed-form expression
$\xi_{1,0}$	$6\sqrt{3}R/\big(4(\pi-3\sqrt{3})\big)$
$\xi_{2,0}$	$\big(8\sqrt{3}\pi+9\big)R^2/\big(8\sqrt{3}\pi-18\big)$
$\xi_{0,1}$	$\Big(\Big(297\sqrt{3}-8\pi\big(9+2\sqrt{3}\pi\big)\Big)R^2+6\big(4\sqrt{3}\pi-27\big)S\Big)\Big/\big(36\big(3\sqrt{3}-4\pi\big)R\big)$
$\xi_{0,2}$	$\Big(\big(64\pi^3-567\sqrt{3}-216\pi\big)R^2+36\big(27-4\pi^2\big)S\Big)\Big/\big(216\big(3\sqrt{3}-4\pi\big)\big)$
$\xi 1,1$	$\Big(\Big(1215\sqrt{3}-8\pi\Big(8\pi\big(3\sqrt{3}+\pi\big)-135\Big)\Big)R^2+36\Big(4\pi\big(2\sqrt{3}+\pi\big)-99\Big)S\Big)\Big/\big(432\big(3\sqrt{3}-4\pi\big)\big)$
$\xi_{1,2}$	$\Big(\Big(-1701\sqrt{3}+40\pi\big(13+2\sqrt{3}\pi\big)\Big)R^3+30\big(19-4\sqrt{3}\pi\big)RS\Big)\Big/\big(30\big(3\sqrt{3}-4\pi\big)\big)$
$\xi_{2,1}$	$\Big(9R\Big(3\sqrt{3}R\big(-1+45R\big)-104S\Big)-54S-16\sqrt{3}\big(1+3R\big)\pi^2R^2+24\pi\Big(3\big(1-5R\big)R^2+\sqrt{3}\big(1+6R\big)S\Big)\Big)\Big/\Big(36\big(3\sqrt{3}-4\pi\big)\Big)$
$\xi_{2,2}$	$\Big(9\Big(243-8\pi\big(3\sqrt{3}+2\pi\big)\Big)R^2S+\Big(4\pi\Big(4\pi\big(9\sqrt{3}+4\pi\big)-189\Big)-1053\sqrt{3}\Big)R^4\Big)\Big/\big(108\big(3\sqrt{3}-4\pi\big)\big)$

TABLE 4.1 – Closed-form expressions of $\xi_{n,m}$ $n,m=0,1,2$.

4.5.3 Proposed algorithm's asymptotic LEE

So far, we derived the average LEE achieved by our localization algorithm and studied its behavior and properties. Motivated by the fact that the LEE is a more practical metric than its average, we investigate in this section its statistical properties more thoroughly for the sake of further highlighting the proposed algorithm's accuracy.

Let us consider again the 2-hop case (i.e., two hops between the i-th sensor and the k-th anchor nodes). Exploiting the fact that m_k is a Binomial random variable, we have from the Chebyshev's inequality we have

$$1-P\left(|\Delta F|<\kappa\right)\leq\frac{F_k(S-F_k)}{N\kappa^2}, \tag{4.34}$$

where κ is any given strictly positive real. If the latter is chosen small enough to guarantee the equivalence $|\Delta F|<\kappa\Leftrightarrow|\Delta F|\simeq 0$, it holds for sufficiently large N that

$$P\left(|\Delta F|\simeq 0\right)\simeq 1. \tag{4.35}$$

Exploiting this result along with (4.27) we obtain

$$P\left(\epsilon_k \simeq 0\right) \simeq 1, \tag{4.36}$$

and, hence, for large N we have $\mathcal{E}_{\mathrm{P},i} \simeq 0$. This further proves the accuracy of the proposed algorithm. Furthermore, it is straightforward to show that $\mathcal{E}_{\mathrm{P},i} \simeq 0$ also holds when the number of hops between the i-th sensor and all anchors is even (but not necessarily 2). This emphasizes even more the importance of the anchor selection scheme discussed above.

4.6 Simulations results

In this section, we validate and illustrate our theoretical results by Monte Carlo simulations. These are conducted to compare under the same network settings the R^2-normalized LEEs (NLEE)s achieved by the proposed algorithm and three of the best representative localization algorithms currently available in the literature, i.e., DV-Hop [4], LAEP [13], and EPHP [20].

All simulation results are obtained by averaging over 600 trials. In all simulations, sensors are uniformly deployed in a 2-D square area $S = 10^4\ m^2$. M is set to 20, expect in Fig. 4.10 where it varies from 15 to 40. R is set to 20 m, expect in Fig. 4.11 where it varies from 12 m to 36 m. Two commonly used anchor placement strategies in the context of WSNs are considered : the perimeter and grid placements as depicted in Figs. 4.8(a) and 4.8(b), respectively.

Fig. 4.9 plots the average NLEE achieved by the proposed algorithm, DV-Hop, and LAEP versus N with two anchor placement strategies : perimeter in Fig. 4.9(a) and grid placement in Fig. 4.9(b). From these figures, the proposed localization algorithm always outperforms in accuracy its counterparts. It is, for instance at $N = 700$, until 12 times more accurate than DV-Hop and until 10 times more accurate than LAEP. This further proves the proposed algorithm's efficiency in WSNs and highlights its advantage over its counterparts.

Fig. 4.10 plots the average NLEE achieved by the proposed algorithm, DV-Hop, LAEP, and EPHP versus the anchor ratio with two anchor placement strategies : perimeter in Fig. 4.10(a) and grid placement in Fig. 4.10(b). From these figures, all algorithms benefit, as expected, from larger anchor ratios. However, the proposed algorithm remains more accurate than its counterparts thereby proving once again its superiority.

Fig. 4.11 displays the average NLEE achieved by all localization algorithms versus both the node degree and communication range with both the perimeter and grid anchor placement

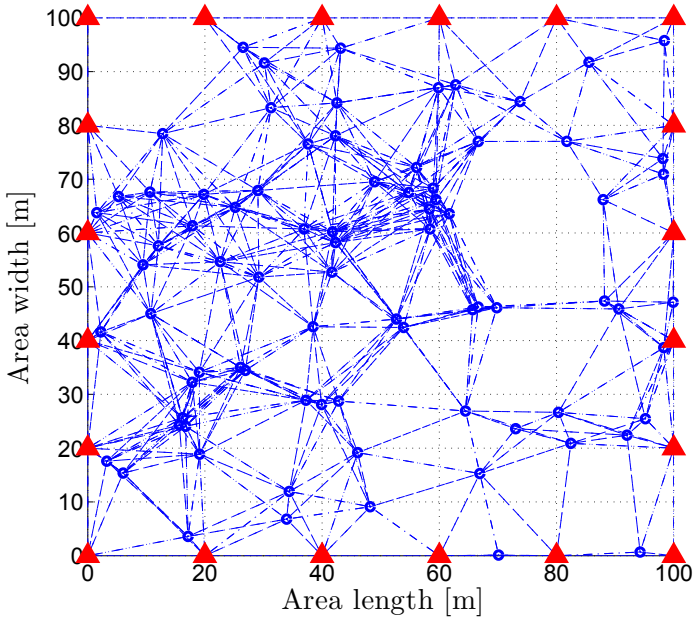

(a) Perimeter anchor placement.

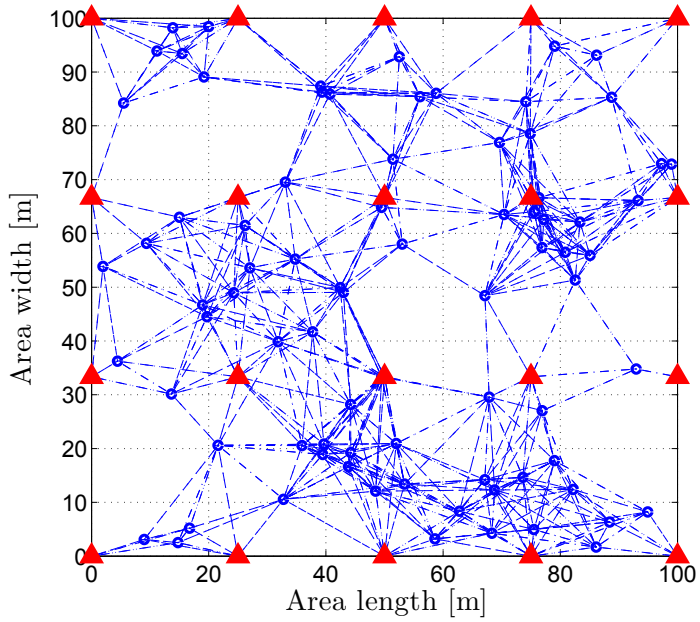

(b) Grid anchor placement.

FIGURE 4.8 – Different anchors placements.

strategies. As can be observed from this figure, the average NLEE of each algorithm decreases, as expected, with both the node degree and communication range. However, the accuracy gain of the proposed algorithm is much more important than those of its counterparts. In contrast

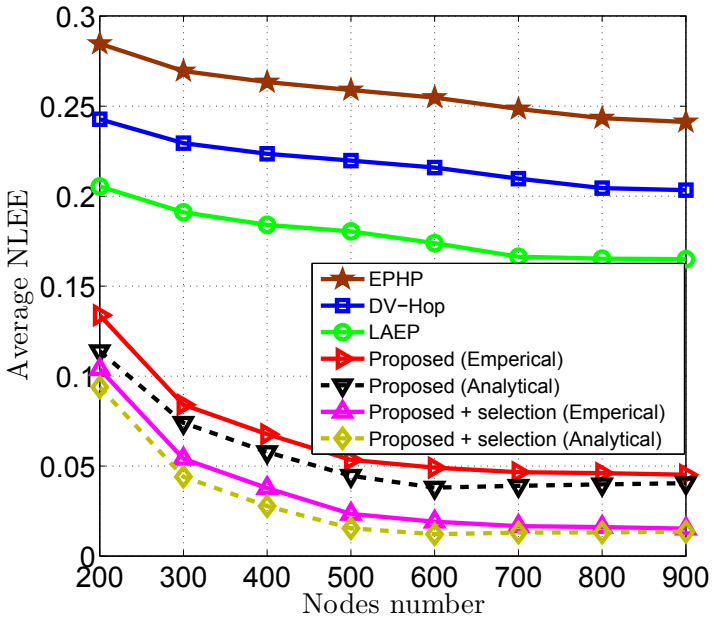

(a) Perimeter anchor placement.

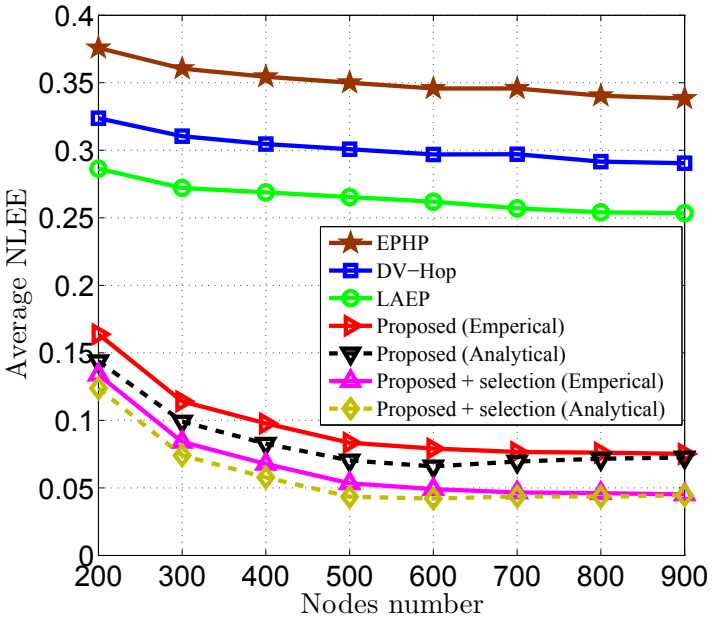

(b) Grid anchor placement.

FIGURE 4.9 – Average NLEE achieved by the proposed algorithm, DV-Hop, LAEP, and EPHP with both perimeter and grid anchor placement strategies versus the nodes number N.

to the latter, its average NLEE approaches 0 when the node degree and/or the communication range increase(s).

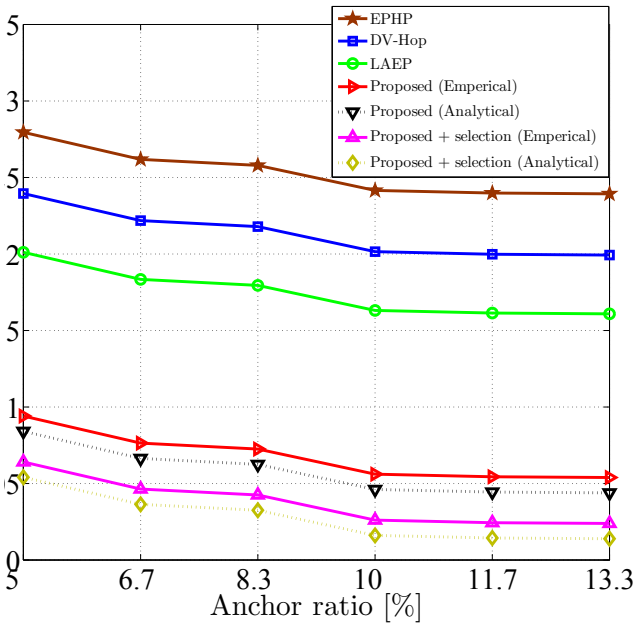

(a) Perimeter anchor placement.

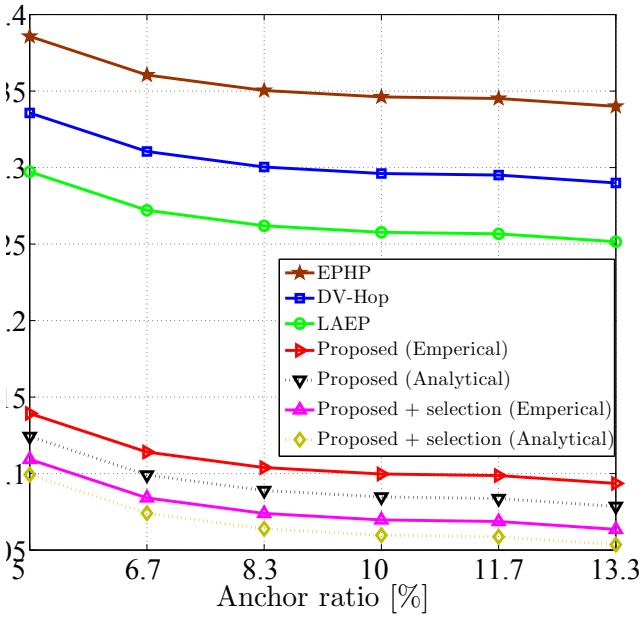

(b) Grid anchor placement.

FIGURE 4.10 – Average NLEE achieved by the proposed algorithm, DV-Hop, LAEP, and EPHP with both perimeter and grid anchor placement strategies versus the anchor ratio when the nodes number $N = 300$.

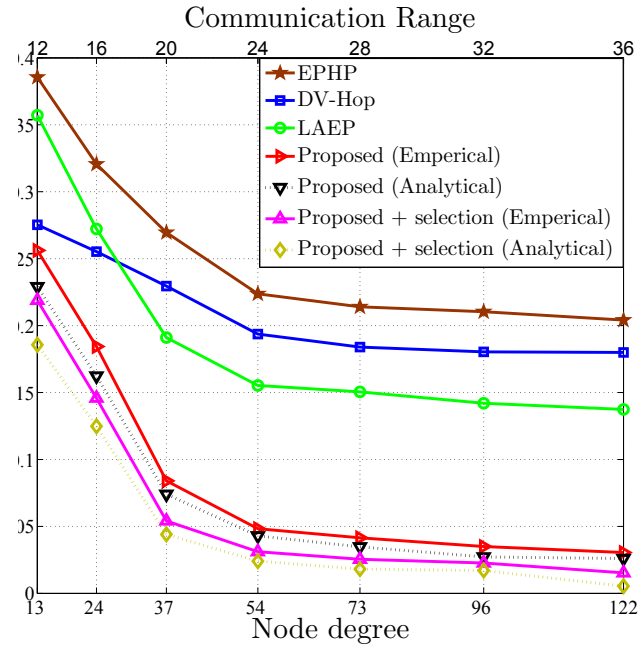

(a) Perimeter anchor placement.

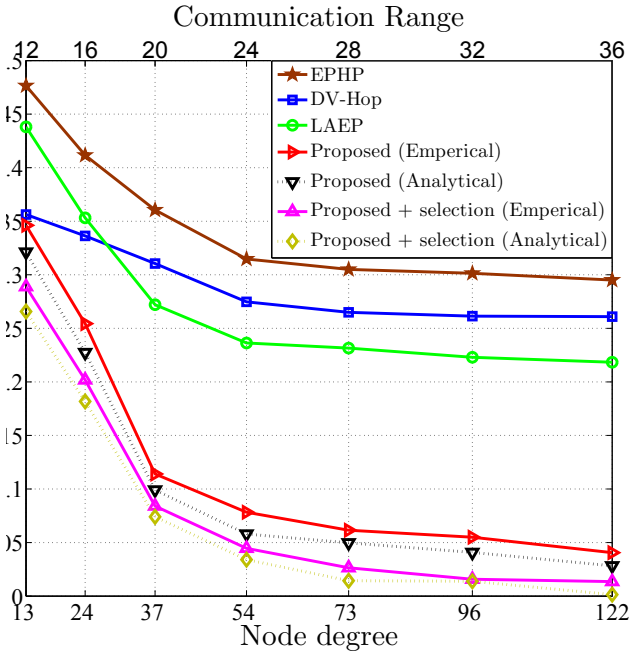

(b) Grid anchor placement.

FIGURE 4.11 – Average NLEE achieved by the proposed algorithm, DV-Hop, LAEP, and EPHP with both perimeter and grid anchor placement strategies versus the node degree and communication range when the nodes number $N = 300$.

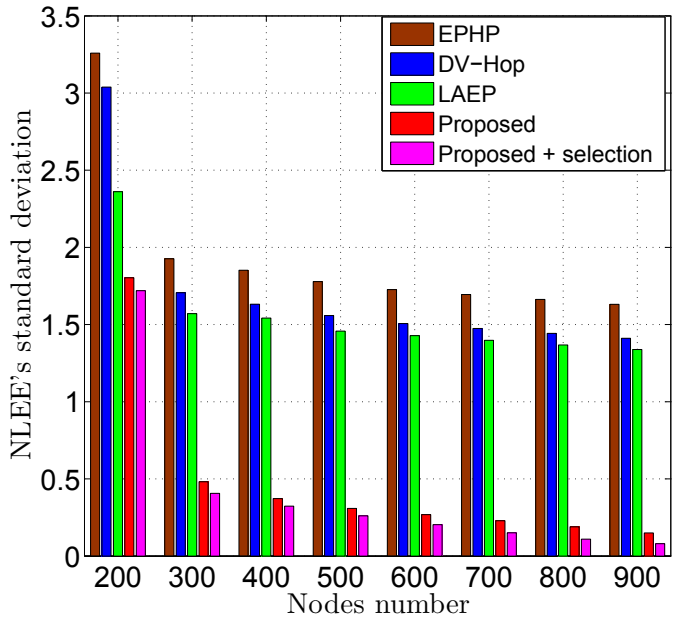

(a) Perimeter anchor placement.

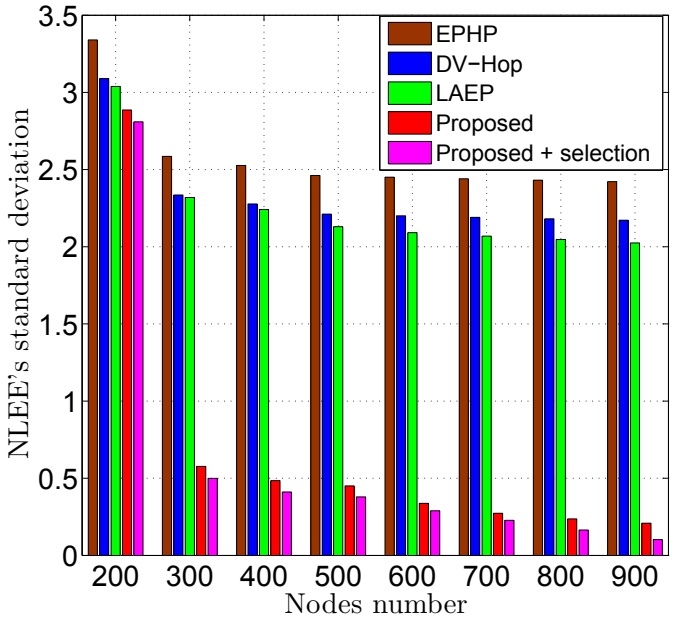

(b) Grid anchor placement.

FIGURE 4.12 – NLEE's standard deviation achieved by the proposed algorithm, DV-Hop, LAEP, and EPHP with both perimeter and grid anchor placement strategies versus the nodes number N.

Fig. 4.12 plots the NLEE's standard deviation achieved by all localization algorithms versus N, for two anchor placement strategies : perimeter in Fig. 4.12(a) and grid placement in Fig. 4.12(b). As it can be observed from these figures, regardless of the anchor placement strategy, the one achieved by the proposed algorithm substantially decreases when N increases while those achieved by the other algorithms slightly decrease. Furthermore, the NLEE's standard deviation achieved by the proposed algorithm with or without anchor selection approaches 0 for any placement strategy. This is due to the fact that the LEE itself being around 0 occurs almost certainly (i.e., with almost probability 1) as stated in Section 4.5.3. On the other hand, Figs. 4.12(a) and 4.12(b) suggest that the proposed algorithm's performance is further improved if the low-cost anchor selection scheme introduced in Section 4.5.2 is implemented at each sensor. All these observations corroborates the results and discussions disclosed in Section 4.5.

Fig. 4.13 illustrates the NLEE's CDF achieved by our proposed localization algorithm with and without the anchor selection scheme as well as that achieved by the other algorithms for two anchor placement strategies : perimeter in Fig. 4.12(a) and grid placement in Fig. 4.12(b). From these figures, using the proposed algorithm, 80% (98% with anchor selection) of the sensors could estimate their position with NLEE less than 0.2. In contrast, 45% of the nodes achieve the same accuracy with LAEP and only about 38% with DV-Hop using the perimeter anchor placement strategy. This proves even more the accuracy of the proposed localization algorithm.

Fig. 4.14 plots the average NLEE achieved by the proposed algorithm and its counterparts versus the degree of range irregularity (DoI). In this figure, the transmission range is no longer assumed circular. A range irregularity model similar to that in [8] was implemented instead. From Fig. 4.14, the average NLEEs achieved by all algorithms deteriorates due to the range irregularity. This is expected since this phenomena is not taken Figs. 4.14(a) and 4.14(b), the proposed algorithm remains more accurate than its counterparts. This further proves the superiority of our proposed algorithm over the latter.

We plot the average NLEE achieved by the proposed algorithm and its counterparts versus N in two different anisotropic topologies commonly used in the context of WSNs : the O-shaped and the U-shaped illustrated in Figs. 4.15(a) and 4.15(b), respectively. We observe from Figs. 4.16 and 4.17, respectively, that From these figures, the average NLEEs achieved by all algorithms deteriorate due to the presence of obstacles (i.e., areas with no nodes, for instance mountains, hills, etc.) in the network. This is expected since such obstacles, which are not taken

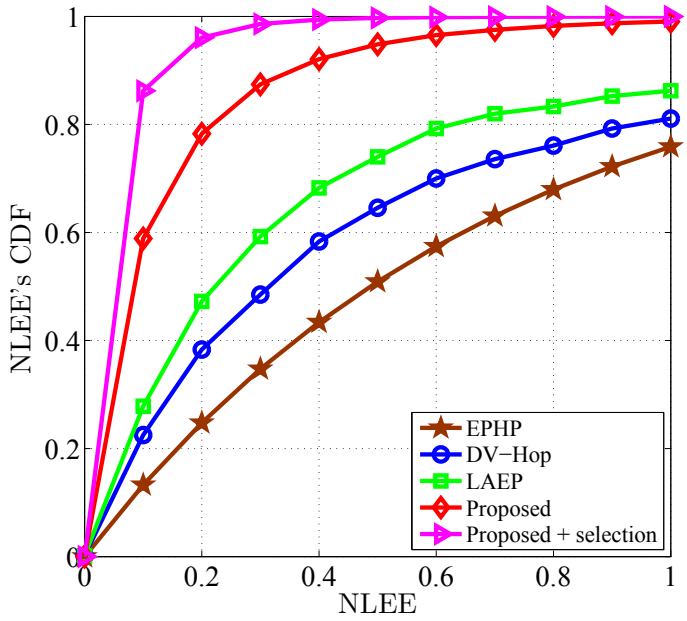

(a) Perimeter anchor placement.

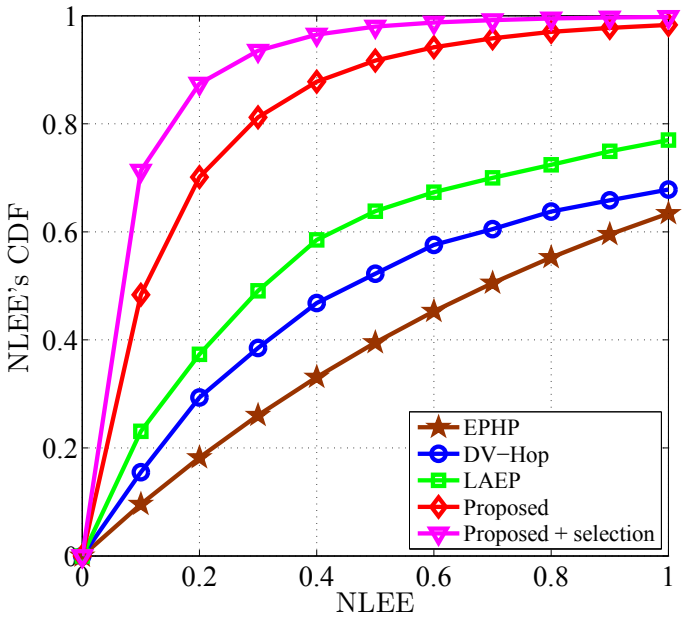

(b) Grid anchor placement.

FIGURE 4.13 – NLEE's CDF achieved by the proposed algorithm, DV-Hop, LAEP, and EPHP with both perimeter and grid anchor placement strategies when the nodes number $N = 300$.

into account when designing theses algorithms, cause DE estimation errors, thereby hindering their accuracies. However, as could be observed from Figs. 4.16 and 4.17, the proposed algorithm

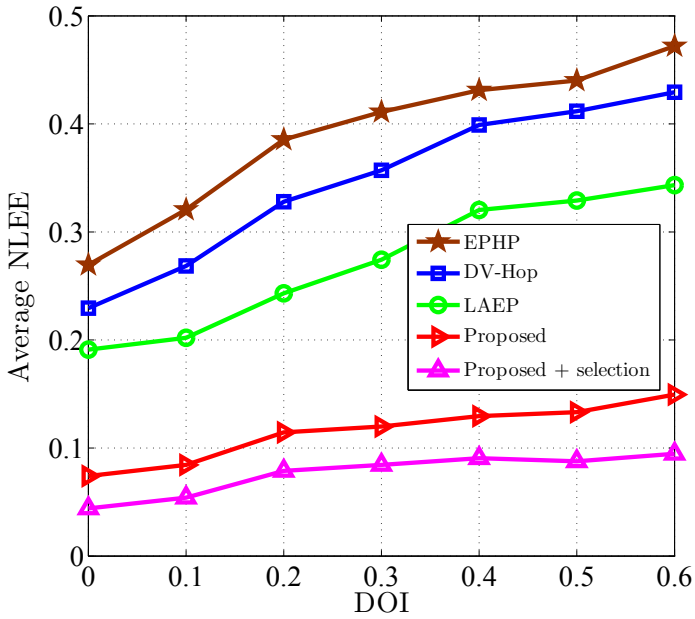

(a) Perimeter anchor placement.

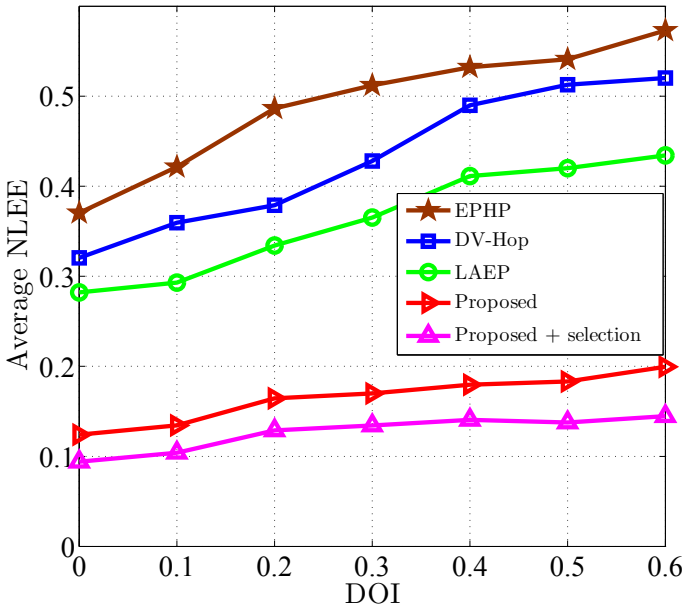

(b) Grid anchor placement.

FIGURE 4.14 – Average NLEE achieved by the proposed algorithm, DV-Hop, LAEP, and EPHP versus the DoI with both perimeter and grid anchor placement strategies when the nodes number $N = 300$.

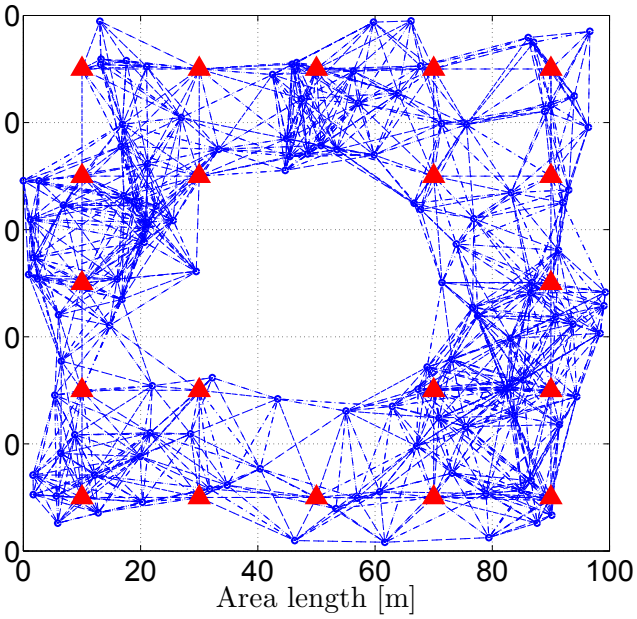

(a) O-shaped topology.

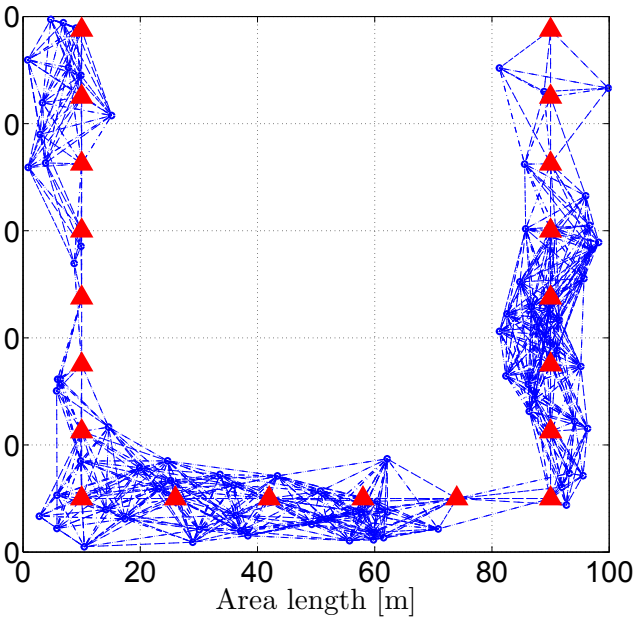

(b) U-shaped topology.

FIGURE 4.15 – Different network topologies.

remains more accurate than its counterparts. This proves its robustness against the latter, in anisotropic environments.

Fig. 4.18 shows the total number of exchanged packets N_{packets} using by the proposed al-

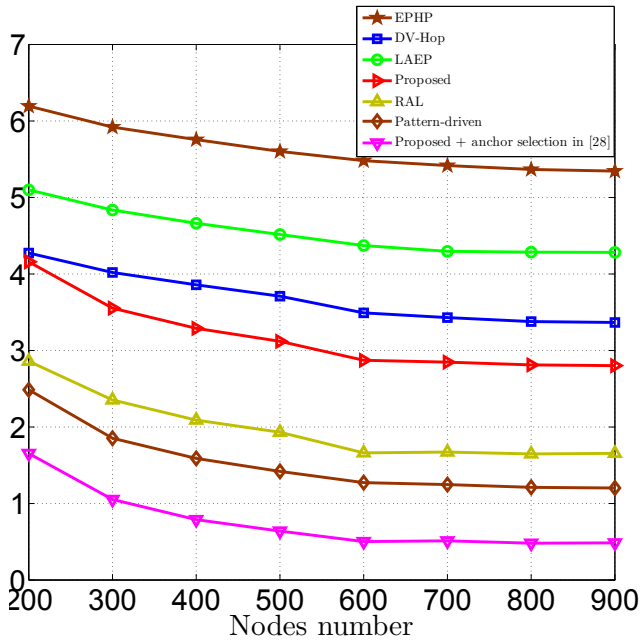

(a) Perimeter anchor placement.

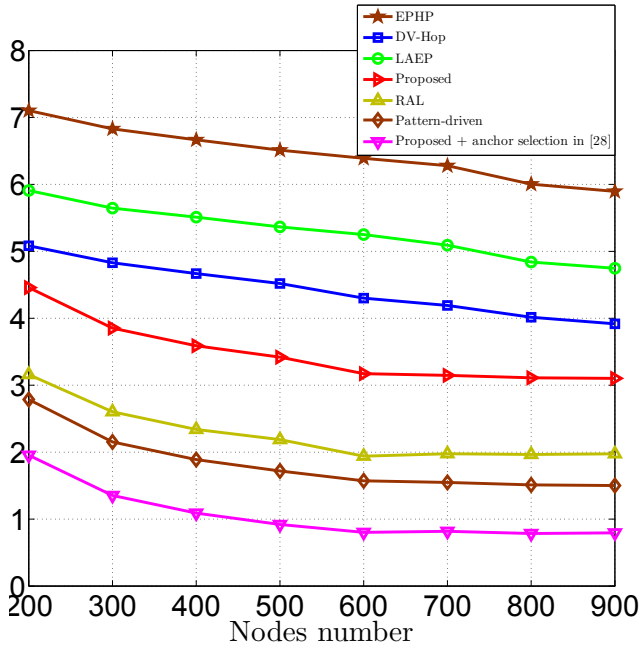

(b) Grid anchor placement.

FIGURE 4.16 – Average NLEE achieved by the proposed algorithm, DV-Hop, LAEP, and EPHP with both perimeter and grid anchor placement strategies versus the nodes number N in the O-Shaped topology.

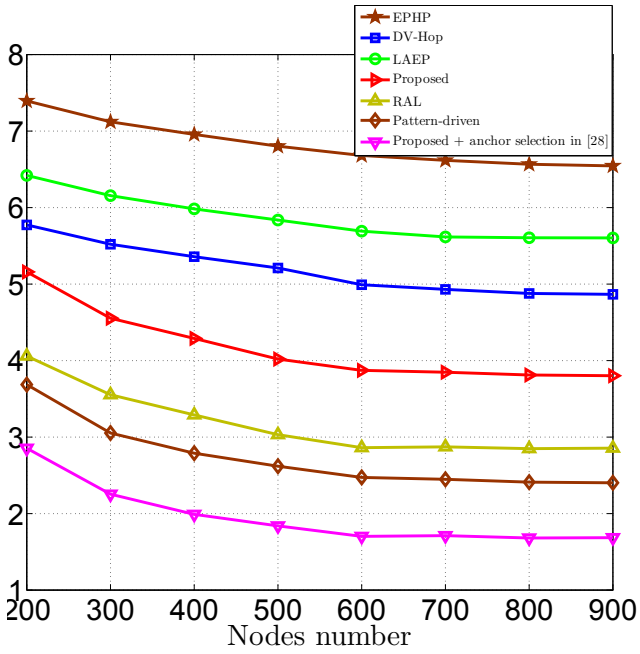

(a) Perimeter anchor placement.

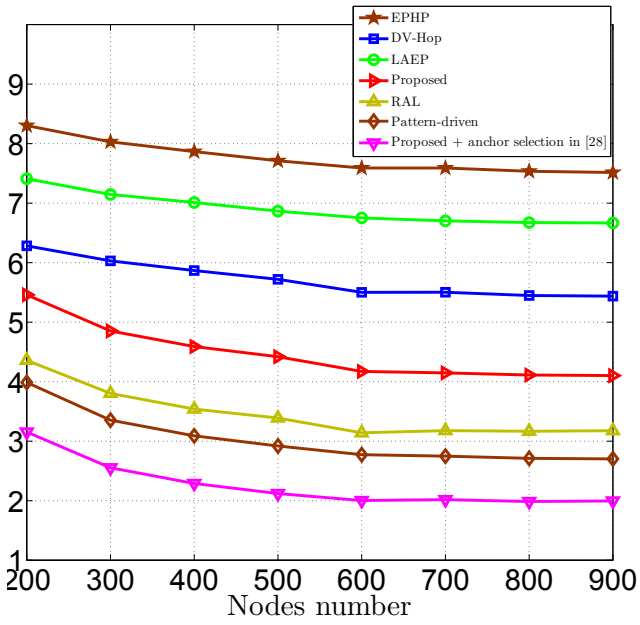

(b) Grid anchor placement.

FIGURE 4.17 – Average NLEE achieved by the proposed algorithm, DV-Hop, LAEP, and EPHP with both perimeter and grid anchor placement strategies versus the nodes number N in the U-Shaped topology.

gorithm and its counterparts versus the node density. As could be seen from this figure, the proposed algorithm requires the same number of exchanged packets as LAEP and EPHP while

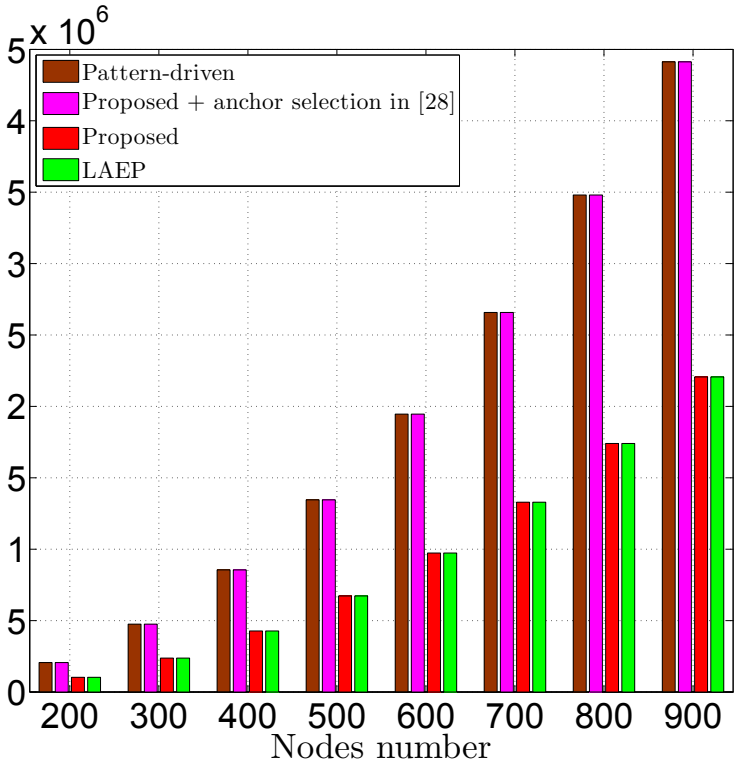

FIGURE 4.18 – The total number of exchanged packets N_{packets} versus the node density.

it requires half the packets exchanged with DV-Hop. This is expected since the three first are analytical algorithms where the EHP evaluation and, hence, the position estimation are locally performed at each node after the initialization step, without requiring any additional information exchange. This is in contrast with DV-hop whose heuristical nature imposes a second broadcast from the anchors to assist regular nodes' self-localization. This implies that the overall power required by our algorithm to transmit and receive the exchanged packets is the same as that required by LAEP and EPHP while it is the half of that needed by DV-Hop. On the other hand, the additional power cost incurred by the proposed algorithm due to the correction mechanism's instructions is negligible and to the few extra bits in each packet is easily avoidable, as discussed in Section 2.6. Therefore, our proposed algorithm incurs almost the same power cost as LAEP and EPHP while it incurs the half cost of DV-hop. This proves that the proposed algorithm outperforms in accuracy all its counterparts, yet a no extra power cost, thereby highlighting its superiority.

4.7 Conclusion

In this paper, we proposed a novel localization algorithm which properly exploits, in addition to the hop-based information, the forwarding nodes' number between any anchor-sensor pair. Its average location estimation error (LEE) was derived in closed-form and compared to those of the best representative algorithms in the literature. We showed that the proposed algorithm outperforms them in accuracy. Furthermore, we proved that, in contrast to the latter, our algorithm is able to achieve an average LEE of about 0, when the total sensors' number N is large enough. We also proved in such a condition that any realization of its achieved LEE approaches 0, which confirms unambiguously its high accuracy.

Appendix A

In order to compute $\mathrm{E}\{\epsilon_k\}$ and $\mathrm{E}\{\epsilon_k^2\}$ for any given n_h, one should distinguish two cases : a) n_h is even and b) n_h is odd. Let us first assume that n_h is even. In such a case, $n_h/2$ 2-hop distances exist between the i-th sensor and the k-th anchor nodes and, hence,

$$d_{i-k} = \sum_{r=1}^{n_h/2} d_r, \tag{4.37}$$

where d_r denotes the r-th 2-hop distance. ϵ_k is then given by

$$\epsilon_k = \left(\sum_{r=1}^{n_h/2} \hat{d}_r \right)^2 - \left(\sum_{r=1}^{n_h/2} d_r \right)^2, \tag{4.38}$$

where $\hat{d}_r$ is the estimated r-th 2-hop distance. Applying (4.26) to $\hat{d}_r$ and retaining the two first non-zero terms, ϵ_k could be equivalently expressed as

$$\epsilon_k = \left(\sum_{r=1}^{n_h/2} \zeta\left(F_{k,r}\right) \right)^2 + 2 \sum_{r=1}^{n_h/2} \Psi\left(F_{k,r}\right) \sum_{r=1}^{n_h/2} \zeta\left(F_{k,r}\right), \tag{4.39}$$

where $F_{k,r}$ is the forwarding area associated with d_r and

$$\zeta\left(F_{k,r}\right) = \Psi^{(1)}\left(F_{k,r}\right)\left(\frac{m_{k,r}}{\lambda} - F_{k,r}\right) + \frac{\Psi^{(2)}\left(F_{k,r}\right)}{2}\left(\frac{m_{k,r}}{\lambda} - F_{k,r}\right)^2, \tag{4.40}$$

where $m_{k,r}$ is the number of forwarding sensors in $F_{k,r}$. It follows from (4.39) that

$$\mathrm{E}\left\{\epsilon_k\right\}=\frac{n_h}{2N}\left(\xi_{0,2}+2\xi_{1,1}+2\xi_{0,1}\left(\frac{n_h}{2}-1\right)\left(\frac{\xi_{0,1}}{N}+\xi_{1,0}\right)\right), \tag{4.41}$$

where $\xi_{1,0}=\mathrm{E}\left\{\Psi\left(F_{k,r}\right)\right\}$, $\xi_{2,0}=\mathrm{E}\left\{\Psi\left(F_{k,r}\right)^2\right\}$, and $\xi_{n,m}=N\mathrm{E}\left\{\Psi\left(F_{k,r}\right)^n\zeta\left(F_{k,r}\right)^m\right\}$ for $(n,m)\in\left\{(i,j)|i,j=0,1,2\right\}\setminus\left\{(1,0),(2,0)\right\}$. In order to obtain (4.41), please note that, we resort to the Multinomial theorem to break $\left(\sum_{r=1}^{n_h/2}\zeta\left(F_{k,r}\right)\right)^2$ into several terms.

Now, let us turn our attention to the computation of $\xi_{n,m}$. We first start by $\xi_{0,1}=N\mathrm{E}\left\{\zeta\left(F_{k,r}\right)\right\}$. Since the sensors are uniformly deployed in S, the probability of having $m_{k,r}$ sensors in $F_{k,r}$ follows a Binomial distribution $\mathrm{Bin}\left(N,\frac{F_{k,r}}{S}\right)$ and, hence, we have

$$\mathrm{E}_{m_{k,r}}\left\{\zeta\left(F_{k,r}\right)\right\}=\Psi^{(2)}\left(F_{k,r}\right)F_{k,r}\left(1-\frac{F_{k,r}}{S}\right), \tag{4.42}$$

where $\mathrm{E}_{m_{k,r}}$ refers to the expectation with respect to $m_{k,r}$. Using (4.42) and integrating by parts twice yields

$$\begin{aligned}\xi_{0,1}=&\frac{S}{2F_{\max}}\left[\Psi^{(1)}\left(F\right)F\left(1-\frac{F}{S}\right)-\Psi\left(F\right)\left(1-2\frac{F}{S}\right)\right]_0^{F_{\max}}-\\&\frac{1}{F_{\max}}\int_0^{F_{\max}}\Psi\left(F\right)dF.\end{aligned} \tag{4.43}$$

$\xi_{0,1}$'s expression is then obtained by substituting $\Psi\left(F_{\max}\right)$ with R and $F_{\max}$ with its expression.

As far as $\xi_{0,2}$ is concerned, it can be readily shown that

$$\xi_{0,2}=\frac{S}{2F_{\max}}\int_0^{F_{\max}}\left(\Psi^{(1)}\left(F\right)\right)^2F\left(1-\frac{F}{S}\right)dF. \tag{4.44}$$

In order to compute the above integral, one could apply the variable change $F=\Phi(x)$. From (4.4), this implies that $dF=\sqrt{4R^2-x^2}dx$ where $x\in[R,2R]$. $\xi_{0,2}$ is then easily obtained by integrating over x. It is noteworthy that, using similar approaches as above, all the expressions of $\xi_{n,m}$ $n,m=0,1,2$ could be derived.

Let us focus now on the case where n_h is odd. It follows from (4.26), (4.8), and (4.13) that ϵ_k is given by

$$\begin{aligned}\epsilon_k=&\left(\sum_{r=1}^{(n_h-1)/2}\zeta\left(F_{k,r}\right)\right)^2+2\sum_{r=1}^{(n_h-1)/2}\Psi\left(F_{k,r}\right)\sum_{r=1}^{(n_h-1)/2}\zeta\left(F_{k,r}\right)+\\&\frac{4R}{3}\sum_{r=1}^{(n_h-1)/2}\zeta\left(F\right)+\frac{4R^2}{9}-Z^2.\end{aligned} \tag{4.45}$$

Recall here that Z refers to the random variable d^{Last}. It follows then from (4.45) that

$$\begin{aligned}\mathrm{E}\{\epsilon_k\} = & \frac{n_h-1}{2N}\Big(2\xi_{0,1}\left(\left(\frac{n_h-1}{2}-1\right)\left(\frac{\xi_{0,1}}{N}+\xi_{1,0}\right)+\frac{2R}{3}\right) \\ & +\xi_{0,2}+2\xi_{1,1}\Big). \end{aligned} \tag{4.46}$$

Finally, using (4.41) and (4.41), (4.31) is obtained.

Following similar above steps, (4.32) is also obtained.

Bibliographie

[1] D.P. Agrawal and Q.-A. Zeng, *Introduction to Wireless and Mobile Systems,* 3^{rd} edition Cengage Learning, USA, 2010.

[2] F. Akyildiz, W. Su, Y. Sankarasubramaniam, and E. Cayirci, "A survey on sensor networks," *IEEE Commun. Mag.,* vol. 40, no. 8, pp. 102-114, August 2002.

[3] J.N. Al-Karaki and A.E. Kamal, "Routing techniques in wireless sensor networks : a survey," *IEEE Wireless Commun.* vol. 11, no. 6, pp. 6-8, December 2004.

[4] F. Gustafsson and F. Gunnarsson, "Mobile Positioning Using Wireless Networks : Possibilities and Fundamental Limitations Based on Available Wireless Network Measurements," *IEEE Signal Process. Mag.,* vol. 22, no. 4, pp. 41-53, July 2005.

[5] V. Lakafosis and M.M. Tentzeris, "From single-to multihop : The status of wireless localization," *IEEE Microw. Mag.,* vol. 10 , no. 7, pp. 34-41, December 2009.

[6] J. Rezazadeh, M. Moradi, A.S. Ismail and E. Dutkiewicz, "Superior Path Planning Mechanism for Mobile Beacon-Assisted Localization in Wireless Sensor Networks," *IEEE Sensors J.,* vol. 14, no. 9, pp. 3052-3064, May 2014.

[7] H. Shen, Z. Ding, S. Dasgupta, and C. Zhao, "Multiple Source Localization in Wireless Sensor Networks Based on Time of Arrival Measurement," *IEEE Trans. Signal Process.,* vol. 62, no. 8, pp. 1938-1949, February 2014.

[8] D. Niculescu and B. Nath, "Ad hoc positioning system (APS)," *Proc. IEEE GLOBECOM'2001,* San Antonio, TX, USA, November 25-29, 2001.

[9] Z. Ziguo and T. He,"RSD : A Metric for Achieving Range-Free Localization beyond Connectivity," *IEEE Trans. parallel and distributed Sys.,* vol. 24, no. 11, pp. 1943-1951 , November 2011.

[10] T. He, C. Huang, B. M. Blum, J. A. Stankovic, and T. Abdelzaher, "Range-free localization schemes for large scale sensor networks," *Proc. ACM MobiCom'03,* San Diego, California, USA, September 14-19, 2003.

[11] A. Boukerche, H.A.B.F. Oliveira, E.F. Nakamura, A.A.F. Loureiro, "DV-Loc : a scalable localization protocol using Voronoi diagrams for wireless sensor networks," *IEEE Wireless. Commun. Mag.,* vol. 16, no. 2, pp. 50-55, April 2009.

[12] L. Gui, T. Val, A. Wei, "Improving Localization Accuracy Using Selective 3-Anchor DV-Hop Algorithm," *Proc. IEEE VTC'2011,* San Francisco, CA, USA, Septembre 5-8, 2011.

[13] C. Bettstetter, J. Eberspacher, "Hop distances in homogeneous ad hoc networks," *Proc. IEEE VTC'2003,* Jeju Island, Korea, April 22-25, 2003.

[14] C. Buschmann, H. Hellbrück, S. Fischer, A. Kroller and S. Fekete, "Radio Propagation-A ware Distance Estimation Based on Neighborhood Comparison," *Proc. EWSN'07,* Delft, Netherlands, January 29-31, 2007.

[15] B. Huang, C. Yu, B. D. O. Anderson and G. Mao, "Estimating distances via connectivity in wireless sensor networks," *Wirel. Commun. Mob. Com.,* vol. 14, no. 5, pp. 541-556, April 2014.

[16] X. Ta, G. Mao, and B. D. Anderson, "On the probability of k-hop connection in wireless sensor networks," *IEEE Commun. Lett.,* vol. 11, no. 9, pp. 662-664, August 2007.

[17] R. Yates and D. Goodman, *Probability and Stochastic Process,* 2^{nd} edition Wiley, New York, USA, 2004.

[18] X. Ta, G. Mao, and B. D. Anderson, "Evaluation of the probability of k-hop connection in homogeneous wireless sensor networks," *Proc. IEEE GLOBECOM'2007,* Washington, DC, USA, November 26-30, 2007.

[19] Y. Wang, X. Wang, D. Wang, and D. P. Agrawal, "Range-Free Localization Using Expected Hop Progress in Wireless Sensor Networks," *IEEE Trans. Parallel Distrib. Syst.,* vol. 25, no. 10, pp. 1540-1552, October 2009.

[20] L. Kleinrock and J. Silvester, "Optimum Transmission Radii for Packet Radio Networks or Why Six is a Magic Number," *in Proc. IEEE NTC '1978,* Birmingham, AL, Alabama, December 4-6, 1978.

[21] A. El Assaf, S. Zaidi, S. Affes, and N. Kandil, "Efficient Range-Free Localization Algorithm for Randomly Distributed Wireless Sensor Networks," *IEEE GLOBECOM'2013,* Atlanta, GA, December 9-13, 2013.

[22] A. EL Assaf, S. Zaidi, S. Affes, and N. Kandil, "Range-free localization algorithm for heterogeneous wireless sensors networks," *Proc. IEEE WCNC'2014,* Istanbul, Turkey, Apr. 6-9, 2014.

[23] S. Vural and E. Ekici, "On Multihop Distances in Wireless Sensor Networks with Random Node Locations," *IEEE Trans. Mobile Comput.,* vol. 9, no. 4, pp. 540-552, April 2010.

[24] M. Haenggi, "On distances in uniformly random networks," *IEEE Trans. Inf. Theory,* vol. 51 , no. 10 , pp. 3584-3586, October 2005.

[25] JC. Kuo, W. Liao, "Hop Count Distribution of Multihop Paths in Wireless Networks With Arbitrary Node Density : Modeling and Its Applications," *IEEE Trans. Veh. Technol.,* vol. 56, no. 4, pp. 2321-2331, July 2007.

[26] M. Li and Y. Liu,, "Rendered path : Range-free localization in anisotropic sensor networks with holes," *IEEE/ACM Trans. Netw.,* vol. 18, no. 1, pp. 320-332, February 2010.

[27] Z. Shigeng, C. Jiannong, L.-J. Chen , C. Daoxu Chen, "Accurate and Energy-Efficient Range-Free Localization for Mobile Sensor Networks," *IEEE Trans. Mobile Comput.,* vol. 9, no. 6, pp. 897-910, June 2010.

[28] A. El Assaf, S. Zaidi, S. Affes, and N. Kandil, "Accurate Nodes Localization in Anisotropic Wireless Sensor Networks,". *Inter. J. Dist. Sensor Net.*, vol. 2015, pp. 1-17, April 2015.

[29] B. Xiao, L. Chen, Q. Xiao, M. Li , "Reliable Anchor-Based Sensor Localization in Irregular Areas," *IEEE Trans. Mobile Comput.,* vol. 9, no. 1, pp. 60-72, January 2010.

[30] Q. Xiao, B. Xiao, J. Cao, J. Wang, "Multihop Range-Free Localization in Anisotropic Wireless Sensor Networks : A Pattern-Driven Scheme," *IEEE Trans. Mobile Comput.,* vol. 9, no. 11, pp. 1592-1607, November 2010.

[31] W. Dargie and C. Poellabauer, *Fundamentals of Wireless Sensor Networks : Theory and Practice,* 1^{st} edition Wiley, New York, USA, 2010.

[32] R. N. Duche and N. P. Sarwade, "Sensor Node Failure Detection Based on Round Trip Delay and Paths in WSNs," *IEEE Sensors J.,* vol. 14, no. 2, pp. 455-464, February 2014.

[33] N. Patwari, J.N. Ash, S. Kyperountas, A.O. Hero, R.L. Moses and N.S. Correal, "Locating the nodes : cooperative localization in wireless sensor networks," *IEEE Signal Processing Mag.,* vol. 22, no. 4, pp. 54-69, July 2005.

[34] J.C. Chen, K. Yao, and R.E. Hudson, "Source localization and beamforming," *IEEE Signal Processing Mag.,* vol. 19, no. 2, pp. 30-39, March 2002.

[35] S. Biaz, Ji. Yiming, Q. Bing, Wu. Shaoen, "Realistic radio range irregularity model and its impact on localization for wireless sensor networks," *IEEE WiCOM'2005,* Wuhan, China, Sept. 23-26 2005.

Chapitre 5

Robust ANNs-based WSN Localization in the Presence of Anisotropic Signal Attenuation

Ahmad El Assaf, Slim Zaidi, Sofiène Affes and Nahi Kandil

Accepted for publication in *IEEE Wireless Communications Letter,* July 2016.

Résumé : Afin d'élargir encore plus les domaines d'application des algorithmes de localisation proposés, ce chapitre propose un nouvel algorithme de localisation *range-free* pour les réseaux de capteurs sans fil (WSN)s qui est robuste contre l'atténuation anisotrope du signal induite l'évanouissement (fading), effet de masque (shadowing), et les interférences, etc., présents dans n'importe quel canal sans fil, et de développer par la présente une technique robuste d'estimation des distances entre les nœuds. En exploitant les réseaux de neurones artificiels (ANNs), on a réussi à développer un mécanisme de correction des distances estimées à faible coût qui tient compte correctement pour l'atténuation anisotrope du signal. Il est prouvé que l'algorithme proposé surpasse les algorithmes de localisation la plus représentatifs, non seulement de la précision, mais aussi dans la robustesse.

Abstract

We propose a novel range-free localization algorithm for wireless sensor networks (WSN)s that is robust against the anisotropic signal attenuation induced by fading, shadowing, and interference, etc., present in any wireless channel, and hereby develop a new distance estimation (DE) approach able to efficiently derive distances' estimates in closed-form. Exploiting artificial neural networks (ANN)s, we also develop a power-efficient DE correction mechanism that properly accounts for anisotropic signal attenuation. Simulation results show that the proposed algorithm significantly outperforms most representative range-free localization algorithms, not only in accuracy, but also in robustness against anisotropic attenuation.

5.1 Introduction

Localization is crucial for many WSN applications such as environment monitoring, disaster relief, and target tracking [2]. So far, several localization algorithms have been proposed in the literature. These algorithms can be roughly classified into two categories : range-based and range-free [2]. To properly localize the regular or position-unaware node positions, range-based algorithms exploit the measurements of some specific received signals' characteristics such as the time of arrival (TOA), the angle of arrival (AOA), or the received signal strength (RSS). These signals are, in fact, transmitted by nodes aware of their positions called anchors (or landmarks). Although range-based algorithms are very accurate, in general, they are unsuitable for WSNs. Indeed, these algorithms require high power to ensure communication between anchors and regular nodes which are small battery-powered units. Furthermore, additional hardware is usually required at both anchors and regular nodes [3], thereby increasing the overall cost of the network. Unlike range-based algorithms, range-free algorithms, which rely on the network connectivity to estimate the regular node positions, are more power-efficient and do not require any additional hardware and, hence, are suitable for WSNs. Due to their practical merits, range-free localization algorithms have garnered the attention of the research community. The range-free techniques developed so far fall in two classes : heuristic and analytical [4]-[6]. Heuristic algorithms are more or less a variation of the well-known DV-HOP [4] whose implementation in WSNs requires the overhead-burdened calculation (by input reception) and broadcast (by

output transmission) of a correction factor by each anchor. Such undesired impediment incurs prohibitive overhead and power consumption thereby increasing the overall cost of the network. On the other hand, analytical algorithms [13]-[6] evaluate theoretically the distances between the anchors and regular nodes. These distances are in fact locally computable at each node, thereby avoiding the above-mentioned impediments of heuristic algorithms. In spite of their valuable contributions [13]-[6], these techniques rely on the unrealistic assumption that nodes have a circular radio propagation pattern (RPP). However, due to real-world phenomena such as fading, shadowing, and interference, etc., present in any wireless channel, anisotropic signal attenuation (i.e., different from a direction to another) occurs, thereby resulting in practice to irregular nodes' RPPs [8]. Hence, if the latter are not properly taken into account, distance estimation (DE) errors increase significantly and severely hinder localization accuracy.

In this letter, we propose a novel analytical algorithm robust against the anisotropic signal attenuation and develop a new DE approach able to efficiently derive distances' estimates in closed-form. Exploiting ANNs, we also develop a power-efficient DE correction mechanism that properly accounts for anisotropic signal attenuation. Simulation results show that the proposed algorithm outperforms most representative range-free localization algorithms, not only in accuracy, but also in robustness against anisotropic attenuation.

5.2 Network model

Fig. 5.1(a) illustrates the system model of N WSN nodes uniformly and independently deployed in a 2-D square area S. Due to the high cost of the global positioning system (GPS) technology, only a few nodes commonly known as anchors are equipped with it and, hence, are aware of their positions. The other nodes, called hereafter position-unaware or regular nodes for the sake of simplicity, are oblivious to this information. In Fig. 5.1(a), the anchor nodes are marked with red triangles while the regular ones are marked with blue discs. Without loss of generality, let $(x_i, y_i)\,,\ i = 1, \ldots, N_a$ be the coordinates of the anchor nodes and $(x_i, y_i)\,,\ i = N_a + 1, \ldots, N$ those of the regular ones. All nodes are assumed to have the same transmission capability (i.e., range) denoted by R. An anisotropic signal attenuation (i.e., varies from a direction to another) is also assumed, due to phenomena such as fading, shadowing, and interference, etc., present in any wireless channel. This leads, as illustrated in Fig. 5.1(a), to irregular RPPs. Hence, the green

curves there represent the nodes' irregular RPPs while the black circles represent their idealistic ones (i.e., without accounting for fading, shadowing, and interference, etc.).

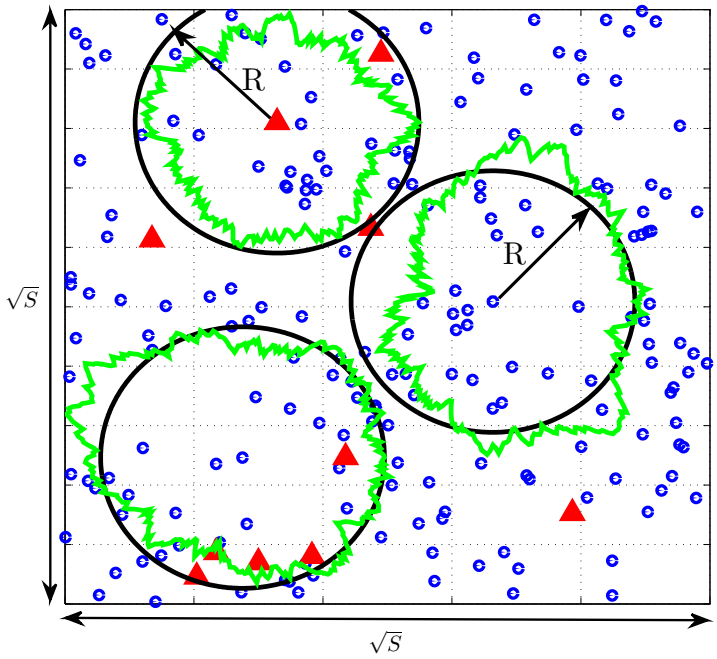

(a) Network model.

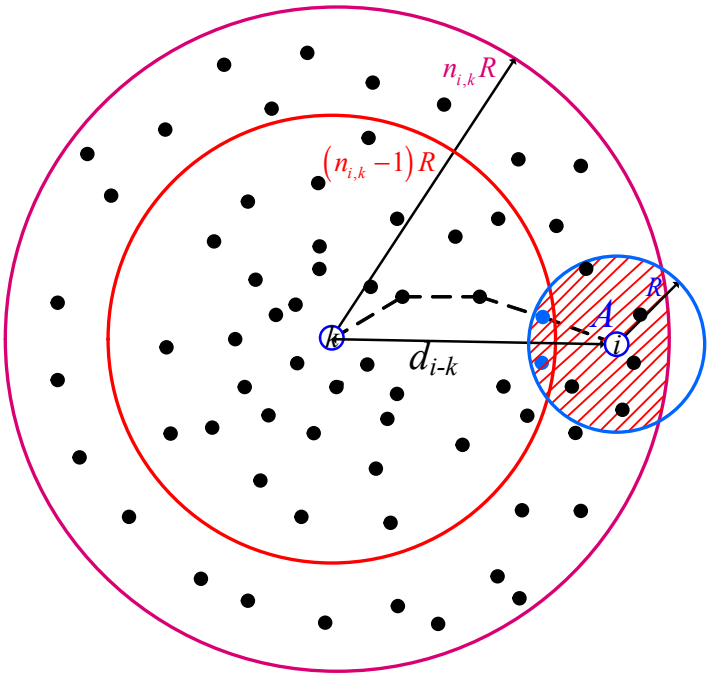

(b) Distance estimation.

FIGURE 5.1

In what follows, we propose an efficient localization algorithm which accounts for the nodes' irregular RPPs when estimating the regular nodes' positions. Such an algorithm requires that these nodes estimate their distances to 3 anchors, at least, and be aware of their coordinates [4]-[6]. The more accurate is DE, the more reliable is localization. Hence, we propose in the next section a novel DE approach for proper integration later in our proposed WSN localization algorithm.

5.3 Proposed DE approach

So far, in most previous algorithms, the i-th regular node (i.e., $(N_a + i)$-th node) estimates its distance to the k-th anchor d_{i-k} as

$$\hat{d}_{i-k} = n_{i,k} h_{\text{av}}, \tag{5.1}$$

where $n_{i,k}$ is the number of hops between the two nodes and h_{av} is a predefined average hop size (AHS). Unfortunately, this approach exhibits a major drawback. Indeed, AHS is usually derived either analytically by exploiting the Poisson Limit Theorem valid for high nodes densities [13]-[6] or heuristically by computing the mean hop size of all the shortest paths between anchors [4]. It is, however, very likely that AHS be different from the mean hop size of the shortest path between the k-th and $(N_a + i)$-th nodes (i.e., $h_{\text{av}} \neq \left(\sum_{l=1}^{n_{i,k}} h_l\right) / n_{i,k}$ where h_l is the l-th hop's size). Hence, large DE errors may occur, thereby hindering the i-th regular node's localization accuracy. In order to circumvent this issue, we propose in this paper to directly estimate d_{i-k} without resorting to AHS. Indeed, it was shown that the minimum mean square error (MMSE) of the distance estimation can be obtained if [6]

$$\hat{d}_{i-k} = \mathrm{E}\left\{Z | n_{i,k}\right\}, \tag{5.2}$$

where Z denotes the random variable that represents the real distance d_{i-k}, and $\mathrm{E}\left\{\cdot | n_{i,k}\right\}$ is the expectation conditioned on $n_{i,k}$. However, due to the randomness of the nodes' irregular RPPs, the derivation of $\hat{d}_{i-k}$ in closed-form is a priori a very tedious task, if not impossible. For the sake of both simplicity and tractability, we assume herein, only temporarily, idealistic circular RPPs (i.e., there is no interference, fading or shadowing) when computing $\hat{d}_{i-k}$. In the next section, we will propose a correction mechanism that properly accounts for the effects of the nodes' irregular RPPs in the calculation of $\hat{d}_{i-k}$.

Assuming idealistic circular nodes' RPPs, it is straightforward to show that the i-th regular node is located, as illustrated in Fig. 5.1(b), in the area

$$A = D\left(k, n_{i,k}R\right) \cap D\left(i, R\right), \tag{5.3}$$

where $D(\star, x)$ is the disc having the $\star$-th node as a center and x as a radius. An in-depth look at this figure reveals that d_{i-k} is strongly dependent on A. Indeed, d_{i-k} decreases as A widens and it increases as this area narrows down. $\hat{d}_{i-k}$ could be then obtained by averaging d_{i-k} over all possible values of A and, hence, we have

$$\hat{d}_{i-k} = \int_{A_{\text{Min}}}^{A_{\text{Max}}} \Psi(A)\, f_A(a)\, da, \tag{5.4}$$

where $\Psi(A)$ is the functional relationship between d_{i-k} and A, A_{Max} and A_{Min} are the maximum and minimum value of the latter, respectively, and $f_A(a)$ is its probability density function (pdf). According to (5.4), it is clear that $\Psi(A)$ and $f_A(a)$ are crucial to obtain $\hat{d}_{i-k}$'s expression. First, let us focus on $\Psi(A)$. Using some geometrical properties and trigonometric transformations, one can show that

$$\begin{aligned} A = \Phi(d_{i-k}) &= R^2 \cos^{-1}\left(\frac{d_{i-k}^2 + R^2\left(1 - n_{i,k}^2\right)}{2Rd_{i-k}}\right) + n_{i,k}^2 R^2 \cos^{-1}\left(\frac{d_{i-k}^2 - R^2\left(1 - n_{i,k}^2\right)}{2n_{i,k}Rd_{i-k}}\right)\Bigg) \\ &- \frac{1}{2}\sqrt{\Big(R^2(1+n_{i,k})^2 - d_{i-k}^2\Big)\Big(d_{i-k}^2 - R^2(1-n_{i,k})^2\Big)}, \end{aligned} \tag{5.5}$$

where $\Phi = \Psi^{-1}$ is the inverse function of Ψ. As $\Phi(d_{i-k})$ is a complex function of d_{i-k}, $\Psi(A)$ cannot be unfortunately obtained in closed-form. We will, however, prove in the sequel that it is possible to compute the integral in (5.4) by solely exploiting the right-hand-side (RHS) of (5.5). Now let us turn our attention to $f_A(a)$. Since A could take any value in $[A_{\text{Min}}, A_{\text{Max}}]$ with the same probability, $f_A(a)$ can be considered as uniform (i.e., $f_A(a) = (A_{\text{Max}} - A_{\text{Min}})^{-1}$). Furthermore, using (5.5) alongside the fact that A_{Max} occurs when $d = (n_{i,k} - 1)\, R$ and A_{Min} occurs when $d = (n_{i,k})\, R$, we have

$$f_A(a) = \left(R^2\left(\pi - \cos^{-1}\left(\frac{1}{2n_{i,k}}\right) - n_{i,k}^2 \cos^{-1}\left(1 - \frac{1}{2n_{i,k}^2}\right) + \frac{1}{2}\sqrt{4n_{i,k}^2 - 1}\right)\right)^{-1}. \tag{5.6}$$

In order to compute $\hat{d}_{i-k}$, we propose to resort to the variable change $z = d_{i-k} = \Psi(A)$ in the integral of (5.4). This implies that $dz = \Psi^{(1)}(A)\, da$ where $\Psi^{(1)}$ is the first derivative of Ψ given by

$$\Psi^{(1)}(A) = \left(\Phi^{(1)}\left(\Psi^{(1)}(A)\right)\right)^{-1} = \left(\Phi^{(1)}\left(z\right)\right)^{-1} = -z \Big/ \sqrt{2\left(1 + n_{i,k}^2\right) R^2 z^2 - \left(n_{i,k}^2 - 1\right)^2 R^4 - z^4}, \tag{5.7}$$

where $\Phi^{(1)}$ is the first derivative of Φ. Actually, this key property - that the inverse function's first derivative depends only on the original function's first derivative - is the one to allow us compute $\hat{d}_{k-i}$ as

$$\hat{d}_{i-k} = f_A(a) \int_{(n_{i,k}-1)R}^{n_{i,k}R} \sqrt{2\left(1+n_{i,k}^2\right)R^2z^2 - \left(n_{i,k}^2-1\right)^2 R^4 - z^4}dz. \tag{5.8}$$

In (5.8), please note that we account for the fact that if $A = A_{\text{Max}}$ (or, $A = A_{\text{Min}}$), then $z = (n_{i,k}-1)\,R$ (or, $z = n_{i,k}R$). It is also noteworthy that the integral in (5.8) can be easily obtained in closed-form expressed using Elliptic functions. It follows from (5.8) that $\hat{d}_{i-k}$ depends solely on R and $n_{i,k}$ which will be shown to be locally available at every regular node in the next sections.

5.4 Proposed localization algorithm

We propose in this section a novel three-step localization algorithm. In the first step, the regular nodes receive in a multi-hop fashion all the information required to estimate their respective distances to all anchors using the DE approach developed in (5.8). In the second step, a correction mechanism that properly accounts for the effects of the real irregular nodes' RPPs is locally performed at each node in order to minimize the DE errors. In the third and last step, the regular nodes' positions are computed using the obtained distances alongside the anchors positions by resorting to conventional multilateration. Due to space limitation, only steps one and two are described in the following. Interested readers can be, however, referred to [2] for ample details on the multilateration process.

5.4.1 Step 1 : Initialization

As a first step of any anchor-based localization algorithm, the k-th anchor broadcasts through the network a packet which consists of a header followed by a data payload. The header contains the anchor position (x_k, y_k) while the data payload contains the hop-count value n initialized to one. When a node receives this packet, it stores the k-th anchor position as well as the received hop-count $n_k = n$ in its database, increments the latter (i.e., $n = n+1$), and then broadcasts the resulting message. Once this message is received by an another node, its database information is checked. If the k-th anchor information is already available and the received hop-count value

n is smaller than the one previously stored n_k, the node updates the latter, increments n by 1, then broadcasts the resulting message. If n_k is smaller than n, the node discards the received message. However, when the node is oblivious to the k-th anchor position, it adds this information to its database and forwards the received message after incrementing n by 1. This mechanism will continue until all nodes become aware of all anchors' positions and their corresponding minimum hops' numbers. Using its available information, the i-th regular node is then able to compute an estimate $\hat{d}_{i-k}$ of its distance to the k-th anchor using the DE approach developed in (5.8). Unfortunately, since this approach does not account for the real irregular nodes' RPPs significant errors occur, thereby hindering severely localization accuracy. In the sequel, we propose a new DE correction mechanism that properly accounts for the effects of the real irregular nodes' RPPs.

5.4.2 Step 2 : Distance correction

An important feature that might allow substantial reduction of DE errors, if properly exploited, is that anchors are fully aware of their true inter-distances and, further, could easily estimate them from (5.8). In order to capitalize on these data (i.e., true and estimated anchor inter-distances), we propose the exploitation in this paper of ANNs due to their ability to build the complex relationship between the true and estimated distances. ANNs consist of groups of interconnected artificial neurons. Depending on the nature of these neurons' connections, several types of ANNs exist in the literature [7]. In this letter, we only consider the multi-layer perceptron (MLP)-type feed-forward back-propagation ANNs whose efficiency has been already proven in the context of WSN localization [7]. Using all the estimated distances between anchors as inputs and the true distances as outputs of the ANN during the learning phase, we are able to generate a model or a set of parameters also known as weights and biases that governs the ANN's input-output relationship or function. It is the use of the latter through the very same ANN type at the regular nodes during the so-called generalization phase, i.e., over previously unobserved data, that allows extrapolation - through the very same linkage established over anchor inter-distances - any new ANN-input distances $\hat{d}_{i-k}$ estimated at the regular nodes assuming idealistic circular RPPs into ANN-output calibrated ones $\bar{d}_{i-k}$ that properly account for real irregular RPPs.

Nevertheless, one pending issue needs to be addressed before of our new ANN-based distance correction mechanism can be implemented properly. Indeed, as discussed above, the latter impe-

ratively requires a training phase that must necessarily be performed at a node with large power resources. In this letter, we propose that one of the anchors, called hereafter super anchor, play this role (i.e., generation through training then broadcast for generalization at other nodes the obtained generic ANN model throughout the network). The main reason for this choice is that an anchor already stores a good part of the required training data and, hence, allows substantial overall reduction of overhead, hardware complexity, and power. Actually, in many applications some anchors are nothing but access points (AP)s with large-enough power resources. Should such APs be unavailable, the so-called super anchor could be equipped with a longer lifetime battery (and/or even energy-harvesting capabilities) that maintains an adequate power level for all its tasks to be achieved.

Furthermore, to be able to perform ANN training, the super anchor needs to be aware of all true and estimated anchor inter-distances (i.e., $N_a(N_a-1)$ distance pairs). Otherwise, each anchor should be solicited for a second power and overhead consuming broadcast to share its data with the super anchor. To avoid this situation, we propose in what follows a power-efficient information sharing protocol where anchors periodically broadcast their positions alongside the training data. In fact, during the first time slot, only the super anchor should broadcast its position while the (N_a-1) other anchors only execute the tasks described in Section 5.4.1. At the second time slot, one of the latter calculates its pair true (e.g., GPS-based) and estimated (as described in Section 5.3) distances to the super anchor then broadcast it along with its own position throughout the network. Upon reception of these information, all nodes become a priori aware of the super anchor and first anchor positions and their inter-distance pairs. A second anchor then calculates its true and estimated inter-distances to both the super and first anchors and broadcasts them along with its position throughout the network. Within N_a time slots, all nodes, including the super anchor, become a priori aware of all the anchors' positions and all $N_a(N_a-1)/2$ inter-distance pairs (i.e., true and estimated). The super anchor is hence able to progressively accumulate up to $\left(N_a^2+N_a-2\right)/2$ distance pairs. Although a relatively larger training data could be collected if each anchor were to broadcast separately its position and distances, we will show below that the one gathered through the power-efficient information sharing protocol proposed above is more than enough for the proposed ANN-based WSN localization technique to outperform most representative range-free algorithms currently available in the literature.

5.5 Simulations results

Monte-Carlo simulations are provided in this section to support the theoretical and analytical results established previously. These simulations are conducted to compare, under the same network settings, the proposed algorithm with three of the best benchmarks currently available in the literature, namely, DV-Hop [4], LAEP [13] and MLPNN-CGFR [7]. All simulation results are obtained by averaging over 500 trials. In all simulations, nodes are uniformly deployed in a 2-D square area $S = 10^4 m^2$ and R and N_a are, respectively, set to $18m$ and 20. Furthermore, a nodes' RPP model characterized by a degree of irregularity (DoI) similar to that in [8] is considered.

As a performance metric, we propose the normalized root mean square error (NRMSE) defined as

$$\text{NRMSE} = \sum_{i=1}^{N-N_a} \sqrt{(x_i - \hat{x}_i)^2 + (y_i - \hat{y}_i)^2} \Big/ \Big((N - N_a)\, R \Big). \tag{5.9}$$

Fig. 5.2 plots the localization NRMSE achieved by the proposed algorithm, LAEP, DV-Hop, and MLPNN-CGFR for different values of N and DoI. As can be observed there, the proposed algorithm always outperforms its counterparts as it turns out to be until about four, three, and two times more accurate than LAEP, DV-Hop, and MLPNN-CGFR, respectively. In Fig. 5.2(b), the localization NRMSE achieved by all algorithms deteriorates as expected with DoI. However, the proposed algorithm show much more robustness to DoI and its accuracy losses than its counterparts.

Figs. 6.4 and 5.3(b) plot the NRMSE's standard deviation achieved by all localization algorithms for different values of N and DoI, respectively. They show that it decreases as expected for all algorithms when the node density increases. However, the one achieved by our algorithm, in contrast to its counterparts, remains relatively very small and even approaches zeros when N becomes large enough. Furthermore, Fig. 5.3(b) shows that the NRMSE's standard deviation's increase with the DoI is relatively slow and moderate with the proposed algorithm, but steep and significant with all three benchmarks.

Fig. 6.6 illustrates the NRMSE's CDF achieved by all algorithms and suggests that 99% of the sensors could estimate their position within a NRMSE value of less than 1 with the proposed technique. In contrast, only 61% of the nodes achieve the same accuracy with MLPNN-CGFR, 43% with Dv-Hop, and only 30% with LAEP. This further proves the superiority of our new WSN

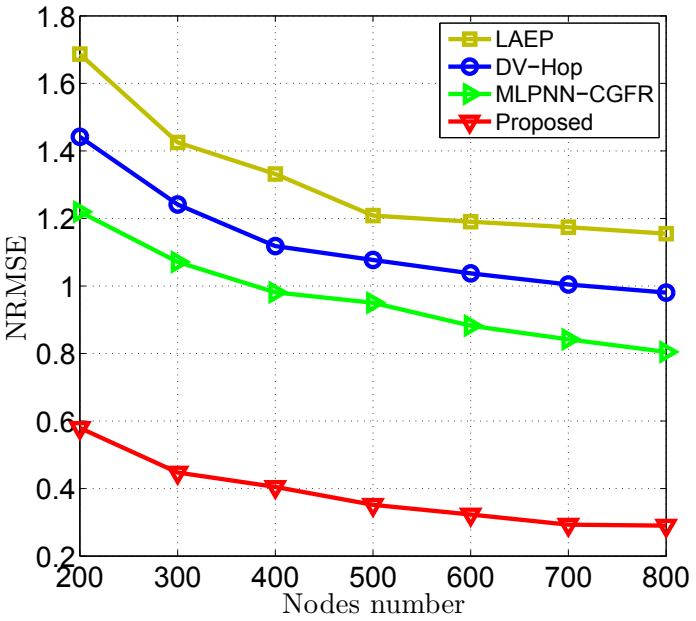

(a) DoI = 0.06.

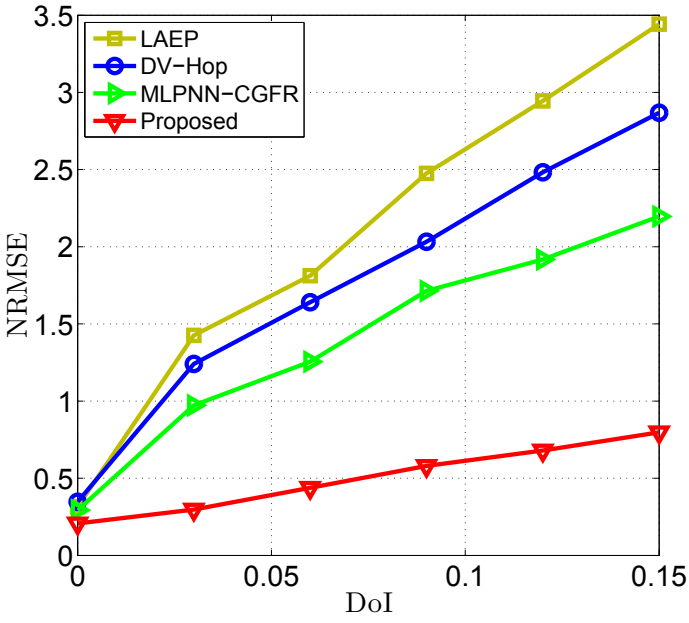

(b) $N = 300$.

FIGURE 5.2 – Localization NRMSE achieved by the proposed algorithm and its counterparts for different values of N and DoI.

localization algorithm over its counterparts in the presence of anisotropic signal attenuation.

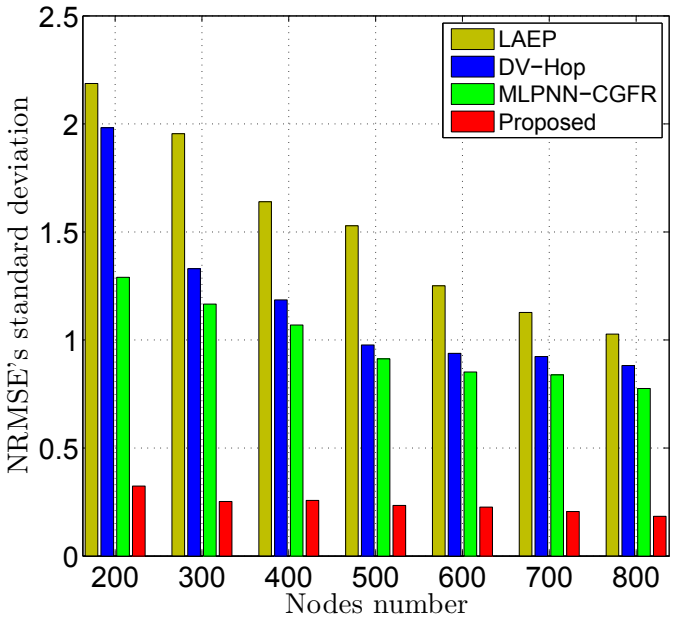

(a) DoI = 0.06.

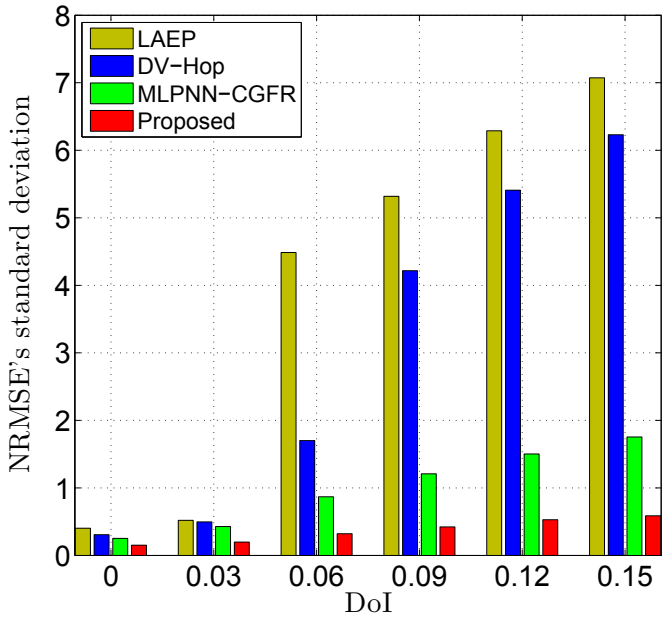

(b) $N = 300$.

FIGURE 5.3 – NRMSE's standard deviation achieved by the proposed algorithm and its counterparts for different values of N and DoI.

5.6 Conclusion

In this letter, we proposed a novel range-free localization algorithm robust against the anisotropic signal attenuation induced by fading, shadowing, and interference, etc., present in any

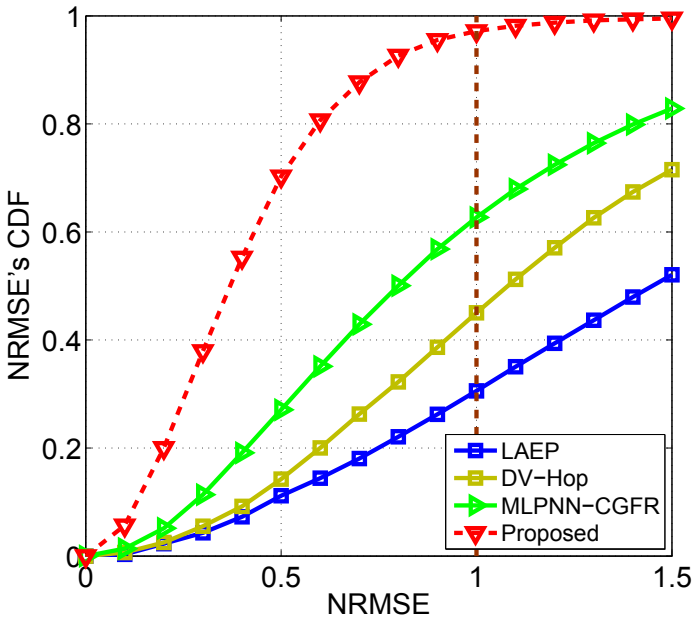

FIGURE 5.4 – NRMSE's CDF achieved by the proposed algorithm and its counterparts for $N = 300$ and $\text{DoI} = 0.06$.

wireless channel. To do so, we developed a new DE approach able to efficiently derive distance estimates in closed-form. We also developed an ANN-based power-efficient DE correction mechanism that accounts for anisotropic signal attenuation. The proposed algorithm significantly and unambiguously outperforms most representative range-free localization algorithms, not only in accuracy, but also in robustness against anisotropic attenuation.

Bibliographie

[1] W. Dargie and C. Poellabauer, *Fundamentals of Wireless Sensor Networks : Theory and Practice,* 1^{st} edition Wiley, New York, USA, 2010.

[2] A. Boukerche, H.A.B. Oliveira, E.F Nakamura, and A.A.F. Loureiro, "Localization systems for wireless sensor networks", *IEEE. Wireless Commun.*, vol. 14, no. 6, pp. 6-12, December 2007.

[3] H. Liu, H. Darabi, P. Banerjee, and j. Liu, "Survey of Wireless Indoor Positioning Techniques and Systems," *IEEE Trans. Syst., Man, Cybern., Syst.,* vol. 37, no. 6, pp. 1067-1080, november 2007.

[4] D. Niculescu and B. Nath, "Ad hoc Positioning System (APS)," *Proc. IEEE GLOBECOM,* San Antonio, USA, November 2001.

[5] Y. Wang, X. Wang, D. Wang, and D. P. Agrawal, "Range-Free Localization using Expected Hop Progress in Wireless Sensor Networks," *IEEE Trans. Parallel Distrib. Syst.,* vol. 25, no. 10, pp. 1540-1552, October 2009.

[6] S. Lee, B. Koo, and S. Kim, "RAPS : Reliable Anchor Pair Selection for Range-Free Localization in Anisotropic Networks," *IEEE Commun. Lett.,* vol. 18, no. 8, pp. 1403-1406, July 2014.

[7] A. Chatterjee, "A Fletcher-Reeves Conjugate Gradient Neural-Network-Based Localization Algorithm for Wireless Sensor Networks," *IEEE Trans. Veh. Technol.,* vol. 59, no. 2, pp. 823-830, February 2010.

[8] S. Biaz, Ji. Yiming, Q. Bing, and Wu. Shaoen, "Realistic Radio Range Irregularity Model and its Impact on Localization for Wireless Sensor Networks," *IEEE WiCOM,* Wuhan, China, September 2005.

Chapitre 6

Optimal Anchors Placement Strategy for Super Accurate Nodes Localization in Anisotropic Wireless Sensor Networks

Ahmad El Assaf, Slim Zaidi, Sofiène Affes and Nahi Kandil

Proc. IEEE IWCMC'2016, Paphos, Cyprus, September 5-9, 2016.

Résumé : Étant donné que la précision de localisation est fortement dépendante des positions de nœuds des ancres, ce chapitre élabore une stratégie de placement optimal de nœuds d'ancre capables de garantir une haute précision de localisation dans les réseaux de capteurs sans fil distribués dans des environnements anisotropes (AWSNs). En recourant à l'optimisation par essaim de particules bien connu ("Particle swarm optimization PSO"), nous dérivons les positions optimales des ancres qui minimisent l'erreur moyenne d'estimation de position (LEE). Il a été prouvé que notre stratégie de placement offre des gains de précision considérables si elles sont utilisées à la place des stratégies classiques et qu'il est en mesure de réduire non seulement la moyenne LEE mais aussi la LEE lui-même et, par conséquent, garantit une grande précision pour toute configuration de WSN.

Abstract

In this paper, we develop a novel optimal anchors placement strategy tailored for anisotropic WSNs. By resorting to the well-known particle swarm optimization (PSO), we derive the optimal anchors' positions that minimize the average location estimation error (LEE). We show that our placement strategy provides substantial accuracy gains if used instead of the conventional ones and that it is able to reduce not only the average LEE but also the LEE itself and, hence, guarantees high accuracy for any WSN configuration.

6.1 Introduction

Recent advances in wireless communications and low-power circuits technologies have led to proliferation of wireless sensor networks (WSNs). A WSN is a set of small and low-cost sensor nodes often equipped with small batteries. The latter are often deployed in a random fashion to sense or collect from the surrounding environments some physical phenomena such as temperature, light, pressure, etc. [1]-[3]. Since power is a scarce resource in such networks, sensors usually resort to multi-hop transmission in order to send their gathered data to an access point (AP). However, the received data at the latter are often fully or partially meaningless if the location from where they have been measured is unknown [4], making sensors' localization an essential task in WSNs. Many localization algorithms available in the literature [5]-[13] were designed to comply with such networks. To properly localize each sensor, most of these algorithms require the distance between the latter and at least three position-aware nodes called hereafter anchors [1]. Since it is very likely in WSNs that some sensors be unable to directly communicate with all anchors, the distance between each anchor-sensor pair is usually estimated using their shortest path. This distance is in fact approximated by the sum of the distances between any consecutive intermediate nodes located on this path. Several approaches have been so far developed to estimate these distances. Although efficient, they were unfortunately unable to guarantee high accuracy, especially in anisotropic environments where the shortest multi-hop path between each

1. In practice, an anchor node refers to a sensor, base station, or a nearby access point (AP) with known position. This information is usually acquired using global positioning system (GPS) technology, configured, or manually entered into the node memory prior to deployment.

anchor-sensor pair is often much longer than the actual distance separating them. This is actually due to the fact that the accuracy of any localization algorithm is governed not only by the distance estimation (DE) efficiency, but also the position of the anchors themselves. Significant research endeavors have been recently devoted to developing anchor placement strategies able to guarantee high sensor localization accuracy [14]-[22]. In [15], it has been proven that perimeter placement is the optimal strategy in isotropic environments free of obstacles (e.g., mountains, coverage holes, etc.). In [18], this strategy was investigated and compared in accuracy performance to other strategies in anisotropic environments. It was shown in [18] and [19] that the perimeter placement performs poorly in anisotropic environments. Some attempts to derive the optimal anchors positions in such environments have been made in [20]-[22] without providing significant accuracy gains.

In this paper, we develop a novel optimal anchors placement strategy properly tailored for anisotropic WSNs. By resorting to the well-known particle swarm optimization (PSO), we derive the optimal anchors' positions that minimize the average location estimation error (LEE). We show that our placement strategy provides substantial accuracy gains if used instead of the conventional ones and that it is able to reduce not only the average LEE but also the LEE itself and, hence, guarantees high accuracy for any WSN configuration.

The rest of this paper is organized as follows : Section 6.2 describes the network model. Section 6.3 introduces the average LEE and proves its adequacy to anchor-based localization. Section 6.4 proposes a novel optimal anchors placement strategy. Simulation results are discussed in Section 6.5 and concluding remarks are made in Section 6.6.

6.2 Network model

Fig. 6.1 illustrates a network model of M anchors and N sensors deployed in a 2-D square area S. The anchors are aware of their positions while the sensors are oblivious to this information. These sensors are assumed to be uniformly distributed in S. All anchor and sensor nodes are assumed to have the same transmission capability (i.e., range) denoted by R. Each node is able to directly communicate with any other node located in the disc having that node as a center and R as a radius, while it communicates in a multi-hop fashion with the nodes located outside. As shown in Fig. 6.1, the anchors are marked with red triangles and the senors are marked with

blue circles. If two nodes are able to directly communicate, they are linked with a dashed line that represents one hop.

Let us denote by $(a_i, b_i)\,,\ i = 1, \ldots, M$ the coordinates of the anchor nodes and $(x_i, y_i)\,,\ i = 1, \ldots, N$ those of the regular ones.

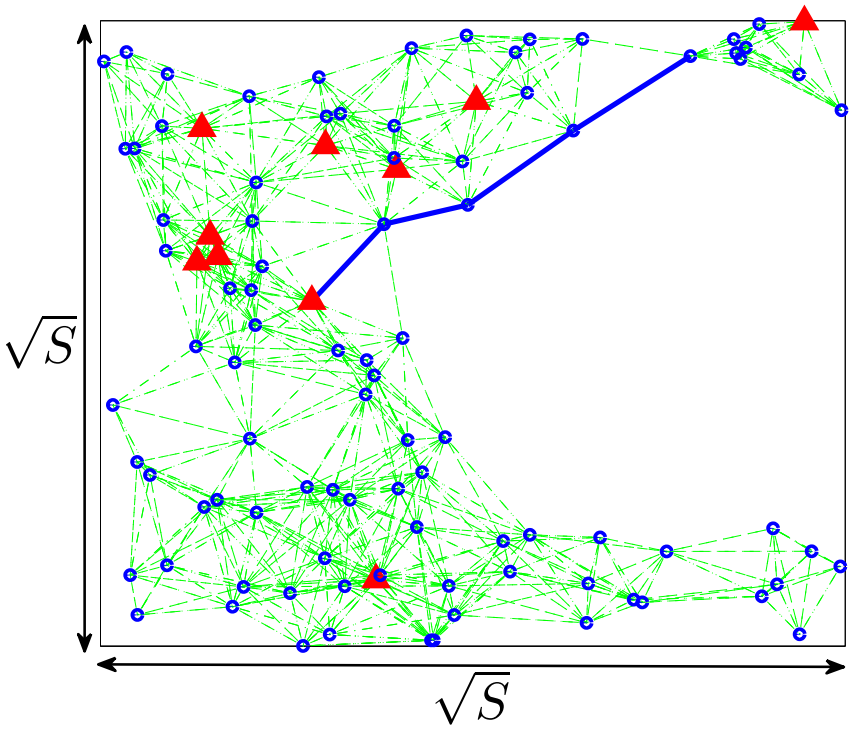

FIGURE 6.1 – Network model.

In what follows, we propose an efficient anchor placement strategy able to significantly enhance the accuracy of any anchor-based localization algorithm. To this end, one should first determine the metric which properly gauges the accuracy of such algorithms. From this perspective, Section 6.3 presents a new metric and proves its adequacy to anchor-based localization algorithms.

6.3 Average location estimation error (LEE)

As a first step of any anchor-based localization algorithm, the k-th anchor broadcasts its coordinate (a_k, b_k) in the network. The regular nodes receive these information either directly or through multi-hop communication. Once the i-th regular node obtains all anchors' coordinates and computes their corresponding distances, either heuristically or analytically, it derives its own

position by solving the following nonlinear equations system :

$$\begin{cases} (a_1 - \hat{x}_i)^2 + (b_1 - \hat{y}_i)^2 = & \hat{d}_{i-1}^2 \\ (a_2 - \hat{x}_i)^2 + (b_2 - \hat{y}_i)^2 = & \hat{d}_{i-2}^2 \\ \vdots & \vdots \\ (a_M - \hat{x}_i)^2 + (b_M - \hat{y}_i)^2 = & \hat{d}_{i-M}^2 \end{cases}, \tag{6.1}$$

where $(\hat{x}_i, \hat{y}_i)$ are the estimated i-th sensor's coordinates and $\hat{d}_{i-k}$ is its estimated distance to the k-th anchor. After some rearrangements aiming to linearize the above system , we obtain

$$\boldsymbol{\Upsilon}\hat{\boldsymbol{\alpha}}_i = -\frac{1}{2}\boldsymbol{\kappa_i}, \tag{6.2}$$

where $\hat{\boldsymbol{\alpha}}_i = [\hat{x}_i, \hat{y}_i]^T$,

$$\boldsymbol{\Upsilon} = \begin{bmatrix} a_1 - a_M & b_1 - b_M \\ a_2 - a_M & b_2 - b_M \\ \vdots & \vdots \\ a_{(M-1)} - a_M & b_{(M-1)} - b_M \end{bmatrix}, \tag{6.3}$$

and

$$\boldsymbol{\kappa_i} = \begin{bmatrix} \hat{d}_{i-1}^2 - \hat{d}_{i-M}^2 + a_M^2 - a_1^2 + b_M^2 - b_1^2 \\ \hat{d}_{i-2}^2 - \hat{d}_{i-M}^2 + a_M^2 - a_2^2 + b_M^2 - b_2^2 \\ \vdots \\ \hat{d}_{i-(M-1)}^2 - \hat{d}_{i-M}^2 + a_M^2 - a_{(M-1)}^2 + b_M^2 - b_{(M-1)}^2 \end{bmatrix}. \tag{6.4}$$

Since $\boldsymbol{\Upsilon}$ is a non-invertible matrix, $\hat{\boldsymbol{\alpha}}_i$ could be estimated with the pseudo-inverse of $\boldsymbol{\Upsilon}$ as follows :

$$\hat{\boldsymbol{\alpha}}_i = -\frac{1}{2}\left(\boldsymbol{\Upsilon}^T\boldsymbol{\Upsilon}\right)^{-1}\boldsymbol{\Upsilon}^T\boldsymbol{\kappa_i}. \tag{6.5}$$

Therefore, the i-th sensor is able to obtain an estimate of its coordinates as $\hat{x}_i = [\hat{\boldsymbol{\alpha}}_i]_1$, and $\hat{y}_i = [\hat{\boldsymbol{\alpha}}_i]_2$. Let $\mathcal{E}_{\mathrm{P},i}$ denote the i-th sensor's location estimation error (LEE) given by

$$\mathcal{E}_{\mathrm{P},i} = \left\|\boldsymbol{\alpha}_i - \hat{\boldsymbol{\alpha}}_i\right\|^2, \tag{6.6}$$

where $\boldsymbol{\alpha}_i = [x_i, y_i]^T$ is a vector whose entries are the true i-th sensor coordinates. From (6.6), $\mathcal{E}_{\mathrm{P},i}$ is an excessively complex function of the random variables $(x_i, y_i), i = 1, \ldots, N$, d_{i-k} and $\hat{d}_{i-k}, k = 1, \ldots, M$ and, hence, a random quantity of its own. Optimizing the anchors' locations using such a metric would not only be a tedious task, but it would also result in locations strongly dependent on the sensors' coordinates. Recall here that such information are not available. A

much more appealing metric would be then the average LEE $\bar{\mathcal{E}}_{\mathrm{P}}(N) = \mathrm{E}\{\mathcal{E}_{\mathrm{P},i}\}$ where the expectation is taken with respect to all the sensors' coordinates. Actually, $\bar{\mathcal{E}}_{\mathrm{P}}(N)$ could be differently defined as

$$\bar{\mathcal{E}}_{\mathrm{P}}(N) = \mathrm{E}\left\{\mathcal{G}_{\mathrm{P}}^{\mathrm{Net}}(N)\right\}, \tag{6.7}$$

where

$$\mathcal{G}_{\mathrm{P}}^{\mathrm{Net}}(N) = \frac{1}{N}\sum_{i=1}^{N}\mathcal{E}_{\mathrm{P},i}, \tag{6.8}$$

refers to the global LEE through the network. Furthermore, using the strong law of large numbers, we show for large N that we have

$$\mathcal{G}_{\mathrm{P}}^{\mathrm{Net}}(N) \xrightarrow{p1} \bar{\mathcal{E}}_{\mathrm{P}}(N), \tag{6.9}$$

where $\xrightarrow{p1}$ stands for convergence with probability one. From (6.9), $\bar{\mathcal{E}}_{\mathrm{P}}(N)$ is not only the statistical average of $\mathcal{G}_{\mathrm{P}}^{\mathrm{Net}}(N)$, but also it approaches the latter for any given realization (i.e., any given $(x_i, y_i), i = 1, \ldots, N$). All the above proves unambiguously that $\bar{\mathcal{E}}_{\mathrm{P}}(N)$ is a meaningful and useful performance metric. It follows from (6.5) that

$$\mathcal{E}_{\mathrm{P},i} \;=\; \frac{1}{4}\left\|\left(\boldsymbol{\Upsilon}^T\boldsymbol{\Upsilon}\right)^{-1}\boldsymbol{\Upsilon}^T\boldsymbol{\delta}_i\right\|^2, \tag{6.10}$$

where $[\boldsymbol{\delta}_i] = [\epsilon_1 - \epsilon_M, \ldots, \epsilon_{M-1} - \epsilon_M]^T$ with $\epsilon_k = \hat{d}_{i-k}^2 - d_{i-k}^2$ being the squared-distance estimation error. $\mathcal{E}_{\mathrm{P},i}$ is then given by

$$\begin{aligned}\mathcal{E}_{\mathrm{P},i} &= \mathrm{Tr}\left(\left(\boldsymbol{\Upsilon}^T\boldsymbol{\Upsilon}\right)^{-1}\boldsymbol{\Upsilon}^T\boldsymbol{\delta}_i\boldsymbol{\delta}_i^T\boldsymbol{\Upsilon}\left(\boldsymbol{\Upsilon}^T\boldsymbol{\Upsilon}\right)^{-1}\right)\\ &= \mathrm{Tr}\left(\boldsymbol{\Omega}\boldsymbol{\delta}_i\boldsymbol{\delta}_i^T\right)\\ &= \sum_{k=1}^{M-1}\boldsymbol{\Omega}_{kk}\left([\boldsymbol{\delta}_i]_k\right)^2 + \sum_{k=1}^{M-1}\sum_{l=1,l\neq k}^{M-1}\boldsymbol{\Omega}_{kl}[\boldsymbol{\delta}_i]_l[\boldsymbol{\delta}_i]_k,\end{aligned} \tag{6.11}$$

where $\mathrm{Tr}(\mathbf{X})$ is the trace of the matrix $\mathbf{X}$ and $\boldsymbol{\Omega} = \boldsymbol{\Upsilon}\left(\boldsymbol{\Upsilon}^T\boldsymbol{\Upsilon}\right)^{-2}\boldsymbol{\Upsilon}^T$. Note in the second line of (6.11) that we exploit the cyclic property of the trace. Since $\epsilon_k, k = 1, \ldots, M$ are i.i.d random variables, we have from (6.11) the following

$$\bar{\mathcal{E}}_{\mathrm{P}}(N) = \sigma_\epsilon^2\left(2\mathrm{Tr}(\boldsymbol{\Omega}) + \sum_{k=1}^{M-1}\sum_{l=1,l\neq k}^{M-1}\boldsymbol{\Omega}_{kl}\right) = \sigma_\epsilon^2 F(\Omega). \tag{6.12}$$

Therefore, in order to reduce $\bar{\mathcal{E}}_{\mathrm{P}}(N)$ (i.e., improve the localization accuracy), one should minimize both σ_ϵ^2 and $F(\boldsymbol{\Omega}) = 2\mathrm{Tr}(\boldsymbol{\Omega}) + \sum_{k=1}^{M-1}\sum_{l=1,l\neq k}^{M-1}\boldsymbol{\Omega}_{kl}$, the former by use of accurate DE techniques [5]-[13] while $F(\boldsymbol{\Omega})$ requires the optimization of the anchors positions. In the next section, adopt $F(\Omega)$ as a new design cost function to develop a novel optimal anchors placement strategy.

6.4 Proposed anchor placement strategy

In order to improve the localization accuracy in the anisotropic environments of our concern, one could compute the optimal set of anchors' positions $\mathcal{S}_{\text{opt}}$ that satisfies

$$\begin{aligned} \mathcal{S}_{\text{opt}} &= \arg\min F(\mathbf{\Omega}) \\ \text{s.t.} \quad & L_a \leq a_i \leq U_a \qquad i = 1, 2, \cdots, N_a \\ & L_b \leq b_i \leq U_b \qquad i = 1, 2, \cdots, N_a \\ & \|P_i - P_j\| \geq d_{min} \qquad \forall\, i \neq j \end{aligned} \tag{6.13}$$

where $P_i = [a_i, b_i]^T$ is the vector of the i-th anchors coordinates and L_a, L_b, U_a, and U_b are lower and upper bounds on all anchors coordinates. These bounds depend on the obstacle form and position. Please note that the first two constraints ensure that anchors be located within the obstacle surrounding area. Whereas the third constraint imposes a minimum distance d_{min} between the anchors and, hence, guarantees their deployment all over the available area.

Several effective optimization algorithms that require a moderate memory and reasonable computational resources have been proposed so far to solve such complex optimization problem, for instance the simulated annealing algorithm (SA), genetic algorithms (GA), artificial intelligence (AI), and particle swarm optimization (PSO) [23]. Due to its ease of implementation, high resolution, and speed of convergence, the latter has attracted a lot of attention in the research community and has been recently introduced as a promising tool for solving a wide range of optimization problems in different contexts such as UWB antenna design, data mining, acoustic communication, and localization [24]. However, despite their advantage, traditional PSO-based algorithms may easily fall into local optima, especially when solving a complex multimodal problem such as the one of our concern [25]. In order to overcome this issue, we propose in this paper a novel non-linear fitness-based inertia weight expression given by

$$\phi^k = w_{\max} \left(1 - \frac{(w_{\max} - w_{\min})\,\mu + w_{\min}}{1 + e^{\left(-2w_{\min} \frac{\min f_i^k - \max f_i^k}{\bar{f}_i^k}\right)}} \right), \tag{6.14}$$

where μ is a random variable uniformly distributed in the interval $[0, 1]$ and $\bar{f}_i^k$ is the average fitness value at the k-th generation. From (6.14), the value of the inertia weight will be then dynamically updated at each iteration in a non-linear manner according to the calculated fitness.

Algorithm 4 Optimal anchor nodes placement algorithm

% s_k is the set of anchor nodes%

Initialize the first two anchor nodes positions

$s_k = [0 \quad S; S \quad S]$

Initialize the cognitive and social scaling parameters c_1 and c_2, respectively

Initialize the maximum number of iterations k_{max}

Initialize γ_g in such a way that the fitness of γ_g is as close to infinity as possible

Initialize position and velocity boundaries

$m = 3$

for $m \leq N_a$ **do**

$X_0 = s_k\,(m-1)$

while Constraints criteria are not met **do**

$k = 1$

for each particle i **do**

$P_i = |X_0 + rand\,(1,2)|$

$V_i = V_{max} \times rand\,(1,2)$

Compute $f\,(P_i)$

if $f\,(P_i) < f\,(\gamma_g)$ **then**

$\gamma_g = P_i$

$f\,(\gamma_g) = f\,(P_i)$

end if

end for

while $k \neq k_{max} v$ **do**

$\phi^{k+1} \leftarrow$ Equation (6.14)

for each particle i **do**

$V_i^{k+1} \leftarrow$ Equation (6.15)

$P_i^{k+1} \leftarrow$ Equation (6.16)

Check the velocity and position boundaries

Compute $f\,(P_i)$

if $f\,(P_i) < f\,(\rho_i)$ **then**

$\rho_i = P_i$

$f\,(\rho_i) = f\,(P_i)$

end if

if $f\,(P_i) < f\,(\gamma_g)$ **then**

$\gamma_g = P_i$

This allows a shorter exploration time than with existing approaches such as the linear, random, constant, and chaotic ones [26]-[29]. Once we get ϕ^k, the velocity and position of each particle are updated using the following equations

$$V_i^{k+1} = \phi^k V_i^k + c_1\alpha\left(\rho_i^k - P_i^k\right) + +c_2\beta\left(\gamma_g^k - P_i^k\right), \tag{6.15}$$

and

$$P_i^{k+1} = P_i^k + V_i^{k+1}, \tag{6.16}$$

where ρ_i^k is the best previous position of the i-th particle, γ_g^k is the best global position at the k-th generation, c_1 and c_2 are the cognitive and social scaling parameters, respectively, and α and β are two random variables uniformly distributed within the interval $[0, 1]$. The rest of the proposed PSO-based estimation algorithm of the optimal anchors positions with a minimum average LEE is summarized in Algorithm 4.

In the next section, we prove that placing the anchors in the positions obtained using our PSO-based algorithm can enhance localization accuracy in anisotropic environments substantially.

6.5 Simulations results

Monte-Carlo simulations are provided in this section to verify the efficiency of the proposed anchors placement strategy. These simulations are conducted to compare, under the same network settings, the latter with three commonly adopted benchmarks, namely the grid [14], perimeter [15], and random [13] placement strategies. All these strategies are tested using two localization algorithms : the well-known RAPS [8] and one of our recently developed algorithms [9]. All simulation results are obtained by averaging over 800 trials. In all simulations, nodes are uniformly deployed in a 2-D square area in the presence of a rectangle obstacle which makes the network topology C-shaped, except in Fig. 6.2 where we consider an isotropic environment. S and R are set to 50^2 m^2 and 10 m, respectively. M is set to 12, expect in Fig. 6.5 where it varies from 5% to 10%.

Figs. 6.2(a) and 6.2(b) plot the average R^2-normalized LEE (NLEE) achieved by RAPS [8] and our localization algorithm in [9] using the proposed anchor placement, grid, perimeter, and random strategies for different values of N in an isotropic environment. From these figures, the accuracy of both localization algorithms is improved using the proposed strategy instead of the

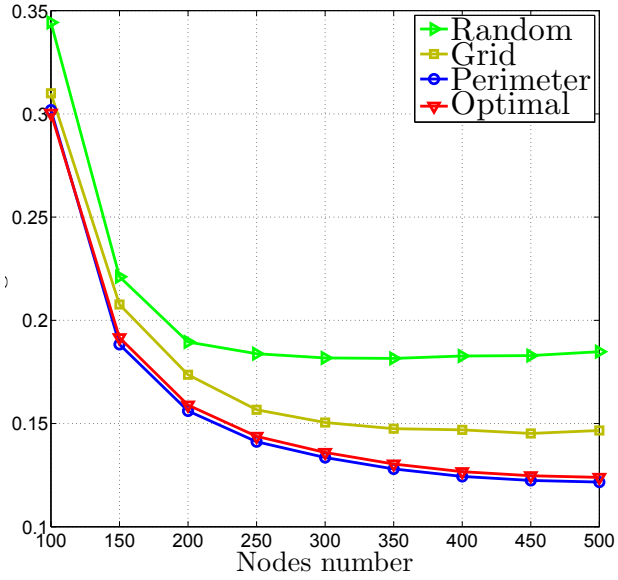

(a) RAPS [8].

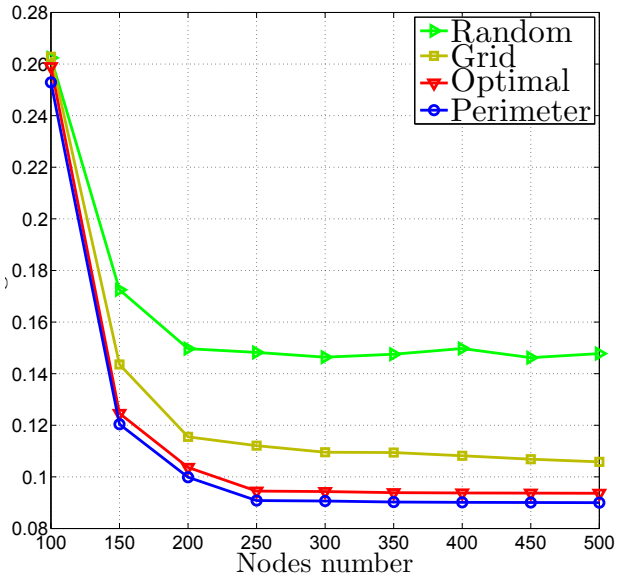

(b) Our localization algorithm in [9].

FIGURE 6.2 – Average NLEE achieved by RAPS [8] and our localization algorithm in [9] using the proposed anchor placement, grid, perimeter, and random strategies for different values of N in an isotropic environment.

grid and random strategies. Furthermore, the proposed strategy guarantees almost the same accuracy as the perimeter placement, which was previously proven to be the optimal one in

any isotropic environment [15]. This validates the optimality of the proposed anchors placement strategy.

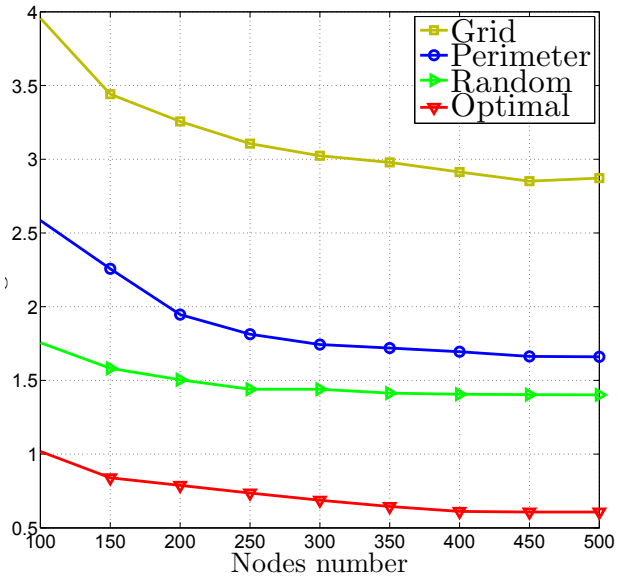

(a) RAPS [8].

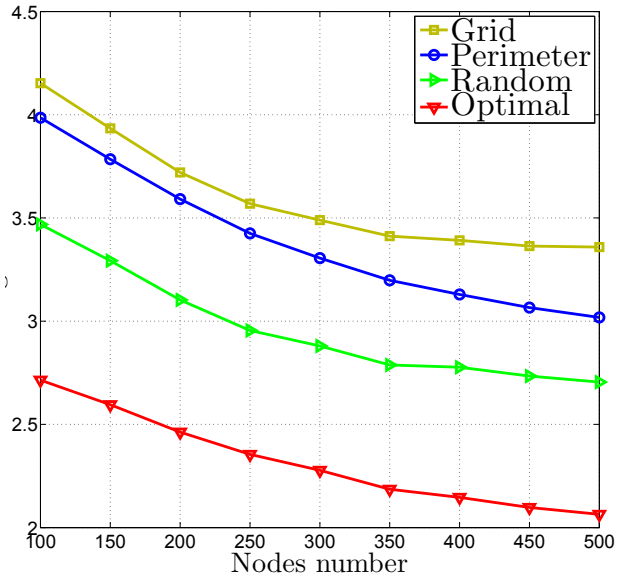

(b) Our localization algorithm in [9].

FIGURE 6.3 – Average NLEE achieved by RAPS [8] and our localization algorithm in [9] using the proposed anchor placement, grid, perimeter, and random strategies for different values of N in an anisotropic environment.

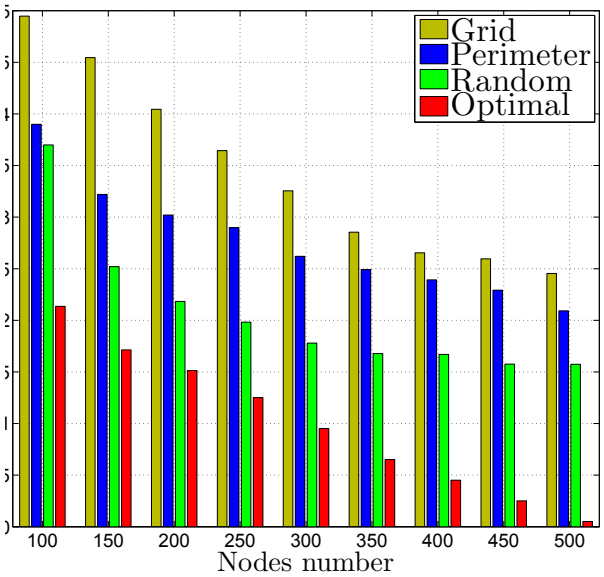

(a) RAPS [8].

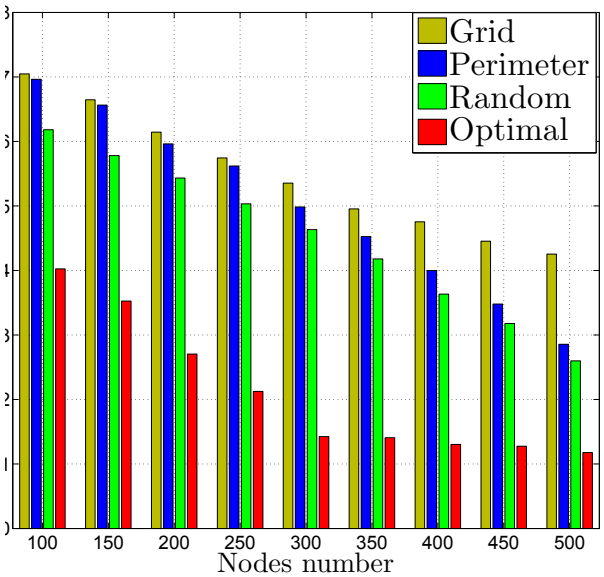

(b) Our localization algorithm in [9].

FIGURE 6.4 – NLEE's standard deviation achieved by RAPS [8] and our localization algorithm in [9] using the proposed anchor placement, grid, perimeter, and random strategies for different values of N in an anisotropic environment.

Figs. 6.3(a) and 6.3(b) display the average NLEE achieved by RAPS [8] and our localization algorithm in [9] using the proposed anchor placement, grid, perimeter, and random strategies

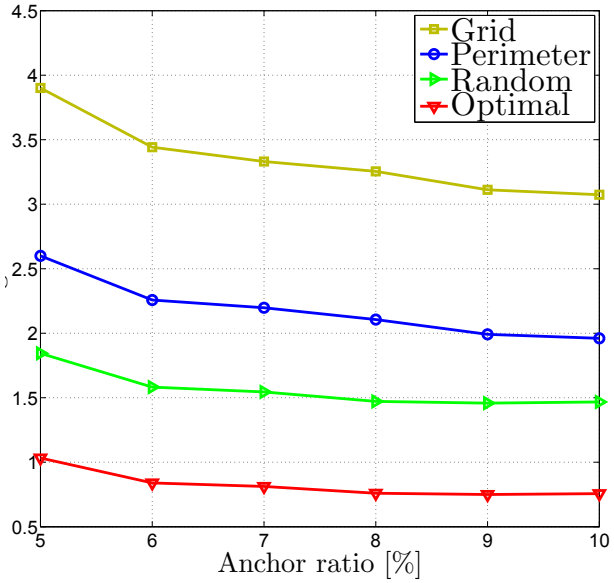

(a) RAPS [8].

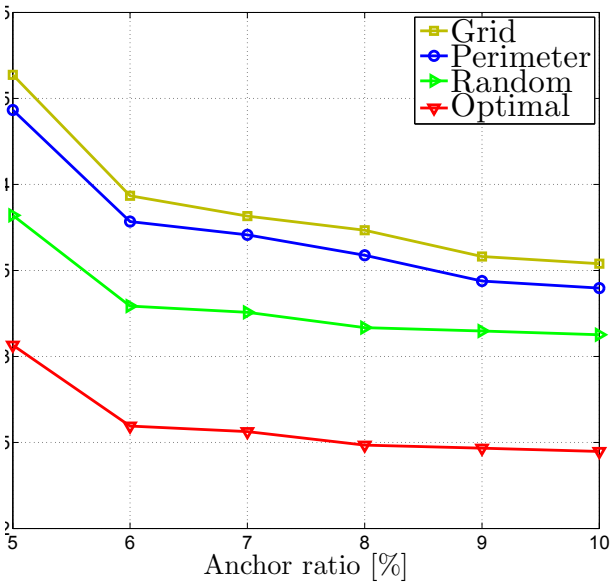

(b) Our localization algorithm in [9].

FIGURE 6.5 – Average NLEE achieved by RAPS [8] and our localization algorithm in [9] using the proposed anchor placement, grid, perimeter, and random strategies for different values of M with $N = 150$ in an anisotropic environment.

for different values of N in an anisotropic environment. As could be observed from these figures, the lowest average NLEE is always achieved by the proposed strategy. The latter turns out to be

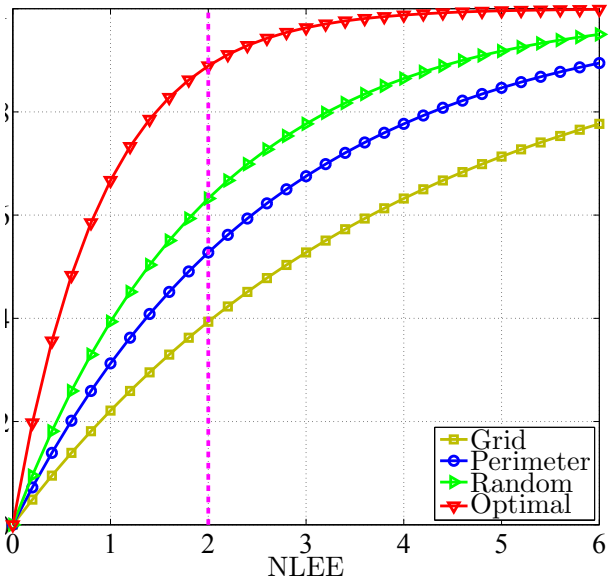

(a) RAPS [8].

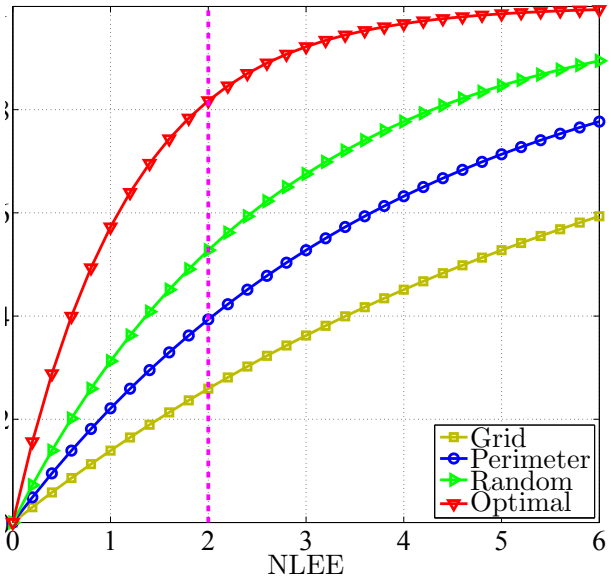

(b) Our localization algorithm in [9].

FIGURE 6.6 – NLEE's CDF achieved by RAPS [8] and our localization algorithm in [9] the proposed anchor placement, grid, perimeter, and random strategies with $N = 150$ in an anisotropic environment.

until about 76.8%, 61.62%, and 50.64% more accurate than than grid, perimeter, and random strategies, respectively. This proves the superiority of the proposed PSO-based anchor placement

strategy.

Figs. 6.4(a) and 6.4(b) plot the NLEE's standard deviation achieved by RAPS [8] and our localization algorithm in [9] using all anchors placement strategies for different values of N. From these figures, using any strategy, the NLEE's standard deviation decreases as expected when the node density increases. However, the one achieved by the proposed strategy approaches 0 as N grows large, in contrast to all its counterparts. Our strategy is actually able to minimize not only the average NLEE, but also the NLEE itself. This is a highly desirable feature, since it guarantees high accuracy for any WSN configuration.

Figs. 6.5(a) and 6.5(b) show the average NLEE achieved by RAPS [8] and our localization algorithm in [9] using the proposed anchor placement, grid, perimeter, and random strategies for different values of M with $N = 150$. As could be observed from these figures, the localization accuracy is improved as expected when he number of anchors is improved. However, the average NLEE achieved using our new anchor placement strategy remains the lowest, thereby further proving its high efficiency.

Figs. 6.6(a) and 6.6(a) illustrate the NLEE's CDF achieved by RAPS [8] and our localization algorithm in [9] using all the anchor placement strategies. With the proposed strategy, until 90% of the sensors could estimate their position with a NLEE less than 2 using the RAPS algorithm. In contrast, 62% achieve the same accuracy with the random strategy, 52% with the perimeter strategy, and only about 40% with the grid strategy. This highlights again the net advantage of the proposed PSO-based placement strategy against its counterparts in anisotropic environments.

6.6 Conclusion

In this paper, we developed a novel optimal anchor placement strategy tailored for anisotropic WSNs. By resorting to the well-known particle swarm optimization (PSO), we derived the optimal anchors positions that minimize the average location estimation error (LEE). It was shown that our placement strategy provides substantial accuracy gains if used instead of conventional ones and that it is able to reduce not only the average LEE but also the LEE itself and, hence, guarantees high accuracy for any WSN configuration.

Bibliographie

[1] D.P. Agrawal and Q.-A. Zeng, *Introduction to Wireless and Mobile Systems,* 3^{rd} edition Cengage Learning, USA, 2010.

[2] W. Dargie and C. Poellabauer, *Fundamentals of Wireless Sensor Networks : Theory and Practice,* 1^{st} edition Wiley, New York, USA, 2010.

[3] F. Gustafsson and F. Gunnarsson, "Mobile Positioning using Wireless Networks : Possibilities and Fundamental Limitations Based on Available Wireless Network Measurements," *IEEE Signal Process. Mag.,* vol. 22, no. 4, pp. 41-53, July 2005.

[4] V. Lakafosis and M.M. Tentzeris, "From Single-to mMltihop : The status of Wireless Localization," *IEEE Microw. Mag.,* vol. 10 , no. 7, pp. 34-41, December 2009.

[5] J. Rezazadeh, M. Moradi, A.S. Ismail, and E. Dutkiewicz, "Superior Path Planning Mechanism for Mobile Beacon-Assisted Localization in Wireless Sensor Networks," *IEEE Sensors J.,* vol. 14, no. 9, pp. 3052-3064, May 2014.

[6] H. Shen, Z. Ding, S. Dasgupta, and C. Zhao, "Multiple Source Localization in Wireless Sensor Networks Based on Time of Arrival Measurement," *IEEE Trans. Signal Process.,* vol. 62, no. 8, pp. 1938-1949, February 2014.

[7] A. El Assaf, S. Zaidi, S. Affes, and N. Kandil, "Range-Free Localization Algorithm for Heterogeneous Wireless Sensors Networks," *Proc. IEEE WCNC'2014,* Istanbul, Turkey, April 6-9, 2014.

[8] S. Lee, B. Koo, and S. Kim, "RAPS : Reliable Anchor Pair Selection for Range-Free Localization in Anisotropic Networks," *IEEE Commun. Lett.,* vol. 18, no. 8, pp. 1403-1406, July 2014.

[9] A. El Assaf, S. Zaidi, S. Affes, and N. Kandil, "Low-Cost Localization for Multi-hop Heterogeneous Wireless Sensor Networks". *IEEE Trans. Wireless. Commun.*, vol. 15, no. 1, pp. 472-484, January 2016.

[10] Z. Ziguo and T. He,"RSD : A Metric for Achieving Range-Free Localization beyond Connectivity," *IEEE Trans. Parallel and Distributed Sys.,* vol. 24, no. 11, pp. 1943-1951, November 2011.

[11] L. Gui, T. Val, and A. Wei, "Improving Localization Accuracy using Selective 3-Anchor DV-Hop Algorithm," *Proc. IEEE VTC'2011,* San Francisco, CA, USA, September 5-8, 2011.

[12] A. Boukerche, H.A.B.F. Oliveira, E.F. Nakamura, and A.A.F. Loureiro, "DV-LOC : a Scalable Localization Protocol using Voronoi Diagrams for Wireless Sensor Networks," *IEEE Wireless. Commun. Mag.,* vol. 16, no. 2, pp. 50-55, April 2009.

[13] Y. Wang, X. Wang, D. Wang, and D. P. Agrawal, "Range-Free Localization using Expected Hop Progress in Wireless Sensor Networks," *IEEE Trans. Parallel Distrib. Syst.,* vol. 25, no. 10, pp. 1540-1552, October 2009.

[14] S.U. Khan, "Approximate Optimal Sensor Placements in Grid Sensor Fields," *Proc. IEEE VTC'2007,* Dublin, Ireland, April 22-25, 2007.

[15] J. N. Ash and R. L. Moses, "On Optimal Anchor Node Placement in Sensor Localization by Optimization of Subspace Principal Angles," *Proc. IEEE ICASSP'2008,* Las Vegas, Nevada, USA, March 30-April 4, 2008.

[16] J. Bachrach, C. Taylor, *Localization in Sensor Networks,* Handbook of Sensor Networks, pp. 277-310, 2005.

[17] C.-C. Chen and T.-C. Lin, "A low-cost anchor placement strategy for range-free localization problems in wireless sensor networks," *Inter. J. Dist. Sensor Net.*, vol. 2013, pp. 1-12, October 2013.

[18] A. El Assaf, S. Zaidi, S. Affes, and N. Kandil, "Accurate Nodes Localization in Anisotropic Wireless Sensor Networks,". *Inter. J. Dist. Sensor Net.*, vol. 2015, pp. 1-17, April 2015. Invited Paper.

[19] A. El Assaf, S. Zaidi, S. Affes, and N. Kandil, "Range-Free Localization Algorithm for Anisotropic Wireless Sensor Networks," *Proc. IEEE VTC'2014-Fall,* Vancouver, Canada, September 14-17, 2014.

[20] R. Zhang, W. Xia, Z. Jia, L. Shen, and J. Guo, "The Optimal Placement Method of Anchor Nodes toward RSS-Based Localization System," *Proc. IEEE WCS'2014),* Hefei, China, October 23-25, 2014.

[21] D. Wang, H. Feng, T. Xing, and J. Sun, "Optimized Anchor Nodes Placement for Underground Mine Localization System Based on ZigBee Technology," *Proc. IEEE MEC'2011,* Jilin, China, August 19-22, 2011.

[22] S. Roy and N. Mukherjee, "Integer Linear Programming Formulation of Optimal beacon Placement Problem in WSN," *Proc. IEEE AIMoC'2014,* Kolkata, India, February 27-March 1, 2014.

[23] J.-B. Park, Y.-W. Jeong, J.-R. Shin, and K. Y. Lee, "An Improved Particle Swarm Optimization for Nonconvex Economic Dispatch Problems," *IEEE Trans. Power Syst.,* vol. 25, no. 1, pp. 156–166, February 2010.

[24] C. Li, S. Yang and T.T. Nguyen, "A Self-Learning Particle Swarm Optimizer for Global Optimization Problems," *IEEE Trans. Syst., Man, Cybern., Syst.*, vol. 42, no. 13, pp. 627-646, June 2012.

[25] J.J. Liang, A.K. Qin, P.N. Suganthan, and S. Baska, "Comprehensive Learning Particle Swarm Optimizer for Global Optimization of Multimodal Functions," *IEEE Trans. Evol. Comput.,* vol. 10, no. 3, pp. 281-295, June 2006.

[26] J. C. Bansal, P. K. Singh, M. Saraswat, A. Verma, S.S. Jadon, and A. Abraham, "Inertia Weight Strategies in Particle Swarm Optimization," *IEEE NaBIC,* Salamanca, Spain, October 2011.

[27] R.C. Eberhart, and Y. Shi., "Tracking and Optimizing Dynamic Systems with Particle Swarms," *IEEE Proc. CEC'2011,* Seoul, South Korea, May 27-30, 2001.

[28] J. Xin, G. Chen, and Y. Hai., "A Particle Swarm Optimizer with Multistage Linearly-Decreasing Inertia Weight," *IEEE CSO'2009,* Sanya, China, April 24-26, 2009.

[29] Y. Feng, G.F. Teng, A.X. Wang, and Y.M. Yao., "Chaotic Inertia Weight in Particle Swarm Optimization," *IEEE ICICIC,* Kumamoto, Japan, September 5-7, 2007.

Conclusion

Cette thèse propose des algorithmes de localisation novateurs à faible cout qui offre une très haute précision. Au chapitre 2, on a développé un algorithme de localisation adapte pour les WSNs hétérogène ou la portée de transmission est généralement différente d'un capteur a un autre. En exploitant le fait que la distance entre deux nœuds de capteurs dépond à la fois de la portée de transmission du nœud émetteur et celle du nœud intermédiaire, on a réussi à améliorer la précision de l'estimation de distance et, par conséquent, les performances de la localisation. Il a été prouvé que notre algorithme ne nécessite aucun échange d'information supplémentaire entre les capteurs. Un mécanisme de correction capable d'améliorer encore plus la précision a été aussi développé. Il a été démontré que notre algorithme offre plus de que la plupart des algorithmes dans la littérature : DV-hop, LAEP et EPHP dont leur conception ne prend pas en compte l'hétérogénéité des WSNs. Au chapitre 3, un nouvel algorithme robuste contre la présence d'obstacles entre les nœuds a été développé. Cet algorithme exploite une stratégie novatrice de sélection des anchors fiables. En plus, un mécanisme d'économie d'énergie visant à améliorer la durée de vie WSN a été proposé. Visant à améliorer encore plus la précision de la localisation dans les WSNs, un autre algorithme a été développé dans le Chapitre 4. Ce dernier utilise d'autres informations localement disponibles au niveau de chaque nœud, jusqu'ici inexploité. En plus, L'expression analytique de la moyenne de l'erreur de l'estimation de positon a été calculée pour la première fois en *closed-form*. Il a été démontré que, en utilisant notre algorithme, les erreurs d'estimation de la position et de leurs écart-type tendent vers zéro dans les réseaux très denses. Chapitre 5 a proposé un nouvel algorithme de localisation robuste contre l'"atténuation anisotrope du signal. Une nouvelle approche capable de dériver efficacement les distances estimées en *closed-form* a été développée dans ce chapitre. En exploitant les réseaux de neurones artificiels (ANNs), on a réussi à mettre en place un mécanisme de correction des distances estimées à faible coût. La précession et la robustesse de notre algorithme a été prouvé.

Étant donné que la précision de localisation est étroitement liée aux positions des anchors, Chapitre 6 a élaboré une stratégie novatrice de placement optimal des anchors. En recourant à l'optimisation par essaim de particules bien connu ("Particle swarm optimization PSO"), il a été démontré que la nouvelle stratégie de placement offre des gains de précision considérables.

Liste de publications

1. **A. EL Assaf**, S. Zaidi, S. Affes, and N. Kandil, "Robust ANNs-based WSN Localization in the Presence of Anisotropic Signal Attenuation,". *IEEE Wireless Communications Letter*, vol. 5, no. 5, pp. 504-507, July 2016.
2. **A. EL Assaf**, S. Zaidi, S. Affes, and N. Kandil, "Low-cost localization for multi-hop heterogeneous wireless sensor networks". *IEEE Trans. Wireless. commun.*, vol. 15, no. 1, pp. 472-484, January 2016.
3. **A. EL Assaf**, S. Zaidi, S. Affes, and N. Kandil, "Accurate Nodes Localization in Anisotropic Wireless Sensor Networks,". *Inter. J. Dist. Sensor Net.*, vol. 2015, pp. 1-17, April 2015. **Invited Paper**.
4. S. Zaidi, **A. EL Assaf**, S. Affes, and N. Kandil, "Accurate Range-Free Localization in Multi-Hop Wireless Sensor Networks,". *IEEE Transactions on Communications,* vol. 64, no. 9, pp. 3886-3900, September 2016.
5. **A. El Assaf**, S. Zaidi, S. Affes, and N. Kandil, "Optimal Anchors Placement Strategy for Super Accurate Nodes Localization in Anisotropic Wireless Sensor Networks," Proc. IEEE IWCMC'2016, Paphos, Cyprus, September 5-9, 2016.
6. **A. EL Assaf**, S. Zaidi, S. Affes, and N. Kandil, "Efficient Node Localization in Energy-Harvesting Wireless Sensor Networks," *IEEE ICUWB'2015 Workshop on communications with energy harvesting and wireless power transfer,* Montreal, QC, Canada, October 4-7, 2015.
7. **A. EL Assaf**, S. Zaidi, S. Affes, and N. Kandil, "Accurate Sensors Localization in Underground Mines or Tunnels," *IEEE ICUWB'2015 Workshop on Wireless Communications in Underground and Confined Environments,* Montreal, QC, Canada, October 4-7, 2015.
8. **A. EL Assaf**, S. Zaidi, S. Affes, and N. Kandil, "Accurate Nodes Localization in Aniso-

tropic Wireless Sensor Networks," *IEEE ICUWB'2015,* Montreal, QC, Canada, October 4-7, 2015.

9. S. Zaidi, **A. EL Assaf**, S. Affes, and N. Kandil, "Range-Free Nodes Localization in Mobile Wireless Sensor Networks," *IEEE ICUWB'2015 Workshop on V2X Communications : Safety, Automated Driving, and Other Applications,* Montreal, QC, Canada, October 4-7, 2015.
10. **A. EL Assaf**, S. Zaidi, S. Affes, and N. Kandil, "Cost-effective and Accurate Nodes Localization in Heterogeneous Wireless Sensor Networks," *Proc. IEEE ICC'2015,* London, United Kingdom, June. 8-12, 2015.
11. S. Zaidi, **A. EL Assaf**, S. Affes, and N. Kandil, "Range-Free Node Localization in Multi-Hop Wireless Sensor Networks,". Submitted to *IEEE WCNC'16.*
12. **A. EL Assaf**, S. Zaidi, S. Affes, and N. Kandil, "Range-free localization algorithm for anisotropic wireless sensor networks," *Proc. IEEE VTC'2014-Fall,* Vancouver, Canada, Sep. 14-17, 2014.
13. **A. EL Assaf**, S. Zaidi, S. Affes, and N. Kandil, "Range-free localization algorithm for heterogeneous wireless sensors networks," *Proc. IEEE WCNC'2014,* Istanbul, Turkey, Apr. 6-9, 2014.
14. **A. EL Assaf**, S. Zaidi, S. Affes, and N. Kandil, "Efficient range-free localization algorithm for randomly distributed wireless sensor networks," *Proc. IEEE GLOBECOM'2013,* Atlanta, GA, USA, Dec. 9-13,2013.
15. **A. EL Assaf**, S. Zaidi, S. Affes, and N. Kandil, "Hop-Count Based Localization Algorithm for Wireless Sensor Networks," *Proc. IEEE MMS'2013,* Saida, Lebanon, September 2-5, 2013. **Invited Paper**.